MINISTRY OF MINES AND ENERGY

Director: Geological Survey: Dr GIC Schneider

COMMUNICATIONS OF THE GEOLOGICAL SURVEY OF NAMIBIA

VOLUME 15
2013

Referees: H. Mocke, G.I.C. Schneider

COMMUNICATIONS OF THE GEOLOGICAL SURVEY OF NAMIBIA

VOLUME 15
2013

CONTENTS

PAPERS

Radio-isotopic age control for Palaeogene deposits of the Northern Sperrgebiet, Namibia

Martin Pickford[1,4], Yoshihiro Sawada[2], Hironobu Hyodo[3] & Brigitte Senut[4]

1. Collège de France, Paris, France, <pickford @mnhn.fr>
2. Professor Emeritus, Shimane University, Matsue, Japan, <yoshipikotan@nifty.com>
3. Research Institute of Natural Science, Okayama University of Science, Ridai-cho,
Okayama 700-0005, Japan, <hhyodo@rins.ous.ac.jp>.
4. UMR 7207 (CR2P) du CNRS, Case postale 38, 8, rue Buffon, 75005, Paris, France,
<bsenut@mnhn.fr>

The fossiliferous freshwater limestones of the Northern Sperrgebiet accumulated in epikarst depressions that formed in Proterozoic dolomites of the Gariep Group. Geological mapping and stratigraphic superposition reveals that they are younger than the Pomona Quartzite, but older than the Blaubok Conglomerate and many other superficial deposits of Palaeogene and Neogene age, including the Klinghardt Phonolites. Age determinations of phonolite cobbles from the Gemsboktal Conglomerate and from occurrences of lava in the Klinghardt Mountains and at Swartkop indicate that volcanic activity spanned the period 42 – 37 million years. It is concluded from the stratigraphic and radio-isotopic evidence that the freshwater limestones were deposited during the middle Lutetian, ca. 47 - 45 Ma.

Introduction

The discovery of rich assemblages of Palaeogene plants, invertebrates and vertebrates in freshwater limestones in the Northern Sperrgebiet (Silica North, Silica South, Chalcedon Tafelberg, Steffenkop, Black Crow, Gamachab, Eisenkieselklippenbacke) (Pickford *et al*., 2008a, 2008b) throws a great deal of light on the geological history and geomorphological evolution of southwestern Namibia because it provides constraints on the age of maturation of the Namib Unconformity Surface (Ward, 1987, 1988). The terrestrial gastropod fauna yields palaeoclimatic evidence, notably that the region enjoyed a summer rainfall regime at the time of deposition, but with a winter rainfall belt not far away. Some of the mammals (embrithopods, macroscelidids, todralestids) are more primitive than anything from the well known Late Eocene and basal Oligocene Fayum (Egypt) faunas, whereas others, notably the rodents and hyracoids share closer affinities with the North African faunas. The presence in Namibia, of a mammal with South American affinities is particularly intriguing.

The rodents and hyracoid, in particular, have been interpreted to indicate an age for the Namibian fossils close to the Late Eocene faunas of the Fayum, Egypt (Seiffert, 2010) but the other evidence suggests instead that these groups evolved more slowly than the embrithopods, just as they did in the Miocene of Africa, where large mammals tended to evolve more rapidly than rodents.

The aim of this paper is to investigate the stratigraphy and radio-isotopic age of rocks in the Sperrgebiet, with a view to resolving the debate about the age of the fossiliferous freshwater limestones. Phonolite clasts were derived from the Klinghardt Volcanic Province which lies 30-40 km to the east of the limestone deposits. The absence of phonolite clasts in all deposits older than the Gemsboktal Conglomerate indicates that eruptive activity did not commence in the Klinghardt Volcanic Province prior to the Middle Eocene some 42 Ma.

Freshwater limestones

The fossiliferous freshwater limestones in the Northern Sperrgebiet have yielded abundant and diverse plant and animal remains (Pickford *et al*., 2008b). In the main outcrops at Silica North, Silica South and

Black Crow (Fig. 1, 2) these limestones are unconformably overlain by the Blaubok Conglomerate (without phonolite clasts), which is in its turn overlain unconformably by the Gemsboktal Conglomerate (with abundant phonolite cobbles).
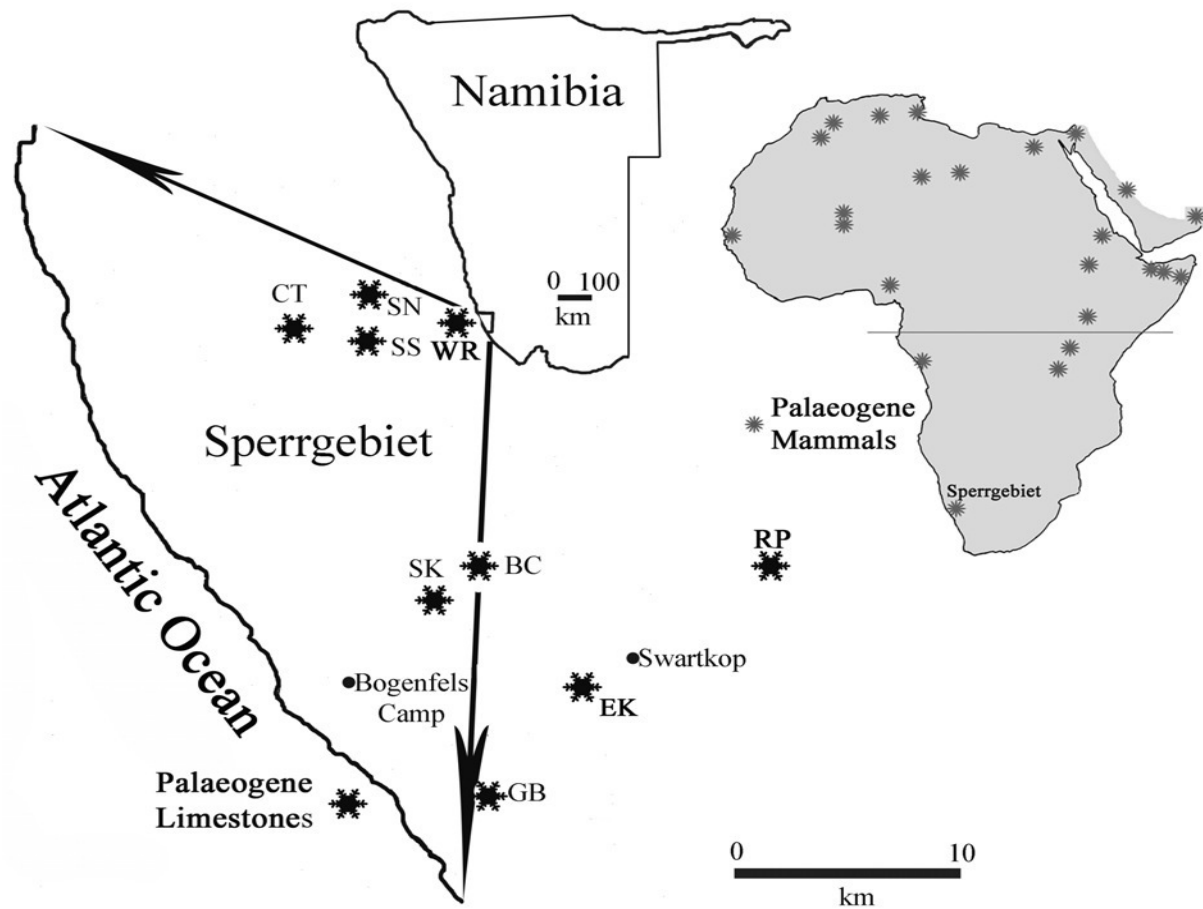
Figure 1: Location map, Northern Sperrgebiet showing Palaeogene terrestrial fossil localities in limestones. BC – Black Crow; CT – Chalcedon Tafelberg; EK – Eisenkieselklippenbacke; GB – Gamachab; RP – Reuning's Pipe; SK – Steffenkop; SN – Silica North; SS – Silica South; WR – White Ring.

Clast assemblages

In the Sperrgebiet in particular, but widely in Southern Africa and other parts of the World, clast assemblages have been studied in order to obtain information concerning the succession of geological events in a region. This is possible if the origin of the clasts can be determined because conglomerates with identifiable clasts must be younger than the stratum or rock unit from which the clasts were derived.

At Black Crow Depression, the Black Crow Carbonates not only underlie the Blaubok Conglomerate, but the latter unit also contains reworked blocks and clasts of Black Crow Carbonate, as well as boulders of Pomona Quartzite and Gariep Group Dolo-

mites, and a variety of unidentified clasts. Some of the clasts in the Blaubok Conglomerate have been silicified, including Gariep Dolomite and Black Crow Carbonate, and this evidence indicates that silicification occurred prior to deposition of the Blaubok Conglomerate.

The Blaubok Conglomerate, which has no volcanic clasts, is widespread in the Sperrgebiet and includes important outcrops close to the Klinghardt Volcanic Mountains (at Graben and Reuning's Pipe for example, Fig. 1) which reveal that this unit was deposited prior to the onset of phonolite volcanism in the region (Fig. 3, 7). Unconformably overlying the Blaubok Conglomerate is another suite of conglomerates called the Gemsboktal Conglomerates, distinguishable
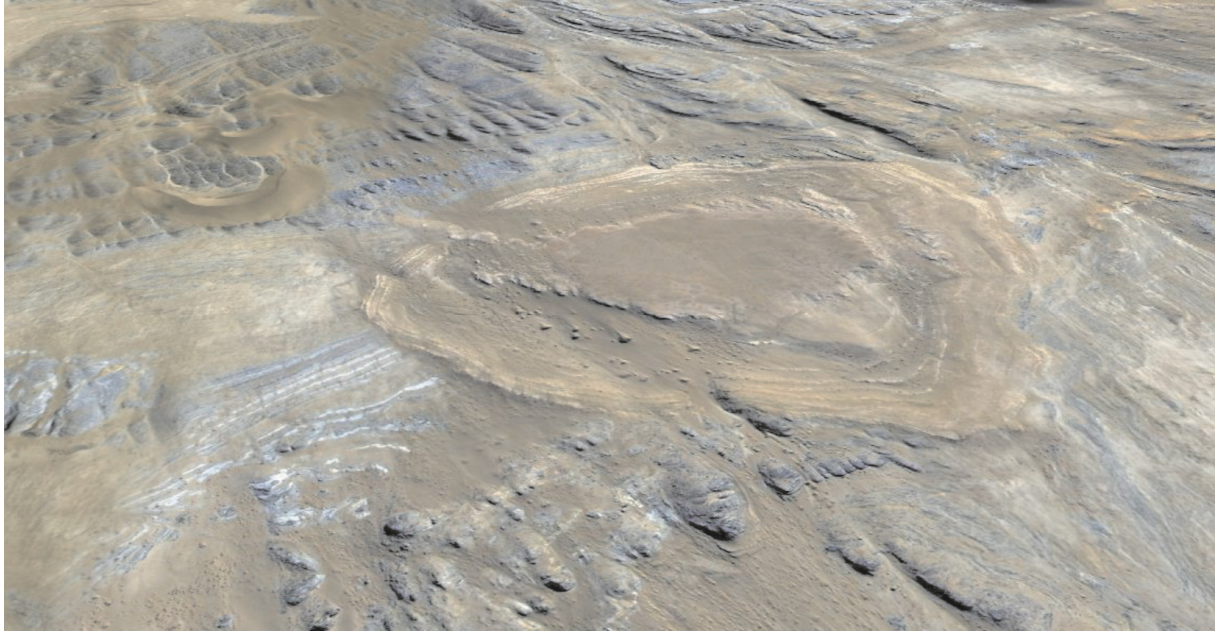
Figure 2: Well-bedded freshwater limestones at Silica South infilling a palaeokamenitza or palaeodoline eroded into Proterozoic Gariep Group Dolomites (grey tones). The well-bedded limestones are unconformably overlain by a cap of cliff forming Blaubok Conglomerate which has been cemented by the cupriferous Older Calc-crust. Note also the extant barchans dunes. The greatest diameter of the oval outcrop of limestone is ca 400 metres. Oblique view towards the north.

from the Blaubok unit by the abundance of phonolite clasts that it contains (Fig. 4, 7). The Gemsboktal Conglomerates must there-fore be younger than the onset of Klinghardt volcanism.

Figure 3: Outcrop of Blaubok Conglomerate cemented by the older cupriferous calc-crust. This widespread sedimentary unit contains abundant honey-coloured silicified limestone pebbles, quartz, quartzite and other basement rock types but no phonolite.

At Black Crow, phonolite clasts are confined to the floors of shallow valleys that incised the countryside after the deposition of the Blaubok Conglomerate. Elsewhere, the Gemsboktal Conglomerates are mapped in superposition above the Blaubok Con-glomerate, as for example at Granit-bergfelder a few km north of Black Crow (Fig. 10). Radio-isotopic age determinations were carried out on phonolite clasts collected from the Gemsboktal Conglomerate at Black Crow and Granitbergfelder (Table 1).

Figure 4: Hamada capped by Gemsboktal Conglomerate rich in phonolite clasts (black pebbles). Note also the purple-brown cement which is the younger calc-crust.

The importance of determining the ages of clasts in conglomerates

It is sometimes considered meaningless (and a waste of funds) to determine the radio-isotopic ages of volcanic rocks in conglomerates. However, in certain geological and stratigraphic situations, the ages of volcanic clasts in conglomerates can provide precious information concerning the timing of geological events in a region. In situations like the one in the Sperrgebiet, where there is a clear differentiation between pre-volcanic and post-volcanic conglomerates, such ages can provide constraints on the ages of deposits older than the conglomerates in which they occur, even though they provide little information about the age of the conglomerate from which they were sampled, save to reveal that said conglomerate must be younger than the age of the clast.

A second excellent reason for determining the ages of volcanic clasts in conglomerates is that reliance exclusively on samples obtained from *in situ* occurrences such as lava flows and intrusions may bias understanding of the development of the volcanic province for two reasons. Firstly, early manifestations of volcanic activity may be subjected to rapid erosion, thereby leaving little or no material remaining *in situ* for researchers to collect, and secondly, as volcanic activity proceeds, earlier lava flows may be completely buried under later volcanic deposits, while intrusive masses of lava may be removed by later eruptions or become buried by later activity and thus be rendered inaccessible.

In the case of the Klinghardt Volcanic Province, previously published age determinations carried out on lava flows and intrusives were not from the main volcanic field but from occurrences some distance away from the Klinghardt Dome (Fig. 7, 8). The range of ages obtained spanned the period 29-37 Ma (Reid *et al.*, 1990) and there is an unconfirmed age of 46 +/- 0.7 Ma (Marsh, 2010). The two phonolite clasts that we analysed yielded ages of 42.2 and 41.4 Ma confirming a Late Middle Eocene age of the on-

set of volcanism in the region.

It would therefore appear that the epikarstic carbonate deposits at Silica North, Silica Southand Black Crow which unconformably underlie the Gemsboktal and Blaubok Conglomerate formations are older than 42 Ma and possibly older than 45 Ma.

Silicification of superficial rocks in the Northern Sperrgebiet

Many of the superficial rocks in the northern Sperrgebiet have been silicified, and these include sediments as well as near-surface exposures of Gariep dolomites and quartzites of Proterozoic age.

Historically there has been much confusion about these silicified rocks, often pooled together under the name Pomona Quartzite. It was only recently that it became clear that the Pomona Quartzite is a composite unit comprising a wide variety of deposits of diverse age (Corbett, 1989). In its type area it is comprised of a series of conglomerates infilling shallow valleys that were silicified, producing valley silcretes, which, because they are extremely resistant to erosion, now stand proud of the surrounding countryside following the more rapid erosion of the Basement complex through which the valleys formerly coursed. Elsewhere, as for example at Black Crow and Swartkop, there

are thin outcrops of well-bedded silicified sandstones, seldom more than a metre or two thick. Close to the margin of the Klinghardt Dome there is a series of well-bedded silicified limestones which have been folded into a series of basinal and domal structures. In many places throughout the Northern Sperrgebiet, outcrops of Gariep rocks show silicified surfaces, as for example at Black Crow, Silica North Silica South, Steffenkop and Eisenkieselklippenbacke. Most of these deposits comprise dark honey-coloured or olive-grey, very fine-grained siliceous rocks, probably formed by the silicification of ancient soil profiles, especially those parts which were close to the soilbedrock interface.

Eocene freshwater limestones at Silica North, Silica South, Chalcedon Tafelberg, Black Crow and Steffenkop, among others (Gamachab, Eisenkieselkippenbacke) have also been subjected to silicification (Fig. 5), but unlike the silicified limestones close to the Klinghardt Dome, they are generally incompletely silicified. The result has been the production of flaggy silicified limestone beds interlarded with pure limestone beds, irregular nodules of silicified limestone, vertical masses of silcified limestone crosscutting bedded limestone and other irregular forms.

Figure 5. Silicified freshwater limestone containing shells of *Hydrobia*, a small freshwater gastropod, from Chalcedon Tafelberg, Northern Sperrgebiet, Namibia.

Although silicification of superficial deposits can result from a variety of processes and at different times, it is not impossible that most of the silicification observed in the Northern Sperrgebiet was due to the same relatively short-lived (ca. 1 Ma) process. The intensity of silicification decreases away from the Klinghardt Dome, which suggests that the silica was mainly of hydrothermal origin related to initial stages of activity in the Klinghardt Volcanic province. It is interesting to note that, if this is the case, then the silicification preceded the commencement of volcanic eruptions by several million years (perhaps 2-3 million years). This in turn suggests the emplacement of a magma chamber deep in the Earth's crust below what eventually became the Klinghardt Dome, and then the Klinghardt Volcanic Field, well before the commencement of surface volcanic activity. The silicification occurred after the deposition of the Black Crow and related feshwater limestones.

Cuprification of the Blaubok Conglomerate

The pre-volcanic Blaubok Conglomerate, which crops out widely to the west of the Klinghardt Dome, was calcified to a depth of a metre or so to produce the so-called "Older Calc-crust" which overlies unconsolidated to indurated conglomerate. In many outcrops, this "Older Calc-crust" shows a pale greenish tinge and sometimes stones caught up in the calc crust (notably quartz pebbles) show a similar colouration (Fig. 6). This is the only unit observed in the region which shows such colouring, and it is possible that the copper, which is responsible for the colour, was ultimately derived by hydrothermal processes related to theKlinghardt magma chamber. It is clear though, that this "copper" event preceded the beginning of volcanic eruptions, because its only manifestation is in rocks laid down prior to the onset of superficial volcanic activity.

Figure 6: Copper staining in the Blaubok Conglomerate at Silica North, Sperrgebiet, Namibia. Note the greenish tinge in the pale calc-crust cementing the conglomerate which contains pebbles of silicified limestone derived from the Silica North freshwater limestones, along with pebbles of quartz, dolomite and quartzite, but no phonolite.

Geomorphology of the Klinghardt Volcanic Field

The Klinghardt Mountains consist of dozens of phonolite flows and intrusives (Fig. 7, 8). The flows are often steep sided and repose on Basement rocks of the Proterozoic Gariep Fold Belt. It is clear that the Basement in the region of the phonolites has been updomed On its western edge the dome is bordered by a series of well-bedded silicified limestones of unknown age containing

traces of fossilised algae (Fig. 8). These deposits have been tectonised into a series of saucer-shaped bodies (Lock & Marsh, 1981) disposed around the western edge of the Klinghardt Dome from the southwest at Graben to the northwest at the so-called Klinghardt Breccia Pipe (which is in fact not a breccia pipe). The diameter of the Klinghardt Dome is approximately 24 km east-west by 23 km north-south, and the Basement rocks near the centre of the dome are ca 300 metres higher than its margins. It should be noted however, that the centre of the dome appears to have collapsed, thereby forming a large circular to slightly ovoid depression about 4 km in diameter in what formerly would have been the tallest part of the dome (Fig. 7). The main lava flows thereby form an irregular, discontinuous ring-shaped outcrop around the central depression.
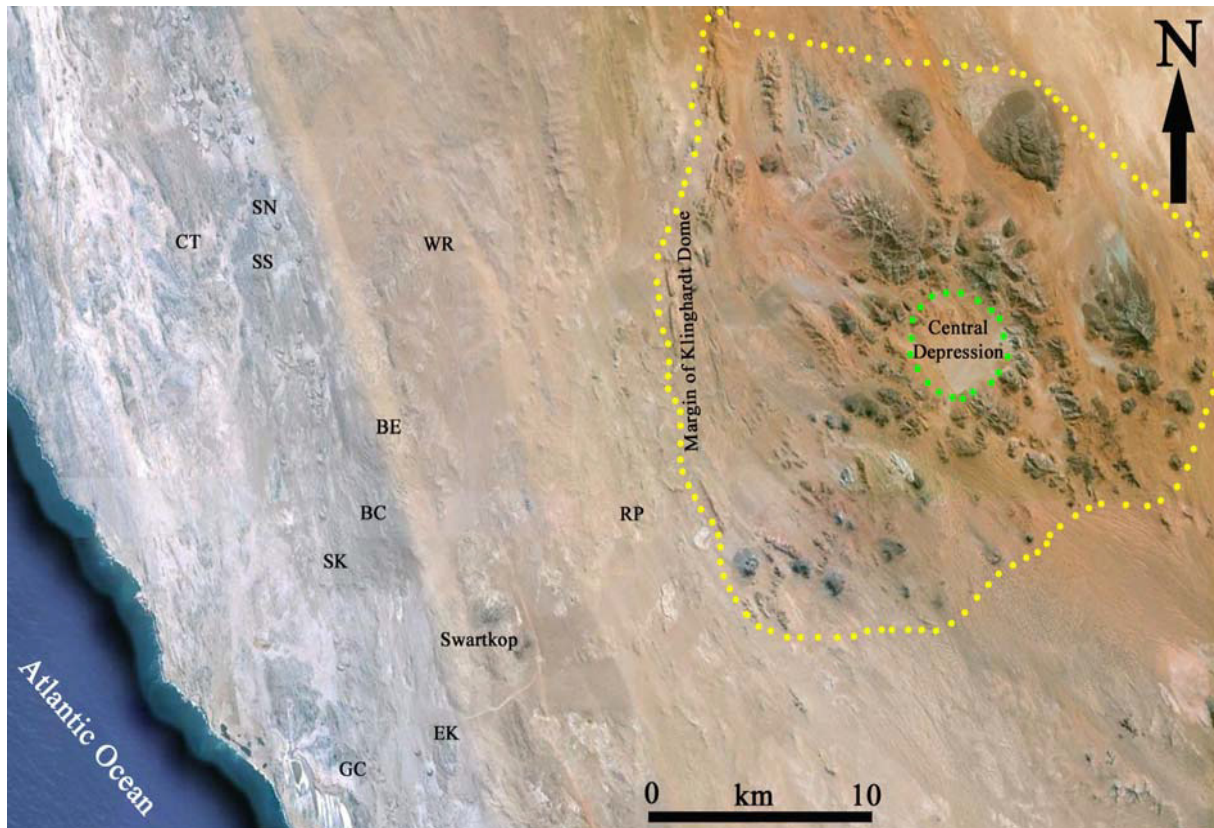
Figure 7: Geomorphology of the Northern Sperrgebiet, Namibia. Note the extent of the Klinghardt Dome (phonolite units are black) and the central depression. Middle Eocene freshwater limestone accumulated in depressions in Gariep Dolomites at BC – Black Crow; BE – Bull's Eye; CT – Chalcedon Tafelberg; EK – Eisenkieselklippenbacke; GC – Gamachab; RP – Reuning's Pipe; SK – Steffenkop; SN – Silica North; SS – Silica South; WR – White Ring.

Uplift of the Klinghardt dome appears to have started prior to the commencement of volcanic eruptions, because the Blaubok Conglomerate, which is widespread in the region west of the Klinghardts, extends right up to the edge of the dome, but nowhere does it contain volcaniclastic debris. The few places where flow direction can be observed, such as Reuning's Pipe (which is not a volcanic pipe), show that it was directed away from the dome.

The dome thus underwent erosion prior to the first eruptions, with the result that most of the phonolite flows in the main volcanic field directly overlie Basement rocks, in contrast to lavas that flowed into the hinterland which may overlie conglomerate and sandstone, as for instance at Swartkop, 24 km south-west of the centre of the dome. Because volcanic activity added to the topographic relief of the Klinghardt Dome, it continued to erode, but now shed huge quantities of volcanic debris into the fluvial systems flowing away from it. These younger

conglomerates, called the Gemsboktal Con-glomerate, are widespread to the west of the Klinghardt Dome (Fig. 8), extending as far as Grillental, 60 km to the northwest and Buntfeldschuh 40 km to the southwest, and probably much further.
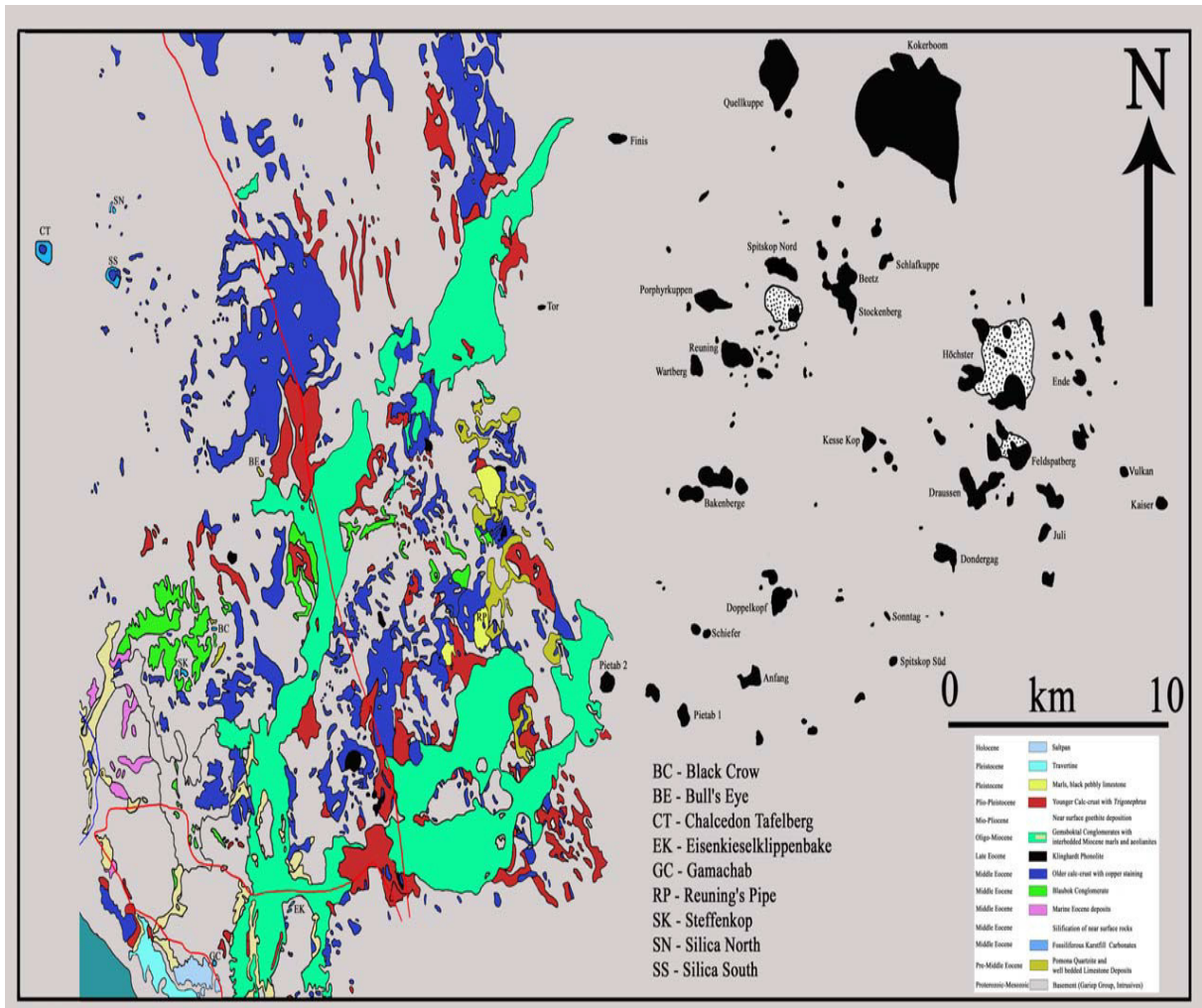
Figure 8. Geological map of Cainozoic deposits in the Northern Sperrgebiet, Namibia (Klinghardt geology based on Lock & Marsh, 1981; the remainder of the map based on Van Greunen's undated map and our own observations).

The Gemsboktal Conglomerates span a considerable period of time, some of the deposits dating from soon after the commencement of volcanic eruptions in the Eocene, and others forming during the Early Miocene (Elisabethfeld, 65 km northwest of the dome) the Pliocene and the Pleistocene. The Mio-Pliocene deposits comprise characteristic hamada topography of vast stone scattered plateaux bordered by scarp-like edges (Fig. 4), whereas the Eocene ones appear to have been confined to river valleys, such as one that cut through the Black Crow depression.

Radio-isotopic ages of Klinghardt Phonolites

1.   Sample description and preparation

Two rock samples were analysed for K-Ar and 40Ar/39Ar age determinations (Tables 1, 2). (1) NB10-1: phonolite cobble from Black Crow. (2) NB10-2: phonolite cobble from Granitberg. Both specimens were collected from the Gemsboktal Conglomerate (Fig. 10). NB10-1 is fresh and highly porphyritic, and consists of phenocrysts of nepheline (Ne87.9 – 83.8 Ks16.2 – 12.1), sanidine (Or70.3 – 60.4 Ab39.3 – 29.4 An0.6 – 0.0) (up to 30 mm in
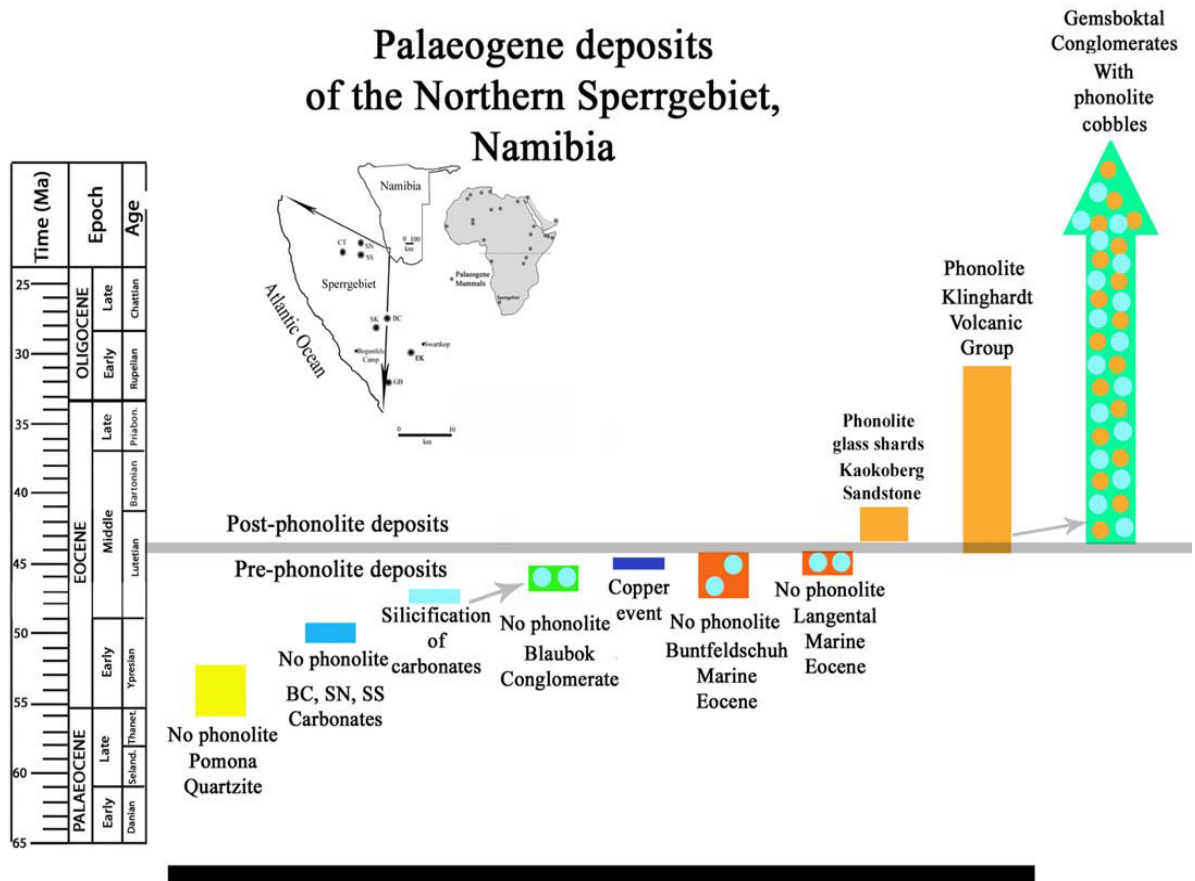
Figure 9: Succession of Cainozoic rocks in the Northern Sperrgebiet, Namibia. The historic basis is the work of Kaiser (1926) which we have modified or checked in the field on the basis of our own observations.
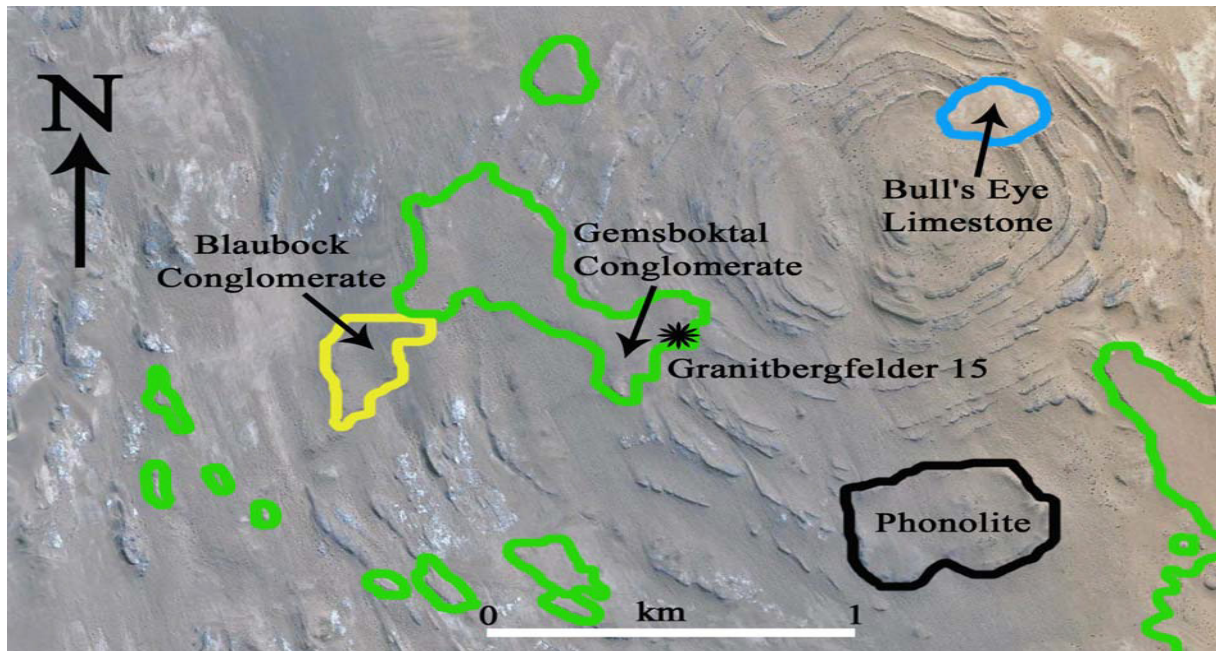
Figure 10: Satellite image of the Bull's Eye area, Northern Sperrgebiet showing the location where the Granitbergfelder 15 phonolite cobble (NB 10-2) was collected (star). The folded strata are dolomites of the Gariep Group, the blue outline is freshwater limestone that accumulated in a kamenitza or doline, the yellow outline is an outcrop of Blaubok Conglomerate unconformably underlying Gemsboktal Conglomerate (green outlines) which forms regionally extensive hamadas.

length), aegirine augite (up to 10 mm in length) and sphene with a groundmass of sanidine (Or65.0 – 62.4Ab37.4 – 34.8 An0.5 – 0.2), albite, aegirine augite, apatite, microlite and mesostasis. NB10-2 is aphyric and consists of a small amount of microphenocrysts of nepheline (Ne86.8 – 84.6 Ks15.4 – 13.2), sanidine (Or75.8 – 68.1 Ab31.8 – 24.2An0.1 – 0.0) (up to 6 mm in length) with a groundmass of sanidine, nepheline, albite, aegirine augite, apatite, zircon, microlite and mesostasis. Abundances of major elements and trace elements of NB10-1 and NB10-2 by X-ray fluorescence spectrometer analysis are shown in Table 1, 2. Both NB10-1 and NB10-2 are peralkaline phonolite. SiO_2, Na_2O and K_2O contents of NB10-1 are 53.72 wt%, 10.63 wt% and 7.24 wt%, respectively. SiO_2, Na_2O and K_2O contents of NB10-2 are 55.21-55.25 wt%, 8.93-8.96 wt% and 7.33-7.35 wt%, respectively.

Sanidine and nepheline phenocrysts and whole rock from NB10-1 and groundmass from NB10-2 were prepared by crushing and sieving for K-Ar age determination. The sieved fraction of 423-254 μm was cleaned in distilled and ion exchanged water then dried in an oven at 110ºC. The magnetic minerals were removed manually by magnet. The sanidine and nepheline grains were removed from the sieved samples by a Frantz isodynamic separator, heavy liquid (bromoform) and additional hand picking. The separated minerals were ultrasonically washed several times in ethanol and ion exchanged water for 10 minutes. The separated sanidine and nepheline (NB10-1Fd-M and NB 10-1L) and whole rock (NB10-1WR) samples were leached two or three times in HCl solutions (HCl : H_2O = 1 : 4) for 15 minutes in order to remove any argillaceous alteration products. The leached samples were cleaned by distilled and ion exchanged water about 20 imes to remove HCl then dried in an oven at 110ºC. A portion of the fraction was ground by hand in an agate mortar, and used for potassium analysis. Fresh coarse-grained sanidine and nepheline

samples (0.5 - 1 mm in size) for 40Ar/39Ar age determination were separated by hand picking under a microscope.

2. Analytical procedure and results of K-Ar and 40Ar/39Ar age determinations

Analytical procedures for potassium and argon and calculations of ages and errors were based on the method described by Nagao *et al.* (1984) and Itaya *et al.* (1991). Potassium was analyzed by flame photometry using a 2000 ppm Cs buffer and has an analytical error of under 2% at 2σ confidence level. Argon was analyzed on a 15 cm radius sector type mass spectrometer with a single collector system using an isotopic dilution method and 38Ar spike.

Calibration of the 38Ar spike is accurate to within 1%. Multiple runs of a standard (JG-1 biotite, 91 Ma) indicate that the error of argon analysis is about 1% at 2σ confidence level. The sample was wrapped in aluminium foil, then preheated for a day or more at about 200 ºC in a vacuum to eliminate any absorbed atmospheric argon. Argon was extracted at 1600ºC on ultrahigh vacuum lines with an atmospheric 40Ar blank of less than 2.5x10-9 ccSTP. The clean up of reactive gas was done by two Ti-Zr getters, and the 38Ar spike added. The decay constants for 40Ar and 40Ca, and 40K content in potassium used in the age calculations are from Steiger & Jäger (1977) and are 0.581x10-10/y, 4.962 x 10-10/y and 1.167 x 10-4 (ratio of atomic abundance), respectively. The results of K-Ar age determinations are shown in Table 1. K-Ar ages of sanidine and nepheline from Black Crow (NB10-1) are 42.2 Ma and 40.1 Ma. The whole rock age is 45.4 Ma. Groundmass K-Ar age of the Granitberg sample (NB10-2) shows 41.4 Ma, and is close to the sanidine and nepheline ages of the phonolite cobble collected at Black Crow (42.2 – 40.1Ma).

Constituent	NB10-1	NB10-2A	NB10-2B
Major elements	Black Crow Namibia	Granitberg Namibia	Granitberg Namibia
SiO_2	53,72	55,25	55,21
TiO_2	0,33	0,40	0,40
Al_2O_3	21,67	20,14	20,13
Fe_2O_3	4,09	5,16	5,22
Total	**100,03**	**99,93**	**99,91**
Loss Ignition	2,21	4,06	4,06
Trace elements ppm			
Ba	114	346	347
Ce	357	344	342
Cr	<10	<10	<10
Ga	25	27	20
Nb	343	865	864
Ni	3	3	n.d.
Pb	39	23	23
Rb	207	183	182
Sr	849	492	493
Th	62	60	68
V	16	13	20
Y	31	15	16
Zr	1183	3060	3057

Table 1: Chemical analyses of two phonolite cobbles from the Gemsboktal Conglomerate, Namibia.

Speci-ment num-ber	Formation	Rock type & occurrence	Local-ity	Material	Grain - size (um)	K content (wt.%)	Rad. 40Ar (10-8 ccSTP/g)	K-Ar age (Ma)	Non Rad. 0Ar (%)
NB10-1Fd-M	Gemsboktal Conglomerate	Phonolite, cobble	Black Crow	Sanidine + nepheline	423-256	5,860±0,117	971,±9,3	42,22 ±0,93	1,2
NB10-1Fd-M	Gemsboktal Conglomerate	Phonolite, cobble	Black Crow	Sanidine+ nepheline	423-257	9,231±0,185	1450,6±14,1	40,05±0,88	1,3
NB10-1Fd-M	Gemsboktal Conglomerate	Phonolite, cobble	Black Crow	Whole rock	423-258	8,374±0,167	1492,6±14,5	45,40±1,00	1,7
NB10-1Fd-M	Gemsboktal Conglomerate	Phonolite, cobble	Granit-berg	groundmass	423-259	5,240±0,105	851,3±9,4	41,39±0,94	13,2

Table 2: Age determinations on phonolite cobbles from the Gemsboktal Conglomerate, Namibia

Discussion and conclusions

Previous geochronological research on the phonolites of the Klinghardt Mountains indicated a late Eocene to Early Oligocene time range for the samples analysed (Lock & Marsh, 1981; Marsh, 1987, 2010; Ried *et al.*, 1990). However, the age determinations published by Kröner (1973) on which this age range was based were obtained not from the Klinghardt Mountains themselves but from isolated bodies of lava some distance away. Kröner (1973) published an age of 37 Ma for the Swartkop Phonolite (conventional K-Ar) (27°25'45.6"S : 15° 32'12.6"E), a flow that overlies silicified sand and conglomerate some 24 km west of the Klinghardt Dome (centre of dome is at 27°18'13"S : 15° 44'33"E) and an age of 35.7 Ma for the Schwarzerberg Nephelinite (whole rock) an intrusive body 33 km northwest (27° 08'47.9"S : 15°25'12.5"E) of the Klinghardts.

Marsh (2010) reported an unpublished age of 46.0 +/- 0.7 Ma (40Ar/39Ar plateau age on sanidine) from an unspecified phonolite in the Klinghardt Mountains (pers. comm. to Marsh by D. Phillips). As it stands, there seems to be no secure age determination from the Klinghardt Mountains themselves, unless the lava analysed by Phillips came from there. We here report additional radio-isotopic age determinations from two cobbles of phonolite collected from different localities in the Gemsboktal Conglomerate, a widespread sedimentary unit west of the Klinghardt Dome and the earliest such deposit to contain lava cobbles (the underlying Blaubok Conglomerate is devoid of lava clasts, even where it crops out close to the Klinghardt Mountains, and it evidently pre-dates the earliest of the eruptions). Both samples yield ages in excess of 40 Ma, the Granitbergfelder 15 specimen an age of 41.39 +/-0.94 Ma (groundmass) and the Black Crow specimen ages of 42.22 +/- 0.93 (sanidine + nepheline), 40.05 +/- 0.88 (sanidine + nepheline) and 45.40 +/- 1.00 (whole rock).

We conclude that Klinghardt eruptive phonolite volcanic activity started somewhat earlier than previously estimated by Lock & Marsh (1981). Our results indicate an onset of volcanism during the Middle Eocene about 40 - 45 million years ago or even earlier, which may have continued until the Early Oligocene about 37 Ma. The age of 29 Ma for the young end of the range published by Ried *et al.*, (1990) needs to be re-examined. The stratigraphic succession in the Sperrgebiet indicates that the prevolcanic strata in the region are older than 40 Ma. The Blaubok Conglomerate and the underlying freshwater carbonates at Black Crow, Silica North and Silica South (and elsewhere) are probably middle Lutetian in age (Fig. 9). A Middle Lutetian age was already estimated for these carbonates on the basis of the fossil mammals collected from them (Pickford *et al.*, 2008a, 2008b).

References

Corbett, I.B., 1989 - *The Sedimentology of Diamondiferous Deflation Deposits within the* Itaya, T., Nagao, K., Inoue, K., Honjou, Y., Okada, T., & Ogata, A., 1991 - Argon isotope analysis by a

newly developed mass spectrometric s ystem for K-Ar dating. *Mineralogical Journal*, **15**: 203-221.

Kaiser, E., 1926 – *Die Diamantenwüste Süd west Afrikas*, Reimer, Berlin, 2 vols.

Kröner, A., 1973 – Comments on "Is the Af rican plate stationary?" *Nature*, **243**: 29-30.

Lock, B.E., & Marsh, J., 1981 – Tertiary pho nolite volcanism in the Klinghardt Mountains of South-West Africa/Na-mibia. *Transactions of the Geological Society of South Africa*, **84**: 1-6.

Marsh, J., 1987 – Evolution of a strongly dif ferentiated suite of phonolites from the Klinghardt Mountains, Namibia. *Lithos*, **20**: 41-58.

Marsh, J., 2010 – The geochemistry and evo lution of Palaeogene phonolites, central Namibia. *Lithos*, doi:10.1016/ j.lithos.2010.02.012.

Nagao, K., Nishido, H., Itaya, T. & Ogata, K., 1984 - K-Ar age determination method. *Bulletin of the Hiruzen Re search Institute*, **9**: 19-38. (in Japanese)

Pickford, M., Senut, B., Morales, J., & San chez, I., 2008a - Fossiliferous Caino zoic Carbonates of the Northern Sperrgebiet. *Memoir of the Geological Survey of Namibia*, **20** : 25-42.

Pickford, M., Senut, B., Morales, J., Mein, P., & Sanchez, I.M., 2008b - Mammalia from the Lutetian of Namibia. *Memoir of the Geological Survey of Namibia*, **20** : 465-514.

Reid, D., Cooper, A., Rex, D., & Harmer, R., 1990 – Timing of post-Karoo alkaline volcanism in southern Namibia. *Geo-logical Magazine*, **127**: 427-433.

Seiffert, E., 2010 – Chronology of Paleogene Mammal Localities. *In*: Werdelin, L., & Sanders W., (Eds) *Cenozoic Mammals of Africa*, Berkeley, Los Angeles, Lon don, University of California Press, pp. 19-26.

Steiger, R., & Jäger, E., 1977 - Subcommis sion on geochronology: convention on the use of decay constants in geo- and cosmochronology. *Earth and Planetary Science Letters*, **36**: 359-362.

Ward, J.D., 1987 – The Cenozoic succession in the Kuiseb Valley, Central Namib Desert. *Memoir of the Geological Sur vey of South-West Africa/Namibia*, **9**: 1-45.

Ward, J.D. 1988 – Eolian, fluvial and pan (playa) facies of the Tertiary Tsondab Sandstone Formation in the Central Na mib Desert, Namibia. *Sedimentary Ge ology*, **55**: 143-162.

Van Greunen, E. (undated) – *Intrusive Rocks and Post-Cretaceous Sediments of the Northwest Sperrgebiet – scale 1:100,000*. Unpublished map, Geologi cal Survey of Namibia, ref 2715 A, C, Map N° 793, CDM.

Mio-Plio-Pleistocene geology and palaeobiology of the Etosha Pan, Namibia

Martin Pickford[1], Brigitte Senut[2], Martin Hipondoka[3], Alain Person[4], Loïc Segalen[4], Chloé Plet[4], Hélène Jousse[5], Pierre Mein[6], Claude Guerin[6], Jorge Morales[7] and Cécile Mourer-Chauvire[8]

[1]*Collège de France, and UMR 7207, CR2P du CNRS, Département Histoire de la Terre, 8, rue Buffon, 75005, Paris, France. <pickford@mnhn.fr>*
[2]*UMR 7207, CR2P du CNRS, Département Histoire de la Terre, 8, rue Buffon, 75005, Paris, France. <bsenut@mnhn.fr>*
[3]*University of Namibia, Private Bag 13301, Windhoek, Namibia. <mhipondoka@unam.na>*
[4]*UPMC Univ Paris6, UMR 7193 ISTEP. Biominéralisations et Environnements Sédimentaires, F75005 Paris, France. <alperson@ccr.jussieu.fr>, <loic.segalen@upmc.fr>, <chloe.plet@etu.upmc.fr>*
[5]*UMR 7209 - Archéozoologie, Archéobotanique: Sociétés, Pratiques et Environnements, CNRS - Muséum national d'Histoire naturelle, USM 303 Département Ecologie et gestion de la biodiversité, Case Postale N° 55, 55 rue Buffon, F-75231, Paris cedex 05, France. <jousse.helene@gmail.com>*
[6]*UMR 5125 "Paléoenvironnements et Paléobiosphère", Université Claude Bernard - Lyon 1, 27 - 43 boulevard du 11 novembre 1918, 69622 Villeurbanne cédex, France. <Pierre.Mein@univ-lyon1.fr>, <Claude.Guerin@univ-lyon1.fr>*
[7]*Paleobiologia, Museo Nacional de Ciencias Naturales, José Guttierez Abascal 2, 28006, Madrid, Spain. <mcnm166@mncn.csic.es>*
[8]*UMR 5125 "Paléoenvironnements et Paléobiosphère", Université Claude Bernard - Lyon 1, 27 - 43 boulevard du 11 novembre 1918, 69622 Villeurbanne cédex, France. <Cecile.Mourer@univ-lyon1.fr>*

The Etosha Pan, northern Namibia, at nearly 5,000 km², is one of the largest in the world. A major hurdle to understanding the geological history of Etosha Pan has been the lack of dated horizons in the local stratigraphic record. We here report the discovery of fossil plants, invertebrates and vertebrates at several distinct horizons within the pan and its immediate vicinity, which reveal the presence of deposits ranging in age from Late Miocene to Late Pleistocene. Most of the floor of the pan consists of Late Miocene deposits whereas in islands and ridges within the pan and along its margins there occurs a discontinuous deposit of Pliocene, Pleistocene sediments up to 20 metres thick. Finally, there are discontinuous patches of green silts on Pelican Island at an altitude of ca 1093 metres, some 8-10 metres above the floor of the pan, which attest to a Late Pleistocene lacustrine episode. Similar aged deposits at the western end of Oshigambo Peninsula have yielded a rich and diverse mammalian fauna containing remains of the aquaphile bovid *Tragelaphus spekei* (the sitatunga).

The discovery of Mio-Pliocene fossils in Etosha is important as it helps to fill what used to be a large geographic gap in the African palaeontological map of this epoch. Late Miocene sites in particular, are poorly represented over much of the continent, being concentratedin the rift valleys of East Africa, the Chad basin, the Maghreb and north African littoral zone.

Introduction

The processes which led to the formation of Etosha Pan, northern Namibia, (Fig. 1, 2) are still a matter of debate, mainly due to a lack of dated stratigraphic horizons within the Tertiary and Quaternary sediments that blanket the Greater Etosha Basin (also known as the Owambo Basin) in which the pan occurs. At almost 5,000 km², Etosha Pan is one of the largest in the world, and it is accompanied by many smaller pans, especially on its western and northern sides. The immense dimensions of the pan have stimu-

lated discussions about its origins, because it has been argued that the usual processes which form small pans may not apply to such a huge one (Hutter, 1910 ; Jaeger, 1926 ; Jaeger & Waibel, 1921 ; Wellington, 1938, 1939).

Hipondoka (2005) wrote that « Etosha Pan is presently an aggradational landform, contrary to conclusions reached by recent studies. Aggradational phases alternated with erosive phases and phases of relative stability and soil formation ». In contrast, for Beugler-Bell & Buch, (1997) the pan's present day form was interpreted as being due to de-

flation.

In 2006 and 2007, Miocene and Pliocene fossils were found in the Etosha Basin, a discovery that provides constraints on the timing of geological activity within the depression. These age determinations will impact on the debate about the origins of Etosha Pan and its substrate. This paper is organised into several parts dealing first with the geological context of the Etosha Basin and its fossil record, followed by the palaeontology of the basin, examining the fauna and flora in stratigraphic order, by a discussion of the biochronological and palaeoenvironmental implications of the fossils, and completed by the conclusions.

Fossiliferous localities of Africa ranging in age from 8 to 4 Ma

Figure 1: Late Miocene and Early Pliocene fossiliferous localities of Africa. The Etosha occurrences help to fill out a huge gap that existed in the palaeontological map of the continent for this epoch. The Berg Aukas karst deposit near Etosha contains microfauna only, whereas the Etosha sites yield a rich and varied macrofauna.

Prior geological, geomorphological and palaeontological studies

The presence of Mio-Pliocene deposits (Andoni Formation) in the Etosha Basin (Hutter, 1910 ; Jaeger, 1926 ; Jaeger & Waibel, 1921 ; Wellington, 1938, 1939) has been reported on several occasions (Buch, 1996 ; Haddon, 2000 ; Hipondoka, 2005 ; Smith & Mason, 1991) but until recently there has been no direct evidence as to the age of the strata. In several papers the Andoni Formation has been broadly referred to the Oligo-Miocene (Buch, 1993 ; Smith & Mason, 1991).

The first fossils reported from the Etosha region were eggshell fragments of « *Struthio* » *oshanai* (now *Namornis oshanai*) (Sauer, 1966) from a borehole at Beisebvlakte (at a depth of 34 m) a few km northeast of the Etosha Pan (18°31'S : 17°04'E) . Similar struthious eggshells were subsequently found in the Namib Desert (Dauphin *et al.*, 1996 ; Mourer-Chauviré *et al.*, 1996 ; Pickford *et al.*, 1993 ; Senut & Pickford, 1995, Senut *et al.*, 1994, 1998) where they are restricted to basal Middle Miocene levels, and this is the likely age of the Beisebvlakte occurrence.

Subsequently stromatolites (oncolites) of unknown age were described (Martin & Wilczewski, 1972 ; Smith, 1980 ; Smith & Mason, 1991 ; Talma & Rust, 1997). Hipondoka (2005 ; Hipondoka *et al.*, 2006) reported the presence of Latest Pleistocene fossil vertebrates at Oshigambo Peninsula and of unknown age at the Ekuma River Delta area. Because the assemblages included remains of sitatunga and *Kobus* sp. the authors concluded that there must have existed perennial lacustrine conditions at the time of deposition. The latter interpretation obtains support from two additional lines of evidence ; a) the occurrence of raised beaches at Poacher's Point and in the Ekuma River valley, about 1.5 to 2 metres above the present day floor of the pan, and b) the presence of green silts on Pelican Island, 8-10 metres above the floor of the pan, where they unconformably overlie Plio-Pleistocene cal-careous deposits (Poacher's Point Carbonate Member), and a widespread rubble horizon containing black sediment nodules (Miller, 2007) (Fig. 3).

The recent discovery of several fossiliferous levels spanning the Late Miocene, Middle Pliocene, Plio-Pleistocene and Holocene (Hipondoka, 2005 ; Hipondoka *et al.*, 2006) provides important constraints on interpretations of the stratigraphy, and therefore of the history, of the Greater Owambo Basin, and the Etosha Pan that occurs in it.

Geological context of the Etosha Basin

The regional geological context of the Etosha Depression (Fig. 2) has been extensively discussed on account of its petroleum potential (Haddon, 2000 ; Hedberg, 1979 ; Hipondoka, 2005 ; Miller, 1997) but most of the information about the subsurface deposits in the basin comes from seismic surveys and shallow boreholes (Miller, 1997).

Infilling a vast depression floored by Proterozoic rocks (the Great Etosha Basin or the Greater Owambo Basin as it is also known) extending from the Otavi Mountains, Namibia, in the south (Fig. 2), to Southern Angola in the north, is a thick sequence of Mesozoic deposits, in turn overlain by Tertiary and Quaternary sediments (Table 1). The Tertiary deposits are generally attributed to the Andoni Formation, an unknown thickness of greenish silts and clays with subordinate quartzite lenses. Miller (2007) formalised several names for subdivisions of the Andoni Formation, and in this contribution, we follow and extend his nomenclature.

Stratigraphy and age of sedimentary deposits exposed in Etosha Pan

The stratigraphy of sediments exposed in the Etosha Pan and around its margins has been summarised by Miller (2007) who subdivided the Andoni Formation of previous authors (Buch, 1996 ; Haddon, 2000 ; Hipondoka, 2005 ; Smith & Mason, 1991) into three members. The Etosha Pan Clay Mem-
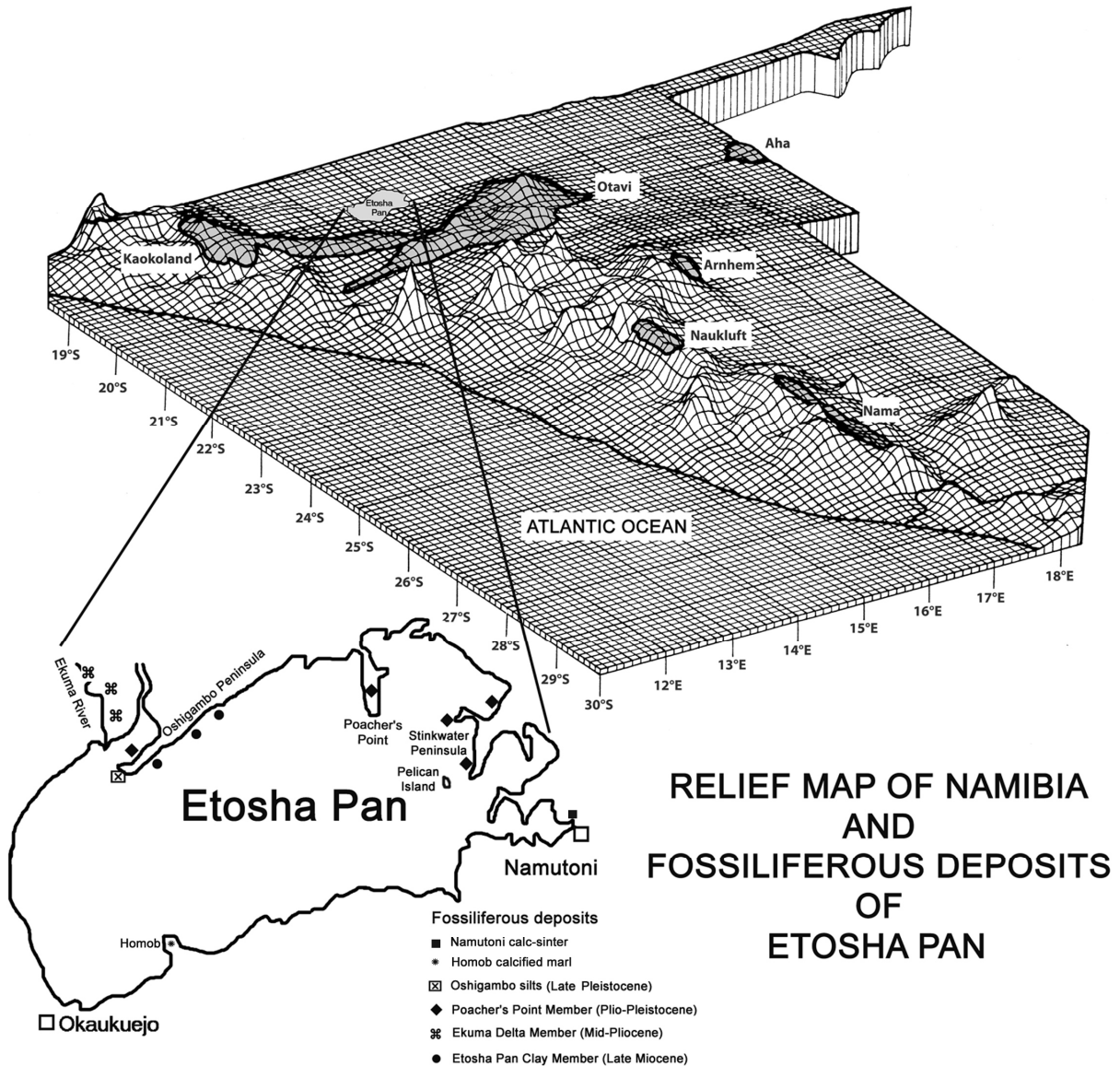
Figure 2: Location of the Etosha Pan, northern Namibia, and fossiliferous deposits discussed in the text. Dolomites of the Otavi Mountains and other parts of Namibia are highlighted by the thick line.

ber (EPCM) is exposed extensively in the floor of the pan, the Ekuma Delta Member (EDM) crops out widely in the Ekuma and Oshigambo drainages close to the pan, and the Poacher's Point Carbonate Member (PPCM) is exposed widely on steep ground along the northern flank of Oshigambo Peninsula, around the flanks of Poacher's Point, the Stinkwater Peninsula and Pelican Island. The PPCM is overlain by the Etosha Limestone, a calcrete of diverse origin, being a groundwater calcrete in the south, and a pedogenic calcrete in the north. Unconformably overlying the Etosha Limestone, is a

variety of poorly indurated to unindurated sediments comprising widespread but thin Oshigambo Pan-loess deposits, Okondeka lunette dunes, Pelican Island green silts, unnamed beach deposits about 1.5 – 2 metres above the present day pan floor (eg at Poacher's Point and in the Ekuma River Valley), calc-tufa deposits, calcified marls in water holes, and salt crusts. The geological sequence is summarised in Table 1.

The Poacher's Point Carbonate Member is overlain by the Etosha Limestone, a widespread calcrete up to 3 metres thick in the vicinity of the pan (Fig. 3), but consid-

Sediment unit	Thickness	Age	Fossil content
Aeolian sands (Okondeka lunette dunes), beach deposits, fans at river mouths, salt crusts	Up to 6 metres	Holocene to Present	Extant snails, *Struthio camelus* eggshells, Mammals
Unnamed calc-tufa at Namutoni	1 metre	Holocene	Planorbidae,
Unnamed calcified marl in Homob Waterhole depression	1 metre	Holocene	*Xerocerastus*, Planorbidae
Oshigambo Pan-loess	1-1.5 metres	Latest Pleistocene	Snails, *Struthio camelus* eggshells, Mammals
Pelican Island Green Silts	3 metres	Latest Pleistocene	
Elevated beach deposits (1.5-2 m above floor of pan)	0.5 – 2 metres	Latest Pleistocene	*Hodotermes* bio-constructions, reworked oncolites, *Melanoides tuberculata*, *Bellamya unicolor*, *Mutela* sp.
Erosional unconformity	Incision of up to 20 metres	Middle to Late Pleistocene	
Etosha Limestone (fossiliferous calcrete and calcreted sands)	1-3 metres in the north, thicker in the south	Early Pleistocene	Oncolites (reworked), plant root networks, *Achatina*, *Xerocerastus*
Unnamed thin but widespread rubble horizon containing black sediment nodules (Ekuma and Oshigambo Valleys; Pelican Island)	10 cm	Early Pleistocene	Reworked fragments of fish and turtles from the Ekuma Delta Member
Poacher's Point Member (fossiliferous micro-ooid strata becoming ooliticwith Magadi-type chert on Pelican Island)	3-20 metres	Late Pliocene to Early Pleistocene	Oncolites, Ostracoda *Xerocerastus*, *Achatina*, *Succinea*, *Struthio camelus* eggshells
Ekuma Delta Member (cross-bedded clean quarztite with minor green clay)	50 cm to 2 metres	Middle Pliocene (ca 4 Ma)	*Bellamya*, *Mutela*, *Clarias*, Cyclanorbinae, *Pelusios*, *Crocodylus*, Phoenicopteridae, *Struthio daberasensis* eggshells, Mammals
Etosha Pan Clay Member (green clay and silt with quartzite stringers)	At least 3 metres (probably considerably thicker)	Late Miocene (ca 6 Ma)	Oncolites, *Clarias*, Cyclanorbinae, *Pelusios*, *Crocodylus*, *Phoenicopterus*, Mammals
Beisebvlakte Borehole (?Andoni Formation)	At ca 34 metres depth	Base of the Middle Miocene (16 Ma)	*Namornis oshanai* eggshells
Subsurface mudstones, shales	--	Mesozoic	*Palynomorphs*
Subsurface dolomites, limestones	--	Proterozoic	*Stromatolites*

Table 1: Stratigraphic succession in the north and east parts of the Etosha Pan, Namibia.

Etosha Limestone (alt. 1120m)
(calcrete with oncolites)

Poacher's Point
Carbonate Member
(micro-ooids, gastropods)

Holocene beach deposit
(oncolites, fossiliferous sand)

Etosha Pan Clay Member
(cliff)

Floor of Pan (alt. 1084m)

Figure 3: Stratigraphic succession at Poacher's Point, Etosha Pan, Namibia.

erably thicker in the south towards the Otavi Mountains (Gevers, 1930 ; Miller, 2007). Unconformably overlying an eroded and deeply incised surface of calcrete and older rocks, there is a series of unindurated or weakly indurated lacustrine, marginal lacustrine, fluvial, aeolian and pedogenic deposits, and salt crust (Beugler-Bell & Buch, 1997 ; Buch, 1993 ; Buch & Zoller, 1992 ; Buch *et al.,* 1992 ; Rust, 1984).

The Late Pleistocene Oshigambo Peninsula fossils (Hipondoka, 2005 ; Hipondoka *et al.,* 2006) occur in grey to yellow clays and silts representing an accumulation of dust derived from the floor of Etosha Pan which was trapped and fixed by vegetation growing on its margins ; These are fine sand, and the ridges are essentially shorelines. These loess-like deposits are here named the Oshigambo Pan-loess, which is a widespread but thin horizon (up to 1.5 metres) that extends over much of the Greater Etosha Basin, but is absent from pans in the region. It unconformably overlies the Andoni Forma-
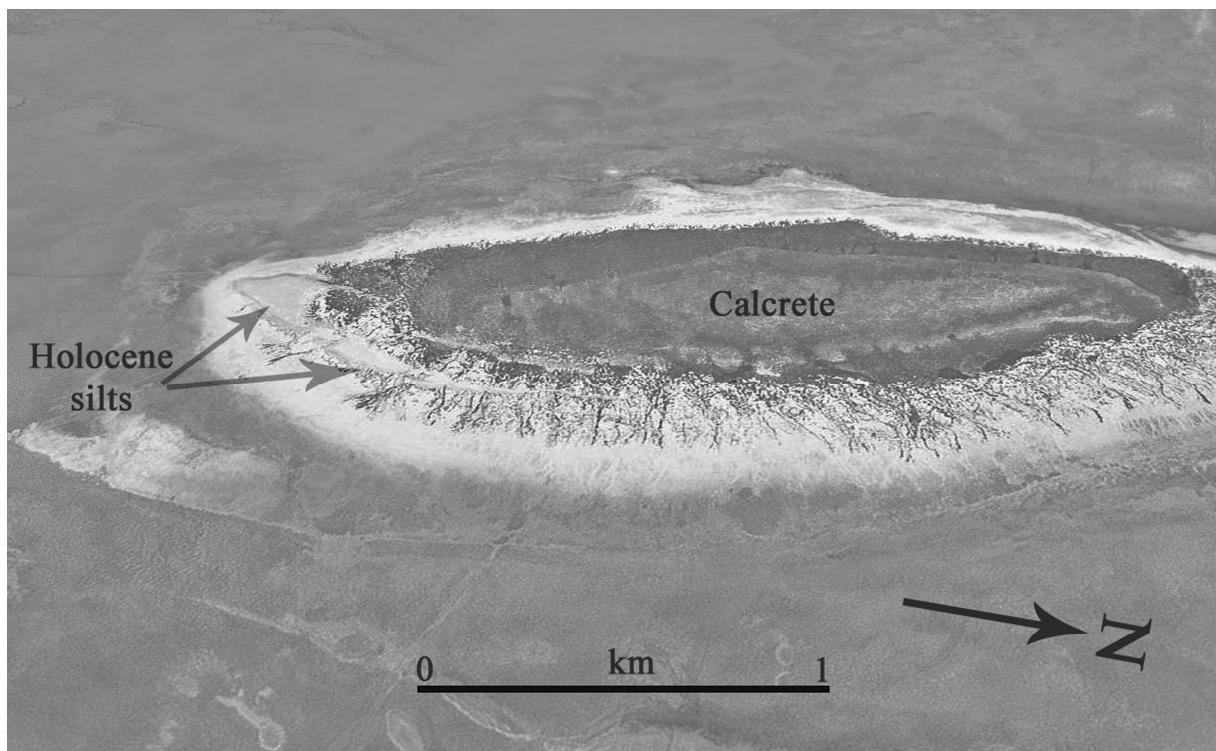
Figure 4: Oblique view of Pelican Island from the East, showing the distribution of the Pelican Island Green Silts (Holocene) on the southern end of the island. Note also the Etosha Calcrete which forms the resistant cap of the island. Image modified from Google Earth.

tion, the Etosha Limestone and the raised beach deposits and is of Latest Pleistocene age (Table 1). Another, more localised latest Pleistocene deposit occurs on the southern end of Pelican Island (Fig. 4) and consists of green silts which drape the incised margins of the island.

Geological processes active in the Etosha Basin

At present there is a complex interplay of erosion, sediment transportation, deposition and diagenesis within the Greater Etosha Basin, with a net loss of fine sediment and salts from Etosha Pan itself, principally by deflation accompanied by short to long distance aeolian transportation (Fig. 5) (Bittner & Plöthner, 2001 ; Bryant, 2003 ; Buch, 1997 ; Buch & Zoller, 1992 ; Buch *et al.,* 1992 ; Engert, 1997 ; Hipondoka, 2005 ; Hipondoka *et al.*, 2004b, 2006; Kempf & Hipondoka, 2003 ; Lindeque & Archibald, 1991 ; Rahm & Buch, 1997 ; Rust, 1981, 1984, 1985 ; Stuart-Williams, 1992 ; Talma & Rust, 1997). There is also considerable aeolian and aquatic redistribution of sand and silt within the confines of the basin (Hipondoka *et al.*, 2004a ; Beugler-Bell & Buch, 1997) and much sediment is brought into the pan by seasonal rivers flowing in from the north and to a lesser extent from the south. The southern margins of the basin have experienced widespread, active groundwater calcrete genesis with the build-up of large, low angle, megadomes of dolomitic carbonate which often have a depression at the top in which water holes occur (Gevers, 1930 ; Rahm & Buch, 1997) whereas the northern parts of the basin experienced pedogenic calcrete formation, often with the preservation of extensive rhizolith networks.

Figure 5: Dust storm on Etosha Pan, 19th November, 2007. The storm front was about 40 km wide and the height of the advancing dust cloud was ca 1 km. Much dust settled onto vegetated ground (dark horizontal features in the background) but some was blown right out of the Etosha Basin towards the Atlantic Ocean.

Sedimentology and Palaeoenvironment

A comprehensive study of the Etosha palaeoenvironment was carried out by Hipondoka (2005) who was interested in the origins and development of the Etosha Pan. His studies revealed that many of the previous hypotheses about pan formation are debatable, even if much of the geological and geomorphological observation upon which they were based is sound. Part of the uncertainty about the origins and history of the pan relates to the fact that the sedimentary deposits lacked precise geological age control, and this chronological uncertainty impacted on ideas concerning processes and rates of pan formation. Various dating methods have been tried, but most of the deposits

are beyond the range of the ^{14}C method or the methods used are inherently imprecise.

The Andoni Formation comprises lacustrine (green silts and quartzite lenses of the Etosha Pan Clay Member), fluvio-lacustrine (quartzite stringers and lenses in the Ekuma Delta Member) and shallow-water carbonates (micro-ooids of the Poacher's Point Carbonate Member). This succession suggests a progressive infilling of a palaeolake in the Etosha Basin, resulting in a shallowing upwards sequence of deposits. The bulk of the fauna from this formation, in particular the fish, turtles and crocodiles, belongs to fresh water species, whereas the fla-

mingos indicate a saline or alkaline environment. The presence of chert nodules in certain localities at Poacher's Point and Pelican Island (Fig. 6) similar to those that formed in Lake Magadi, Kenya, suggests that at some stages of the lake basin development, there must have been hyper-alkaline conditions (pH greater than 12). These cherty deposits occur *in situ* in the Poacher's Point Carbonate Member at Pelican Island (Fig. 6). As the palaeolake became shallower and shallower, there was a progression from freshwater deposition in the Late Miocene to hyper-alkaline deposition during the Plio-Pleistocene.
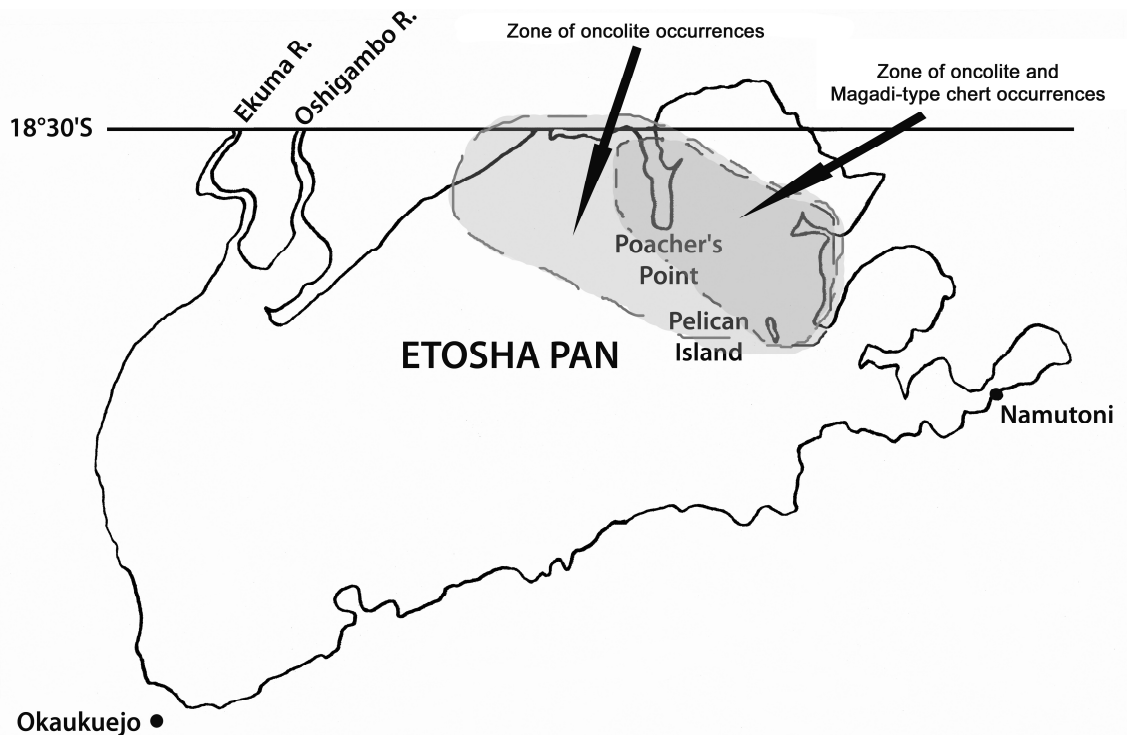
Figure 6: Distribution of oncolites and Magadi-type chert nodules in Etosha Pan. These deposits attest to a highly alkaline depositional environment during the Plio-Pleistocene.

The Etosha Pan Clay Member and the Poacher's Point Carbonate Member host abundant oncolites (Fig. 7, 8). The richest *in situ* occurrences of oncolites occur at the Stinkwater Peninsula and Pelican Island, but they occur widely in the pan (Fig. 6).

The Ekuma Delta quartzite and green silts contain rich assemblages of freshwater gastropods (*Bellamya unicolor*) and bivalves (*Mutela* preserved as articulated couplets) which indicate freshwater deposition and

well oxygenated waters. The abundant presence of rhizoliths and casts of tree trunks *in situ* in the quartzites indicate shallow water deposition followed by subaerial exposure.

The Poacher's Point Member at Oshigambo and Poacher's Point comprises a 15-20 metre thick micro-ooid horizon containing abundant arid-adapted terrestrial snails (small *Achatina*, *Xerocerastus* and *Succinea*) indicating a semi-arid to sub-humid regional environment. It also contains oncolites. At

Figure 7: Abundant oncolites occur in the Poacher's Point Carbonate Member on the northern margin of the Stinkwater Peninsula. The outcrop has been affected by calcrete pedogenesis.
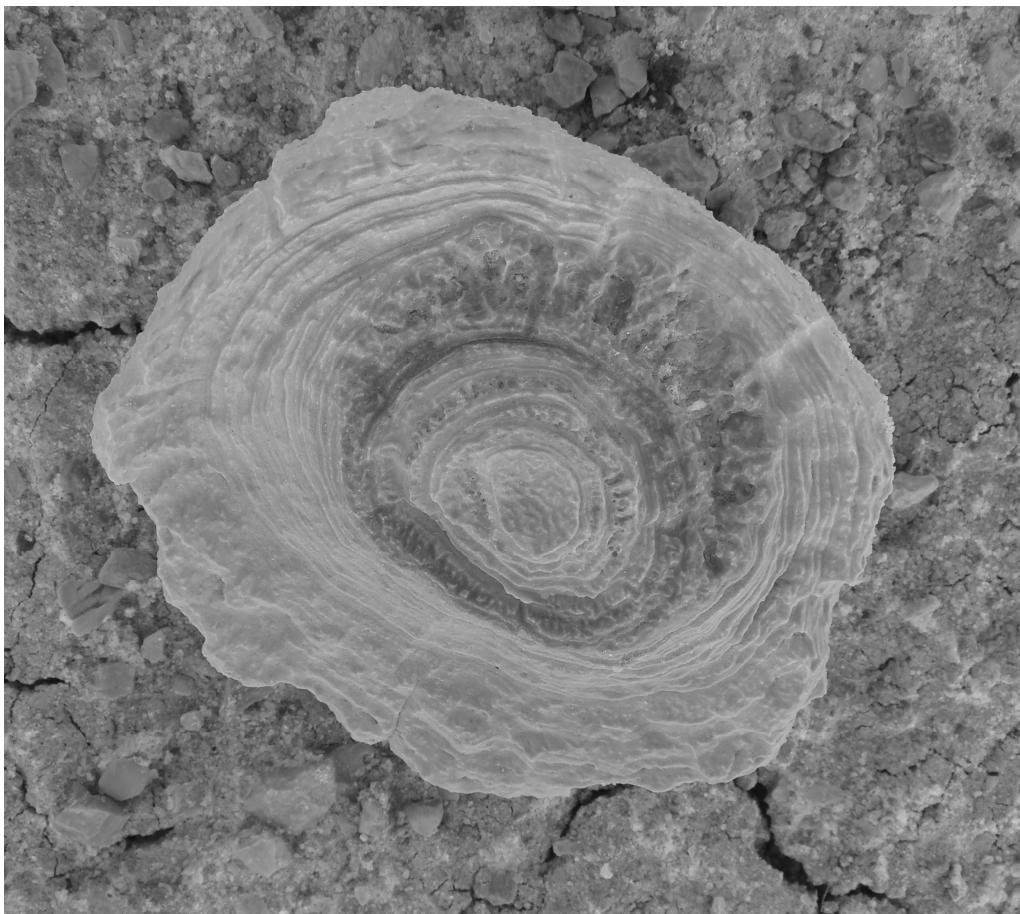
Figure 8: Naturally sectioned and slightly weathered oncolite from the western margin of Poacher's Point, showing multiple growth phases (diameter of specimen ca 25 cm).

Pelican Island, this unit contains limestone horizons comprised of ooliths up to 2 mm in diameter (Fig. 9), interbedded with horizons containing Magadi type chert plates. The latter deposits indicate highly alkaline conditions in palaeolake Etosha during the early Pleistocene, contrasting with the fresher conditions that likely prevailed earlier in its history.

Figure 9: Oolitic limestone in the Poacher's Point Carbonate Member at Pelican Island, Etosha Pan, Namibia.

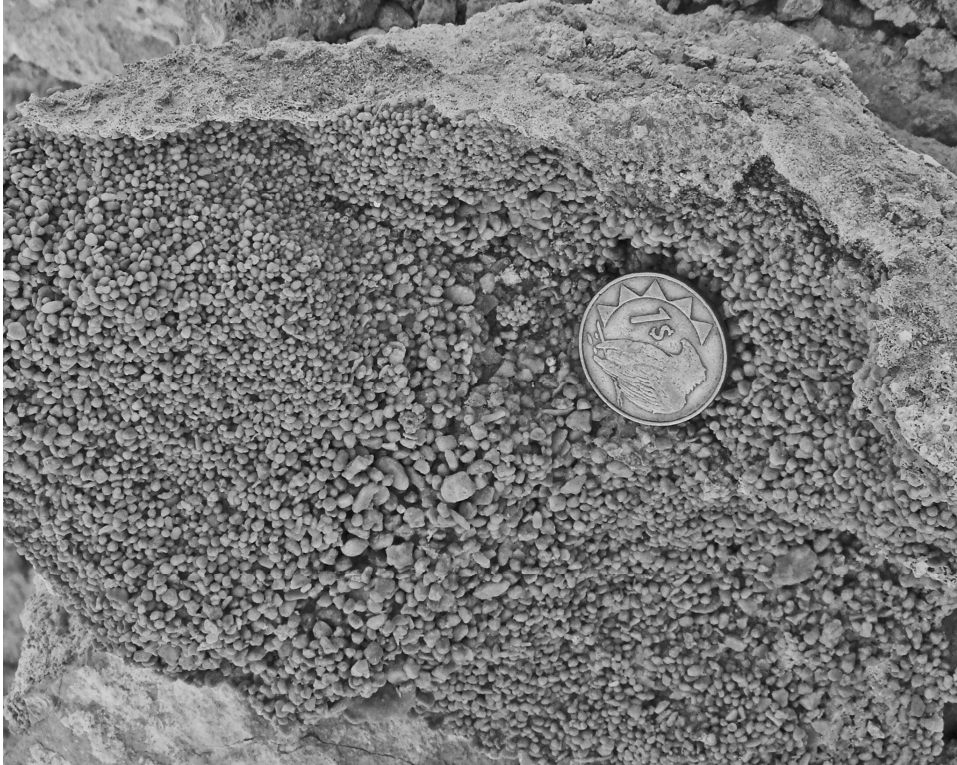The Etosha Limestone (pedogenic and groundwater calcrete) contains termite hives (*Hodotermes*) and abundant terrestrial snails, similar to those that occur in the region today. The discovery of reworked oncolites in the calcrete that caps the cliffs at Poacher's Point, suggests that there was a lake at this altitude (1120 masl) well above the present day floor of the pan (1084 masl). Abundant oncolites occur along the edges of the Etosha Pan at Stinkwater Peninsula and at Pelican Island, associated with the Poacher's Point Carbonate Member of the Andoni Formation. Similar oncolites have been observed littering the floor of the Etosha Pan at various localities where they lie on green silts of the Etosha Pan Clay Member (Fig. 6).

Beach deposits are preserved on a terrace ca 1.5-2 metres above the present day floor of the pan at Poacher's Point and similar deposits occur in the Ekuma River Valley, stratigraphically between the Ekuma Delta Member beneath, and the Oshigambo Pan-loess above. In both areas the beach deposits are fossiliferous, those at Poacher's Point yielding calcified termite hives in indurated sand which also contains quantities of reworked oncolites, and those at Ekuma containing abundant shells of *Melanoides tuberculata* and rarer shells of *Mutela* sp. and *Bellamya unicolor*. These pale orange, partly calcified beach deposits underlie the Oshigambo Pan-loess deposits, and they attest to widespread lacustrine conditions at the time of deposition.

Tertiary and Quaternary Palaeontology of the Etosha Basin

The palaeontological descriptions that follow are arranged in stratigraphic order. This approach leads to some repetition, but it yields a better comprehension of the content of each fauna and thereby provides a surer

Figure 10: Section in the east bank of the Ekuma River Valley exposing at the base, quartzite of the Ekuma Delta Member, above which lies a pale orange silty sand horizon 1.5 metres thick (small eroded embayment surrounded by vegetation) rich in lacustrine molluscs. The top of the succession comprises 1 to 1.5 metres of Oshigambo Pan-loess, on which the vegetation is growing.

foundation for palaeoenvironmental and biochronological studies which flow from the faunal study.

Fauna from the Etosha Pan Clay Member of the Andoni Formation

In Etosha Pan, green silts and quartzites of the Etosha Pan Clay Member of the Andoni Formation have yielded abundant vertebrate fossils (Fig. 15-19) from several distinct localities along the northern rim of the pan. By far the most common fossils are cranial and skeletal fragments of clariid fish which are accompanied by scutes of freshwater turtles and crocodiles as well as leg bones of flamingos, and rarer terrestrial mammal remains. Deposition in shallow lacustrine conditions, near end points of rivers flowing into the palaeolake appears to have occurred.

Bivalvia (MP)

Internal and external molds of a large bivalve were found in quartzite of the EPCM on the south side of the Oshigambo Penin-

sula. The dimensions and shape of the specimens suggest a mutelid (Fig. 12). The specimens are poorly preserved but they probably belong to *Mutela* sp.

Pisces (HJ)

The fish bones collected in the green silts of the EPCM belong above all to the skull roof, ornamented in the characteristic fashion of Siluriformes, in which the shape and distribution of granules is typical of that of Clariidae (*Clarias, Heterobranchus*). Among the other skull bones, the commonest are articulars, dentaries and mesethmoids. The cleithral belt has yielded abundant pectoral spines and a few fragments of cleithrum. Vertebrae are abundant, but determining their position along the vertebral column neccessitates a detailed comparison with extant Clariidae. Of these elements of the skeleton, only the pectoral spines permit an accurate identification. They possess well developed parallel striae along the cleithral articular surface, a character that is typical of the genus *Clarias* (Gayet & Van Neer; 1990). The sample is monospecific, without

Figure 11: Outcrops of Pelican Island Green Silt reposing unconformably on an incised rubble-covered erosional terrace at Pelican Island, Etosha. A) the silts (to left of the people) drape an incised topography some 10 metres above the floor of the pan (southeast edge of Pelican Island), B) the geologist is standing on Pelican Island green silts which drape a rubble covered slope beneath a cliff of Etosha Pan Clay Member locally rich in oncolites (the undercut in shadow) and Poacher's Point Carbonate Member (cliff forming strata) (southern end of Pelican Island).

any sign of another taxon. We therefore identify the Etosha fossils as Siluriformes, Clariidae, cf. *Clarias* sp.

Employing the equations developed for the genus *Clarias* by Van Neer & Lesur (2004), we can estimate the dimensions of individuals represented by fossil at Etosha, by measuring mesethmoids, dentaries, ar-

ticulars, quadrates, operculars, urohyals, cleithra and pectoral spines (Tab. 2, Fig. 13). Most of the specimens are large with the size profile centred on 70 cm, and the largest reaching a length of 110 cm. Individuals smaller than 50 cm are undoubtedly present at Etosha but would require fine screening to sample.

Figure 12: ET 55'07, internal and external molds of shells of *Mutela* sp., in quartzite of the Etosha Pan Clay Member, Etosha, Namibia.

Dimensions (cm) / Samples	40	50	60	70	80	90	100	110	120
ET16´07		1		2	1				
ET28´07			2	8	3	2	1	1	
ET35´07		4	5	4	2			1	
ET43´07			3	2	3	1	1		
ET47´07			1						
ETOSHA total	0	5	11	16	9	3	2	2	0

Table 2: Dimensions (in cm) calculated for individual specimens of *Clarias* sp.

Monospecific assemblages of *Clarias* are common in shallow, poorly oxygenated waters of Africa. *Clarias* are fish that can survive in anoxic waters thanks to a certain number of physiological and anatomical adaptations. They possess two respiratory organs derived from their pharyngeal cavity, which permits them to obtain oxygen directly from the air. Assemblages comprising individuals of all sizes can be found together embedded in mud around dessicated water holes during the dry season (Paugy *et al.*, 2003).
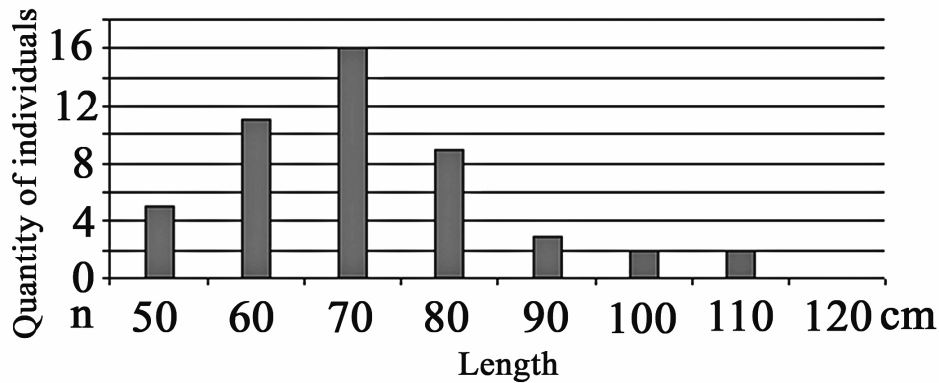
Figure 13: Profile of dimensions (preliminary) of *Clarias* sp. from the Etosha Pan Clay Member of the Andoni Formation, Etosha.
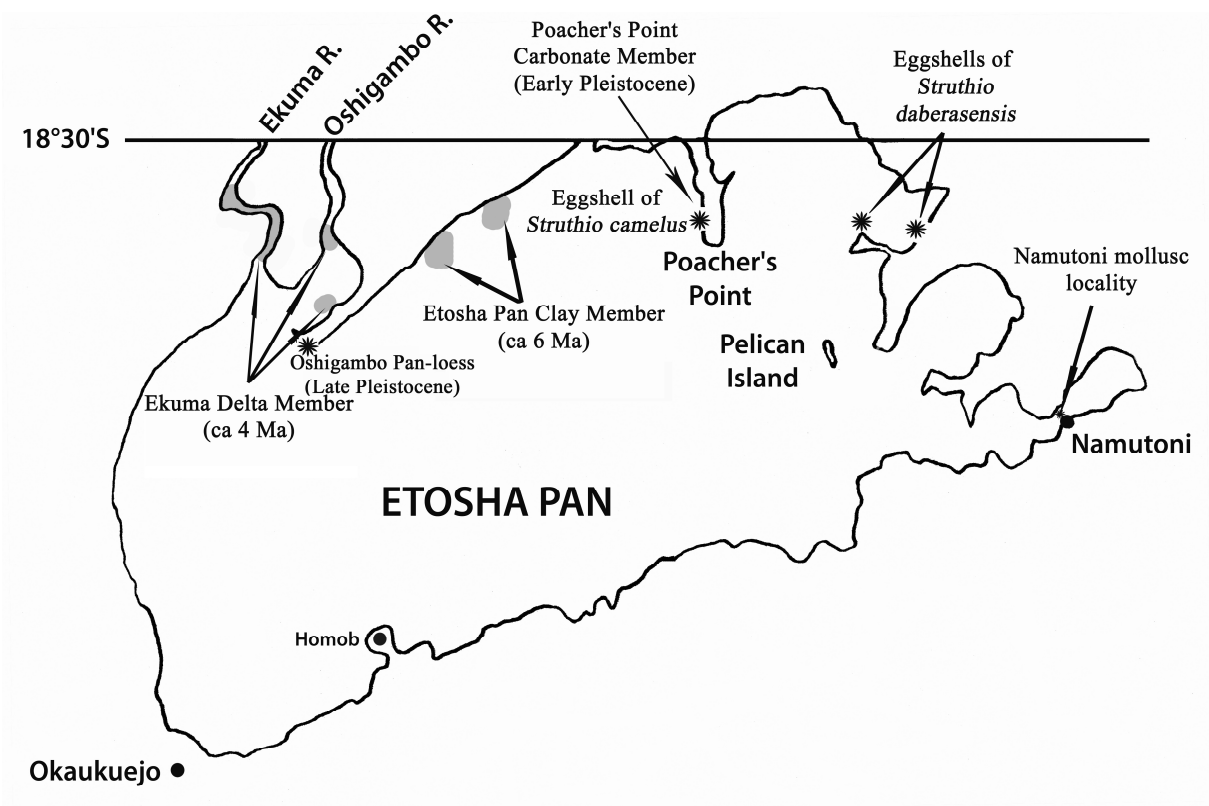
Figure 14: Main Late Miocene, Pliocene and Pleistocene vertebrate fossil localities at Etosha Pan.

Chelonia (de Lapparent de Broin, pers. comm.)

Pelusios is represented in the EPCM by several scutes (ET 34'07) (Fig. 15) with the characteristic surface texture of the genus, but without ridges and pustules. The grooves corresponding to the edges of the shell that overslies the scutes is clearly visible, as are growth ridges (Fig. 15 B).

Cyclanorbidae is represented in the EPCM by a characteristic scute (ET 33'07) which is patterned with anastomosing worm-like ridges and bony pustules characteristic of this family (de Lapparent de Broin, pers. comm.) The scute is dorsally concavo-convex round its margin (Fig. 16 A) and possesses an apophysis at one corner.

The two chelonian taxa from the EPCM are freshwater turtles that are widespread in tropical Africa (de Lapparent de Broin, 2000).
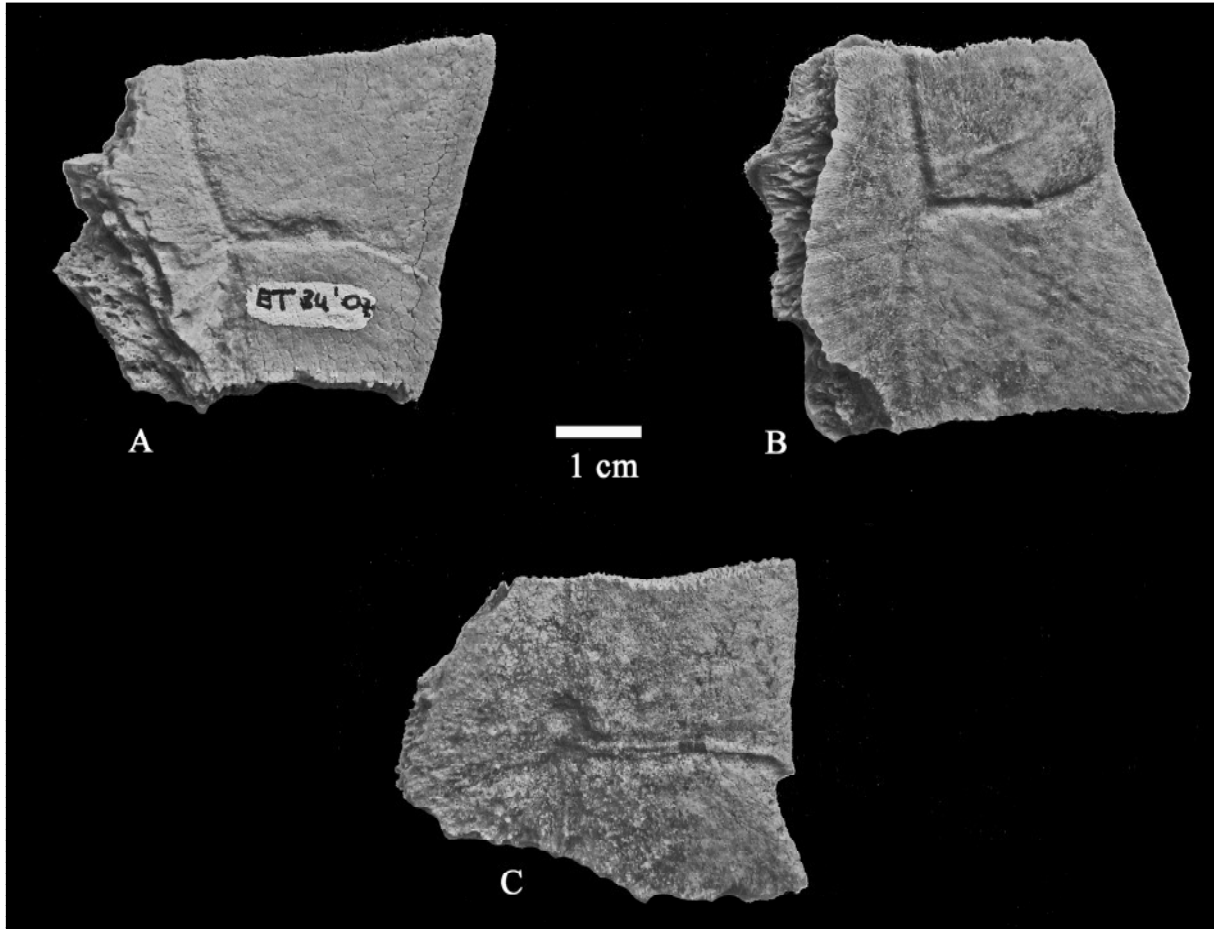
Figure 15: ET 34'07, *Pelusios* scutes from the Etosha Pan Clay Member, south of Oshigambo Peninsula, Etosha, Namibia.

Crocodylia (MP)

Crocodiles are common in the EPCM, being represented by cranial fragments, vertebrae and appendicular elements and by abundant scutes, some of large dimensions. Teeth are relatively rare.

Phoenicopteridae (CM-C)
Order Phoenicopteriformes
Family Phoenicopteridae
Phoenicopterus ruber Linnaeus, 1758

Material
ET 42'07 Right tibiotarsus, distal part, female size
ET 42'07 Left tarsometatarsus, proximal part and fragment of shaft, female size
ET 26'07 Right tibiotarsus, distal part, male size
ET 26'07 Right tarsometatarsus, fragment of

shaft, female size

Description and comparisons -
Comparison with recent forms

The Etosha fossils (Fig. 16 B-D) display the morphological characteristics of the genus *Phoenicopterus*, the Greater Flamingo, and differ from the genus *Phoeniconaias*, the Lesser Flamingo. In *Phoeniconaias*, on the distal part of the tibiotarsus, on the caudal side, the trochlea cartilaginis tibialis (Baumel and Witmer, 1993) is not very projecting caudally and not very developed in the proximo-distal direction. In distal view, the two cristae trochleae are almost symmetrical and are separated by a sulcus directed proximo-distally and situated in a median position. In *Phoenicopterus* the trochlea cartilaginis tibialis is strongly projecting caudally and more developed proximo-distally. The crista trochleae later-

30

alis (external condyle in Howard, 1929) is more projecting caudally than the crista trochleae medialis (internal condyle in Howard, 1929). These two cristae are separated by a proximo-distally directed groove which is closer to the medial side and the crista trochleae medialis has the shape of a cutting edge. On the tarsometatatarsus, in *Phoeniconaias*, the eminentia intercotylaris in proximal view makes a medio-laterally elongated ridge, while in *Phoenicopterus* it makes a tubercle more rounded in the dorso-plantar direction and more projecting in the proximal direction. In *Phoenicopterus* there is a conspicuous narrowing between the proximal articular surface and the hypotarsus, while in *Phoeniconaias* this narrowing is barely perceptible.

Both tibiotarsi from Etosha are characterized by the strong projection of the trochlea cartilaginis tibialis in the caudal direction. However this characteristic is subject to a certain amount of variation in the extant forms of *Phoenicopterus ruber*. This characteristic can be expressed by the ratio Distal Depth : Distal Width (Table 3). Inside the same subspecies, in *P. ruber ruber*, the Caribbean Flamingo, which lives in the Caribbean and the Galapagos, as well as in *P. ruber roseus*, the Rosy Flamingo, which lives in Eurasia and Africa, the females have a larger D/W ratio than the males, which corresponds to a trochlea cartilaginis tibialis proportionally more projecting than that of the males. In addition, in the subspecies *P. ruber ruber*, both sexes have a D/W ratio greater than both sexes of *P. ruber roseus*, thus a trochlea cartilaginis tibialis proportionally more projecting. This last characteristic had already been reported by L. Miller (1944). For the two tibiotarsi from Etosha, ET 26'07, male size, and ET 42'07, female size, the D/W ratios are included in the variation range of both extant subspecies of *Phoenicopterus ruber*.

The other characteristics of the Etosha form are the wide distal opening of the canalis extensorius, which is almost circular on the tibiotarsus ET 26'07, male size. This characteristic is also variable in the extant

forms: some individuals have an elliptical opening, medio-laterally elongate and proximo-distally narrow, and some others have an almost circular opening. The shape of the trochlea cartilaginis tibialis is also variable, the extant small-sized individuals often have a proximo-distal sulcus situated closer to the medial side, and a crista trochleae medialis with the shape of a cutting edge, as in both specimens from Etosha.

The dimensions of the tibiotarsi and tarsometatarsi from Etosha are included in the variation range of both extant subspecies of *Phoenicopterus ruber* and are larger than those to the extant species *Phoeniconaias minor*.

Comparison with fossil forms

An extinct genus and species of flamingo, *Leakeyornis aethiopicus*, was described from the early and middle Miocene of Kenya (Dyke and Walker, 2008; Harrison and Walker, 1976; Pickford, 1986; Rich and Walker, 1983). In *Leakeyornis aethiopicus*, on the tibiotarsus, the prominence on the distal end of the pons supratendineus is lower and less pronounced than in the extant flamingos, the proximal opening of the canalis extensorius is narrow, the sulcus extensorius running proximal to it is deep and well defined, the distal opening of the canalis extensorius is directed antero-distally, not anteriorly. Still in *Leakeyornis*, on the tarsometatarsus, the shelf between the articular surfaces and the hypotarsus does not slope off posteriorly at such a high angle as in the extant flamingos (Rich and Walker, 1983). The characteristics of the Etosha flamingo remains correspond to the genus *Phoenicopterus* and differ from the genus *Leakeyornis*, and they are larger than *L. aethiopicus*.

Phoenicopterus floridanus was described on the basis of a distal part of tibiotarsus from the Pliocene of the Bone Valley Fm., in Florida (Brodkorb, 1953). The measurements of seven distal parts of tibiotarsus of *P. floridanus*, from the same locality, are given by Olson and Rasmussen (2001). One of the main specific characteristics given by P. Brodkorb, i.e. the low value of the ratio D/
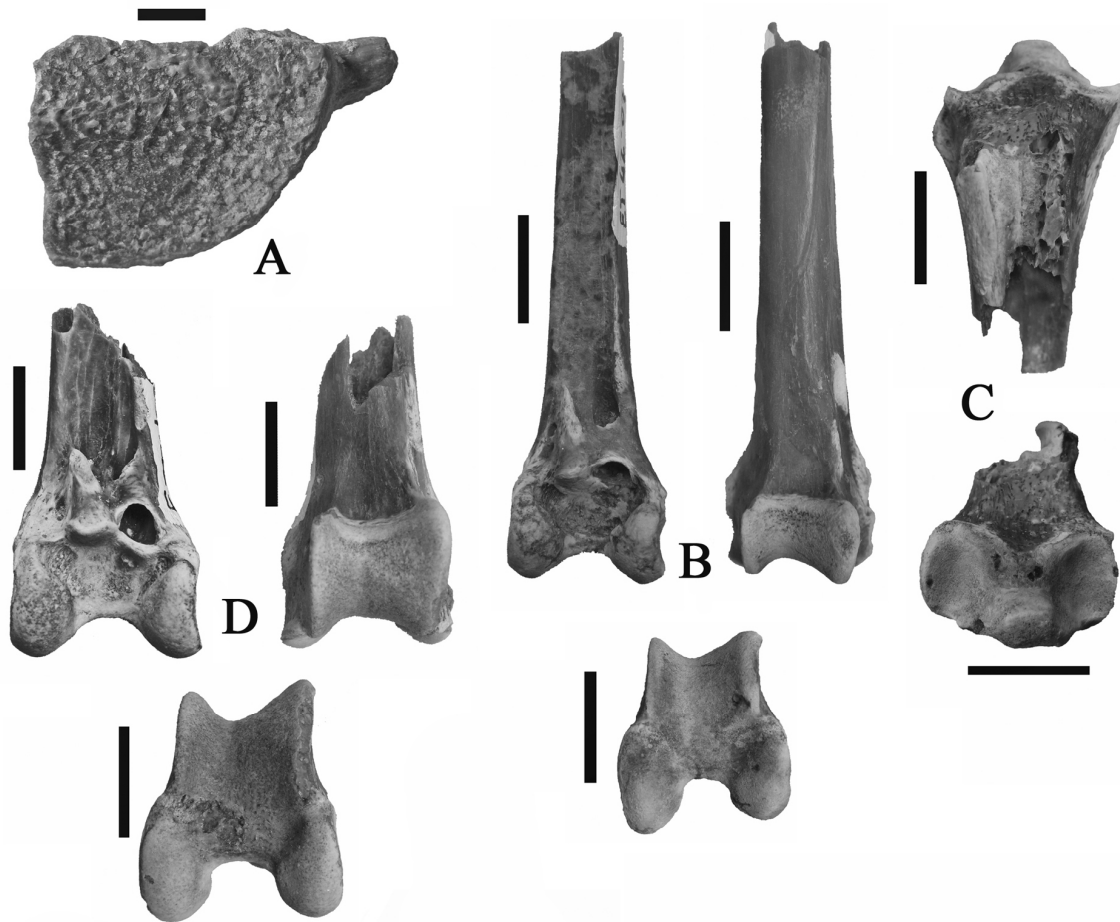
Figure 16: Vertebrates from the Etosha Pan Clay Member, northern rim of Etosha Pan, Namibia (scale bars : 1 cm). A) ET 33'07, Cyclanorbidae scute ; B) *Phoenicopterus ruber*, ET 42'07, right tibiotarsus, distal part, female size, cranial, caudal, and distal views ; C) *Phoenicopterus ruber*, ET 42'07, left tarsometatarsus, proximal part, female size, dorsal and proximal views ; D) *Phoenicopterus ruber*, ET 26'07, right tibiotarsus, distal part, male size, cranial, caudal, and distal views.

W (Distal width: 16.5; Distal of lateral condyle: ca. 17.6; D/W: 1.067), is not confirmed when a larger sample is available (Mean of distal depth: 18.3; mean of distal width: 15.3, D/W: 1,196). The dimensions of *P. floridanus* are almost entirely included in the range of variation of the extant *P. ruber*. Another specific characteristic of *P. floridanus* is the small width of the trochlea cartilaginis tibialis in relation to the distal width. This characteristic is not present in the Etosha forms where the width of this trochlea is comparable to that of the extant forms.

Phoenicopterus stocki was described in the Rincón Pliocene of Chihuahua, Mexico, the holotype of which is a distal part of tibiotarsus (L. Miller, 1944). It is very small and the distal width is comparable to that of

Phoeniconaias minor, but ratio D/W (1.255) is larger than in *P. minor* and comparable to the values found in *Phoenicopterus ruber*.

Another genus, *Phoeniconotius*, and another species of *Phoenicopterus*, *P. novaehollandiae*, were described in the late Oligocene or the early Miocene of Australia (A. H. Miller, 1963). They are only represented by distal parts of tarsometatarsi and they are much older than the Etosha specimens.

In conclusion, the fossil flamingos from Etosha can be ascribed to the extant species, *Phoenicopterus ruber*. The other data from the litterature show that a form very close to the extant species is already present in the Pliocene (Olson and Rasmussen, 2001).

Tibiotarsus	Distal width	Distal depth	Ratio D/W
ET 26'07	18.0	22.3	1.239
ET 42'07	14.3	17.3	1.210
Phoenicopterus ruber ruber			
males, extremes	15.8-17.3	18.9-21.2	1.16-1.28
mean (n)	16.66 (9)	20.01 (9)	1.207 (9)
females, extremes	14.3-17.3	16.5-20.0	1.10-1.30
mean (n)	15.30 (10)	18.36 (10)	1.198 (10)
Phoenicopterus ruber roseus			
males, extremes	16.7-19.0	19.4-20.6	1.07-1.19
mean	17.98 (4)	20.15 (4)	1.123 (4)
females, extremes	14.4-17.0	17.9-18.5	1.09-1.24
mean	15.93 (3)	18.23 (3)	1.146 (3)
Leakeyornis aethiopicus			
extremes	11.2-11.8	13.8-14.3	-
n	3	3	
Tarsometatarsus and Phalanx 1 post. digit III	Tarsometatarsus Proximal width (1)	Tarsometatarsus Depth of prox. art. surf. (2)	Total length of phal. 1 post. digit III
ET 42'07	17.5	9.6	-
GPS 69	-	-	44.9
Phoenicopterus ruber ruber			
males, extremes	19.0-21.0	10.7-12.3	44.1-49.5
mean (n)	19.93 (10)	11.48 (10)	46.99 (9)
females, extremes	17.2-19.9	9.5-10.6	39.7-45.7
mean (n)	18.09 (10)	10.14 (10)	43.23 (8)
Phoenicopterus ruber roseus			
males, extremes	18.6-20.5	12.0-12.7	47.7-50.0
mean (n)	19.64 (5)	12.26 (5)	48.48 (4)
females, extremes	17.4-18.2	9.9-11.0	42.1-43.2
mean (n)	17.90 (3)	10.50 (3)	42.60 (3)
Leakeyornis aethiopicus			
extremes (n)	9.4-15.0 (10)	-	-

Table 3: Measurements (in mm) of the fossil material of *Phoenicopterus ruber* from Etosha Pan and Ekuma River, compared to modern individuals of *P. ruber* and fossil *Leakeyornis aethiopicus*, after Rich and Walker (1983).
(1) For the tarsometatarsus the proximal width is measured including a small tubercle which is situated on the lateral side, just distally to the lateral cotyle.
(2) The depth of the proximal articular surface is measured from the eminentia intercotylaris to the plantar border of the articular cotyles, i. e. without the hypotarsus.

Biostratigraphic distribution

Phoenicopteridae are present in a certain number of localities from the early and middle Miocene of Kenya, with *Leakeyornis aethiopicus* (Rich and Walker, 1983), or undetermined Phoenicopteridae (Pickford, 1986). According to Rich and Walker all these localities are early Miocene in age, but the locality of Maboko which has yielded a femur of *L. aethiopicus* is of middle Miocene age (Pickford, 1986). But later on the Phoenicopteridae are unknown in the African localities. They are absent from the middle Miocene Kenyan localities of the Nyakach Fm., and Fort Ternan (Pickford, 1986), from the late Miocene localities of Ethiopia and Chad (Louchart *et al*., 2008), of Kenya (Lothagam, Harris and Leakey, 2003), of Tanzania (Laetoli, Harrison and Msuya, 2005), of Tunisia (Fm. Beglia, Rich, 1972) and of Libya (Sahabi, Ballmann, 1987; Louchart 2005b). They are still absent from the Pliocene localities of Chad (Louchart *et al*., 2004, 2005a), of Ethiopia (Hadar and Omo, Brodkorb and Mourer-Chauviré, 1982; Louchart *et al*. 2005a), and from the Pliocene of Langebaanweg, South Africa (Rich, 1980). This is all the more surprising since all these avifaunas, with the exception of Langebaanweg, are almost uniquely composed of aquatic forms, such as Podicipedidae, Pelecanidae, Phalacrocoracidae, Anhingidae, Ardeidae, Ciconiidae, Balaenicipitidae, Anatidae, Gruidae, Rallidae and Heliornithidae. The Phoenicopteridae occur again only in Olduvai, Bed I, Tanzania, dating from the latest Pliocene, where they are plentiful and correspond to the recent species *Phoenicopterus ruber* (Mourer-Chauviré, unpublished results; Harrison, 1980). Their absence from most of the sites is probably linked to ecological factors.

Paleoecology

The flamingos of the recent genus *Phoenicopterus* only live in saline or alkaline waters, such as saline lagoons, salt pans, and highly alkaline or saline inland lakes (del Hoyo *et al*., 1992).

Felidae (JM)

A distal radius of a large felid, ET 29'07 (Fig. 17) was collected from the EPCM south of the Oshigambo Peninsula. The specimen accords in morphology and dimensions to that of extant lions, *Panthera leo* Linnaeus.

The fragment is a left distal radius, comprising about a third of the bone. The eipiphysis is slightly eroded medially and laterally, but the articular surface is well preserved. The bone has the characteristic morphology of Pantherines, medio-laterally broad and narrow dorso-palmarly (Fig. 17). The articular surface for the scaphoid is concave, but moderately deep, except at the dorsal and palmar borders. The dimensions of the specimen are provided in Table 4.

Maximal medio-lateral diameter	57.2 mm
Medio lateral diameter of the articular surface	39.9 mm
Maximal dorso palmar diameter	31.7 mm
Dorso palmar diameter of the articular surface	25.0 mm

Table 4: Dimensions of the radius of *Panthera* cf *leo* from the EPCM, Namibia
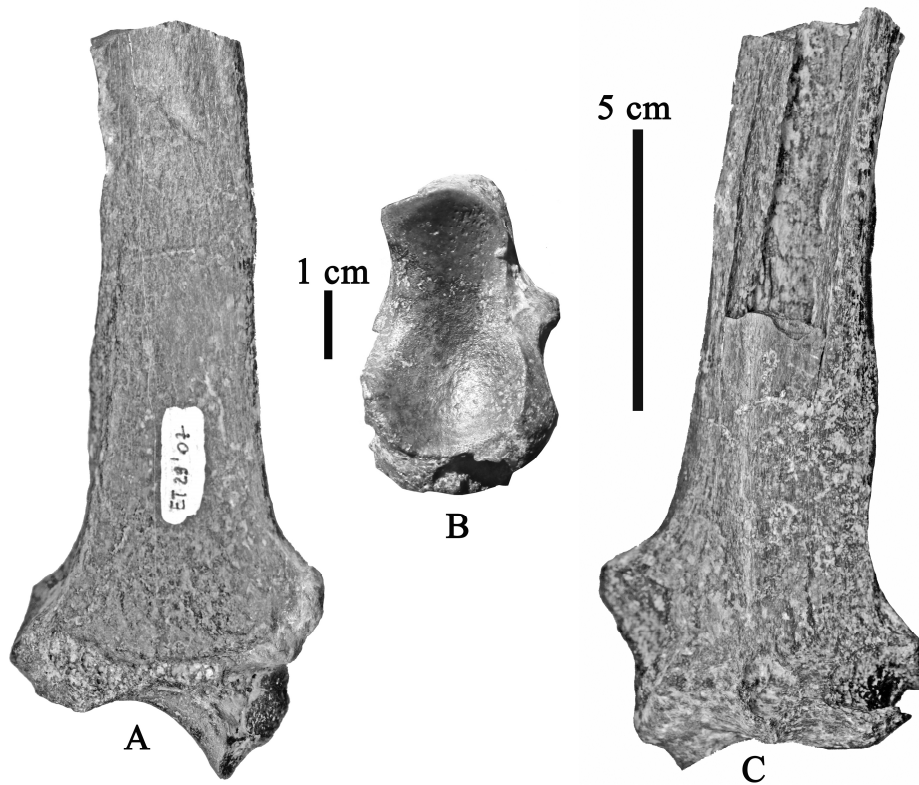
Figure 17: ET 29'07, distal left radius attributed to *Panthera* cf *leo*, from the Etosha Pan Clay Member. A) palmar, B) distal, and C) dorsal views.

The morphology of this radius is similar to that observed in *Panthera leo* and *Panthera pardus*. It differs from radii of more primitive machairodontines such as *Machairodus aphanistus* and *Paramachairodus ogygia* from the Late Miocene locality of Batallones, Spain, which show a tendency to broaden the facet for articulation with the scaphoid, while maintaining overall proportions close to those of pantherines. However, in these machairodonts the scaphoid articulation is notably deeper, in consequence of the greater height of the dorsal border. These two primitive machairodontines are similar in morphology to each other despite the major difference in size of the two species, which indicates the validity of the character which is not related to size. More derived machairodontines such as *Homotherium* or *Smilodon*, have a shorter and broader articular surface than those of pantherines and primitive machairodontines (Ballesio, 1963; Merrian & Stock, 1932).

Proboscidea (MP)

The loxodont teeth from the EPCM of the Andoni Formation are incomplete, but they reveal potentially useful data. Enamel thickness in one specimen (Fig. 18 A) about 30% up from the base of the crown ranges between 3.7 to 5.6 mm (n = 9), unworn crown height is 77.4 and 80 mm in two fragments, the greatest breadth is low down (the pretrite half consists of a single cusp that diminishes in medio-lateral breadth from 30 mm at ca 30% crown height to 22 mm at 50% crown height to 9.5 mm near its occlusal apex (measured from the contact with the sinus)). The loxodont sinus is large, increasing in dimensions rootwards.

A complete molar loph (Fig. 18 B) is 65.8 mm broad at the base, narrowing occlusally to 33.5 mm at the broadest part of the apex. Pre-trite and post-trite halves comprise 5 columns each at the base, but these crowd each other apically so that only 4 tubercles reach the apex. The loxodont sinus, which is the innermost column on both the pre-trite and post-trite sides, is well devel-

oped apically where they twist away from the other cusps and come to lie mesially and distally respectively of the loph axis. The loxodont sinus in this specimen fades out towards cervix. In radicular view, the squared off margin of the tooth is evident on one side, as in primitive species of *Loxodonta*.
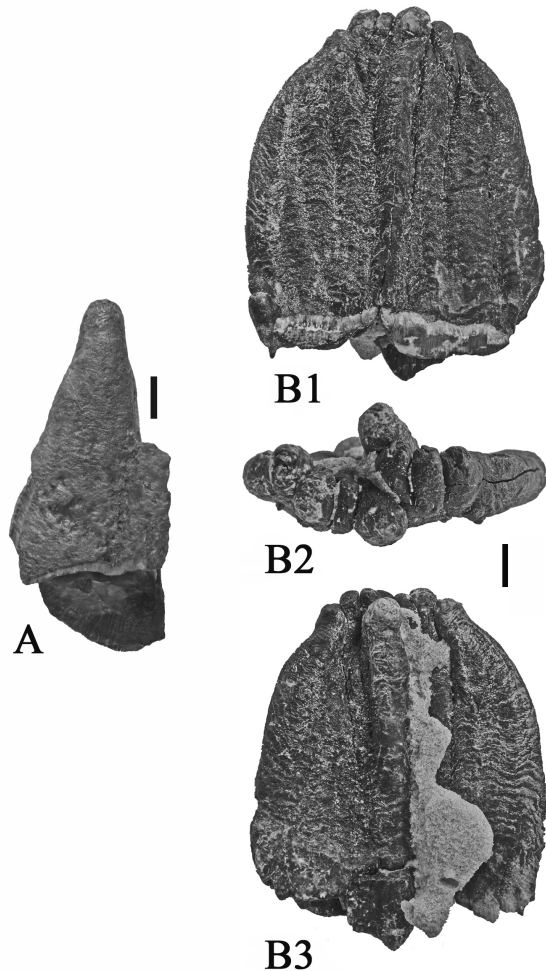
Figure 18: Fossil Proboscidea from the Etosha Pan Clay Member, northern rim of Etosha Pan, Namibia (scale bar : 1 cm). A) ET 10'07, *Loxodonta* cf *cookei*, half molar plate anterior view ; B) ET 53'07, *Loxodonta* cf *cookei* complete molar plate, B1) anterior, B2) occlusal and B3) posterior views.

The overall pattern of the proboscidean teeth from the EPCM is compatible with the species *Loxodonta cookei* from Langebaanweg, South Africa, and various late Miocene and early Pliocene sites in East Africa (Lukeino, Mabaget, Nkondo) (Sanders, 2007).

Suidae (MP)

The suid from the EPCM of the Andoni Formation is a very large one (Fig. 19) (patellar dimensions of EK 30'07 are 65 x 41 mm (proximo-distal x medio-lateral)) with an antero-posterior height of 48 mm (measured from the central articular ridge to the outermost extremity of the patella). Although the genus and species to which this patella belongs cannot be determined, it is larger than that of any extant suid (in *Potamochoerus porcus larvatus* (Fig. 19) the proximo-distal dimension is 36.7 mm) and its dimensions are compatible with large species of *Nyanzachoerus*, *Notochoerus* and *Metridiochoerus*. Extant *Potamochoerus* range in weight from 45-120 kg. The fossil patella from Etosha has almost twice the linear dimensions of a patella of *Potamochoerus porcus larvatus* from Madagascar, with which it was compared (Fig. 19). This would imply that the Etosha suid weighed between 360 and 960 kg (ie 8 x the weight of *P. porcus*).

Bovidae (JM & MP)

Two bovid horn cores and several unidentifiable bovid post-cranial bones have been found in the EPCM belonging to 2-3 size groups.

Tribe Alcelaphini
Genus *Damalacra* Gentry, 1980
Damalacra acalla Gentry, 1980

ET 21'07, a right horn-core lacking the apex, whose total length is ca. 180 mm, preserves part of the frontal with about 25 mm of the interfrontal suture, which indicates that the horns were close together at their bases (Fig. 20 A). The horns diverge outwards, and curve slightly towards the exterior. The pedicle has a strongly developed sinus, which penetrates as far as the base of the horn-core. The transverse section at the base of the horn-core is rounded (54 x 45 mm) (Fig. 21). The medial surface of the horn-core is clearly convex and the lateral side flattened. The margin between the two
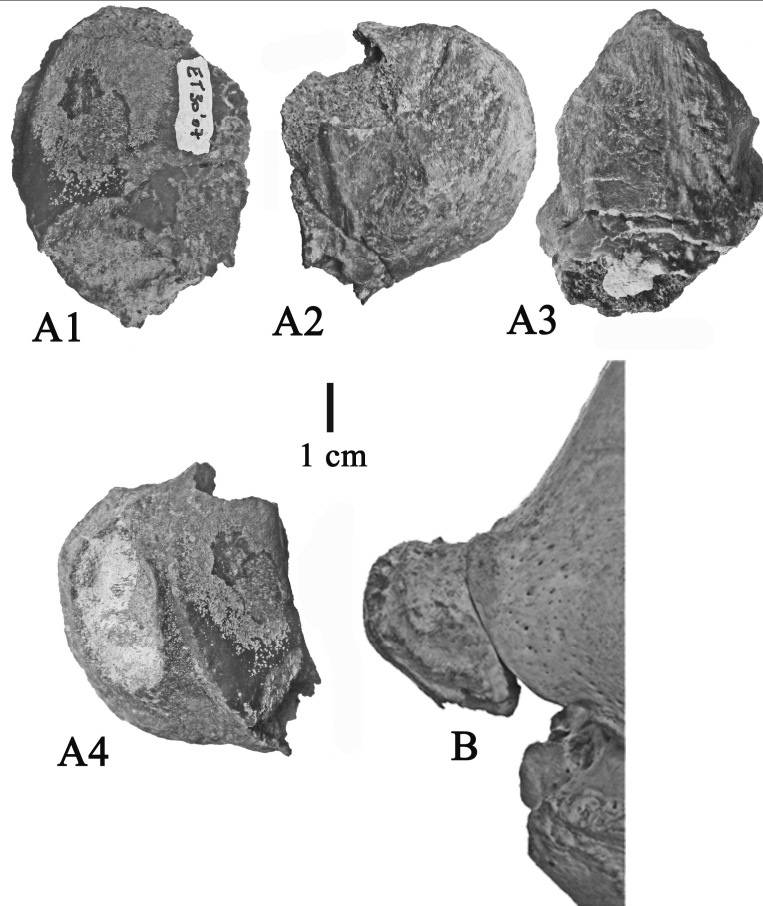
Figure 19: ET 30'07, suid right patella from the Etosha Pan Clay Member (A) ; A1) articular surface, A2) lateral surface, A3) distal view, A4) medial view, (B) medial view of right knee joint of *Potamochorus porcus larvatus* from Madagascar.

surfaces is lightly keeled, visible in anterior view, whereas posteriorly the keel is stronger and is accompanied by a deep groove. The base of the lateral surface possesses many strong grooves, which are weaker medially. However, the medial surface is more ornamented up to the apex than the lateral side is.

ET 54'07 (GPS 108) a right horn core preserving part of the pedicle, is almost straight, with a slight curve which increases apically and outwards (Fig. 20 B). There is a strong sinus in the pedicle (enlarged by breakage of the internal base of the horn-core). The section is quasicircular (45 x ca. 35.5 mm). The anterior surface is convex and quite narrow. The medial side is convex and the lateral side flattened. The posterior surface is narrow and has strongly developed vertical grooves, especially towards the apex.

Discussion

The dimensions and morphology of the two Etosha horn-cores reveal that they are close to species of the genus *Damalacra* Gentry, 1980. Among other features, we should cite the narrow extent of the frontal between the horns which insert close together. They also have a strongly developed pedicular sinus. The horn-cores are conical in aspect, with slight compression and are almost straight, without obvious signs of curvature or torsion. The basal dimensions of the horn-cores are similar to those of *Damalacra acalla* (Fig. 21), and somewhat more compressed than those of *Damalacra neanica*. In particular, the horn-cores from Etosha are morphologically and metrically closer to specimens L1836 (Gentry, 1980, fig.32) and L46075 from Langebaanweg than they are to the holotype of the species (L40001, Gentry, 1980, fig. 31).

Damalacra is a primitive member of the Alcelaphini, a bovid tribe which is today widespread in open country in Africa. The genus has been reported from the Mio-Pliocene of Lothagam, Kenya, and the basal Pliocene of Wadi Natrun, Egypt (the latter record requires confirmation, as the sole specimen known from the site is fragmentary). All the Lothagam fossils (Harris, 2003) are smaller than the Etosha specimens (Fig. 21). The Wadi Natrun horn-core is broken (Vrba 1997), but its dimensions fall within the range of metric variation of *Damalcra neanica* from Langebaanweg.

Although the early stages of the evolution of alcelaphines are still relatively obscure, it would seem that the tribe originated in southern Africa and spread northwards as
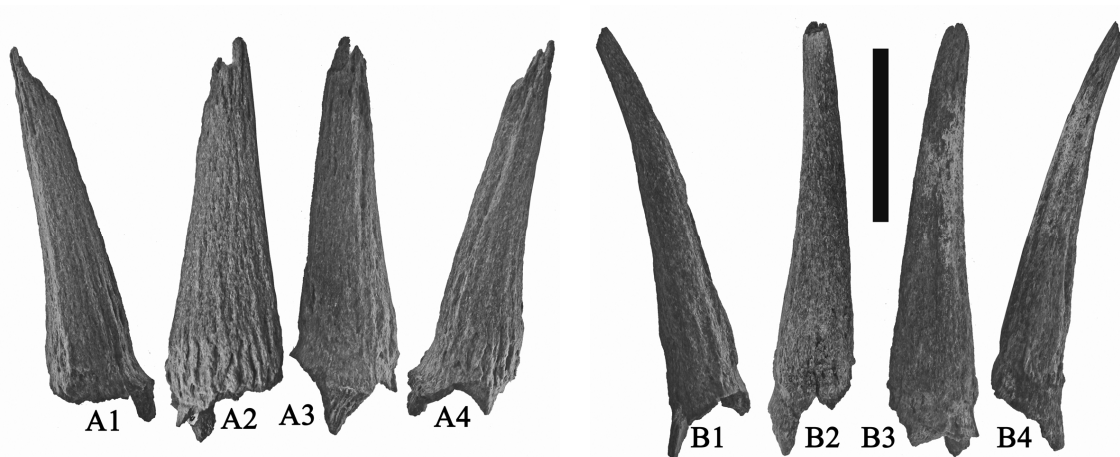

Figure 20: *Damalacra acalla*, A) ET 21'07, right horn-core, B) ET 54'07, right horn-core, 1) anterior, 2) lat-
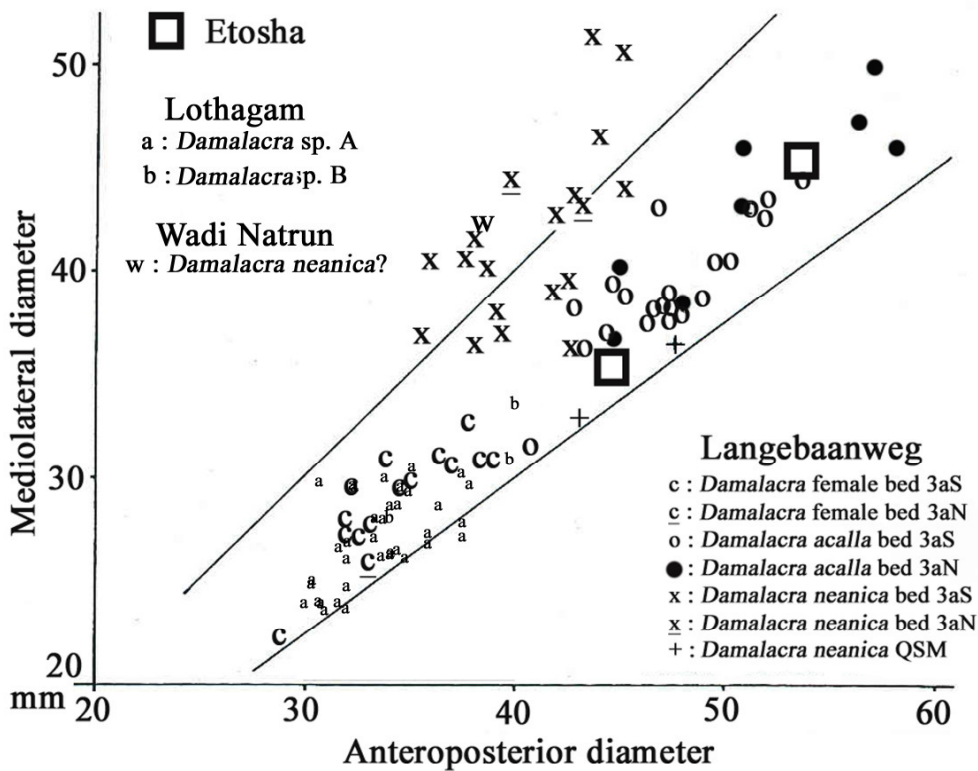

Figure 21: Bivariate plot of anteroposterior and mediolateral diameter of the base of the horn cores of *Damalacra* spp. The two specimens from the Etosha Pan Clay Member (large open squares) fall within the range of variation of *Damalacra acalla*.

open country habitats developed there. The Etosha horn-cores are sufficiently close morphometrically to those from Langebaanweg, that we may postulate similar habitats in the two areas and similar biochronology.

Although the diversity of vertebrates from the Etosha Pan Clay Member of the Andoni Formation is not very great, the overall aspect of the fauna suggests links to the Mio-Pliocene occurrences at Langebaanweg, South Africa, indicating an age between 5 and 6 Ma for the Namibian sites.

Flora and fauna from the Ekuma Delta Member of the Andoni Formation

Plant remains are common in the Ekuma Delta Member of the Andoni Formation, in particular casts of root systems and tree trunks. By their nature these fossils are difficult to identify (Fig. 22 B), but in one case the cast of a tree trunk surrounded by a swarm of narrow roots is sufficiently informative to reveal that it belongs to a palm tree (Fig. 22 A).
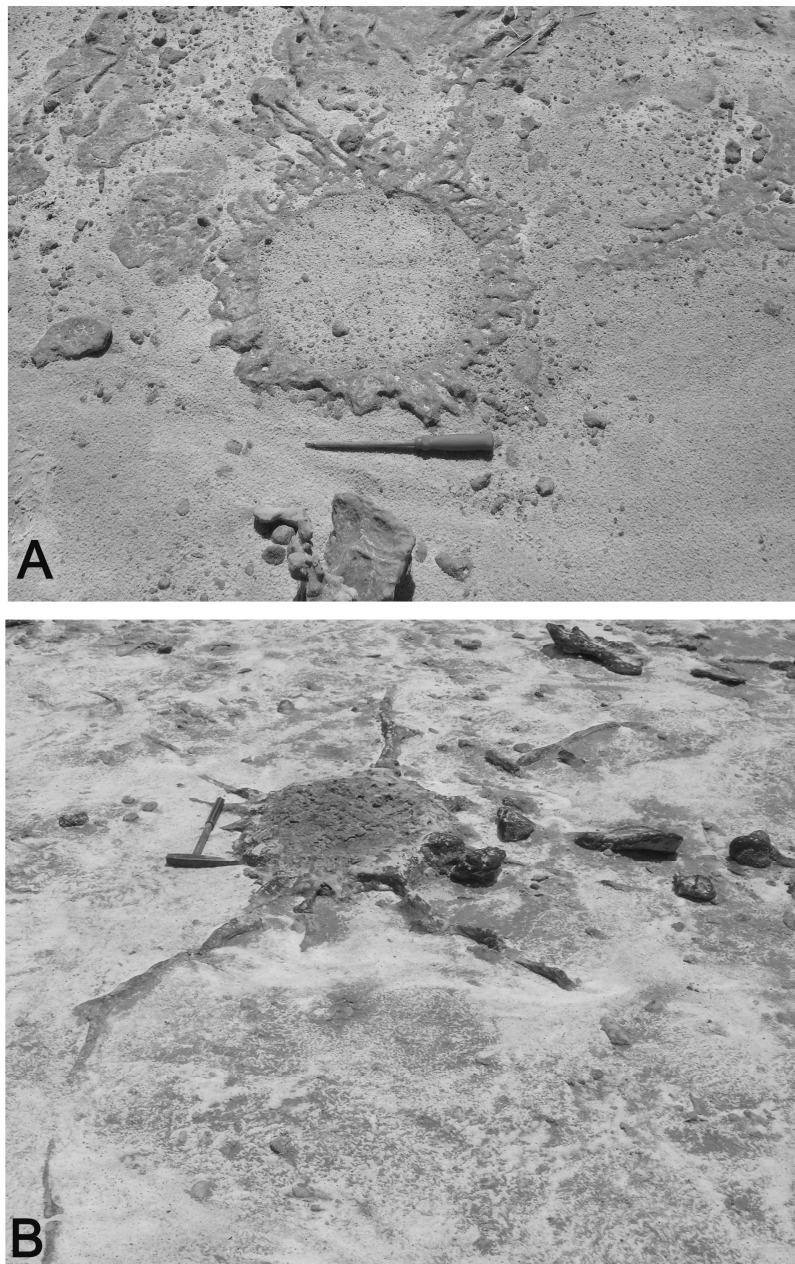
Figure 22: Tree boles and roots in quartzite of the Ekuma Delta Member, Ekuma River Valley, Etosha, Namibia. A) palm tree cast surrounded by dense root system, B) dicoltyledon tree bole and root network (screw driver and geological hammer for scale)

Invertebrates occur in the quartzites of the EDM, the richest deposits consisting of shell banks containing abundant *Bellamya unicolor* (Fig. 23 A) and bivalves (probably *Mutela*) (Fig. 23 B) both of which indicate freshwater deposition and well oxygenated water.

Apart from numerous fish remains which often occur as complete skulls and sometimes even as articulated skeletons (Fig. 25), the vertebrates in the EDM tend to be fragmentary and disarticulated (Fig. 24 D-H). Preliminary identifications of these fos-

sils indicate an age of about 4 Ma for the deposits.

Gastropoda (MP)

Abundant shells and internal molds of freshwater gastropods occur in quartzites of the EDM, sometimes in large concentrations (Fig. 21 A ; 24 A). The shape of the whorls, the finely pointed protoconch and the dimensions serve to identify these snails as *Bellamya unicolor*, a freshwater mollusc common throughout Africa.
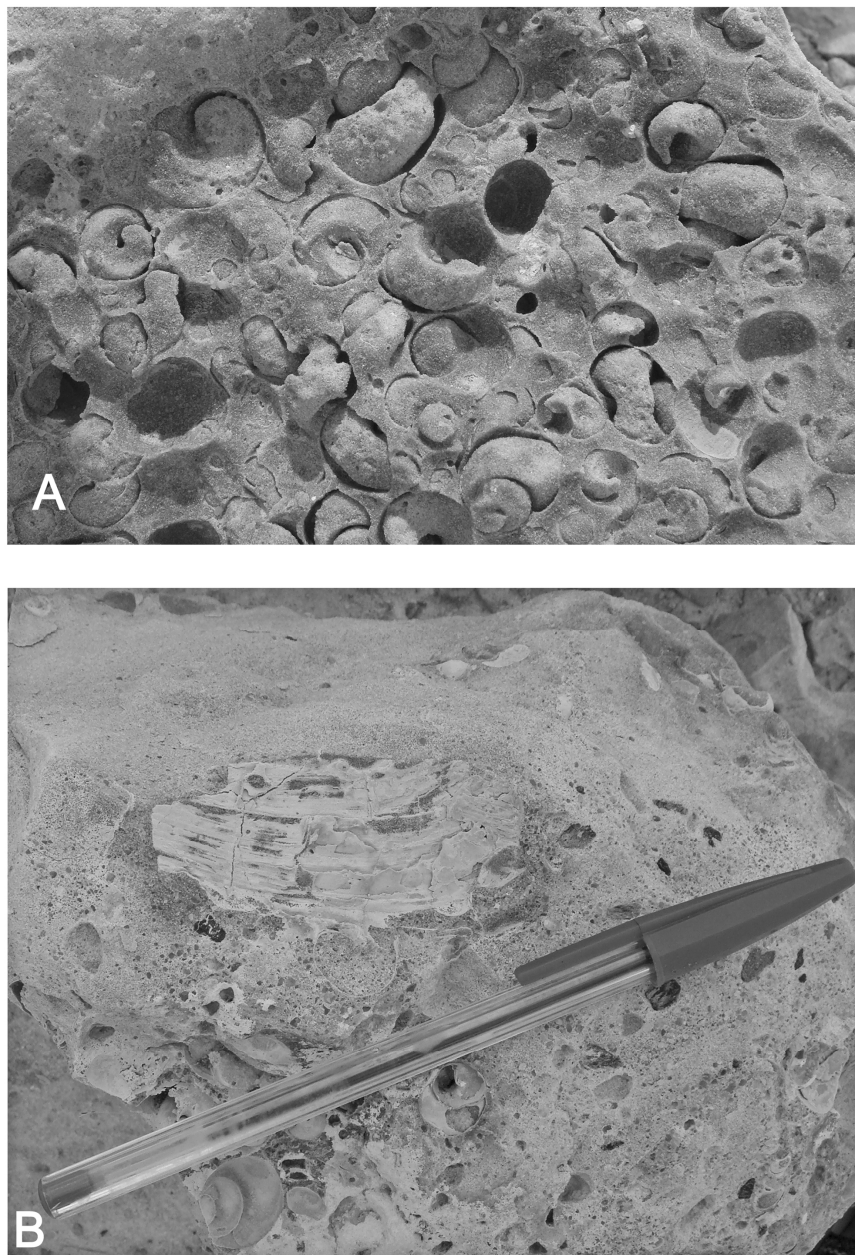
Figure 23: Mollusca in quartzite of the Ekuma Delta Member, Etosha, Namibia. A) a rich concentration of *Bellamya unicolor*, B) a shell of *Mutela* sp. accompanied by *Bellamya unicolor*.

Bivalvia (MP)

Internal molds and steinkern of mutelid bivalves are common in the EDM. The shell is usually absent, but in some individuals the characteristic concentric growth lines of mutelids can be observed (Fig. 23 B ; 24 B). Given the generally poor preservation of the samples, we prefer to identify the shells only to the genus level as *Mutela* sp. There are however, indications of a second species of bivalve at Ekuma, resembling the freshwater Donacidae *Egeria* (Van Damme, pers. comm.). Whatever the genera however, these bivalve specimens indicate the availablity of well-oxygenated, fresh water at the time that the EDM was being deposited.

Pisces (HJ)

The fish remains from the EDM are similar to those from the EPCM, and we accordingly identify them as *Clarias* sp. (Fig. 24 D-H).

Cyclanorbidae

Patterned scutes characteristic of Cyclanorbidae have been found in the EDM (Fig. 24 K).

Pelusios

The scutes of *Pelusios* are common in the EDM (Fig. 24 I-J).

Crocodylia (MP)

Crocodile teeth, scutes, vertebrae and limb bones are frequently encountered in the EDM (Fig. 24 L, 24 M).
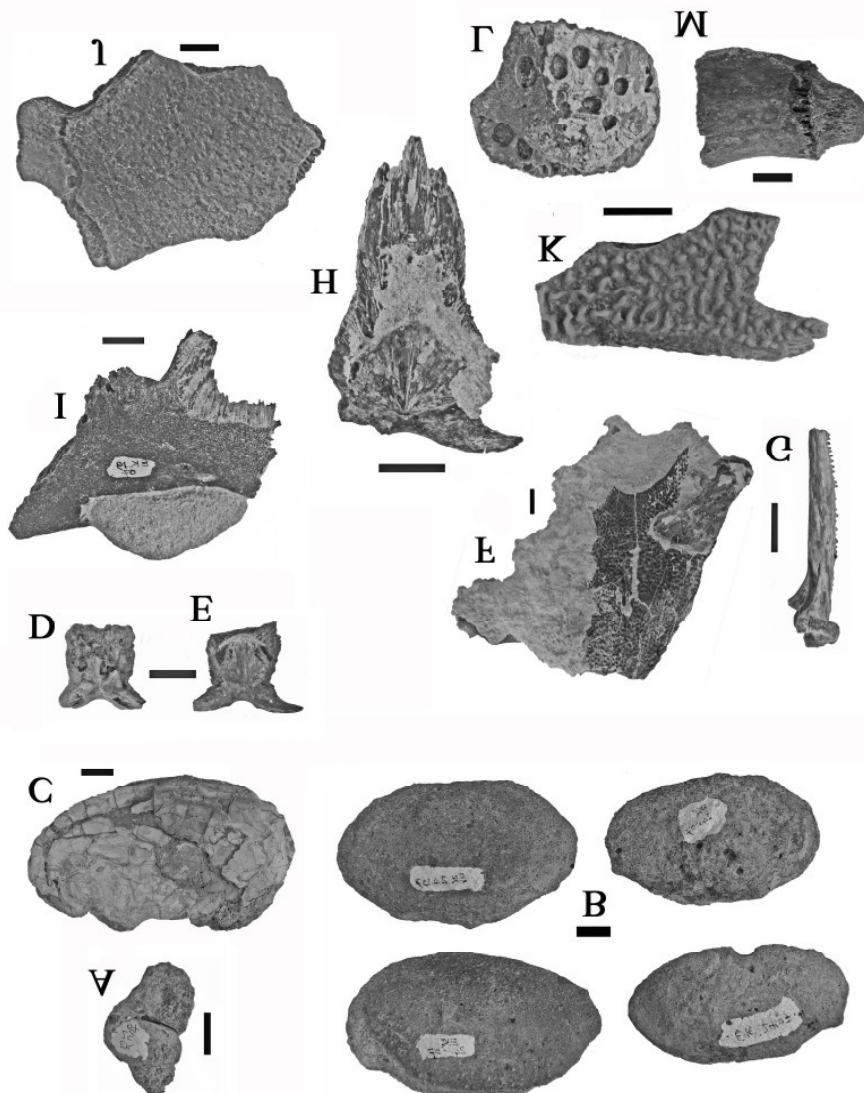
Figure 24: Invertebrates and vertebrates from the Ekuma Delta Member (ca 4 Ma) Ekuma River, Namibia (scale bars : 1 cm except N : 5 cm). A) EK 25'07, *Bellamya unicolor*, shell ; B) EK 24'07, four specimens of *Mutela* sp., internal molds ; C) *Mutela* steinkern ; D-E) *Clarias*, two vomers, ventral view ; F) *Clarias*, skull, dorsal view ; G) *Clarias*, pectoral spine ; H) *Clarias*, vomer, ventral view ; I-J) EK 19'07, *Pelusios* sp., scute, dorsal view ; K) Cyclanorbidae, scute, dorsal view ; L) *Crocodylus* sp., scute, dorsal view ; M) Crocodile vertebra.

Figure 25: EK 52'07, *Clarias* sp., articulated skeleton in quartzite of the Ekuma Delta Member, Namibia.

Aves (Fig. 26, 27, 28, 29)

Two bird bones were collected in the EDM of the Ekuma River valley. GPS 69 Phalanx 1 of posterior digit III (Fig. 28). The size of this phalanx is included in the variation range of the extant species *Phoenicopterus ruber* (Table 1).

EK 21'07 right humerus, fragment of proximal part. This cannot belong to an Anseriform because there is a fossa on the cranial side, at the level of the impressio coracobrachialis.

Bird footprints are locally common in the Ekuma Delta Quartzites (Fig. 29).

Struthio daberasensis (LS, MP & BS).

Two fragments of ostrich egg shell were found on the northern margin of the Stinkwater Peninsula (Fig. 26, 27). The specimens preserve the characteristic pore structure and shell thickness of the species *Struthio daberasensis* (Senut and Pickford, 1995).

Preliminary results of isotope analyses of extant and Holocene eggshells of *Struthio*

camelus from Etosha (Fig. 26 ; Table 5) indicate that they have similar d^{13}C isotope signatures (-6 to -1.8‰) as those from the Central Namib Desert. Both samples inhabit regions of summer rainfall, and the values reflect the presence of C4 plants in their diets. The main difference concerns the values of d^{18}O, which at Etosha, range between 0 and 4‰ whereas in the Central Namib they range from 12 to 16‰. This difference shows that the Namib ostriches consumed water that was more evaporated and lived in an arid environment whereas those from Etosha indicate a more humid environment. The variation observed at Etosha between the extant and Holocene samples is linked to climatic change during the Quaternary, but estimates of the ages of the localities are necessary to interpret the differences in a reliable chronological framework.

The shells of *Struthio daberasensis* from the Namib Desert are discriminating from the point of view of isotope composition. The differences noted reflect the presence of C3 and C4 plants in the central re-

gion and C3 and CAM plants in the south (Ségalen *et al*., 2006, 2007). Furthermore, the central Namib is more arid than the southern part where the localities, being closer to the Atlantic Ocean, are more humid. For the egg shells from Etosha attributed to *Struthio daberasensis*, it is interesting to note that the $d^{18}O$ is similar to that of egg shells from the Southern Namib (ranging between 3 and 9‰). In contrast the $d^{13}C$ is much more enriched ($d^{13}C_{mean} \sim -5.4$‰ n=3 ; versus ~ -9.5‰ n=19), the large range of variation is due to the small quantity of egg shells analysed but suggests the presence of C4 plants. This proportion would otherwise be greater than in the Central Namib for this period. Nevertheless the preliminary interpretations need to be confirmed by isotopic analyses of larger samples of egg shells.
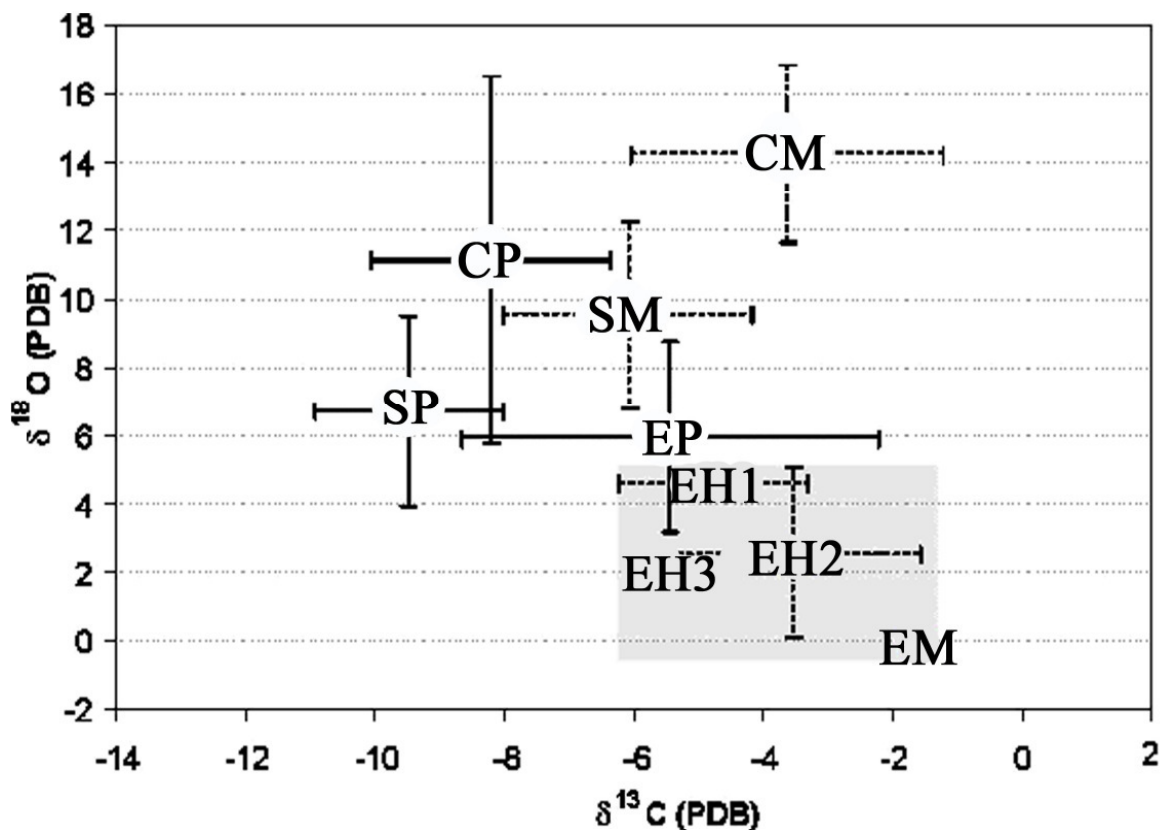
Struthio camelus

Struthio daberasensis

CM - Central Namib Modern
SM - Southern Namib Modern
EM - Etosha Modern

CP - Central Namib Pliocene
SP - Southern Namib Pliocene
EP - Etosha Pliocene

EH1 - Etosha Holocene (GPS 112)
EH2 - Etosha Holocene (GPS 117)
EH3 - Etosha Holocene (161107)

Figure 26: $\delta^{13}C$ et $\delta^{18}O$ of extant and fossil ratites of Namibia (GPS 112, 18°37'43.3''S : 16°12'01.7''E ; GPS 117, 18°41.770'S : 16°04.012'E).

Sample	δ^{13}C	*Struthio camelus* (modern) δ^{13}C	*Struthio camelus* (Holocene) δ^{18}O	*Struthio daberasensis* (Pliocene) δ^{18}O
ETO GPS 75	-8.1			7.6
ETO GPS 78 1	-6.3			2.7
ETO GPS 78 2	-1.9			7.5
ETO GPS 102 1	-7.1		5.3	
ETO GPS 102 2	-4.4		4.9	
ETO GPS 102 3	-3.6		4.6	
ETO GPS 102 4	-5.2		4.4	
ETO GPS 102 5	-3.6		4.1	
ETO GPS 117 1	-6.3		3.8	
ETO GPS 117 2	-2.7		1.7	
ETO GPS 117 3	-3.2		5.2	
ETO GPS 117 4	-1.5		-0.5	
ETO 161107 1	-1.6	-0.2		
ETO 161107 2	-5.5		1.9	
ETO Modern	-1.5	-0.3		
Central Namib (n = 11)	-3.6	14.2		
Central Namib (n = 16)	-8.2	14.2		11.1
Southern Namib (n = 21)	-6.1	9.6		
Southern Namib (n = 19)	-9.5			6.7

Table 5: δ^{13}C and δ^{18}O of fossil and extant ratite egg shells from Etosha and the Namib Desert, Namibia.
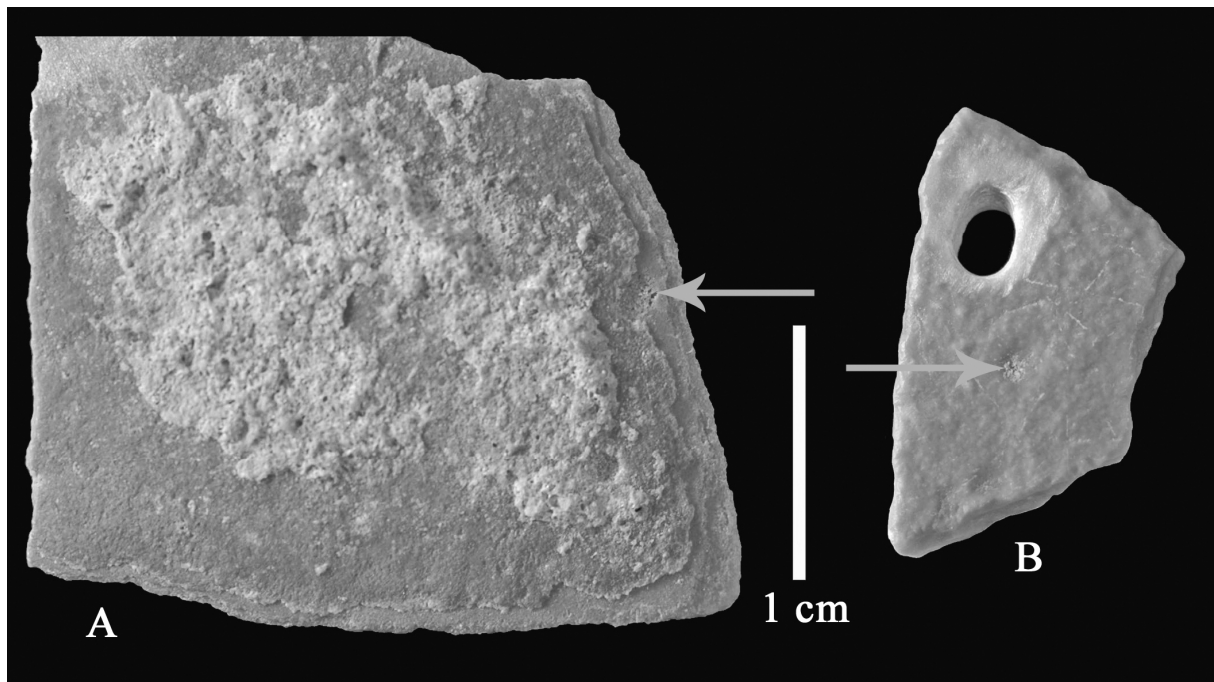
Figure 27: *Struthio daberasensis* fossil egg shells from the Andoni Formation at Stinkwater Peninsula, Etosha Pan, Namibia A) GPS 75 (18°36'58.0''S : 16°45'08.7E'') and B) GPS 78 (18°36'13.2''S : 16°41'51.9''E) (arrows point to pores, the dimensions and scattering are characteristic of this species).

Pedetidae (PM)

A molar of a pedetid from the Ekuma Delta Member is curved from occlusal surface to root, and is very hypsodont. EK18'07 (Fig. 30 A) is interpreted as a P4/ due to the strong anterior curvature of its basal part. The posterior lobe is higher than the anterior one (the opposite is the case in m/3). The tooth is almost unworn and preserves both grooves : a small hypostria 1.3 mm tall, and a mesostria, 7.4 mm tall, which terminates almost at the base of the crown. The occlusal length of the tooth is 3.14 mm and its basal length is slightly greater at 3.27 mm. The occlusal breadth of the anterior lobe is 2.96 mm and its basal breadth is 3.40 mm. The occlusal breadth of the posterior lobe is 2.94 mm and at its base it is 4.20 mm. The height of the tooth is 10.7 mm, but its base is damaged. The buccal closure of the base of the

Figure 28: EK 68'07, Pedal phalanx of a wading bird, Phoenicopteridae, from the Ekuma Delta Member, Ekuma River valley near the Horse Camp, Namibia (dorsal, lateral, plantar, proximal and distal views).
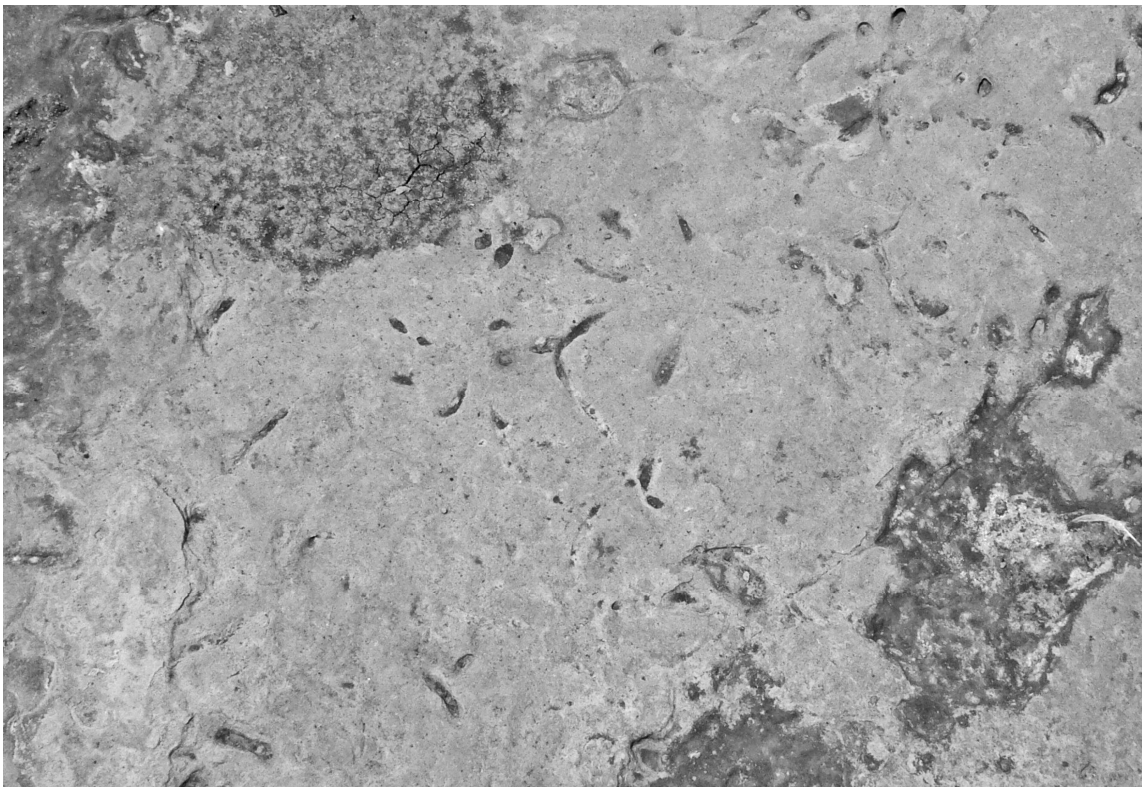
Figure 29: Bird foot prints and other traces in quartzite of the Ekuma Delta Member, Ekuma River Valley, Etosha, Namibia. The dimensions of the foot prints accord with those of ducks and flamingos.
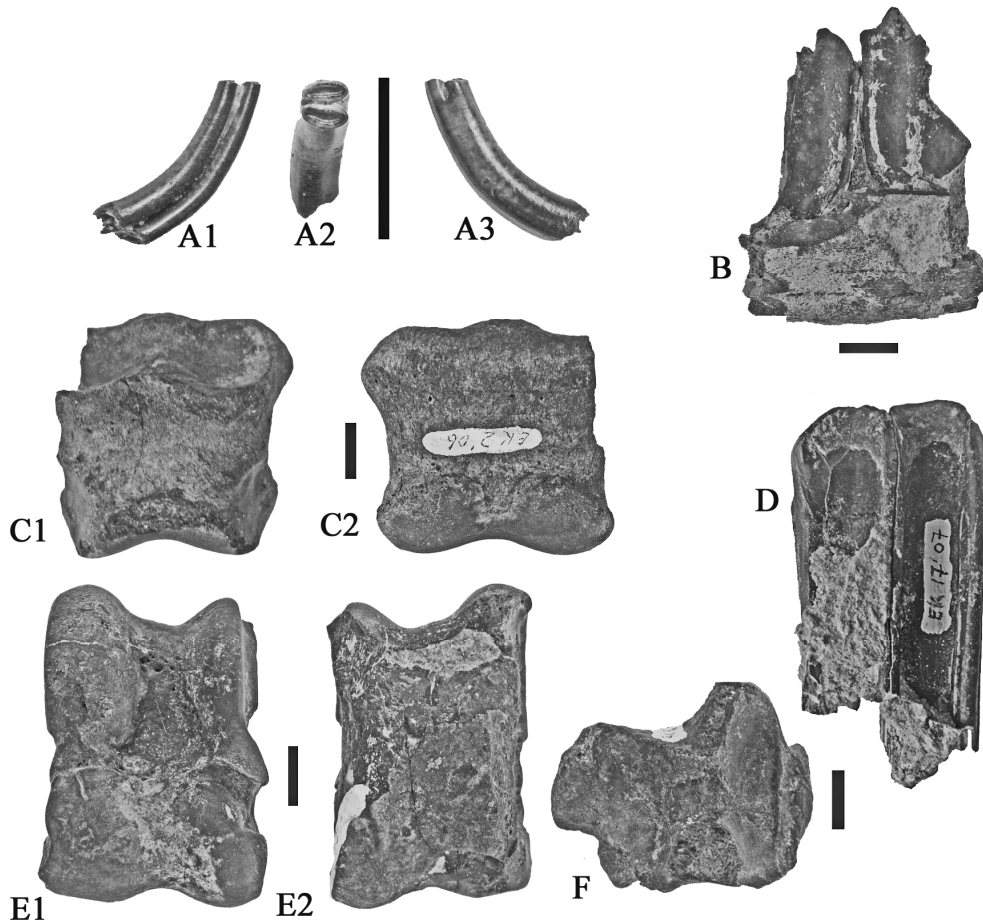
Figure 30: Mammals from the Ekuma Delta Member, Etosha, Namibia. A) EK 18'07, *Propedetes* sp. P4/, A1) lingual, A2) occlusal and A3) buccal views ; B) EK 1'06, *Redunca darti*, juvenile mandible fragment containing damaged teeth, buccal view ; C) EK 2'06, *Hipparion* sp. second phalanx, C1) dorsal and C2) plantar views ; D) EK 17'07, *Hipparion* sp. ectoloph of upper cheek tooth ; E) EK 9'06, Bovidae, left talus, E1) anterior and E2) posterior views ; F) EK 8'06, Bovidae distal tibia, distal view.

mesostria, as well as the absence of cementum indicates that this specimen belongs to a new genus of pedetid being described from the Sperrgebiet, Namibia. Its hypsodonty exceeds all the other known teeth of this genus, and it is therefore most likely the youngest.

Comparable teeth, belonging to *Propedetes*, have been found in various localities in Namibia (Tree Pan, Awasib) but no P4/ is known from these localities. Such a degree of hypsodonty is however less than that expressed in *Pedetes*. At Taung, South Africa, *Pedetes gracilis*, which we were able to study, has a longer and more curved P4/ and its height is 19 mm. In addition the mesostria does not close, the tooth is rootless, and there are traces of cementum.

In conclusion, The Ekuma pedetid likely represents a new species of *Propedetes*, probably older than the Laetoli (Davies, 1987) and Taung species (Broom, 1937) but younger than the species from the *Diamantornis laini* level (ca 10-8 Ma) (Senut and Pickford, 1995).

Proboscidea (MP)

Loxodont enamel fragments are common in the EDM, and there is a partial skeleton eroding out on the banks of the Ekuma River. However, none of the tooth fragments is complete enough for confident identification, but enamel is as thick as in material from the Etosha Pan Clay Member and the crown is relatively low. We attribute these specimens to *Loxodonta* cf *cookei*.

Specimen	Total height	Height of mesostria
Rooilepel RL 16'94, P4/	l0.7	7.4
Ekuma EK 18'07, P4/	13.0	13.1
Taung 4194c, P4/	19.0	19.0

Table 6: Measurements (in mm) of the P4/ of pedetids from Namibia and South Africa.

Rhinocerotidae (CG)

Material

A left talus Ekuma EK 064 (Fig. 31 A), two first central phalanges, one abaxial second phalanx, a distal metapodial, a fragment of left magnum, and a fragment of left pyramidal, all numbered EK 063, were found close together, and thus probably represent a single individual. Only the talus, the two incomplete carpals and a first phalanx are well enough preserved for study.
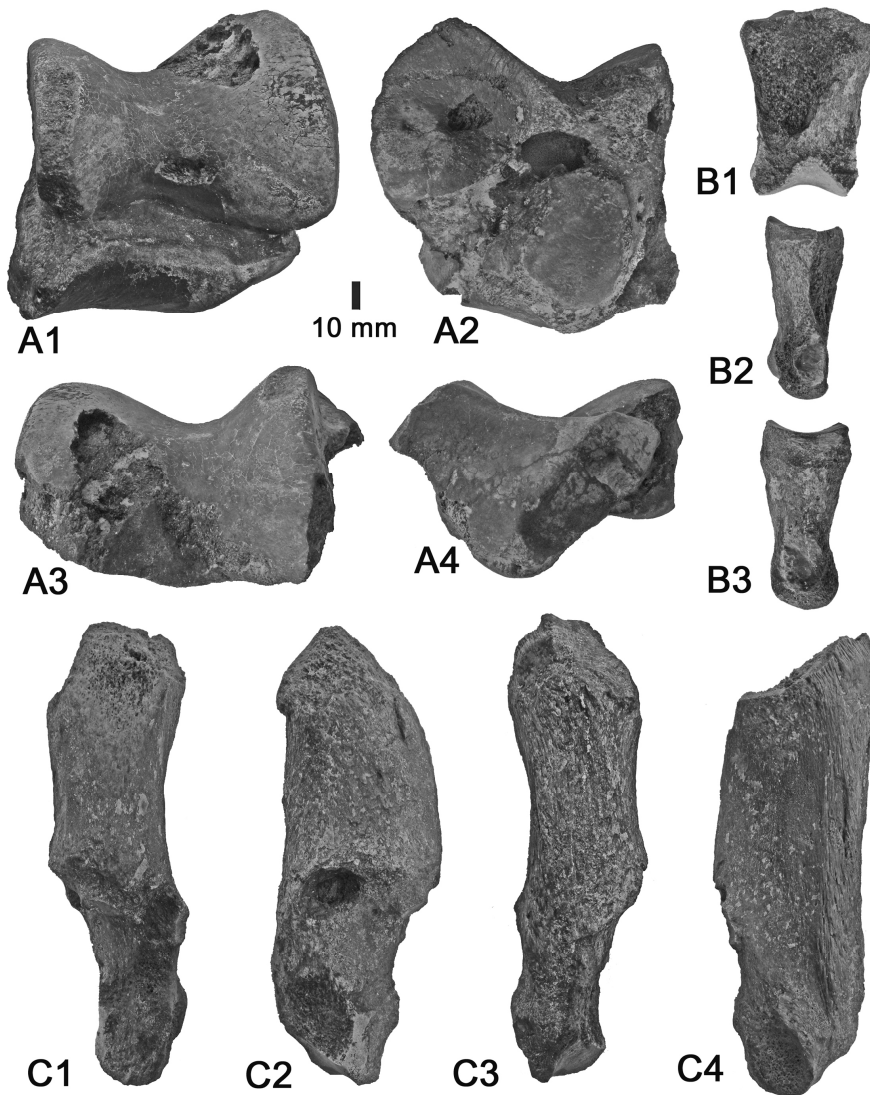
Figure 31: (A) EK 66'07, *Ceratotherium praecox* and (B, C) EK 67'07, *Hippopotamus* sp. from the Ekuma Delta Member (ca 4 Ma). A1) dorsal, A2) plantar, A3) cranial and A4) caudal views of left talus ; B1) dorsal, B2) lateral and B3) medial views of central 1st phalanx ; C1) cranial, C2) medial) C3) caudal and C4) lateral views of left calcaneum.

Magnum :

The bone which lacks the posterior apophysis and a small part of the lateral margin of the anterior surface, resemble that of extant *Ceratotherium simum* but are taller and narrower. The anterior surface has a rounded pentagonal contour which is asymmetric distally. The medial transverse extension is pointed but not very strong, but is better developed than in extant *C. simum*. The proximal articulation is wide. The articular height is at least 66 mm. For 11 specimens of *Ceratotherium praecox* from Laetoli (Tanzania) Hadar (Ethiopia) and Nkondo (Uganda), this dimension ranges from 60 to 70 mm (mean 65.05, standard deviation 3.037). It reaches 78.5 mm in *C. germanoafricanum* from Olduvai, Tanzania and 56 mm in fossil *Diceros bicornis* from Olduvai.

Pyramidal :

This specimen lacks the antero-external surface. It resembles that of extant *C. simum* but differs in its proportions : it is taller and slightly narrower. The antero-external surface is slightly broader than tall. The breadth is at least 58 mm. In 15 specimens of *Ceratotherium praecox* from Laetoli and Nkondo it ranges in dimensions from 57 to 69 mm (mean 61.7 mm, standard deviation 3.453). It ranges from 72.5 to 74 mm (mean 73.5 mm) in three fossil specimens of *C. simum* from the Afar (Ethiopia) and Olduvai, and from 56 to 57.5 mm (mean 56.83 mm) for three fossils of *D. bicornis* from Laetoli and Olduvai.

Talus :

This bone is relatively well preserved, save for the postero-distal quarter of the medial surface. The morphological characters are very close to those of extant *C. simum*. The articular pulley is broad and deep (Fig. 28 A1, A2, A3). The distal tubercle of the medial surface is positioned well above the distal margin. The distal articulation has a weakly concave anterior margin, without an encoche between the facets for the navicular and cuboid ; these facets are not offset (Fig.

28 A4). All these characters are typical of the genus *Ceratotherium*. The dimensions are provided in Table 7. They are close to the upper limit of a sample of 10 to 16 *Ceratotherium praecox* from Hadar, Laetoli and Kanam W (Kenya), and the mean values of a sample of 6-9 *C. germanoafricanum* from East Turkana (Kenya), Omo-Shungura (Ethiopia), Olduvai and Hadar. They exceed most of the maximal values obtained from a sample of 11 to 12 extant *C. simum*, and also those of 2 fossil *C. simum* from Omo-Shungura and Olduvai. They are much larger than a sample of 23 to 27 extant *D. bicornis* and 4 fossil *D. bicornis* from East Turkana and Omo.

Axial first phalanx :

This phalanx is 54.5 mm long, and its greatest proximal breadth is 60 mm.

Identification:

Morphologically, the rhino from Ekuma belongs to the genus *Ceratotherium*. The dimensions and proportions of the talus are compatible with those of a large *C. praecox* or a medium-sized *C. germanoafricanum*, but the height of the magnum and the breadth of the pyramidal support the former identification. The Ekuma rhinoceros is thus identified as *Ceratotherium praecox* Hooijer & Patterson, 1972.

Biostratigraphic and palaeoenvironmental implications:

The species *C. praecox* is frequently reported from the Neogene of Africa (Hooijer & Patterson, 1972; Guérin, 1979, 1980, 1985, 1987, 1994). It was originally defined at Kanapoi (Kenya ; 4.5 Ma). In the same country it is also present at Lothagam-1 Members B and C (7.2 to 5.5 Ma), Ekora (4 to 3.5 Ma), in the Aterir Beds (4 Ma), in the Chemeron Formation loc. JM 507, at Koobi Fora (Kubi Algi, 4 to 2.5 Ma), at Lukeino (6 to 5.7 Ma), and at Mpesida (6.5 to 6 Ma). *C. praecox* is also known from Ethiopia at Omo (Mursi and base of the Shungura Formations, more than 4 to 3 Ma), from Hadar (Sidi Hakoma, 3.4 to 3.1 Ma). It

Talus	EK 064					
Maximum length		106				
Height		ca 102				
DAP int.		ca 69				
DT artic.dist.		ca 87.5				
DAP artic.dist.		62				
Dist. 2 lips		84				
DT dist.		ca 91				

Ceratotherium praecox

	N	mean	min.	max.	std dev	coef. var.
Maximum length	16	100.1	92.5	112.5	5.4	5.4
Height	15	91.9	82.5	103	5.4	5.9
DAP int.	10	61.7	57	67	3.7	6.0
DT artic.dist.	14	81.5	70	92	5.7	7.0
DAP artic.dist.	11	49.0	39	60	5.9	12.1
Dist. 2 lips	15	70.5	67	79.5	3.9	5.5
DT dist.	15	89.3	83.5	101	4.6	5.2

Ceratotherium germanoafricanum

	N	mean	min.	max.	std dev	coef. var.
Maximum length	9	109.4	104	116	4.9	4.5
Height	9	101.9	94	112	7.3	7.2
DAP int.	7	68.5	65	74.5	3.8	5.5
DT artic.dist.	9	91.8	81.5	102.5	6.2	6.7
DAP artic.dist.	6	56.0	50.5	66	5.7	10.1
Dist. 2 lips	8	76.4	68	84	5.4	7.0
DT dist.	9	97.7	90.5	106	4.9	5.0

Ceratotherium simum **extant**

	N	mean	min.	max.	std dev	coef. var.
Maximum length	12	95.1	88	111	6.3	6.7
Height	12	84.5	80	92	3.9	4.6
DAP int.	12	58.5	53.5	65	3.6	6.1
DT artic.dist.	11	80.0	74	86	4.6	5.7
DAP artic.dist.	11	48.0	44	52	2.7	5.6
Dist. 2 lips	11	64.9	60	71	3.2	5.0
DT dist.	12	86.5	81	93	3.8	4.4

Ceratotherium simum **fossils**

	N	mean	min.	max.		
Maximum length	2	98.5	95	102		
Height	2	87.0	84	90		
DAP int.	2	62.2	60.5	64		
DT artic.dist.	2	78.0	77	79		
DAP artic.dist.	1	50.0	50	50		
Dist. 2 lips	2	65.5	62	69		
DT dist.	2	87.5	86	89		

Table 7: Measurements in mm of the Ekuma rhino talus and comparisons with extant and fossil *Ceratotherium* and *Diceros* species.

Diceros bicornis **extant**						
	N	mean	min.	max.	std dev	coef. var.
Maximum length	25	84.8	78	96	4.4	5.2
Height	23	77.9	73	88	4.2	5.4
DAP int.	27	56.0	50.5	61	2.5	4.5
DT artic.dist.	23	68.7	60	79	4.4	6.4
DAP artic.dist.	23	43.9	40	49.5	2.7	6.2
Dist. 2 lips	25	62.6	55.5	73	4.3	6.9
DT dist.	26	75.3	68.5	85.5	4.4	5.8

Diceros bicornis **fossils**					
	N	mean	min.	max.	std dev
Maximum length	4	79.5	70.5	94	10.3
Height	4	78.2	73	90	8.1
DAP int.	4	54.5	50.5	63.5	6.1
DT artic.dist.	4	67.2	59.5	82	10.2
DAP artic.dist.	4	42.2	37.5	50.5	5.8
Dist. 2 lips	4	52.9	47	61.5	6.2
DT dist.	4	73.2	63.5	91.5	12.5

Table 7: (continued)

has also been reported from Laetoli (3.8 to 3.5 Ma) in Tanzania and in the Nkondo (5 Ma), Warwire (4.5 Ma) and Hohwa Formations (2.3 Ma) in Uganda. The species is also present in South Africa at Langebaanweg-E quarry (5 to 4 Ma), Limeworks Cave-Makapansgat (3.4 to 3 Ma) and at Swartlintjes Farm, Hondeklipbaai (Namaqualand, Cape Province). Finally, Likius (2002) identified it in the Pliocene of Tchad at Kollé (5 to 4 Ma) and Koro Toro (3.5 to 3 Ma). *C. praecox* is thus known from deposits in eastern, central and southern Africa ranging in age between 7 and 2.5 Ma. It is likely the ancestor of *C. mauritanicum*, *C. germanoafricanum* and *C. simum* of the Quaternary, which continued the same evolutionary tendencies : hypsodonty, extension towards the rear of the lingual extremity of the protoloph of the upper cheek teeth lowering of the head, and passage towards a graviportal locomotion. *C. praecox* was a denizen of the savannah, grazing mainly on grass.

Equidae (V. Eisenmamm, pers. comm.)

The equid *Hipparion* is represented in the EDM by a characteristic axial phalanx (Fig. 30 C), showing the distal narrowing that is not as well developed in *Equus*. An unworn upper cheek tooth ectoloph (Fig. 30 D) shows the medium degree of hypsodonty

(66 mm tall x 33 mesio-distal length near apex, 29 mm mesio-distal length near cervix) characteristic of Pliocene examples of this genus.

Hippopotamidae (M. Faure, pers. comm.)

The Ekuma deposits yielded two bones of *Hippopotamus*, EK 064, left calcaneum (Fig. 31 C C) ; first central phalanx (Fig. 31 B), and diverse fragments including a badly damaged navicular and some sesamoids.

Calcaneum: The bone is poorly preserved, the sustentaculum tali is broken and the two extremities are incomplete. It is however, possible to compare two of its dimensions with those of a sample of extant *Hippopotamus amphibius* (Faure, 1985). The height is greater than 180 mm. For 16 specimens of extant *Hippopotamus amphibius* this dimension ranges from 159 to 204 mm (mean 177.8 mm, standard deviation 13.558). The transverse diameter of the diaphysis above the sustentafculum is 43 mm. For 16 specimens of extant *Hippopotamus amphibius* this dimension ranges from 31 to 41 mm (mean 34.7 mm, standard deviation 3.177).

Phalanx I central: It is broken along its anterior surface and at the distal extremity. It is 72 mm long, its proximal breadth attains 50.5 mm and the transvers diameter of the

diaphysis is 38.5 mm. The homologous measurements for a posterior phalanx I central of extant *Hippopotamus amphibius* in the Musée d'Histoire naturelle de Lyon (n° OST 361) are respectively 68.5, 42 and 30.5 mm.

Identification: The calcaneum and the central first phalanx from Ekuma undoubtedly belong to a hippopotamus, but the preservation is too poor for species identification. Nevertheless these two bones are the same length as those of a medium sized extant *Hippopotamus amphibius* and their breadth is greater. More than 15 species of the genus *Hexaprotodon* (in the broad sense) and *Hippopotamus* are known in the Pliocene and Pleistocene of Africa. (Gèze, 1980, 1985 ; Boisserie, 2005). Only three are more or less compatible in dimensions and age with the Ekuma specimens : *Hexaprotodon harvardi* Coryndon, 1977, *Hexaprotodon protamphibius* Arambourg, 1944 and *Hippopotamus kaisensis* Hopwood, 1926. The first two are somewhat smaller than *H. amphibius* and their extremities are more slender ; the last is the same size as *H. amphibius* but its extremities are more elongated. It is therefore necessary to obtain better material before the Ekuma hippo can be identified.

Bovidae (JM & MP)

Bovid remains are quite common in the Ekuma Delta Member, but most of them are damaged. There are however two horn cores and a frontlet with both horns and partial dentition. Bovid dental postcranial remains from the same area (Fig. 30 B, E, F) suggest that there are two or three additional species of bovid in the deposits, but they are not identifiable at the species level.

Tribe Reduncini
Genus *Redunca* Smith, 1827
Redunca aff. *darti* Wells & Cooke 1956

ETO 19'06, a left horn-core with almost circular section, (49.4 mm x 53.5 mm) without keels. The thickening of the frontal is transversal to a suture fades out at the posterior base of the horn (Fig. 32 B). It is difficult to discern how many surfaces there are due to the almost round section and the very attenuated keels.

There is no hint of frontal sinuses. The frontal is thick (even though not well preserved), the pedicle is broad, especially anteromedially. There is a shallow but large post-cornual fossa.

The anterior zone of the base of the horn is inflated, clearly visible in lateral and medial views. In anterior view the horn is quite straight, with a slight inclination towards the exterior. In lateral and medial views, it is possible to observe that towards its apex the horn curves forwards.

The anterior surface is convex and the posterior one flattened which makes the section almost circular with the anteroposterior diameter slightly less than the mediolateral one. Because of this, the medial and lateral surfaces are difficult to delimit, medially the horn is slightly keeled, whereas the transition between the anterior and lateral surfaces is marked by deep, vertical grooves.

The ornamentation is strong, comprising vertical grooves, especially prominent postero-laterally, and anterolaterally there are at least three subhorizontal growth ridges arranged parallel to each other.

EK 1'07 (ETO 231) a right horn-core with a subrounded section, is smaller (37.9 mm x 44.1 mm) than the previous specimen (Fig. 32 A). Despite the poor preservation of the horn-core, it is possible to see a shallow but extensive post-cornual fossa. Overall, this fossil looks like a gracile version of the preceding one. The base of the horn is slightly inflated anteriorly, the anterior surface is convex, but up to the apex there are deep grooves which have a tendency to become keels. The posterior surface is flattened basally becoming convex towards the apex. The delimitation between the anterior and posterior surfaces is clearer than in the previous specimen, hinting at the presence of keels medially and laterally which fade out progressively towards the apex. In anterior and posterior views, the horn is straight, while in lateral and medial views it is possible to see that the horn is inclined backwards near the base and curves forwards near the apex.
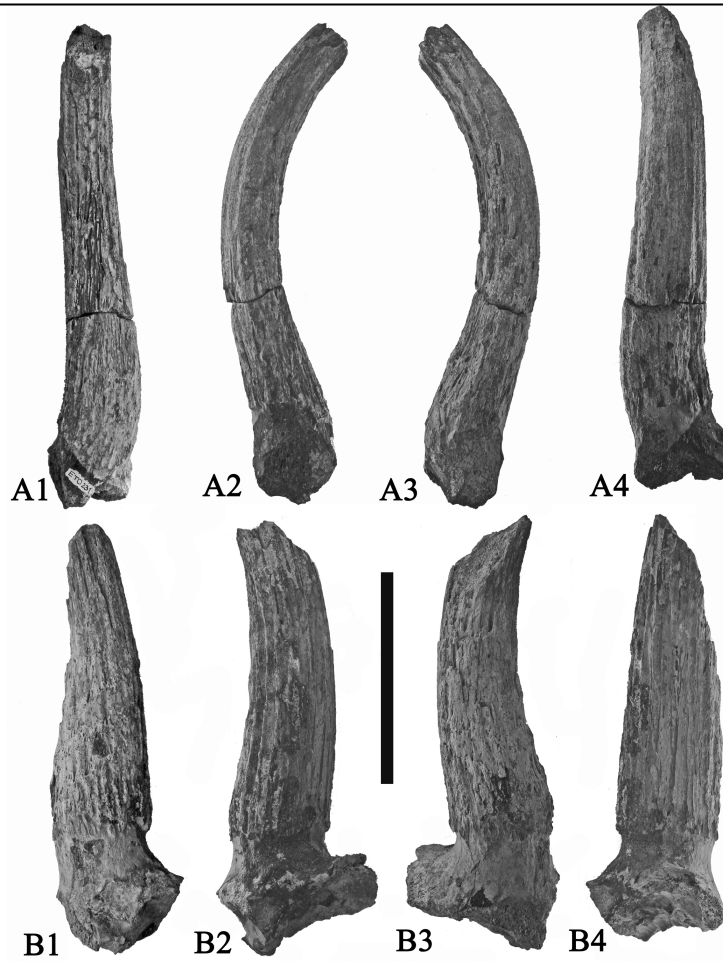
Figure 32. *Redunca* aff. *darti*, from the Ekuma Delta Member, Namibia, A) EK 1'07, right horn-core, B) ETO 19'06, left horn-core, 1) anterior, 2) lateral, 3) medial, 4) posterior views (scale : 10 cm).
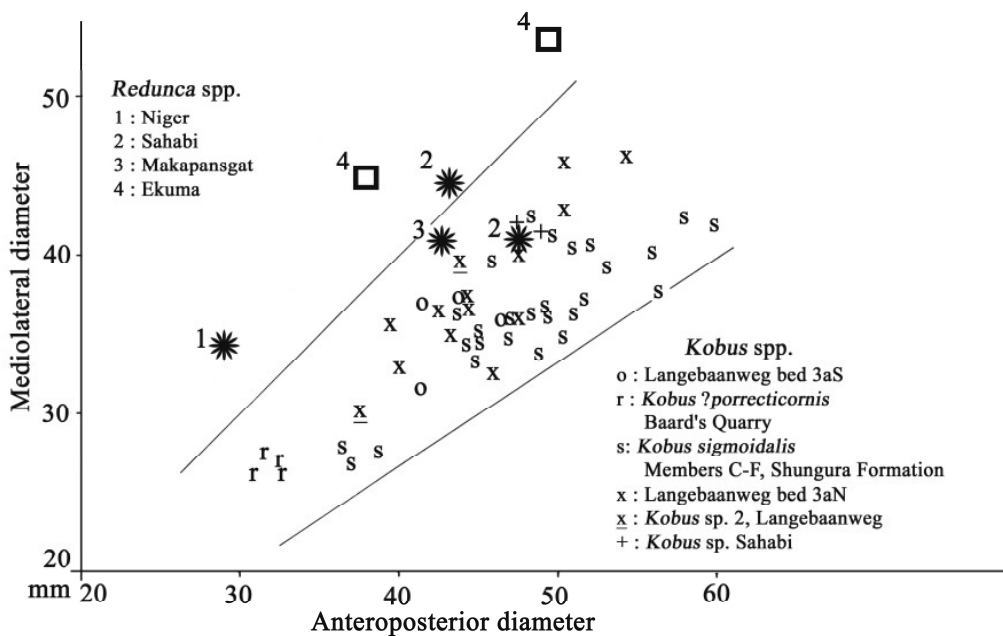

Figure 33. Bivariate plots of anteroposterior and mediolateral diameters of horn cores of *Redunca* spp. The two specimens from the Ekuma Delta Member are closest to *Redunca darti* from Makapansgat, South Africa and fossils attributed to this species from Sahabi, Libya.

Discussion

The morphological features of these two horn-cores are encountered in representatives of the tribe Reduncini. In general, they differ from those of species of *Kobus* by the transverse section of the horn-core, which is more circular, even though a few individuals have medio-lateral diameters greater than the anteroposterior one. Lehmann & Thomas (1987) employed this more circular morphology of the horn-core section to attribute to *Redunca* aff. *darti* Wells & Cooke (1956) two frontals and a horn-core from Sahabi, Libya, distancing them from *Kobus subdolus* from Langebaanweg (Gentry, 1980) and from the ruminants from Mpesida and Lukeino (Thomas, 1980). The two best preserved horn-cores from Ekuma have almost circular transverse sections, in which the transverse diameter (mediolateral) is slightly greater than the anteroposterior one (Fig. 33). This is also the case in *Redunca* aff. *darti* from Niger (Pickford et al, 2008) and the frontals described from Sahabi by Lehmann & Thomas (1987), despite the fact that the second specimen from Sahabi has an anteroposterior diameter somewhat greater than the transverse one. As in *Redunca darti* from Makapansgat, South Africa (the type locality) and in the Sahabi form, those from Ekuma are inflated near the base of the horn-core, clearly visible in lateral and medial views, and the apex of the horn curves forwards. Apart from the localites cited above, *Redunca darti*, or a similar species, occurs at Langebaanweg, where two specimens (L10672 and L1748) present the characteristsic features of *Redunca*, although the lateral compression is slightly stronger, as in one of the specimens from Sahabi. In the Natural History Museum, London, there is a horn-core (NHM M 15925) from Kanam Museum Cliff (Kenya) (Kent, 1942) which is comparable in morphology and dimensions to the Ekuma *Redunca*.
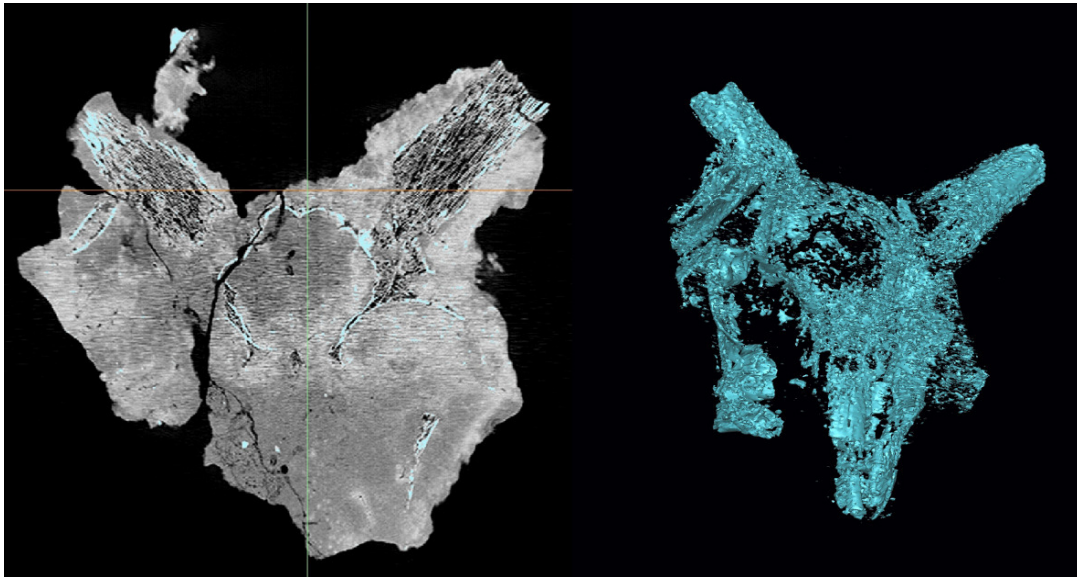
Figure 34: EK 5'07, fragmentary skull of a reduncine embedded in quartzite. Left image is a section through the block showing the quartzite and bone, right image is a 3D view after digital removal of matrix.

EK 05'07, a fragmentary reduncine skull embedded in quartzite preserves the posterior part of the palate and much of the frontals and the two horn-cores (Fig. 34). Interpretation is difficult due to the cover of matrix, but it seems that the two horn-cores are inserted far apart in the frontals, diverging strongly towards the exterior. The transverse section of the right horn-core about 110 mm from the base is almost circular, without any signs of compression. Both M3/s are preserved (L= 24-26.7, W=15.3-16.1) and the roots or alveoli of the anterior molars are present. The molar series is about 65 mm long.

EK 1'06, an unerupted right lower pre-

molar row (p/2-p/4) is approximately 37 mm long, and could correspond to the same species as the skull. The p/4 has an open lingual wall and the mesiolingual conid is directed backwards.

Flora and Fauna from the Poacher's Point Carbonate Member of the Andoni Formation

The Poacher's Point Member of the Andoni Formation comprises a deposit of micro-ooids cropping out extensively along the Oshigambo Peninsula, at Poacher's Point, the Stinkwater Peninsula and at Pelican Island where the ooids are larger, forming oolites up to 2 mm in diameter. In many places these deposits have yielded faunal remains comprising terrestrial snails (Fig. 10) similar to those that live in the Etosha Basin today, but thus far the only vertebrate remains found comprise eggshell fragments attributed to *Struthio camelus*. It is therefore difficult to estimate an age for the sediments, although it is evident that they post-date the Ekuma Delta Member, and are most likely to be Pleistocene, an estimate supported by the eggshelll evidence (Senut & Pickford, 1995). The regional palaeoclimate at the time of deposition was probably sub-humid to semi-arid, as it is today.

Oncolites and stromatolites (AP and CP)

Oncolites occur abundantly on the west flank of Poacher's Point and round the shores and in cliffs along the Stinkwater Peninsula, and more rarely near Oshigambo in the floor of Etosha Pan (Fig. 35-38). These oncolites are polyphase structures, each interruption in growth representing a change from fresh water to evaporitic conditions. The nuclei of the oncolites are varied, ranging from indurated sediment to fragments of pre-existing stromatolites, or even to soft sediment which later developed septaria during desiccation.

Each growth phase represents a return to a more humid climate. Erosional phases can produce either rounded pebbles due to high energy conditions (waves for example) or flatter pebbles produced during paroxysmal storms or in oncolites exposed in outcrops, due to thermal fracture resulting from many cycles of daily temperature changes.

The smectite sediment surrounding the oncolites (sodic smectite, analcime and sometimes halite) is not contemporary with their growth. The sediment originally associated with the growth of the oncolites is a lacustrine limestone containing ostracods, which have been incorporated into the inter-pillar spaces of the oncolites. In thin section abundant spherical globules (168.5 μm in diameter) are visible which probably represent the Chlorophyceae, *Chlorellopsis coloniata*, a thallophyte that is usually associated with lacustrine oncolites and cherts.

Succineidae (MP)

A shell of a succineid gastropod (h x b = 9.8 x 6 mm) (Fig. 39 A) has the same proportions and dimensions as extant *Succinea striata* from Namibia. Connolly (1939) recorded several species of the genus from Namibia, including *S. badia*, *S. arboricola*, and *S. exarata*, which differ from each other in size and shell proportions. The fossil from Poacher's Point is closer in size and shape to *S. striata* than to any of the other species.

Subulinidae (MP)

Subulinid shells are very common in the Poacher's Point Member (Fig. 39 B). They are all referrable to a single species, *Xerocerastus burchelli* (h x b = 17 x 7 h/d 2.43; h x b = 16 x 6.6 h/d; 2.42, h x b =15.7 x 5.7 h/d 2.75). At present there are several species of *Xerocerastus* in Namibia (Connolly, 1939). Van Bruggen (1970) recognised 5 species which differ from each other in dimensions and shell proportions; *X. damarensis* (h/d 2.21-2.61), *X. burchelli* (h/d 2.27-2.46), *X. subteres* (h/d 2.59-3.16), *X. nitens* (h/d 2.00-2.09), *X. hottentotus* (h/d 1.58-1.64) and *X. ovulum* (h/d 1.40-1.61). The material from Poacher's Point is similar in dimensions and shell proportions to two of these species *X. damarensis* and *X. burchelli*, but it appears to be morphologically closer to the latter than to the former.
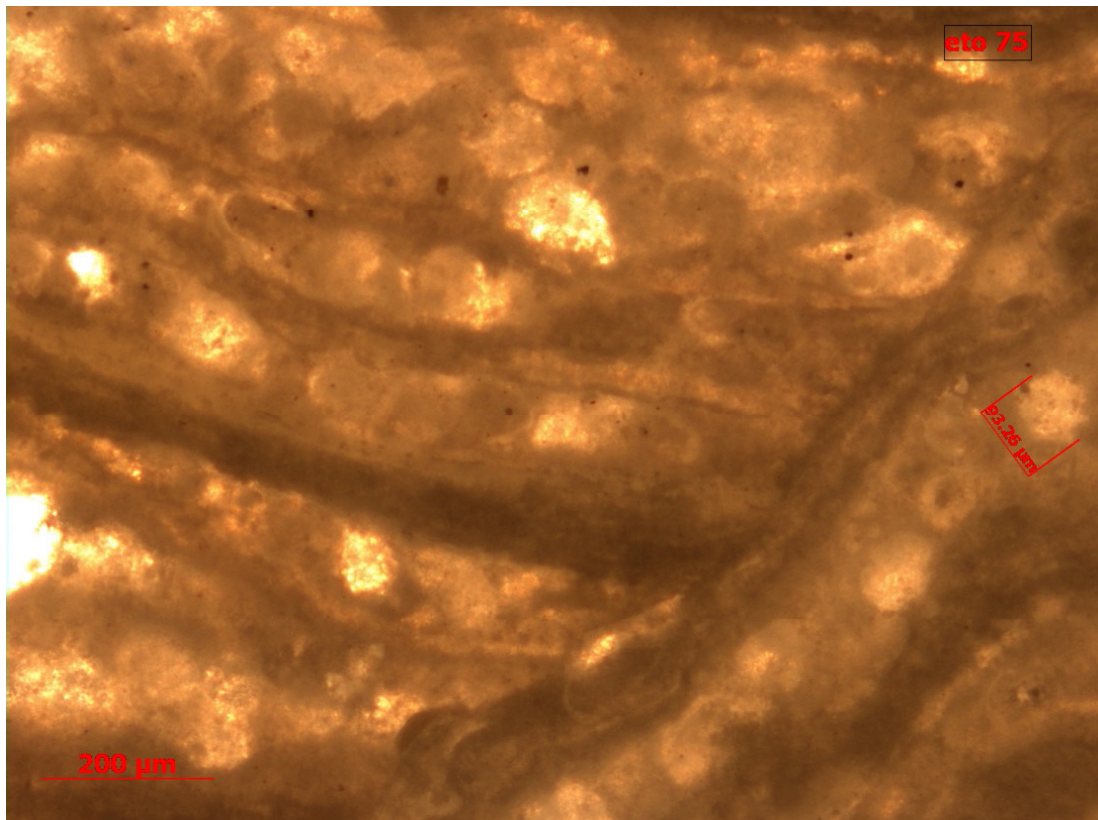
Figure 35: Microglobules (168.5 µm diameter) of organic origin are abundant in the interstices of stromatolites. These probably correspond to *Chlorellopsis coloniata*.
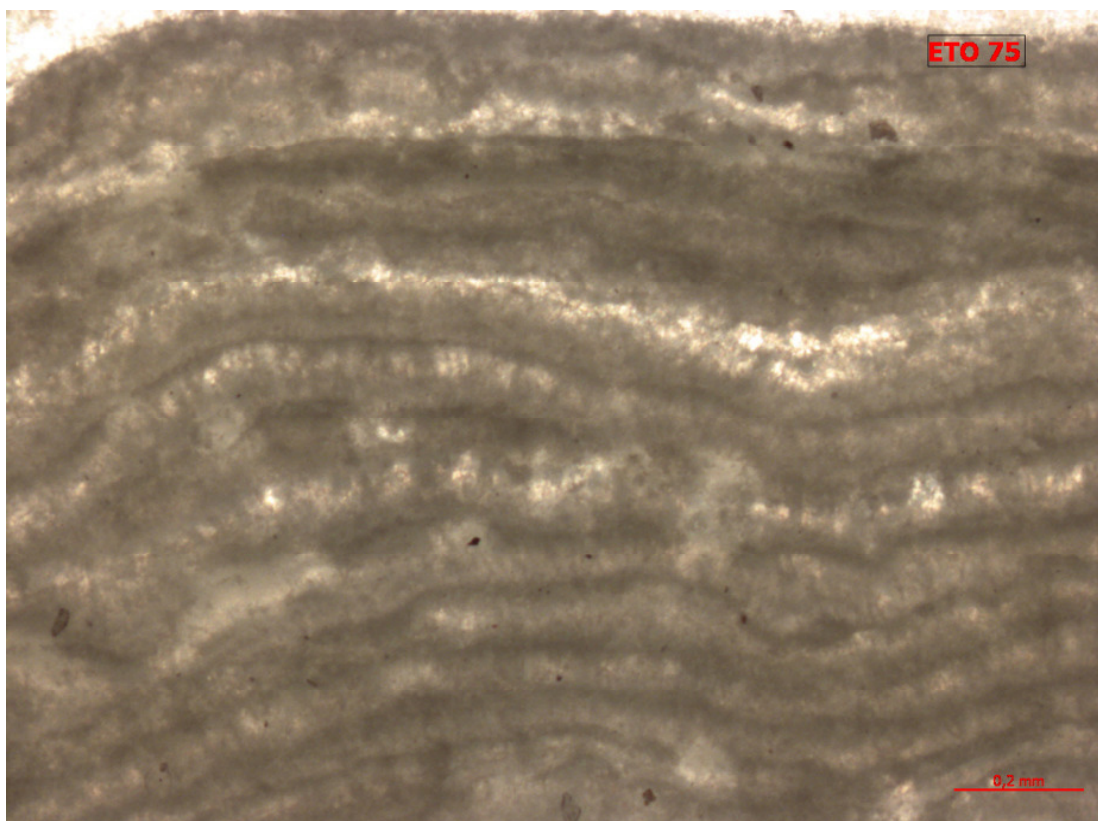

Figure 36: Microlaminations of Etosha oncolites are clearly visible in thin section.

Figure 37: Polished section of an oncolite from Poacher's Point, Etosha. Note the core comprised of sediment which includes phosphatic grains, possibly coprolites or rounded and polished fish bones. The polyphase growth of this individual is clearly demonstrated by a rupture which has removed part of the dark layer (to the left of the image) followed by a second growth phase (paler layers). Note the pillar-like growth pattern in parts of the oncolite, with open or sediment-filled gaps between the pillars.
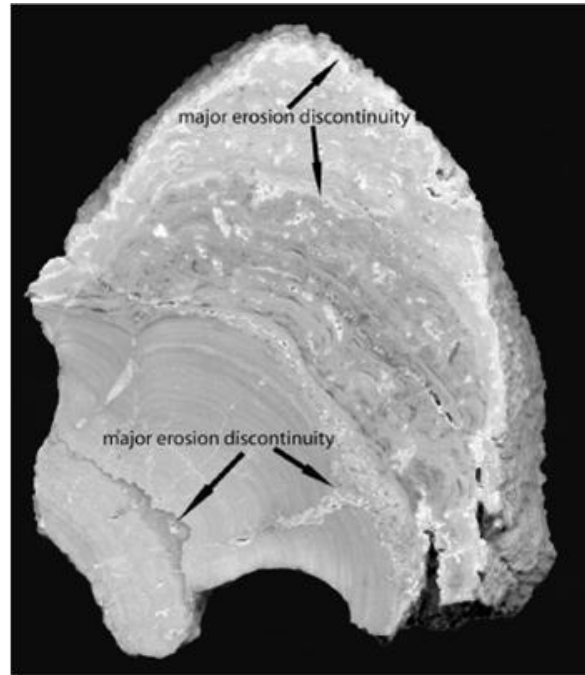
Figure 38: Polished surface of a stromatolite from Poacher's Point showing evidence of at least four periods of erosion and growth.
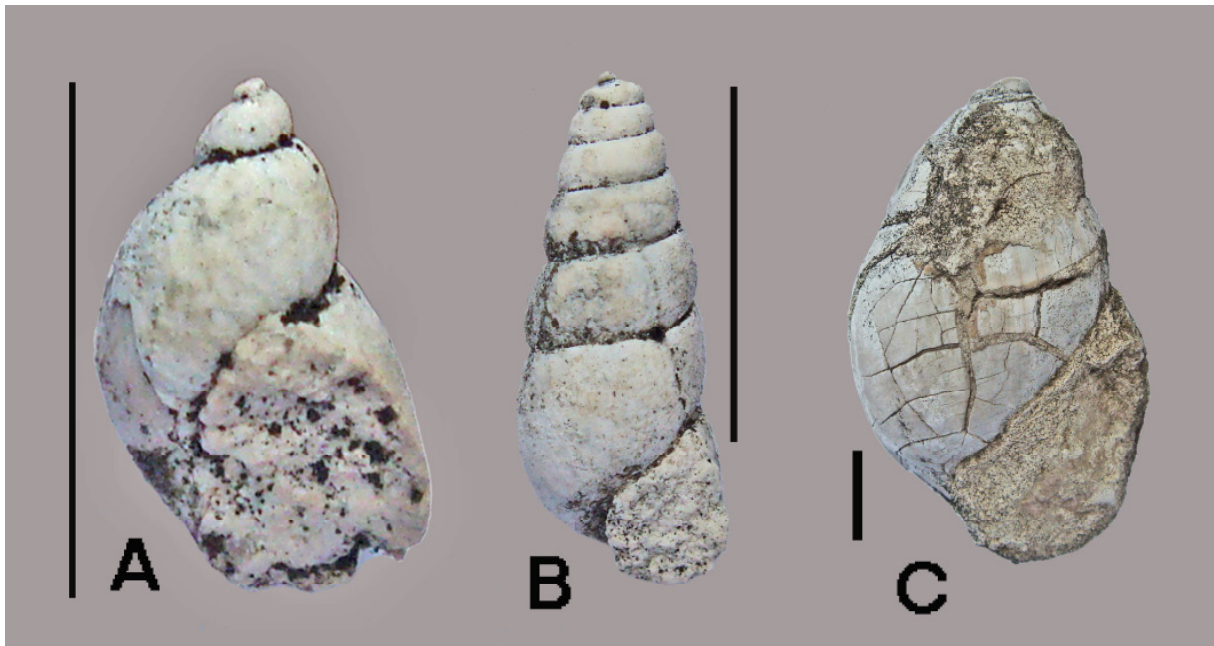
Figure 39: Landsnails from the Poacher's Point Carbonate Member, from the west flank of Poacher's Point. A) *Succinea striata*, B) *Xerocerastus burchelli*, C) *Achatina dammarensis* (apertural views).(scale bars : 10 mm).

Achatinidae (MP)

Achatinid shells are reasonably common at Poacher's Point, but few of them are fully adult or well preserved. An exception is a complete specimen (Fig. 39 C) attributed to *Achatina dammarensis* (h x b = 67 x 40; h/d 1.67). Connolly (1939) recorded several species of *Achatina* from Namibia, which differ from each other in dimensions and superficial shell sculpture such as the way the granulations are arranged on the surface of the shell. The Poacher's Point specimen is close in shape to *Achatina oedigyra* and *A. dammarensis*, but differs from *A. tracheia* and *A. passargei*, which are taller and narrower (Connolly, 1939). We attribute the specimen to *A. dammarensis* despite the somewhat greater dimensions than are usually encountered in this species.

Struthionidae (LS & MP)

The Poacher's Point micro-ooid horizon yielded a single fragment of ostrich egg shell, probably *Struthio camelus* judging from its thickness of 1.9 mm and the presence of pore complexes that are smaller than those of *Struthio daberasensis* (Senut and Pickford, 1995; Senut *et al.*, 1998).

Flora and fauna from the Etosha Limestone

The Etosha Limestone is a widespread calcrete horizon that formed by a variety of processes. In the south it is a groundwater calcrete, whereas in the north it is a pedogenic calcrete often containing abundant rhizoliths (Fig. 40).

The Etosha Limestone has been eroded from much of the surface of the Etosha Pan, and now occurs as discontinuous outcrops at the summit of islands and ridges within and close to the margins of the pan (Miller, 2007). In places such as Poacher's Point and Oshigambo Peninsula, the calcrete has yielded abundant fossils of terrestrial snails

Figure 40: Etosha Limestone in the banks of the Ekuma River Valley. This calcrete horizon is widespread in the Etosha Basin, frequently showing abundant rhizolith networks. Locally, at Ekuma River, this unit unconformably overlies an irregular surface incised into the Ekuma Delta Member, the Poacher's Point Carbonate Member, and an un-named rubble horizon containing black nodules (also present on Pelican Island).

(Fig. 41) but no vertebrates have been found. Lacustrine and paludal gastropods are rare in the calcrete and related deposits, but have been found at Homob waterhole on the southern margin of the pan in calcified marly silts that probably accumulated within the waterhole depression and in calcareous tufa deposits close to Namutoni. On stratigraphic and geomorphological grounds, the Etosha Limestone is likely to be Early to Middle Pleistocene in age, but there is no direct evidence for this estimate in the form of datable fossils.
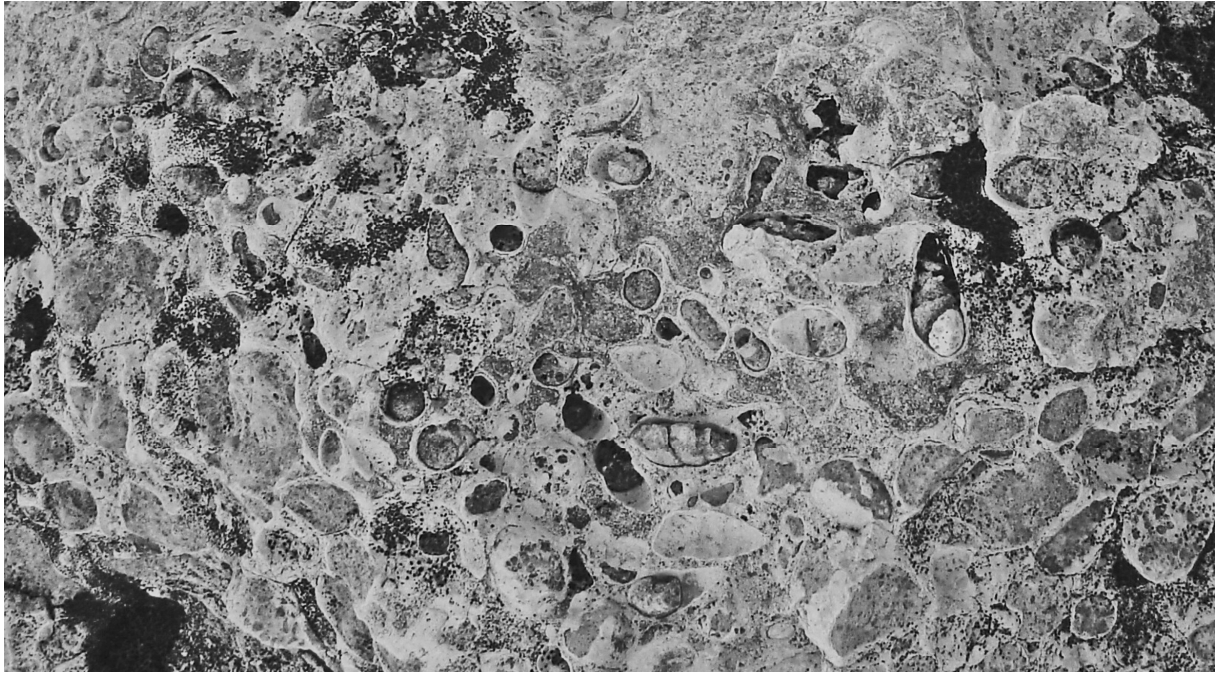
Figure 41: Abundant shells of *Xerocerastus burchelli* in calcrete (Etosha Limestone) atop the Oshigambo Peninsula on its northern flank, Etosha, Namibia (Some of these shells could be "inherited" from the Poacher's Point Carbonate Member on top of which the Etosha Limestone formed).

Fauna from the Etosha raised beaches (1.5 - 2 m beaches)

Pale orange silt and sand, along with cobbles and reworked oncolites, which accumulated in beaches at an altitude of 1.5 to 2 metres above the present day floor of Etosha Pan, have yielded abundant fossils. In the Ekuma River Valley, these deposits have been incompletely indurated to the stage where pea-sized clumps of calcified sand have formed within the bed which is otherwise poorly consolidated. The commonest fossils from this deposit comprise shells of *Melanoides tuberculata*, which are accompanied by rarer shells of *Mutela* sp. and *Bellamya unicolor*. No land snails have been found in these beach deposits.

The assemblage of molluscs in the raised beach deposits comprise freshwater species. Although *Melanoides* is tolerant of slight alkaline or weakly saline water, *Mutela* sp. and *Bellamya unicolor*, in contrast, are intolerant of such conditions, and attest to the presence of well-oxygenated, fresh water conditions. *Melanoides tuberculata* is widespread in Africa, but is absent from forested zones and desert areas (Brown, 1980). It does however occur as an isolated population at Namutoni Springs (Van Bruggen, 1963) well removed from its general distribution in Africa (Fig. 42).

Fauna from the Oshigambo Pan-loess

Late Pleistocene sands and silts exposed along the southern edge of the Oshigambo Peninsula, attributed to the Oshigambo Pan-loess, have yielded a rich variety of fossil vertebrates (Hipondoka, 2005) including aquaphilous bovids such as sitatunga

(*Tragelaphus spekei*) which have been interpreted to indicate the former presence of perennial lacustrine conditions in the area at the end of the Pleistocene (Hipondoka *et al.*, 2006). The inferred presence of a recent highstand of Palaeolake Etosha gains support from the occurrence at Pelican Island, of green silts that overlie an eroded and incised surface of Etosha Limestone and older rocks (Fig. 4). The Oshigambo faunal assemblage contains remains of terrestrial gastropods similar to those that occur in the region today (*Achatina dammarensis*, *Xerocerastus*

burchelli) as well as ostrich egg shells (*Struthio camelus*) (Fig. 43) and fungus gardens of termites, suggesting a sub-humid to semi-arid terrestrial environment nearby. Other mammals from the deposits comprise *Equus quagga* (quagga), *Damaliscus lunatus* (tsessebe), *Antidorcas marsupialis* (springbok), *Aepyceros melampus* (impala), *Tragelaphus spekei* (sitatunga), *Taurotragus oryx* (eland). The sediments also yield terrestrial snails (*Achatina dammarensis* and *Xerocerastus burchelli*) and there are also termite fungus gardens (*Hodotermes* sp.).
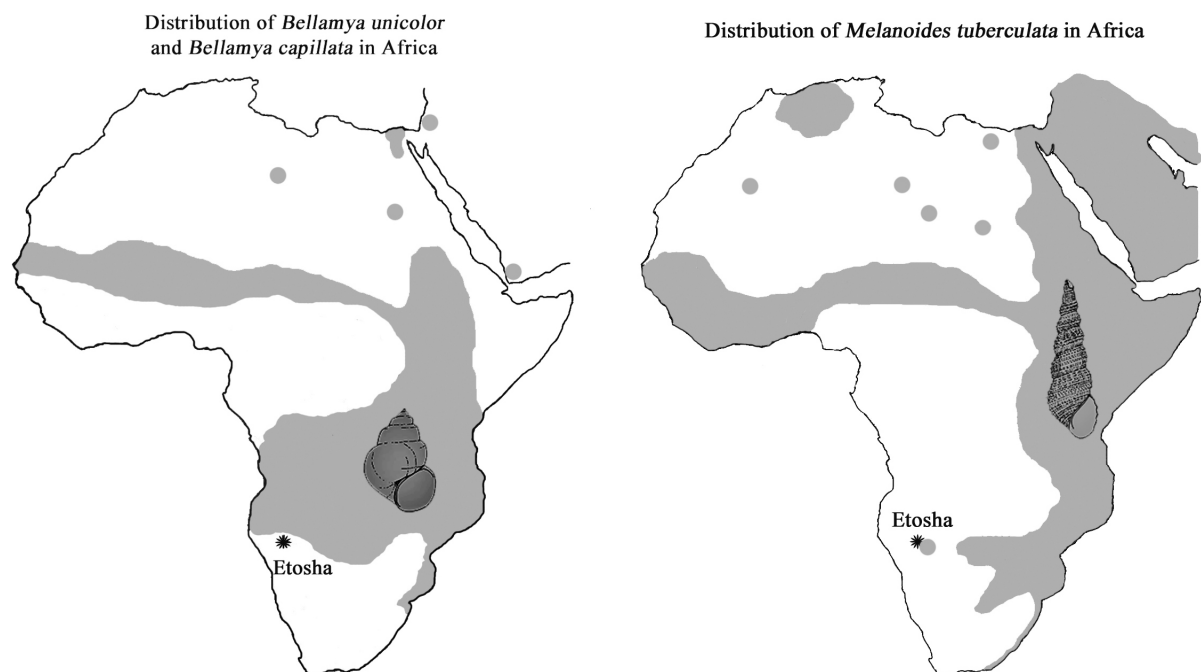
Figure 42: Distribution of *Melanoides* and *Bellamya* relative to Etosha Pan. *Melanoides* occurs today in the Namutoni Springs in the southeast corner of the Etosha Basin, but as an outlier of the main zone of distribution of the genus. The combined presence of these two genera in the raised beach deposits in the Ekuma River Valley implies a climate that was probably somewhat more humid at the time of deposition than it is today. The same is suggested by the presence of the bivalve *Mutela* sp.

Discussion

Biochronology of the Etosha Pan Clay Member and the Ekuma Delta Member of the Andoni Formation

Etosha Pan Clay Member

An age of ca 6 Ma is deduced for the Etosha Pan Clay Member on account of the presence of a primitive loxodont with low crowned molars and thick enamel. The

specimens, even though fragmentary, are close in morphology to material from Late Miocene deposits in South Africa (Langebaanweg) and East Africa (Nkondo, Lukeino) attributed to *Loxodonta cookei* by Sanders (2007). A similar age is indicated by the presence of a primitive alcelaphine, differing slightly in horn core shape from *Damalacra neanica* from Langebaanweg but close to *Damalacra acalla* from the same site (Gentry, 1970).
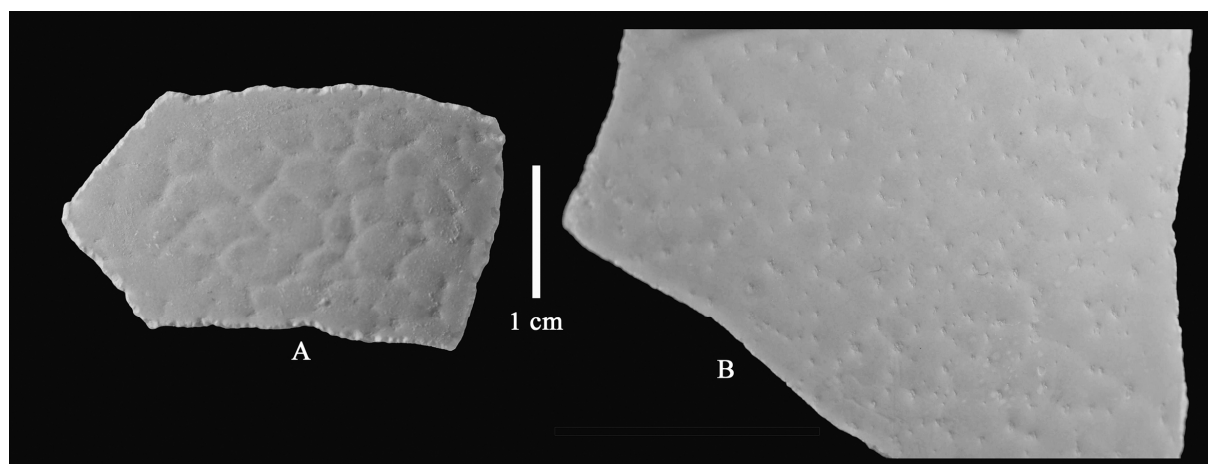
Figure 43: Egg shells of *Struthio camelus* from Etosha, Namibia, A) Holocene, GPS 102 (18°41'23.9''S : 16° 09'22.8''E), and B) Modern, ETO 161107.

Ekuma Delta Member

Horn cores of *Redunca darti* from Ekuma resemble material from East African deposits aged about 4 Ma (Gentry, pers. comm.). The equid from Ekuma is *Hipparion* sp. (Eisenmann, pers. comm.). The pedetid tooth from Ekuma is older than material from Laetoli, Tanzania (3.7-4 Ma) (Davies, 1987) but younger than the *Diamantornis laini* levels at Rooilepel (8-10 Ma). The rhinocerotid from Ekuma is the large extinct species *Ceratotherium praecox* which ranges in age range from 7 to 4.5 Ma. The *Hippopotamus* from Ekuma is a large species, but the re-

mains are too fragmentary for species determination. On the basis of these faunal remains a Middle Pliocene age (ca 4 Ma) is estimated for the Ekuma Delta Member.

Radio-isotopic age determination of the Oshigambo Pan-loess fauna

New age determinations have been obtained from faunal elements from the Oshigambo Pan-loess deposits located at the western extremity of the Oshigambo Peninsula. The results are presented in Table 8, and indicate that the deposits date from the Late Pleisto-

nature	δ^{13}C‰	APGM	ASG	mg C	N°labo	Age AMS	Calibrated age (2s)
Bovid bone bioapatite	0,9	19	11	1,28	Pa650	10778±54 BP	12880-12720 cal bp
Bovid bone bioapatite	0,34	19	11,3	1,28	Pa651	11489±56 BP	13450-13230 cal bp
Bovid enamel bioapatite	0,14	28	17,6	1,95	Pa652	12091±59 BP	14090-13800 cal bp

Table 8: Radio-isotopic age determinations of faunal elements from the Oshigambo pan-loess.

These age determinations are considered to be more reliable than previous estimates obtained by analysing collagen from an equid bone from the site, because in this round of analyses the determinations were made on bioapatite, and not collagen, which is usually poorly preserved. We conclude that the site dates back to the very end of the Pleistocene after the hyper arid phase of the Last Glacial Maximum (18 ka).

Conclusions

Surveys of Etosha in 2006 and 2007 by the Namibia Palaeontology Expedition led to the discovery of fossil sites of Late Miocene and Mid-Pliocene age (Table 9). The flora is dominated by tree boles and root systems, whereas the fauna is rich in invertebrates and vertebrates (Table 9). These discoveries complement those of Hipondoka (2005, Hipondoka *et al.*, 2006) who found a rich and diverse fauna in the Late Pleistocene Oshi-

Formation/ Palaeontology	Etosha Pan Clay Member	Ekuma Delta Member	Poacher's Point Carbon-ate Member	Etosha Lime-stone	Oshigambo Pan-loess
Oncolites	X		X	X (reworked?)	
Chlorellopsis coloniata			X		
Palm		X			
Dicotyledon		X			
Ostracoda	X		X		
Hodotermes sp.				X	X
Succinea striata			X	X	
Xerocerastus burchelli			X	X	X
Achatina dammarensis			X	X	X
Bellamya unicolor		X			
Planorbidae sp.				X	
Mutela sp.	X	X			
?Egeria sp.		?			
Clarias sp.	X	X			
Cyclanorbinae sp.	X	X			
Pelusios sp.	X	X			
Crocodylus sp.	X	X			
Phoenicopterus ruber	X	X			
Struthio daberasensis		X			
Struthio camelus			X	X	X
Propedetes sp.		X			
Panthera cf *leo*	X				
Loxodonta sp. cf *cookei*	X	X			
Ceratotherium praecox		X			
Hipparion sp.		X			
Equus quagga					X
Hippopotamus sp.		X			
Suidae (large sp.)	X				
Damalacra acalla	X				
Redunca darti		X			
Damaliscus lunatus					X
Antidorcas marsupialis					X
Aepyceros melampus					X
Tragelaphus spekei					X
Taurotragus oryx					X
Bovidae 2-3 spp.	X	X			

Table 9: Summary of the distribution of the palaeontological remains in the various stratigraphic units exposed in the floor and flanks of Etosha pan.

gambo Pan-loess, and Mid-Pliocene fossils in the Ekuma Delta, which belong to a wide variety of extant taxa, including aquaphilous antelopes. Palaeontology is proving to be crucial to the determination of the timing of geological events in the basin, and this impacts directly on the interpretation of the history of the basin.

It is clear that there was a complex history of alternating erosional and depositional episodes in the Etosha Basin, at least in the latter part of its history represented by the uppermost 20-30 metres of sedimentary deposits spanning the period 6 Ma to the Late Pleistocene. The three exposed members of the Andoni Formation attest to a shallowing upwards lacustrine system, with the Etosha Pan Clay Member recording fully lacustrine conditions, the overlying Ekuma Delta Member an increase in fluvial deposition, and the oolitic limestones of the Poacher's Point Carbonate Member, deposition in shallow water which towards the end became hyper-alkaline, to such an extent that Magadi-type chert plaquettes formed in abundance. The deposition of this carbonate unit was accompanied by the growth of abundant algal oncoliths. There followed a period of calcrete pedogenesis resulting in the formation of the widespread Etosha Limestone, which incorporated into it elements of the underlying deposits, such as oncolites. In the south of the Etosha basin, calcrete formation was predominantly due to groundwater processes which produced dolomitic calcrete in huge, low-angle megadomes, while in the north, the Etosha Limestone is largely of pedogenic origin, with a rubbly, nodular structure and abundant rhizolith networks.

Unconformably on top of an eroded and incised surface of rocks of the Andoni Formation and Etosha Limestone, which left a widespread rubble horizon containing black nodules of sediment, there occur various Late Pleistocene deposits including fossiliferous raised beach deposits 1 – 1.5 metres above the present day floor of the pan, and the Pelican Island green silt which occurs up to 10 metres above the pan floor. The latter deposits attest to a Late Pleisto-

cene lacustrine high stand which filled Etosha Pan with water to a depth of at least 10 metres. A lake of this depth would cover an area of well over 5,000 km^2. Overlying the raised beach deposits there is an extremely widespread horizon 1 to 1.5 metres thick, of grey silt and clay comprising the Oshigambo Pan-loess. At the western extremity of the Oshigambo Peninsula, this unit has yielded a rich and diverse fauna. Some elements of the fauna, such as sitatunga indicate that there was a perennial lake in the basin some 12,000 to 14,000 years ago. The Pelican Island green silts and the raised beach deposits at Poacher's Point and in the Ekuma River valley, probably represent earlier manifestations of this palaeolake.

Finally, we emphasise that the Etosha Late Miocene and Ekuma Basal Pliocene fossil localities help to fill what used to be an enormous void in the palaeontological map of the African continent for the period between 8 and 4 million years. This is a period of interest to palaeoanthropologists who desire to throw light on hominid origins. The strata in the Etosha Basin are thus crucial not only for understanding the history of the basin, but are also because of their potential for the study of hominid origins and Late Miocene and Pliocene palaeoenvironments.

Acknowledgements

References

Arambourg, C., 1944 - Les hippopotames fossiles d'Afrique. *C. R. Acad. Sci. Paris*, **218**: 602-604.

Ballesio, R., 1963 - Monographie d'un *Machairodus* du gisement Villafranchien de Senèze: *Homotherium crenatidens* Fabrini. *Travaux du Laboratoire Géologique de la Faculté des Sciences de Lyon*, **9**: 1-129.

Ballmann, P., 1987 - A Fossil Bird Fauna from the Pliocene Sahabi Formation of Libya. *In*: N. T. Boaz, A. El-Arnauti, A. W. Gaziri, J. de Heinzelin and D. D. Boaz (Eds) *Neogene Paleontology and Geology of Sahabi*. Alan R. Liss Inc., pp. 113-117.

Baumel, J. J., and Witmer, L. M., 1993 - Osteologia. *In*: Baumel, J. J. (Ed) *Handbook of Avian Anatomy. Nomina Anatomica Avium*. 2nd edition. Nutall Ornithological Club, n° 23, pp. 45-132.

Beugler-Bell, H., and Buch, M.W., 1997 – Soils and soil erosion in the Etosha National Park, northern Namibia. *Madoqua*, **20** (1) : 91-104.

Bittner, A., and Plöthner, D., 2001 – Cuve-lai-Etosha Basin. *In* : G. Christelis and W. Struckmeir (Eds) *Groundwater in Namibia : An Explanation to the Hydrological Map.* pp. 51-58. John Meinert Printing, Windhoek.

Boisserie, J.R., 2005 - The phylogeny and taxonomy of Hippopotamidae (Mammalia: Artiodactyla): a review based on morphology and cladistic analysis. *Zoological Journal of the Linnean Society*, **143** : 1-26.

Brink, J., and Stynder, D., in press – Morphological and trophic distinction of the dentitions of two early alcelaphine bovids from Langebaanweg (genus *Damalacra*). *Palaeontologia africana.*

Brodkorb, P., 1953 - A Pliocene Flamingo from Florida. *Natural History Miscellanea*, **124**: 1-4.

Brodkorb, P., and Mourer-Chauviré, C., 1982 - Fossil Anhingas (*Aves*: *Anhingidae*) from Early Man Sites of Hadar and Omo (Ethiopia), and Olduvai Gorge (Tanzania). *Geobios*, **15** (4): 505-512.

Broom, R., 1937 - On some new Pleistocene mammals from limestone caves of the Transvaal. *S. Afr. J. Sci.* **33**: 750-768.

Brown, D., 1980 – *Freshwater Snails of Africa and their Medical Importance.* London, Taylor and Francis. 487 pp.

Bryant, R.G., 2003 – Monitoring hydrological controls on dust emissions : preliminary observations from Etosha Pan, Namibia. *Geographical Journal*, **169** (2) : 131-141.

Buch, M.W., 1993 – *Känozoischer Klima- und Umweltwandel in Etoscha/Nord-Namibia – Untersuchungen zur Klimasensibilität und Geomorphodynamik eines semiariden Landschaftrumes im südlichen Afrika.* Habilitationsschrift, Institut für Geographie der Universität Regensberg, Teil I/II, Regensberg : Selbsverlag.

Buch, M.W., 1996 – Geochrono-Geomorphostratigraphie der Etoscha-Region, Nord Namibia. *Die Erde*, **127** (1) : 1-22.

Buch, M.W., 1997 – Etosha Pan – the largest

lake in the world? *Madoqua*, **20** : 49-64.

Buch, M.W., and Zöller, L., 1992 – Pedostratigraphy and thermoluminescence chronology of the western margin (lunette) dunes of the Etosha Pan / northern Namibia. *Würzburger Geogr. Arb.* **84** : 361-384.

Buch, M.W., Rose, D., and Zöller, L., 1992 – A TL-calibrated pedostratigraphy of the western lunette dunes of the Etosha Pan / northern Namibia : A reconstruction of the depositional implications for the last 140 Ka. *Palaeoecology of Africa*, **23** : 129-147.

Connolly, M., 1939 - A monographic survey of the South African non-marine Mollusca. *Ann. S. Afr. Mus.* **33**: 1-660.

Coryndon, S.C., 1977 - The taxonomy and nomenclature of the Hippopotamidae (Mammalia, Artiodactyla) and a description of two new fossil species. *Proc. Kon. Ned. Akad. Wetensch.* **B.80 (2)**: 61-88.

Dauphin, Y., Pickford, M., and Senut, B., 1996 - Microstructures des coquilles d'oeufs d'oiseaux fossiles de Namibie. *Revue de Paléobiologie*, **15** : 225-241.

Davies, C., 1987 - Fossil Pedetidae (Rodentia) from Laetoli. *In*: M.D. Leakey and J.M. Harris (Eds) *Laetoli - A Pliocene Site in Northern Tanzania*, pp. 171-189, Oxford, Oxford University Press.

de Lapparent de Broin, F., 2000 – African Chelonians from the Jurassic to the present: phases of development and preliminary catalogue of the fossil record. *Palaeontologia Africana*, **36**: 43-82.

Dyke, G. J., and Walker, C. A., 2008 - New Records of Fossil "Waterbirds" from the Miocene of Kenya. *Amer. Mus. Novit.*, **3610**: 1-10.

Engert, S., 1997 – Spatial variability and temporal periodicity of rainfall in the Etosha National Park and surrounding areas in northern Namibia. *Madoqua*, **20** (1) : 115-120.

Faure, M., 1985 - Les hippopotames quaternaires non-insulaires d'Europe occidentale. *Nouv. Arch. Mus. Hist. nat. Lyon,* **23** : 13-79.

Gayet, M., and Van Neer, W., 1990 - Caractères diagnostics des épines de quelques silures africains. *Journal African Zoology*, **104** : 241-252.

Gentry, A.W., 1970 - The Langebaanweg Bovidae. *Ann. S. Afr. Mus.*, **56**: 114-117.

Gentry, A.W., 1980 - Fossil Bovidae (Mammalia) from Langebaanweg, South Africa. *Annals of the South African Museum*, **79**: 213-337.

Gevers, T.W., 1930 – Terrestrial dolomite in the Etosha Pan, Southwest Africa. *Centralblatt für Mineralogie, Geologie und Paläontologie*, **6** : 224-230.

Gèze, R., 1980 - Les *Hippopotamidae* (Mammalia, Artiodactyla) du Plio-Pleistocène de l'Ethiopie (Afrique orientale). *Thèse doctorat 3ème cycle, Univ. Paris VI,* 116 p.

Gèze, R., 1985 - Répartition paléoécologique et relations phylogénétiques des Hippopotamidae (Mammalia, Artiodactyla) du Néogène d'Afrique orientale. Colloque Internat. Fondation Singer-Polignac, "L'environnement des Hominidés au Plio-pléistocène", Paris Juin 1981, *Masson édit.,* Paris, pp. 81-100.

Guérin, C., 1979 - Chalicotheriidae et Rhinocerotidae (Mammalia, Perissodactyla) du Miocène au Pléistocène de la Rift Valley (Afrique orientale). Un exemple d'évolution: le squelette post-cranien des *Diceros* et *Ceratotherium* plio-pléistocènes. *Bull. Soc. géol. Fr.*, Paris, (7), **21 (3)** : 283-288.

Guérin, C., 1980 - A propos des rhinocéros (Mammalia, Perissodactyla) néogènes et quaternaires d'Afrique: essai de synthèse sur les espèces et sur les gisements. *Proc. 8th Panaf. Congress Prehist. Quat. stud.,* Nairobi 1977, pp. 58-63.

Guérin, C., 1985 - Les rhinocéros et les chalicothères (Mammalia, Perissodactyla) des gisements de la vallée de l'Omo en

Ethiopie. (Collections françaises). *In* : Y. Coppens and F. Clark Howell (Eds) "Les faunes plio-pléistocènes de la basse vallée de l'Omo (Ethiopie)", *Cahiers de Paléontologie - Travaux de Paléontologie Est-africaine,* CNRS*,* Paris, **1** : 67-95.

Guérin, C., 1987 - Fossil Rhinocerotidae (Mammalia, Perissodactyla) from Laetoli, In M.D. Leakey and J.M. Harris (eds.), *Laetoli, a Pliocene Site in Northern Tanzania*, p. 320-348, Clarendon Press*,* Oxford.

Guérin, C., 1994 - Les Rhinocéros (Mammalia, Perissodactyla) du Néogène de l'Ouganda, *In* : B. Senut and M. Pickford (Eds), *Geology and Palaeobiology of the Albertine Rift Valley, Uganda-Zaire, vol. II: Palaeobiology*, CIFEG édit., Orléans, occasional publication **1994/29** : 263-279.

Haddon, I.G., 2000 – Kalahari Group Sediments. *In* : T.C. Partridge and R.R. Maud (Eds) *The Cenozoic of Southern Africa*. Oxford University Press, Oxford, pp. 173-181.

Harris, J., 2003 - Bovidae from the Lothagam Succession. *In*: M. Leakey and J. Harris (Eds) *Lothagam: The Dawn of Humanity in Eastern Africa*, pp. 531-579, New York, Columbia University Press.

Harris, J. M., and Leakey, M. G., 2003 - Lothagam Birds. *In*: M. G. Leakey and J. M. Harris (Eds) *Lothagam: the Dawn of Humanity in Eastern Africa*. Columbia Univ. Press, New York, pp. 161-166.

Harrison, C. J. O., 1980 - Fossil birds from Afrotropical Africa in the collection of the British Museum (Natural History). *Ostrich*, **51**: 92-98.

Harrison, C. J. O., and Walker, C. A., 1976 - Cranial material of Oligocene and Miocene flamingos: with a description of a new species from Africa. *Bull. Brit. Mus. natur. Hist.*, *Geology*, **27** (4): 305-314.

Harrison, T., and Msuya, C. P., 2005 - Fossil struthionid eggshells from Laetoli,

Tanzania: Taxonomic and biostratigraphic significance. *Journal of African Earth Sciences*, **41**: 303-315.

Hedberg, R.M., 1979 – Stratigraphy of the Owamboland Basin, SWA. *Bulletin Precambrian Research Unit*, **24** : 1-325.

Hipondoka, M., 2005 – *The Development and Evolution of Etosha Pan, Namibia.* PhD Thesis, Würzburg, 152 pp.

Hipondoka, M., Busche, D., and Kempf, J., 2004a – Source of lunette dune sediments : A geomorphic terrain analysis approach in Etosha National Park, Namibia. *Erdekunde*, **58** : 212-220.

Hipondoka, M., Jousse, H., Kempf, J., and Busche, D., 2006 - Fossil evidence for perennial lake conditions during the Holocene at Etosha Pan, Namibia. *S. Afr. J. Sci.*, **102**: 93-95

Hipondoka, M., Versfeld, W.D., and Kapner, J.S., 2004b – Assessment and application of annual field rain gauges in Etosha National Park. *Namibia Scientific Society*, **52** : 43-52.

Hooijer, D.A., and Patterson, B., 1972 - Rhinoceroses from the Pliocene of Northwestern Kenya. *Bull. Mus. Comp. Zool.* Cambridge (Mass.), **144 (1)** : 1-26.

Hopwood, A., 1926 - The geology and palaeontology of the Kaiso Bone Beds. *Uganda Prot. Geol. Surv. Dept. Occas. Pap.*, **2 (2)**: 19-23.

Howard, H., 1929 - The avifauna of Emeryville shellmound. *Univ. Calif. Publ. Zool.*, **32** (2): 301-394.

Hoyo, J. del, Elliott, A., and Sargatal, J., 1992 - *Handbook of the Birds of the World*, vol. 1, Lynx Edicions, 696 pp.

Hutter, F., 1910 – Im gebiet der Etoschapfanne (Deutsch-Südwestafrika). *Globus*, **48** (1) : 1-7 ; **48** (2) : 24-32.

Jaeger, F. 1926 – Die Etoschapfanne. *Mitteilungen aus dem Deutschen Schutzgebieten,* **34** (1) : 1-22.

Jaeger, F., and Waibel, L., 1921 – Beiträge zur Landeskunde von Südwestafrika, II, Teil. Landschaften des nördlichen Südwestafrika. *Mitteilungen aus dem*

Deutschen Schutzgebieten Erganz. Hft., **15** : 1-138.

Kempf, J., and Hipondoka, M., 2003 – Regenzeitliche Hydrodynamik im Bereich der Etoschapfanne, Namibia. *Petermanns Geographische Mitteilungen*, **147** : 4-5.

Kent, P.E., 1942 - The Pleistocene beds of Kanam and Kanjera, Kavirondo, Kenya. *Geol. Mag.* **79**: 72-77.

Lehmann, U., and Thomas, H., 1987 - Fossil Bovidae (Mammalia) from the Mio-Pliocene of Sahabi, Libya. *In:* N. Boaz *et al.,* (eds), *Neogene Paleontology and Geology of Sahabi*, pp. 323-335. New York, Alan Liss.

Likius, A., 2002 - Les grands ongulés du Mio-Pliocène du Tchad (Rhinocerotidae, Giraffidae, Camelidae): systématique, implications paléobiogéographiques et paléoenvironnementales. *Thèse Université de Poitiers*, 188 pp.

Lindeque, M., and Archibald, T.J., 1991 – Seasonal wetlands in Owambo and Etosha National Park. *Madoqua*, **17** (2) : 129-133.

Louchart, A., Hailé-Sélassié, Y., Vignaud, P., Likius, A., and Brunet, M., 2008 - Fossil birds from the Late Miocene of Chad and Ethiopia, and zoogeographical implications. *Oryctos*, **7**: 147-167.

Louchart, A., Mourer-Chauviré, C., Taisso Mackaye, H., Likius, A., Vignaud, P., and Brunet, M., 2004 - Les Oiseaux du Pliocène inférieur du Djourab, Tchad, Afrique Centrale. *Bull. Soc. Géol. Fr.*, **175** (4): 413-421.

Louchart, A., Vignaud, P., Likius, A., Brunet, M., and White, T. D., 2005 a - A large extinct marabou stork in African Pliocene hominid sites, and a review of the fossil species of *Leptoptilos*. *Acta Palaeont. Polon.*, **50** (3): 549-563.

Louchart, A., Vignaud, P., Likius, A., Mackaye, H. T., and Brunet, M., 2005 b - A new swan (Aves: Anatidae) in Africa, from the latest Miocene of Chad and Libya. *Journ. Vert. Paleont.*, **25** (2): 384-392.

Martin, H., and Wilczewski, N., 1972 – Algen-Stromatolithen aus der Etoschapfanne Südwestafrikas. *Neues Jb. Geol. Paläont. Mh.* **12** : 720-726.

Merrian, C.J., and Stock, C., 1932 - The Felidae of Rancho La Brea. Carnegie Institution of Washington, **422**: 3-231.

Miller, A. H., 1963 - The fossil flamingos of Australia. *The Condor*, **65**: 289-299.

Miller, L., 1944 - A Pliocene Flamingo from Mexico. *The Wilson Bull.*, **56** (2): 77-82.

Miller, R., 1997 – The Owambo Basin of Northern Namibia. *In* : R.C. Selley (Ed.) *African Basins : Sedimentary Basins of the World 3*. Elsevier Science, Amsterdam, pp. 237-268.

Miller, R., 2007 – Kalahari Group. *In* : R. Miller (Ed.) *The Geology of Namibia, Volume 3, Palaeozoic to Cenozoic*, **24** : 1-76. Windhoek, Ministry of Mines and Energy.

Mourer-Chauviré, C., Senut, B., Pickford, M., Mein, P., and Dauphin, Y., 1996 - Ostrich eggs, legs and phylogenies. *S. Afr. Jl Sci.*, **92**: 492-495.

Olson, S. L., and Rasmussen, P. C., 2001 - Miocene and Pliocene Birds from the Lee Creek Mine, North Carolina. *In*: C. E. Ray and D. J. Bohaska (Eds) Geology and Paleontology of the Lee Creek Mine, North Carolina, III. *Smiths. Contrib. Paleobiol.*, **90**: 233-265.

Paugy, D., Lévêque, C., and Teugels, G.G., 2003 - *Poissons d'eaux douces et saumâtres de l'Afrique de l'Ouest*. IRD: Paris.

Pickford, M., 1986 - Cainozoic Paleontological Sites of Western Kenya. *Münchner Geowiss. Abh.* (A), **8**: 1-151.

Pickford, M., Senut, B., and Dauphin, Y., 1993 - Chronologie du Néogène continental de Namibie : apport des oeufs fossiles. *Palaeovox,* **2** : 66-67.

Pickford, M., Senut, B., Morales, J., and Braga, J., 2008 – First hominoid from the Late Miocene of Niger. *South Afri-*

can Journal of Science, **104** : 337-339.

Rahm, L., and Buch, M., 1997 – Groundwater flow in the southern part of the Etosha Basin indicated by the chemical composition of water. *Madoqua*, **20** (1) : 129-135.

Rich, P. V., 1972 - A fossil avifauna from the Upper Miocene Beglia formation of Tunisia. *Notes du Service géologique*, n° 35, *Travaux de Géologie Tunisienne*, n° 5, Tunis, Formation Beglia, fasc. **1**: 29-66.

Rich, P. V., 1980 - Preliminary Report on the Fossil Avian Remains from Late Tertiary Sediments at Langebaanweg (Cape Province), South Africa. *South African Journal of Science*, **76**: 166-170.

Rich, P. V., and Walker, C. A., 1983 - A new genus of Miocene flamingo from East Africa. *Ostrich*, **54**: 95-104.

Rust, U., 1981 – Vorläufiges Ergebnis der Geländearbeiten zur Landschaftsgeschichte von Etoscha (Südwestafrika/Namibia). *Newsl. S. W. Afr. Sci. Soc.* **22** : (2-3), appendix, 8 pp.

Rust, U., 1984 – Geomorphic evidence of Quaternary environmental changes in Etosha, South West Africa/Namibia. *In* : J.C. Vogel (Ed.) *Late Cainozoic Palaeoclimates of the Southern Hemisphere.* Balkema, Rotterdam, pp. 279-286 .

Rust, U., 1985 – Die Entstehung der Etoschapfanne im Rahmen der Landeschafteentwicklung des Etoscha Nationalparks (nördliches Südwestafrika/Namibia). *Madoqua*, **14** : 197-266.

Sanders, W., 2007 – Taxonomic review of fossil Proboscidea (Mammalia) from Langebaanweg, South Africa. *Transactions of the Royal Society of South Africa*, **62** : 1-16.

Sauer, E., 1966 – Fossil eggshell of a giant struthious bird (*Struthio oshanai* sp. nov.) from Etosha Pan, SWA. *Cimbebasia*, **14** : 2-51.

Ségalen, L., Lee-Thorp J.A., and Cerling, T.E., 2007 - Timing of C4 grass expansion across sub-Saharan Africa. *Journal of Human Evolution*, **53**: 549-559.

Ségalen, L., Renard, M., Lee-Thorp, J.A., Emmanuel, L., Le Callonnec, L., Rafélis (de), M., Senut, B., Pickford, M., and Melice J.L., 2006 - Neogene climate change and emergence of C_4 grasses in the Namib, south western Africa, as reflected in ratite ^{13}C and ^{18}O. *Earth Planetary and Science Letters*, **244**: 725-734.

Senut, B., Dauphin, Y., and Pickford, M., 1998 - Nouveaux restes aviens du Néogène de la Sperrgebiet (Namibie): complément à la biostratigraphie avienne des éolianites du désert de Namib. *C. R. Acad. Sci. Paris*, **327**: 639-644.

Senut, B., and Pickford, M., 1995 - Fossil eggs and Cenozoic continental biostratigraphy of Namibia. *Palaeont. afr.*, **32** : 33-37.

Senut, B., Pickford, M., and Ward, J.D., 1994 - Biostratigraphie des éolianites néogènes du Sud de la Sperrgebiet (Désert de Namib, Namibie). *C. R. Acad. Sci. Paris*, Sér. II, **318** : 1001-1007.

Smith, A.M., 1980 – *Lacustrine Stromatolites of the Etosha Pan, S.W.A. (Namibia).* MSc Thesis, Univ. Natal (Durban) 140 pp.

Smith, A.M., and Mason, T.R., 1991 – Pleistocene, multiple-growth, lacustrine oncoids from the Poacher's Point Formation, Etosha Pan, northern Namibia. *Sedimentology*, **38** : 591-599.

Smith, C.H., 1827 - Synopsis of the Species of the Class Mammalia as Arranged with Reference to their Organisation by Cuvier and Other Naturalists : with Specific Characters, Synonyma, &c. &c. In : Cuvier, G., Griffith, E., Smith, C.H., Pidgeon, E., Gray, J.E., Latreille, P.A., and Gray, G.R., (eds) *The Animal Kingdom, Arranged in Conformity with its Organisation, by the Baron Cuvier, with Additional Descriptions*

of all the Species hitherto named, and of Many Not Before Noticed by Edward Griffith and others, **5**: 1-392, London, G.B. Whittaker.

Stuart-Williams, V., 1992 – Etosha : third largest lake in the world. *In* : A. Marsh and M. Seely (Eds) *Oshanas – Sustaining People, Environment and Development in Central Owambo, Namibia*. Windhoek, Typoprint, 13 pp.

Talma, A.S., and Rust, U., 1997 – Stable isotope characterization of calcrete, lake marl and stromatolites in the Etosha region, Namibia. *Madoqua*, **20** (1) : 75-80.

Thomas, H., 1980 - Les Bovidés du Miocène supérieur des couches de Mpesida et de la formation de Lukeino (District de Baringo, Kenya). *In:* R. Leakey and B. Ogot (eds) *Actes du 8ème Congrès Panafricain de Préhistoire: Etudes Quaternaires. Nairobi*, pp. 82-91.

Van Bruggen, A.C., 1963 – Report on the Mollusca of the 1961 Harvard-Smithsonian-Transvaal Museum Kalahari Expedition. *Ann. Transv. Mus.* **24**: 261-270.

Van Bruggen, A.C., 1970 – A contribution to the knowledge of non-marine Mollusca of South West Africa. *Zool. Meded.* **45**: 43-73.

Van Neer, W., and Lesur, J., 2004 - The ancient fish fauna from Asa Koma (Djibouti) and modern osteometric data on three Tilapiini and two *Clarias* catfish species. *Documenta Achaeobiologiae*, **2**: 141-160.

Vrba, E., 1997 - New fossils of Alcelaphini and Caprinae (Bovidae: Mammalia) from Awash, Ethiopia, and phylogenetic analysis of Alcelaphini. *Palaeontologia africana*, **34**: 127-198.

Wellington, J.H., 1938 – The Kunene River and the Etosha Plain. *S. Afr. Geogr. Jl*, **20** : 21-33.

Wellington, J.H ., 1939 – The Great Etosha Basin. *S. Afr. Geogr. Jl*, **21** : 47-48.

Wells, L.H., and Cooke, H.B.S., 1956 - Fossil Bovidae from the Limeworks Quarry, Makapansgat, Potgietersrus. *Palaeontologia africana*, **4**: 1-55.

Brevirhynchocyon gen. nov., a new name for the genus *Brachyrhynchocyon* Senut, 2008 (Mammalia, Macroscelidea) preoccupied by *Brachyrhynchocyon* Loomis, 1936 (Mammalia, Carnivora)

B. Senut[1] and G. Georgalis[2]

[1]Muséum National d'Histoire Naturelle, Département « Histoire de la Terre » & UMR 7207
CNRS, 8, rue Buffon, 75005 Paris, France
bsenut@mnhn.fr
[2]Department of Chemical Engineering, Aristotle University, Thessaloniki, Greece
dimetrodon82@yahoo.gr

In 2008, Senut described a new genus of Macroscelidea from the lower Miocene of the Northern Sperrgebiet in Namibia. As the name suggests, *Brachyrhynchocyon,* is a brachyodont animal with smooth premolars, large multipectinate upper incisors, and lacking m3. The new species *Brachyrhynchocyon jacobi* was erected as the type species of the new genus. In the same paper, *Miorhynchocyon gariepensis* (Senut, 2003) was transferred to the new genus, under the new combination *Brachyrhynchocyon gariepensis*.

However, the name *Brachyrhynchocyon* has already been used for an amphicyonid carnivoran (Loomis, in Scott and Jepsen, 1936). The type species of this genus is *Brachicyon intermedius* Loomis, 1931 from the Oligocene of North America. *Brachicyon* was shown to be preoccupied by *Brachycyon* Filhol, 1872 and so Loomis (1936) erected the new genus *Brachyrhynchocyon.* While compiling vertebrate taxonomic lists, one of us (G.G.) noticed the homonymy between the two genera. According to the International Code of Zoological Nomenclature (ICZN), *Brachyrhynchocyon* Senut, 2008, is a junior homonym of *Brachyrhynchocyon* Loomis, 1936. We therefore propose the new genus name *Brevirhynchocyon* gen. nov. to substitute *Brachyrhynchocyon* Senut, 2008. The new name also refers to the brachyodonty of this macroscelidid. *Brevis* is the latin synonym of the greek word brachys (βραχύς) meaning brief or short and *Rhynchocyon*, a modern genus of Macroscelididae and moreover a common ending for other genera of the family.

The two species of *Brachyrhynchocyon* Senut, 2008 are now reassigned as *Brevirhyn-chocyon jacobi* (Senut, 2008) comb. nov., which is the type species by original designation of the new genus and *Brevirhynchocyon gariepensis* (Senut, 2003) comb. nov.

References

Filhol, H. 1872. Recherches sur les Mammifères fossiles des dépôts de phosphates de chaux dans les départements du Lot, du Tarn et de Tarn-et-Garonne. Première Partie. Carnassiers et Chiroptères. *Ann. Sci. Géol.*, **3**, 7, 1-31.

Loomis, F.B. 1931. A new Oligocene dog. *American Journal of Science*, **22**, 100-102.

Scott, W.B. and Jepsen, G.L. 1936. The mammalian fauna of the White River Oligocene. Part I. Insectivora and Carnivora. *Trans. Amer. Phil. Soc.* (New Series), **28**, 1-149.

Senut, B. 2003. The Macroscelididae from the Miocene of the Orange River, Namibia. In: Pickford, M. and Senut, B. (eds), *Geology and Palaeobiology of the Central and Southern Namib*. Vol 2: Palaeontology of the Orange River Valley. *Mem. Geol. Surv. Namibia*, **19**, 119-141.

Senut, B. 2008. Macroscelididae from the lower Miocene of the Northern Sperrgebiet, Namibia. In: Pickford, M. and Senut, B. (eds) *Geology and Palaeobiology of the Northern Sperrgebiet. Mem. Geol. Surv. Namibia*, **20**, 185-225.

New Ratite Eggshells from the Miocene of Namibia

Martin Pickford

Collège de France, and
Département Histoire de la Terre, UMR 7207, CR2P du CNRS, Case postale 38, 8, rue Buffon, 75005, Paris
e-mail: pickford@mnhn.fr

Namibian Neogene deposits have yielded a remarkably comprehensive register of fossil ratite eggshells spanning the entire Miocene and Plio-Pleistocene. Previous studies recognised three genera of struthious egg types, from oldest to youngest named *Namornis* (1 species) *Diamantornis* (4 species) and *Struthio* (3 species) and one of aepyornithoid type, older than the struthious ones, hitherto left undetermined on account of the relatively poor preservation of the available material.

A palaeontological and geological survey carried out in November, 2010, in the Tsondab Valley and the Tsondab Flats to the west of the end point of the valley, led to the discovery of good samples of two hitherto unrecognised extinct taxa of eggs, one aepyornithoid, and the other, struthionid, from overlying strata. Neither of the samples fits into the previously established taxonomic schema, indicating that we are in the presence of undescribed taxa. We here analyse the eggshells and discuss their systematic and phylogenetic implications. A small, primitive pedetid tooth, found with the aepyornithoid shells, indicates an Early Miocene age for the deposits. This estimate is supported by comparing the new eggs with the established eggshell biochronology of Namibia, itself calibrated by mammalian biostratigraphy.

Introduction

Fossil ratite eggshells from the Neogene of Namibia are useful biochronological and palaeoclimatic resources (Dauphin *et al*., 1996, 1998; Pickford & Dauphin, 1993; Pickford & Senut, 1999; Pickford *et al*., 1993, 1995; Ségalen *et al*., 2002, 2004a, 2004b, 2006a, 2006b; Senut & Pickford, 1995; Senut *et al*., 1995, 1998, 2009). Work by other researchers has extended the Namib eggshell biochronology to other countries, notably Malawi (Stidham, 2004), Tanzania (Harrison & Msuya, 2005), Kenya (Harris & Leakey, 2003), and the Arabian Peninsula (Bibi *et al*., 2006), in cases providing refinement of the initial age estimates.

Previous studies of the Namibian eggs left several questions unanswered. In particular the aepyornithoid type of shell was left undetermined, mainly because of the relatively undiagnostic nature of the available material (Senut *et al*., 1995). It was noted that specimens from Elim attributed to *Namornis oshanai*, were appreciably thinner than material from the type locality, Beisebvlakte, Etosha, Namibia, and other fossils from Rooilepel and Awasib. However, given that the Elim fossils came from only two localities it could not be ruled out that the specimens represented particularly thin examples of *N. oshanai* (Pickford *et al*., 1995).

We are now in a position to address the above uncertainties, due to the collection of good samples of two types of eggshells in the Tsondab Vlei and the Tsondab Flats which lie from 3 to 35 km west of the end point of the Tsondab Valley. At Tsondab Vlei, it has now been established that the aepyornithoid eggs come from stratigraphic levels beneath those that yield eggs of *Namornis* (Fig. 1-3). It is confirmed that the Tsondab aepyornithoid eggs are thicker than those from the Sperrgebiet, whereas eggs from the northern part of the Namib-Naukluft Park previously attributed to *Namornis oshanai* are uniformly thinner than those from the type locality at Etosha and sites in the Sperrgebiet and the southern half of the Namib-Naukluft Park (Fig. 8).

The aim of this report is to describe and analyse the new samples of fossil eggs from Tsondab within the context of previous studies on Namibian ratite eggshells and to refine the biostratigraphy of the Tsondab Sandstone Formation which yielded them.
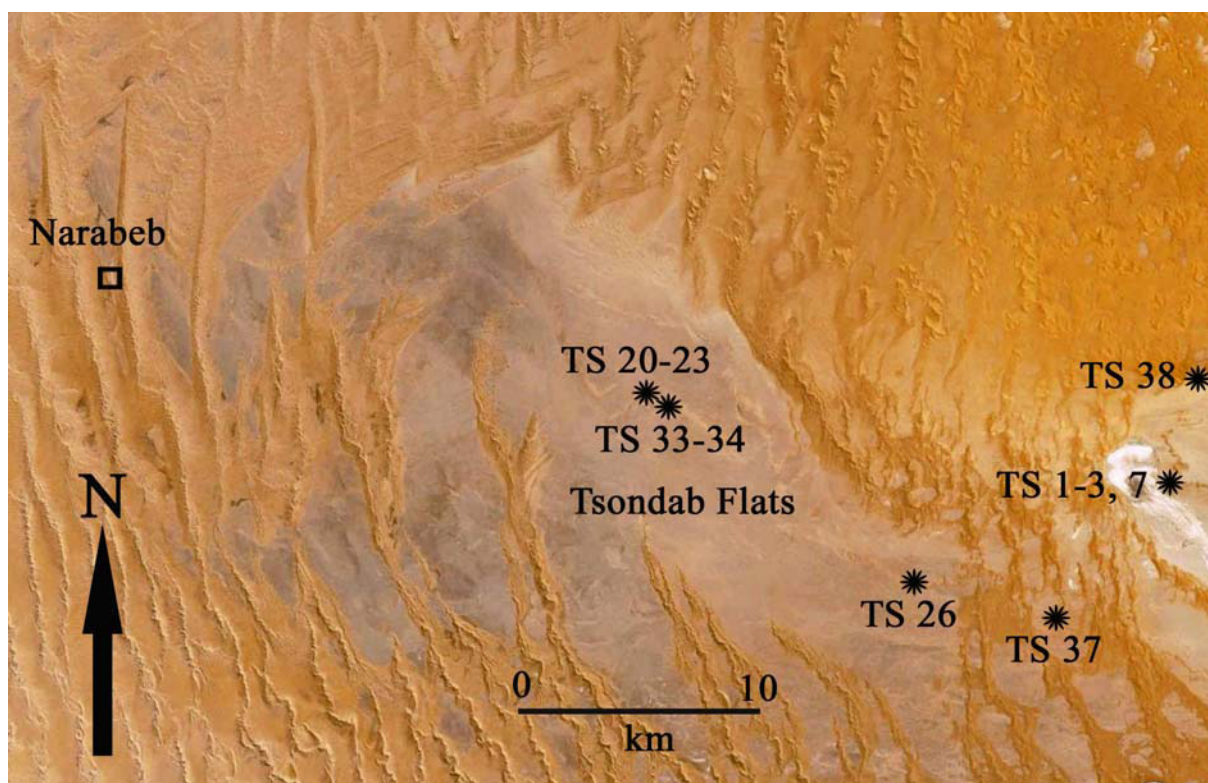
Figure 1: Fossil eggshell localities in the Tsondab Flats and near the end point of the Tsondab Valley, Namib-Naukluft Park, Namibia. TS 7 is the type locality of *Tsondabornis psammoides*, gen. et sp. nov., and of the Tsondab Formation (image modified from Google Earth).
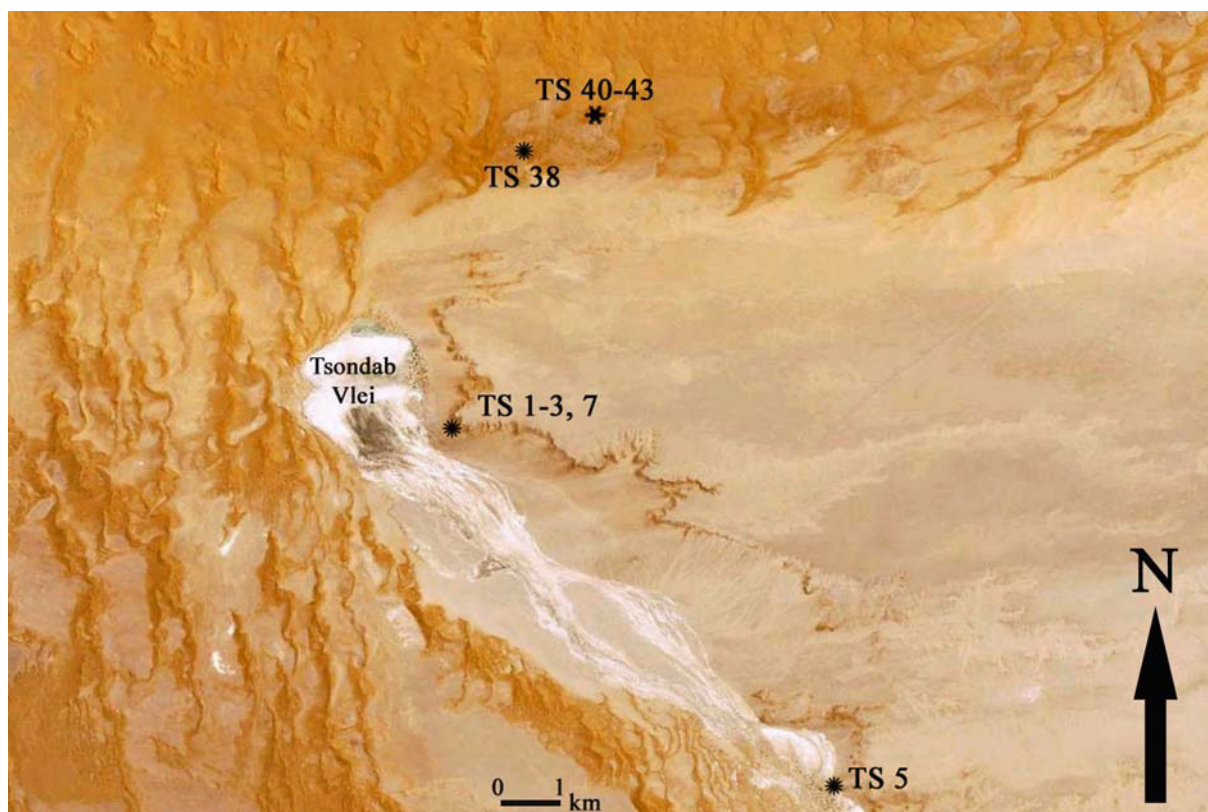
Figure 2: Fossil eggshell localities in the lower reaches of the Tsondab Vlei, Namib-Naukluft Park, Namibia. Localities TS 1-3, 5, 7 and 38 yield eggshells of *Tsondabornis psammoides*, whereas the younger localities TS 40-43, yield eggshells of *Namornis elimensis* (image modified from Google Earth).
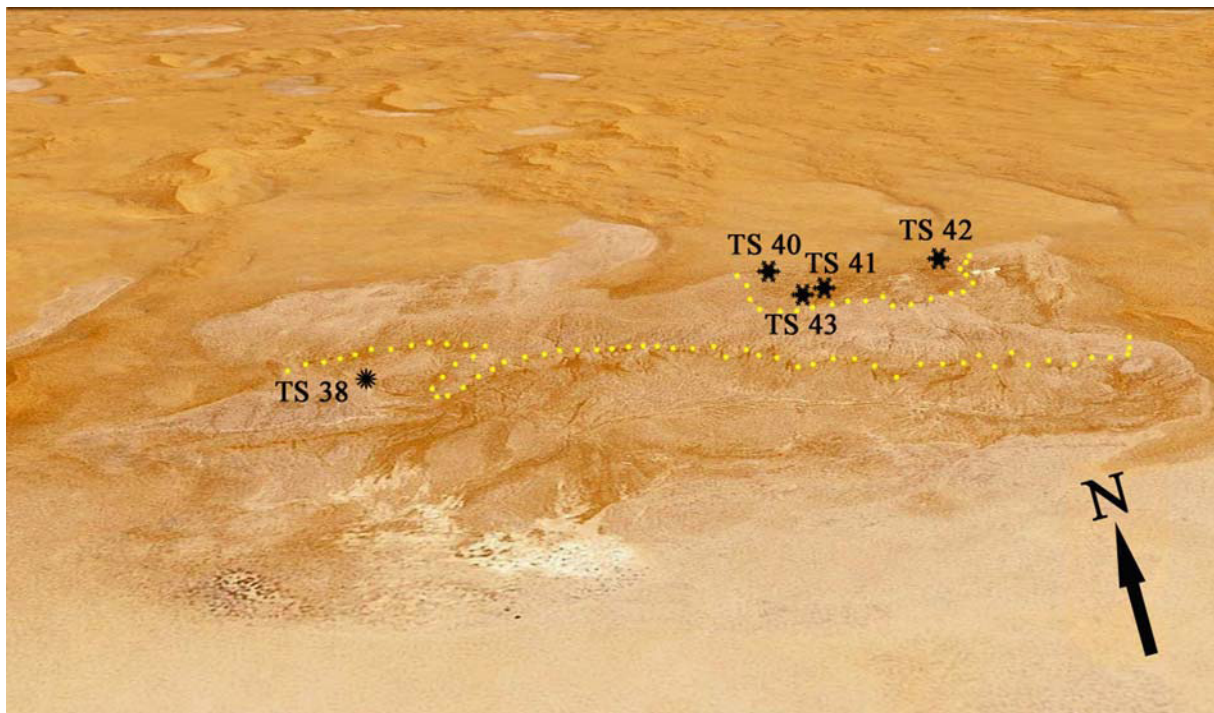
Figure 3: Ratite eggshell localities on the north flank of Tsondab Vlei. Super-bounding surfaces have been highlighted by dotted lines. TS 38 yielded *Tsondabornis psammoides* eggshells, whereas the younger sites TS 40-43 yielded only eggshells of *Namornis elimensis*. Oblique view from the south, extracted from Google Earth - the distance between TS 38 and TS 43 is ca 1 km. Note the Sossus Sand Sea in the background reposing unconformably on the Tsondab Sandstone.

Geological and stratigraphic context

The geology of the northern part of the Namib-Naukluft Park relevant to understanding the Cenozoic deposits, has been studied by numerous researchers (Besler, 1996; Besler & Marker, 1979; Heine, 1985; Lancaster, 1983, 1984a, 1984b; Lancaster & Teller, 1988; Lancaster *et al.*, 1984; Marker, 1977, 1979, 1980-81; Pickford & Senut, 1999; Rust & Wienecke, 1980; Seely & Mitchell, 1986; Selby *et al*, 1979; Teller & Lancaster, 1986, 1987; Teller *et al.*, 1990; Walter, 1986; Ward, 1987a, 1987b, 1988). In brief, overlying the Namib Unconformity Surface (NUS of Ward, 1987a) is a thick and varied sequence of sands and related deposits attributed to the Tsondab Sandstone Formation which accumulated under arid to hyper-arid palaeoclimatic conditions, with intercalated deposits indicative of periods of sub-humid conditions. Overlying the Tsondab Formation there is the Karpfenkliff Conglomerate which is usually cemented by the Kamberg Calcrete. Incision of the Kuiseb

and neighbouring rivers to the north and to the south into their current channels followed the formation of the Kamberg Calcrete. In these valleys there occurs a suite of fluvial deposits ranging from conglomerates to silts dating from the Pleistocene and Recent (Ward, 1987a). Finally, younger than all other deposits are the mobile sands of the Sossus Sand Sea underlain by loose gravel and granule lags.

The fossil eggshells described in this report come from the Mio-Pliocene Tsondab Sandstone Formation. All the eggshells derive from the aeolian facies of the Tsondab Formation, the other facies (fluvial, lacustrine) being poorly fossiliferous. Fossil and sub-fossil eggs of *Struthio camelus* were found but are not included in this analysis.

The Tsondab Vlei and Tsondab Flats to the west comprise a topographically varied landscape consisting of various granule or gravel covered "terraces" cut into extensive aeolianite deposits of Tertiary age (Marker, 1977, 1979, 1980-81), overlain by loose sands of the Sossus Sand Sea. The

Locality	Co-ordinates WGS 84	Altitude	Taxon
TS 01	23°55'20.4"S : 15°23'00.9"E	641 m	*Tsondabornis psammoides*
TS 02	23°55'19.3"S : 15°23'03.0"E	648 m	*Tsondabornis psammoides*
TS 03	23°55'22.0"S : 15°23'07.8"E	670 m	*Tsondabornis psammoides*
TS 05	23°59'01.5"S : 15°26'44.3"E	672 m	*Tsondabornis psammoides*
TS 06	23°58'16.8"S : 15°26'38.3"E	691 m	*Struthio camelus*
TS 07	23°55'19.0"S : 15°23'09.7"E	694 m	*Tsondabornis psammoides*
TS 10	23°57'36.1"S : 15°20'32.9"E	622 m	*Struthio camelus*
TS 20	23°52'36.0"S : 15°10'12.3"E	542 m	*Tsondabornis psammoides*
TS 21	23°52'43.5"S : 15°10'03.5"E	549 m	*Tsondabornis psammoides*
TS 22	23°52'42.8"S : 15°10'02.9"E	546 m	*Tsondabornis psammoides*
TS 23	23°52'37.2"S : 15°10'09.5"E	543 m	*Tsondabornis psammoides*
TS 28	23°57'19.0"S : 15°16'31.9"E	600 m	*Tsondabornis psammoides*
TS 33	23°52'59.2"S : 15°11'10.6"E	565 m	*Tsondabornis psammoides*
TS 34	23°52'56.5"S : 15°11'09.0"E	556 m	*Tsondabornis psammoides*
TS 37	23°58'01.5"S : 15°20'12.0"E	622 m	*Tsondabornis psammoides*
TS 38	23°52'40.9"S : 15°24'02.4"E	686 m	*Tsondabornis psammoides*
TS 40	23°52'25.3"S : 15°24'37.5"E	720 m	*Namornis elimensis*
TS 41	23°52'29.8"S : 15°24'40.9"E	716 m	*Namornis elimensis*
TS 42	23°52'24.9"S : 15°24'53.4"E	720 m	*Namornis elimensis*
TS 43	23°52'31.3"S : 15°24'58.6"E	711 m	*Namornis elimensis*
Gamsberg Pass (Paradys)	23°21'02.3"S : 15°54'00.5"E	1025 m	*Tsondabornis psammoides*
Elim	24°24'45.7"S : 15°45'07.0"E	900 m	*Namornis elimensis*
Diep Rivier Cliffs	24°07'56"S : 15°53'44"E	1075 m	*Namornis elimensis*
Zebra Hill, Kamberg	23°37'40"S : 15°38'43"E	828 m	*Tsondabornis psammoides*
Tsauchab	24°30'14.0"S : 15°43'02.1"E	772 m	*Diamantornis laini*
North of Sesriem Airstrip	24°28'59"S : 15°44'21"E	784 m	*Diamantornis wardi*
Tsondab South	24°00'47"S : 15°29'24"E	723 m	*Diamantornis wardi*
Narabeb	23°49'12.4"S : 14°57'11.8"E	414 m	*Diamantornis wardi*
Narabeb	23°49'12.4"S : 14°57'11.8"E	414 m	*Tsondabornis psammoides*
West Pan	23°34'10.1"S : 14°48'31.6"E	309 m	*Diamantornis corbetti*

Table 1: Fossil eggshell localities mapped during the 2010 field season in the Tsondab region (TS) and previously known localities in the northern part of the Namib-Naukluft Park, Namibia.

most extensive of the "terraces" is the conglomeratic Kamberg Calcrete (Ward, 1987a), a duricrust that varies in character depending on its distance from the Great Escarpment (Fig. 4). Proximal to the scarp it contains large boulders and cobbles and is up to 30-40 metres thick in places close to valleys, thinning in the interfluves (Pickford & Senut, 1999). The calcrete thins westwards away from the scarp and its clastic content becomes finer grained. At the current end point of the Tsondab Vlei, the calcrete is about 1 metre thick with cobbles up to 5 cm in diameter. 25 km further west the duricrust directly overlies indurated white silts and its clastic component is sand-sized to silt-sized.

Here the duricrust is only 2-5 cm thick and it eventually pinches out completely about 40 km west of Tsondab Vlei. In its proximal parts the Kamberg Calcrete is of pedogenic facies (Yaalon & Ward, 1982) but at its western edges where it is only a few cm thick it was formed at the surface during many cycles of condensation and evaporation of dew. The Kamberg Calcrete is a composite unit, but is useful as a geomorphological marker level, as it provides evidence for a widespread, stabilised, almost planar landscape prior to a phase of deep incision, comprising the Kuiseb, Tsondab, Tsauchab and other rivers that currently drain the Great Escarpment.
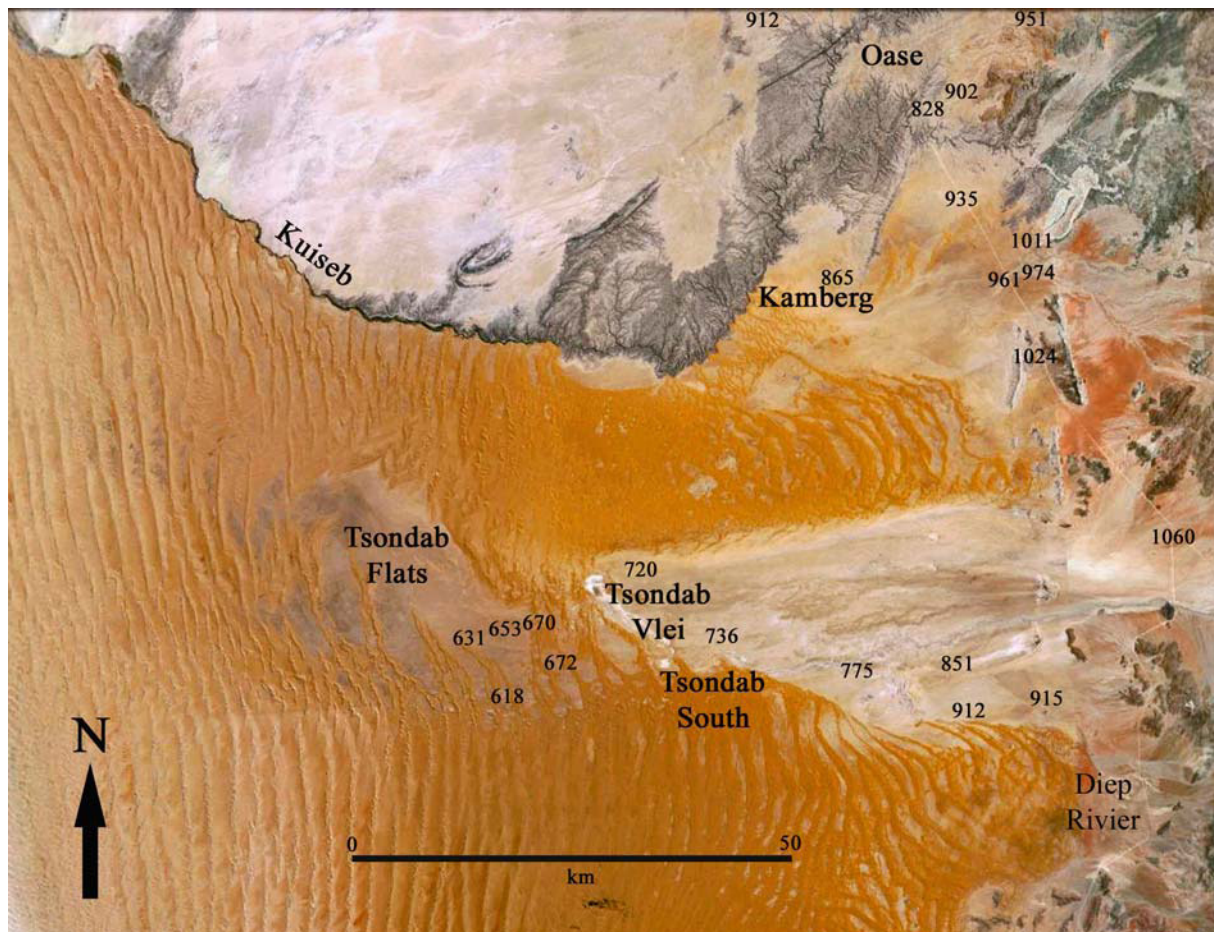
Figure 4: Spot heights (in metres) on calcrete in the northern part of the Namib-Naukluft Park and neighbouring farms. Note the decrease in altitude from the Great Escarpment in the east with spot heights of over 1000 m, decreasing to altitudes of just over 600 metres 80 km to the southwest. At Tsondab South and Elim (see fig. 11), these calcretes contain Pleistocene fossils and stone tools (image modified from Google Earth).

In detail, the Kamberg Calcrete has an undulating surface, draping down into shallow valleys and gullies and up the other side. In its proximal parts, close to the Great Escarpment, it formed under a thin (generally less than 50 cm) vegetated sand cover (grassy plains for the most part), but over much of its present extent it is exposed at the surface and is in the process of being dissolved by rainwater and especially by dew. Cobbles of carbonate rocks (limestone, dolomite, calcrete) often show a runnelled surface which is formed by dew condensing on exposed surfaces of the rocks and trickling down their sides to the ground. Repeated many times, such dew produces a surface that is patterned by runnels dissolved into the surface of the rock. The same happens to fossil eggshells that are exposed for extended periods.

After a long phase of landscape stability (Ward, 1987a, estimated the duration to be about 0.5 million years, but it could have been much shorter than this, perhaps as little as 40,000 years (Leeder, 1975)) fluvial incision started, culminating in the present day drainage network of the region. In the Tsondab Valley, Marker (1979) recognised seven terraces resulting from various phases of incision. Later workers tended to recognise fewer terraces. Nevertheless there are at least three widespread "terraces", not only in the Tsondab Valley, but also close to the base of the Great Escarpment, where at least three flights of calcreted terraces have been noted (Pickford & Senut, 1999).

The importance of this geomorphological development for understanding the palaeontology of the region is that post-Kamberg incision cut into the Tsondab Sandstone For-

mation, thereby exposing different layers from which fossils may be collected. It should be noted that at Diep Rivier, there are impressive cliffs of sandstone (summit at ca 1000 m) which stand proud of the Kamberg Calcrete horizon, and which, at the time of calcrete genesis, comprised bornhardts rising a 80-90 metres above the generally planar Kamberg Plains (altitude in the vicinity ca 915 m (Fig. 4).

The fossils collected by the Namibia Palaeontology Expedition reveal that sedimentation patterns in the Tsondab Formation were complex, with wind driven cut and fill on large and small scales. Super-bounding surfaces are common in the Tsondab region, as are the usual smaller scale dune cross-cutting features. Nevertheless, outcrops are sufficiently informative that the sequence of fossil horizons can in most cases be established by superpositional criteria. By this means we can be sure that the eggs of *Tsondabornis* are older than those attributed to *Namornis* (Fig. 3) which are in their turn older than those of *Diamantornis* and finally those of *Struthio*.

Systematic descriptions

Family Struthionidae Vigors, 1825
Genus *Tsondabornis* nov.

Diagnosis - Eggshells with smooth to lightly undulating external surface, pores arranged in sub-parallel slits and dagger point depressions.

Differential diagnosis - *Tsondabornis* differs from *Namornis*, *Diamantornis* and *Struthio* by possessing pores arranged in sub-parallel slits and dagger point depressions, and not in clumps or clusters. Its outer shell surface is smooth to slightly undulating, which differentiates it from other aepyornithoids and the above taxa. *Tsondabornis* differs from *Psammornis* by its thinner shells and its slit-like pore structures.

Derivatio nominis - The genus name refers to the *Tsondab* area where the material was collected and *ornis*, Greek for bird.

Synonymy - Pending the discovery of diagnostic specimens, in previous literature these Namibian eggs were referred to "aepyornithoid".

Type species - *Tsondabornis psammoides* sp. nov.

Species *Tsondabornis psammoides* nov.

Diagnosis - Eggshells ranging in thickness from 1.5 to 2.2 mm, mode 1.8 mm, some fragments showing incipient vermiform or undulating sculpture of the outer shell surface.

Derivatio nominis - The species name *psammoides* refers to the fact that all the specimens were found in sandstone.

Holotype - TS 7, eggshell fragment associated with dozens of other fragments many of which are *in situ* in the Tsondab Sandstone.

Type locality and age - TS 7, Tsondab Sandstone Formation (type area of the formation) ca 18 Ma.

Material - Numerous eggshell fragments (see Table 1 for complete list of localities).

Description - The eggshells of *Tsondabornis psammoides* generally possess a smooth to slightly undulating outer surface, in which the pores are usually subtle, best viewed in slanting light with a low power lens (4x – 10x). Some specimens have more obvious slits arranged in a sub-parallel pattern, with scattered dagger point depressions scattered here and there.

The eggs attributed to *Tsondabornis psammoides* range in thickness from 1.3 to 2.3 mm, discounting obviously eroded specimens (Fig. 6D, 6E). The mode varies from 1.8 to 2 mm in the different samples.
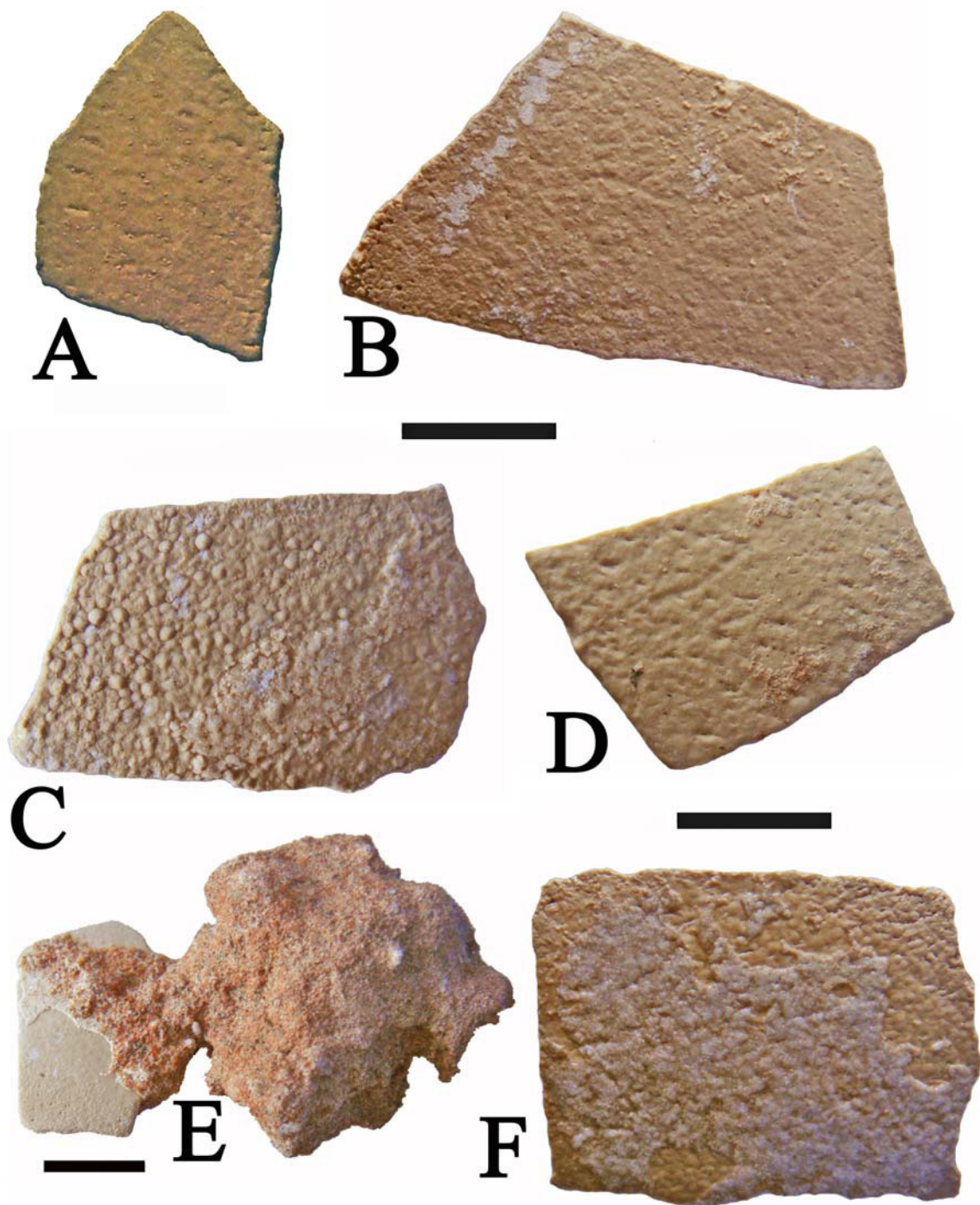
Figure 5: Eggshell fragments of *Tsondabornis psammoides* gen. et sp. nov. from the type locality, TS 7, Tsondab Cliffs, Namib-Naukluft Park. A) holotype showing sub-parallel slits and a few dagger point pits, B) a particularly smooth example in which it is difficult to make out the pores, C) example in which the outer surface either did not form, or has been removed by erosion, exposing the external part of the mammillary layer, D) specimen with sub-parallel slits, dagger point pits and a slightly undulating external shell surface, E) egg-

There were about 200 pores per 4 cm² counted on one specimen which possessed many pores. Some fragments appear to have fewer pores, which could be due either to variability of pore density over the egg, a well known variation in extant ostriches (Sauer, 1966) or to variation between eggs. It is also probable that some pores are so small that they are easily missed during counting.
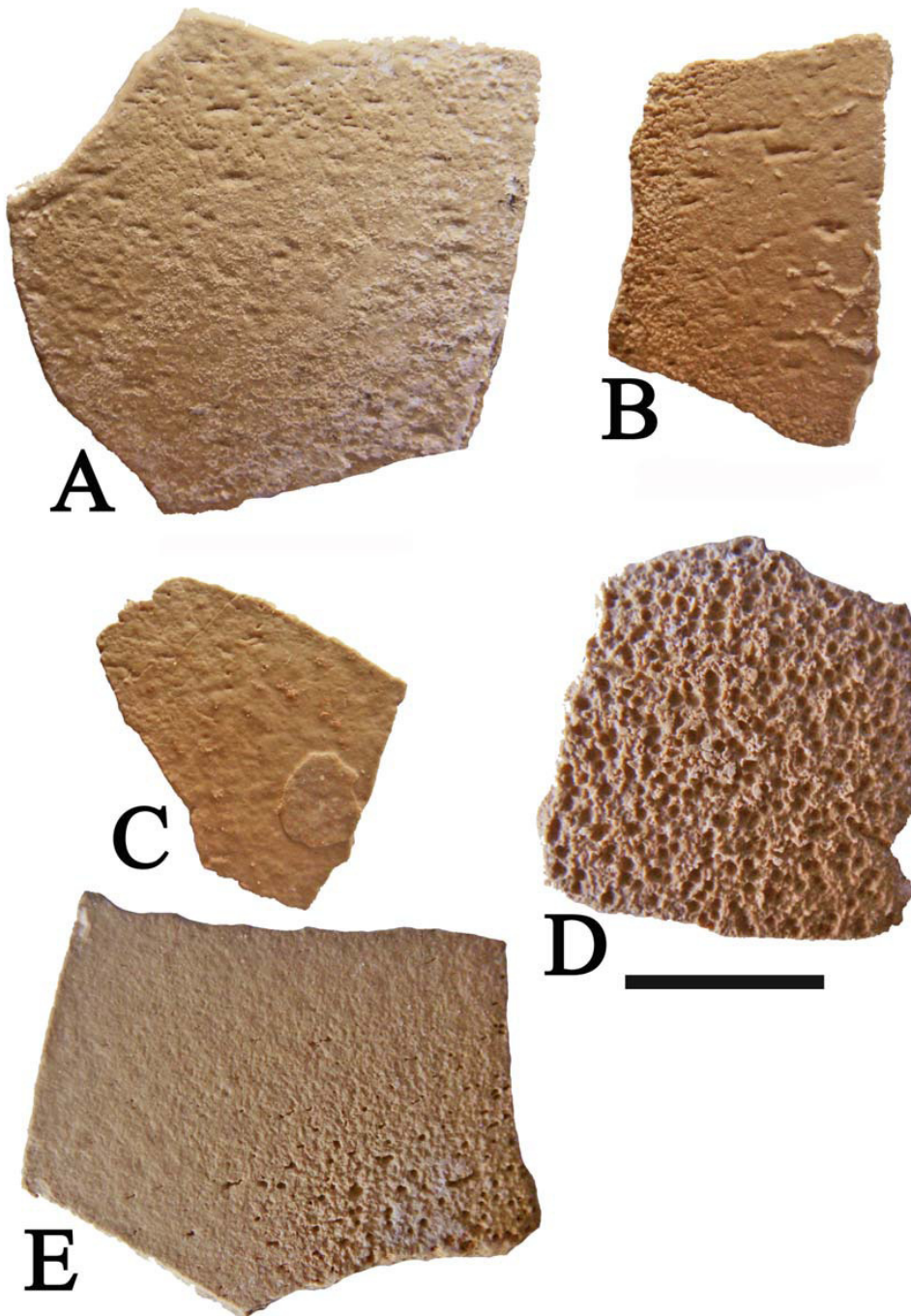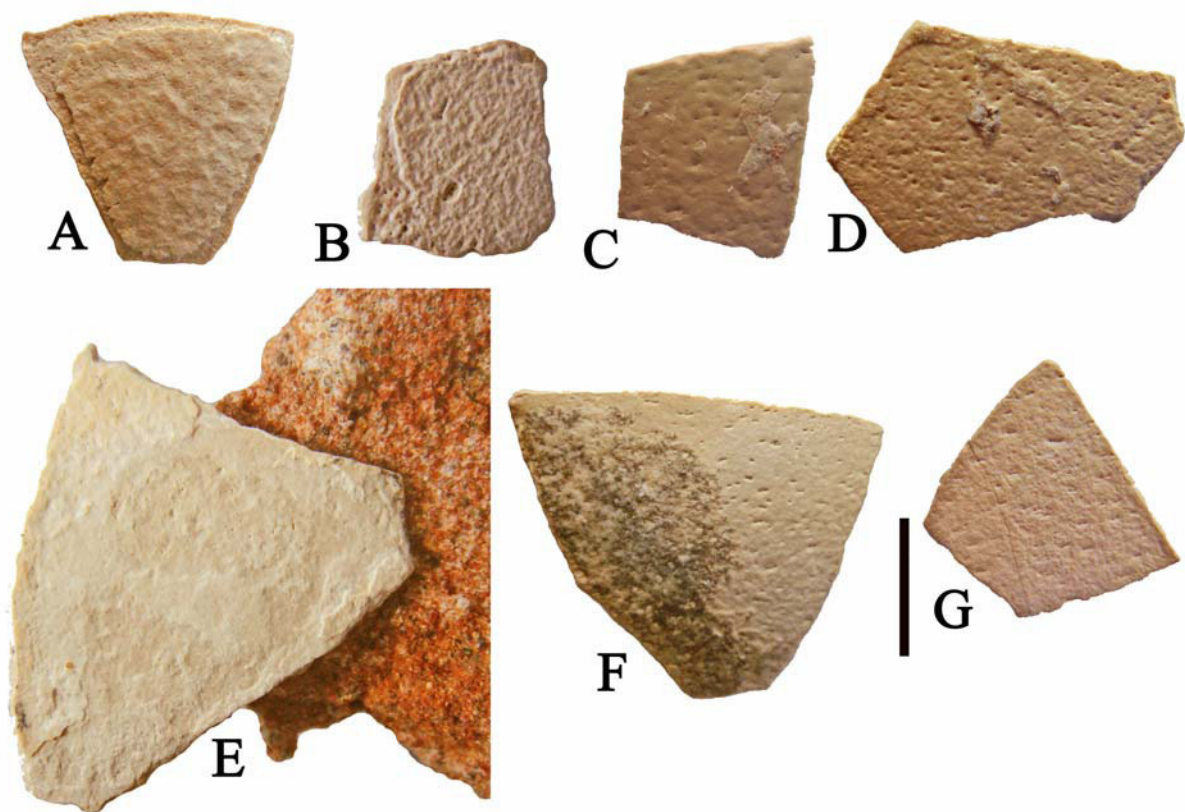

Figure 6: Eggshell fragments of *Tsondabornis psammoides* gen. et sp. nov. from the type locality TS 7, Tsondab Cliffs in the northern part of the Namib-Naukluft Park, Namibia. A) specimen showing sub-parallel slits and dagger point pores, B) specimen with some slits running into each other, C) a specimen with slightly undulating surface with slits and dagger point pore complexes, D) eroded specimen in which the outer layer has been completely removed, exposing the inner parts of the mammillary layer, E) a specimen in which a gradient of erosion exposes deeper and deeper parts of the external surface of the eggshell. Note how the slits are more easily observed in the eroded part than in the fresh part of the shell (scale – 10 mm).

Figure 7:*Tsondabornis psammoides* eggshell fragments from various localities in the Tsondab Vlei and Tsondab Flats, Namib-Naukluft Park, Namibia. A) TS 20, B) TS 22, C) TS 28, D) TS 33, E) TS 23, specimen

Discussion - *Tsondabornis psammoides* eggshells occur widely in the northern part of the Namib-Naukluft Park, but are seldom common save at Zebra Hill. They occur in dark red aeolianites which have been pervasively affected by bioturbation, mostly plant root systems, but also hives (*Namajenga mwichwa* Pickford, 2008a) and foraging tunnels of the termites *Hodotermes* and more rarely *Psammotermes* (Seely & Mitchell, 1986). The same levels of sandstone often yield clumps of white nodules, resembling coprolites, although the true nature of the nodules remains to be determined. In several places, fossil roof webs of the buck-spoor spider, *Seothyra* were found (Pickford, 2000).

The combination of the trace fossils, red colouration of the sands and the widespread outcrops of the Oase Member (fluvial facies of the Tsondab Formation) suggests that the palaeoenvironment at the time of deposition was one of summer rainfall with a semi-arid to arid palaeoclimate.

Species *Tsondabornis minor* nov.

Diagnosis - Eggshells ranging in thickness from 1.0 to1.7 mm, mode 1.3 mm, external surface of eggs generally smooth, without undulating or vermiform sculpture.

Derivatio nominis - The species name *minor* refers to the fact that all the specimens of eggs are appreciably thinner than those of the type species, implying a smaller species.

Holotype - EF 95'01, eggshell fragment.

Type locality and age.- Elisabethfeld, Sperrgebiet, Namibia, Early Miocene ca 21 Ma on the basis of mammalian biochronology.

**Other localities** - Grillental, Langental,

Fiskus

Description - The eggshells of *Tsondabornis minor* are usually smooth with little or no sign of undulations, save in wind-eroded specimens or material in which the shell surface has been dissolved by dew. Pores are arranged in sub-parallel slits with dagger-point pits scattered here and there.

Shell thickness ranges from 1.0 to 1.7 mm, the mode ranging from 1.2 to 1.5 mm at different localities. In the holotype specimen there are about 100 pores per 4 cm², but other specimens have fewer, reflecting within-egg and between-egg variation.

Discussion - The fossil eggshells from the fluvio-paludal deposits of the Sperrgebiet were previously attributed to an unidentified bird species with "aepyornithoid" egg morphology. Elisabethfeld has yielded bones of a diminutive ostrich (*Struthio coppensi*) (Mourer-Chauviré *et al.*, 1996a, 1996b) which could well be the bird responsible for the eggs (they are compatible in dimensions).

The fact that eggshells of *Tsondabornis minor* are common at all four localities in the Northern Sperrgebiet, suggests that the species was well adapted to the palaeoenvironment, which was sub-humid to semi-arid with indications of both summer and winter rainfall. The terrestrial gastropods *Trigonephrus* and *Dorcasia* are common in deposits at Grillental and Elisabethfeld (Pickford, 2008b) as are hives of the harvester termite *Hodotermes*. The mammalian fauna, frogs and tortoises also indicate that the fluvio-paludal deposits of the northern Sperrgebiet accumulated under sub-humid to semi-arid palaeoclimatic conditions close to a winter rainfall zone or within the belt that experienced both winter and summer rainfall.
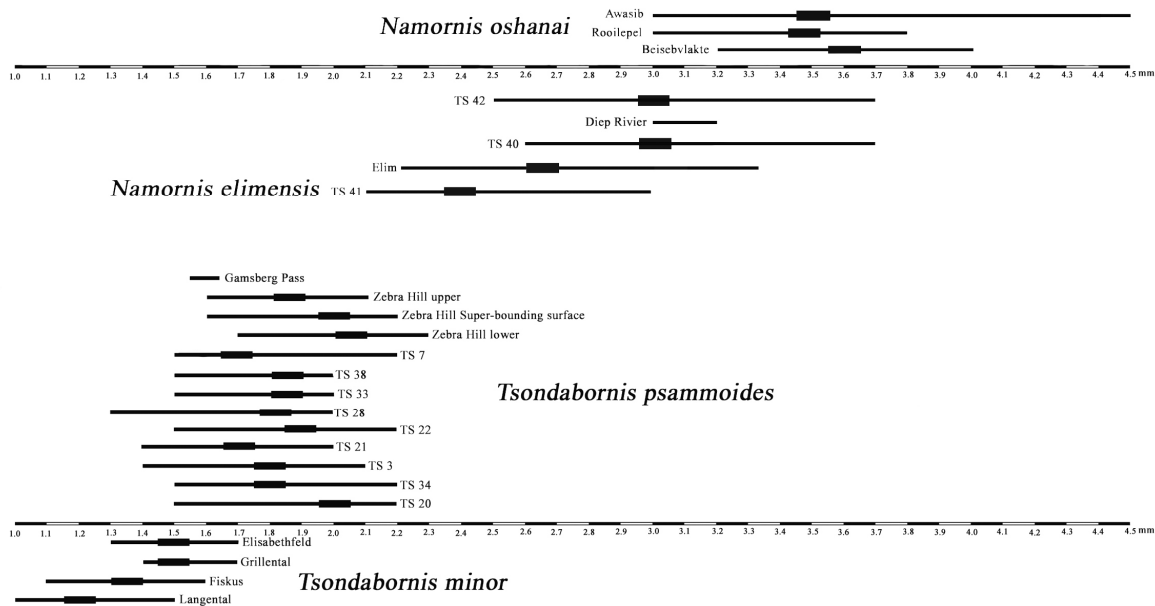
Figure 8: Shell thickness of Early and basal Middle Miocene ratite eggs from Namibia. The thin bar represents the range of variation; the thick bar is the mode.

Genus *Namornis* Pickford, Senut & Dauphin, 1994

Species *Namornis elimensis* nov.

Diagnosis - Eggshells ranging in thickness from 2.5 to 3.7 mm, mean 3.2 mm which is less than the type species, *Namornis osha-*

nai, from Beisebvlakte, Etosha, Namibia (range 3.2 to 4.0 mm, mean 3.6 mm). Pores arranged both in clusters in the depths of vermiform depressions and in sub-parallel slits (like those of aepyornithoids).

Derivatio nominis - The species name refers to the *Elim* Gullies north of Sossus Vlei,

Figure 9: Eggshell (holotype) of *Tsondabornis minor* from Elisabethfeld, Sperrgebiet, Namibia (view of external surface showing sub-parallel slits and dagger point pores (scale - 10 mm).

eroded into the Tsondab Sandstone, where the type series was collected.

Holotype - Eggshell fragment from Elim housed at the Geological Museum, Geological Survey of Namibia, Windhoek (Fig. 10C).

Type locality and age - Elim Gullies, Tsondab Sandstone, ca 17-16.5 Ma.

Description - The external surface of the eggshells of *Namornis elimensis* is patterned by a complex undulating system of depressions and pore complexes (Pickford *et al.*, 1995). In addition in some shells there are parts of the surface in which there are slit-like depressions arranged in sub-parallel fashion, recalling the situation in eggs of *Tsondabornis psammoides* but with swollen slit edges.

Eggshells of *Namornis elimensis* range in thickness from 2.1 to 3.7 mm, with modes ranging from 2.4 to 3.0 mm at different localities, thinner than the eggs attributed to *Namornis oshanai* from the Sperrgebiet (range 3.4 to 4.5, mode ranging from 3.5 to 3.6) and Beisebvlakte (range 3.2 to 4.0 mm, mode 3.6 mm).
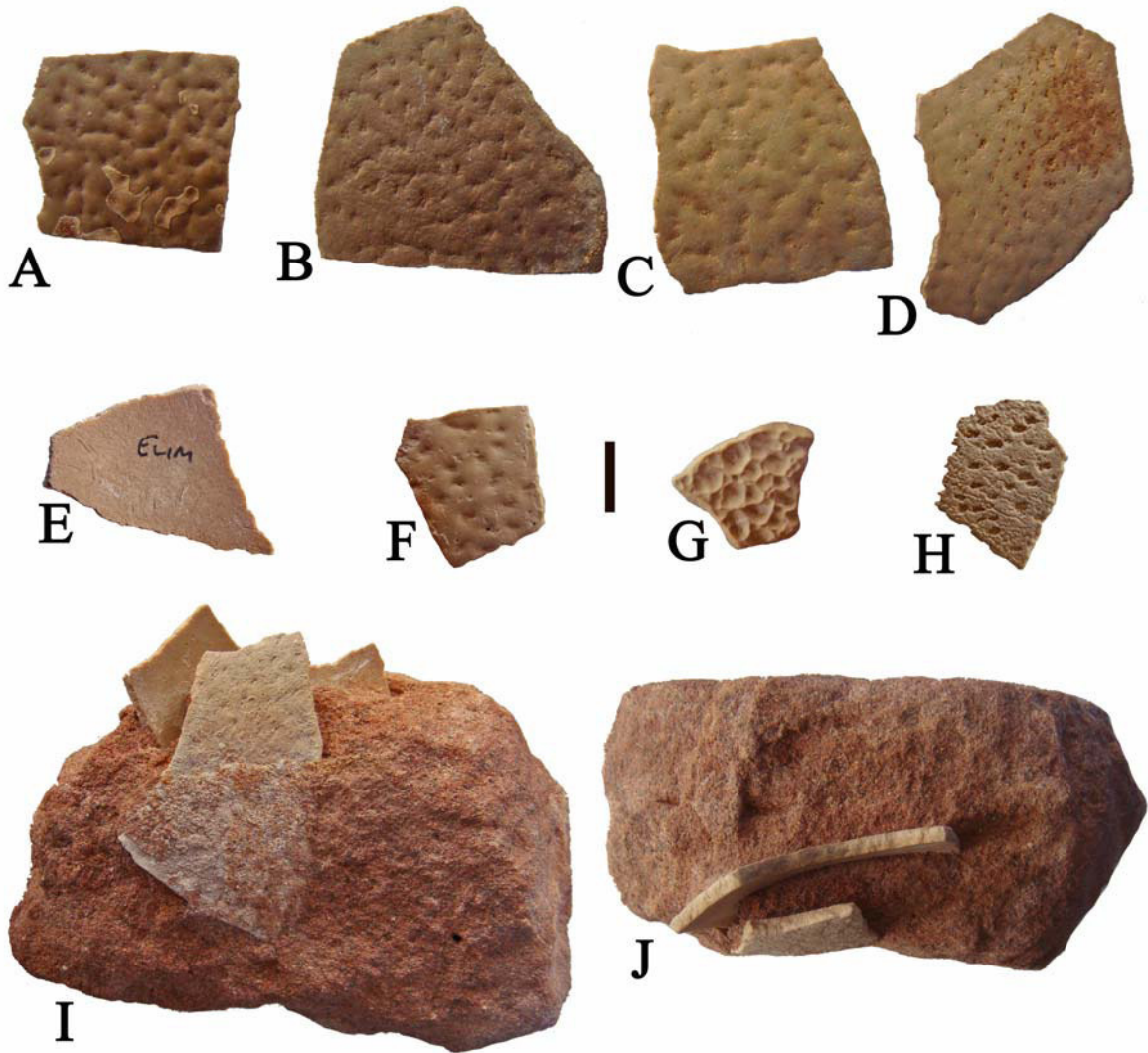
In *Namornis elimensis* from Tsondab Vlei there are about 40 pore complexes per 4 cm². The Elim and Diep Rivier sample were reported to have 24-37 pore complexes per 4 cm² (Pickford *et al.*, 1995). *Namornis oshanai* possesses between 16 and 44 pore complexes per 4 cm² (Sauer, 1966).

Discussion - When fossil eggshells of this species were known from only a single site, it was not clear whether their diminutive thickness should be interpreted as a species character or as a case of a particularly thin egg of *Namornis oshanai*. Now that the same thin egg type has been found at six localities in the northern half of the Namib-Naukluft Park, whereas none of the thicker eggshells of *Namornis oshanai* have been found there (they occur at Awasib in the southern part of the Namib-Naukluft Park and in the Sperrgebiet (Fig. 8)) then it is clear that the eggs from the northern part of the NNP belong to a separate species, here named *Namornis elimensis*.

A striking feature of the eggshells of *Namornis elimensis* is that the pores are arranged not only in clusters in the depths of vermiform depressions, but many of them also occur in sub-parallel slits, as in aepyornithoids. This combination of pore arrangement suggests that the *Namornis* eggshell type evolved from the *Tsondabornis* type, in which the pores are mostly in sub-parallel slits and dagger point depressions. Although the outer surfaces of most of the eggshells of *Tsondabornis* are smooth, there are specimens in which the surface is undulating with shallow vermiform depressions. We interpret these undulations to be precursors of the deeper, better expressed vermiform depressions that occur in eggshells of *Namornis*. If so, then *Tsondabornis* is likely the ancestral group from which *Namornis* evolved.

A strange feature of the eggs of *Namornis elimensis* is that they appear to occur as singletons, or at most in pairs. As a result, the eggs are found in small patches of shell fragments, and not in immense concentrations of broken eggshells such as typify nests of *Diamantornis* and *Struthio*. For this reason, the eggs of *N. elimensis* are more

difficult to locate than those of the other genera. It is still unclear whether the pattern of occurrence is due to the fact that the species was laying small clutches of eggs (K-strategy reproduction) or whether the eggs found were "scatter" eggs, much as extant *Struthio came-* *lus* occasionally lays an egg far from the nest, and immediately abandons it. Further field research is required to determine whether the pattern repeats itself at all of the occurrences or not.


Figure 10: Fossil eggshells of *Namornis elimensis* from the northern part of the Namib-Naukluft Park. A-E, I-J) specimens from the type locality, Elim (C is the holotype, E is the inner surface of the egg); F-H) specimens from TS 40 (Tsondab Vlei) F) un-eroded specimen, G) specimen with wind facetted external surface, H) specimen in which the external layer has been removed by sandblasting, exposing the pore complexes and mammillary layer (scale - 10 mm except I-J, which are reduced).

Discussion on ratite eggshells from the northern part of the Namib-Naukluft Park

The northern part of the Namib-Naukluft Park, north of Sesriem (Fig. 11) has yielded a large variety of fossil avian eggshells spanning much of the Miocene. The samples from this part of Namibia complement and extend downwards the succession of egg types described from the southern part of the park and the Sperrgebiet (Pickford *et al*., 1995) (Fig. 14).
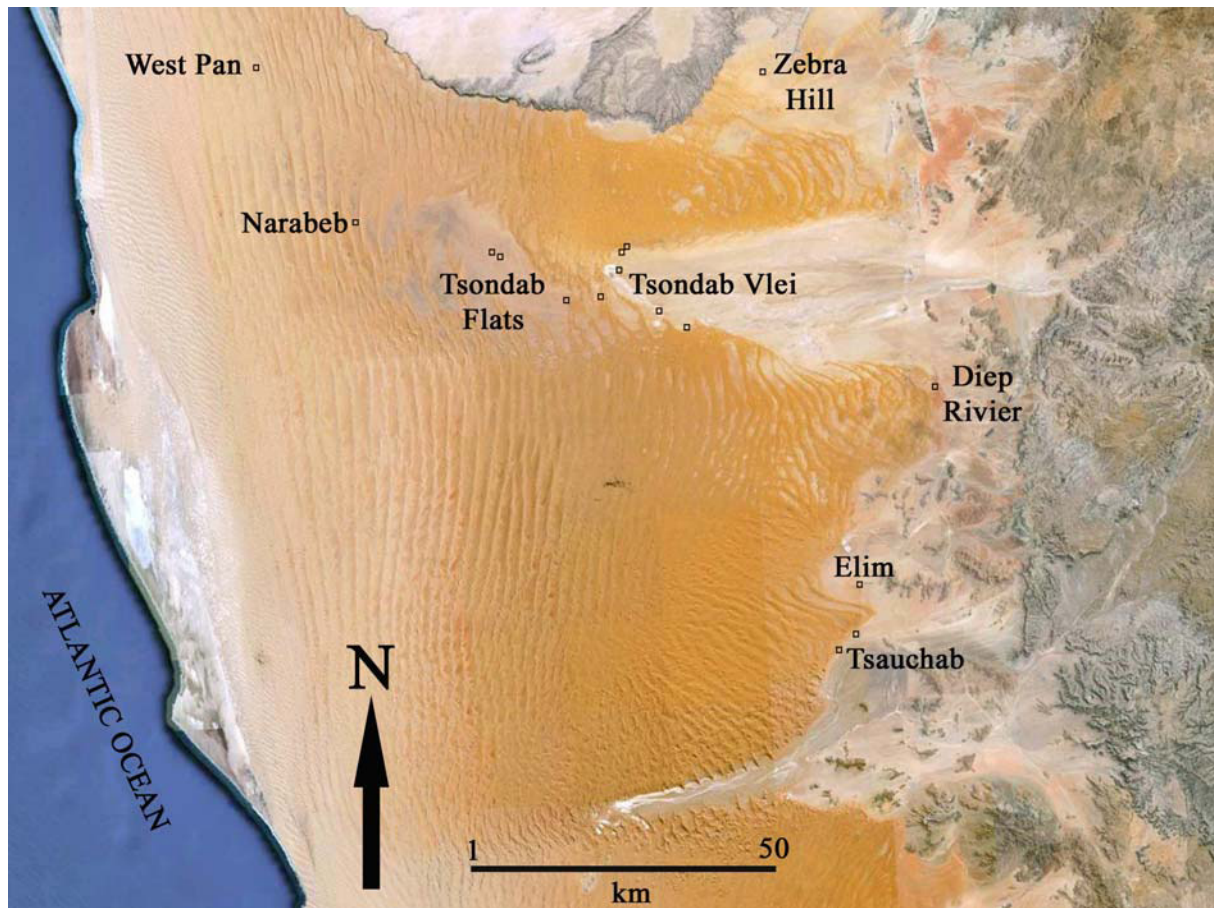
Figure 11: Fossil eggshell localities in the Tsondab Sandstone in the northern part of the Namib-Naukluft Park. Localities that yield fossil eggs of *Struthio camelus* have been omitted (image modified from Google Earth).

Geochronology and Palaeobiogeography

Pickford & Senut (1999) summarised the biochronology of the Neogene and Quaternary struthious eggs of Namibia. The succession of egg types is based on superposition of the strata from which they were collected. Calibration of the succession was based on fossil mammals that occur in the same strata as some of the eggs, but because some levels failed to yield mammals, then there is residual doubt about the age determinations of some of the taxa. For the latter taxa estimates of the age were made by interpolation.

Since then, fossil struthious eggs have been reported from Malawi (Stidham, 2004), Tanzania (Harrison & Msuya, 2005), Kenya (Harris & Leakey, 2003) and the United Arab Emirates (Bibi *et al*., 2006) all of which are associated with fossil mammals and in the case of Tanzania and Kenya, with radio-isotopic age determinations on superjacent volcanic rocks.

Perhaps the most interesting assemblage from the point of view of its diversity is that from Lothagam, Kenya, where eggshells attributed to *Struthio* sp. by Harris & Leakey (2003) belong to *Diamantornis laini* and *Struthio* cf *karingarabensis* (or *daberasensis*). These fossils come from the Lower Nawata (7.4 – 6.5 Ma), Upper Nawata (6.5 – 5 Ma) and Apak Member (5 – 4.2 Ma) respectively. The Lothagam succession also yielded eggs with aepyornithoid morphology.

On the basis of the Lothagam eggshells, Stidham (2004) suggested that the age determinations of the Namibian egg types may need revision upwards by about a million years. Since biochronology based on mammals often has error margins of the order of half a million years, this suggestion may be valid, but before accepting it some

aspects of the evidence need to be considered. According to Stidham (2004) the Lower Nawata levels yielded eggshell of *D. wardi* but Harrison & Msuya (2005) considered that the specimens concerned belong to
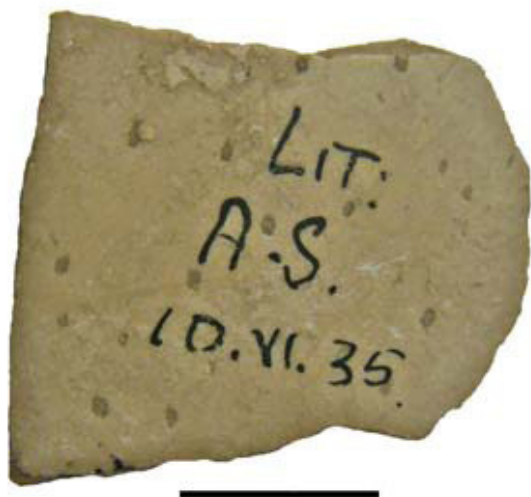
Figure 12: Eggshell fragment from Laetoli, Tanzania, housed in the NHM London, originally identified as *Struthio daberasensis* (Pickford & Senut, 1999). The eggshell is 3.2 mm thick which is substantially thicker than the range of variation in *S. daberasensis* (range 1.7 – 2.5 mm) and supports its re-identification as *Struthio kakesiensis*, even though its pore complexes are comparable to those of *S. daberasensis* (scale – 10 mm).

D. laini, which would resolve the apparent biochronologic problem. The thickness (2.2 – 3.4 mm, mean 3.7 mm) reported by Harrison & Msuya (2005) for their rendering of the Lothagam *D. laini* sample (i.e. a combination of specimens attributed to *D. wardi* and *D. laini* by Stidham, 2004) is similar to that of *D. laini*. Further study is required.

Diamantornis laini* eggs occur in the Late Miocene of the United Arab Emirates (ca 7 Ma). The Malawi eggs attributed to *Struthio daberasensis* are associated with a Pliocene fauna (ca 3.9 - 3.5 Ma) (Stidham, 2004). The Kakesio, Tanzania eggs (Harrison & Msuya, 2005; Kingston & Harrison, 2005) were initially attributed to *Struthio daberasensis* by Pickford & Senut (1999) (Fig. 12), a determination accepted by Stidham (2004), but Harrison & Msuya (2005), on the basis of much enlarged samples, created a new species *Struthio kake-*

siensis for eggs from the Lower Laetoli Beds (ca 4.2 - 3.7 Ma) and from the Upper Laetoli Beds beneath Tuff 3. The same type of eggshell occurs at Kanapoi, Kenya (4.2 – 4.1 Ma) (Harrison & Msuya, 2005). Above Tuff 3 at Laetoli, Harrison & Msuya (2005) recognised eggshells of *Struthio camelus* only, although some of the specimens are appreciably thicker than eggs of extant samples of ostrich from Namibia and Tanzania.

Overall, the sequence and timing of Namibian egg types has withstood the test of discoveries in other African countries and the Arabian Peninsula, although refinement of the biochronology is undoubtedly possible.

It should be noted however, that other kinds of eggshells have been found in Africa and Europe which do not fit into the above scheme. Harris & Leakey (2003) reported the presence of eggshells with aepyornithoid morphology in the Lower Nawata Member at Lothagam, Kenya. The Late Miocene of Spain (including the Canary Islands) has yielded similar eggs (Mein & Dauphin, 1995; Sauer & Roth, 1972) as has Turkey (Sauer, 1976). Eggs attributed to *Psammornis* have been reported from Algeria (Andrews, 1911). Eggshells from the Early Pliocene of Wadi Natrun, Egypt, possibly belong to this genus (Pickford *et al.*, in press).

From this evidence it appears that Africa was populated by at least two taxa of ratites for much of the Miocene and Pliocene, but that their geographic ranges barely overlapped. Only one locality (Lower Nawata, Kenya) is reported to have yielded struthious and aepyornithoid eggs in the same stratigraphic unit.

As far as ratite eggshells are concerned, the presence of the same succession of species of *Diamantornis* and *Struthio* in Namibia, Kenya and the Arabian Peninsula, indicates that diffusion between these regions was likely relatively easy and could therefore take place rapidly, hence their utility for biochronology. This biogeographic pattern indicates the presence of an arid corridor between southwestern Africa and

northeastern Afro-Arabia from about 12 Ma (if not earlier) to the Present.

Palaeoclimatic considerations

The new fossil eggshells from the Tsondab succession are from aeolian deposits indicative of arid to hyper-arid palaeoclimatic conditions. However, the aeolianites are heavily affected by bioturbation represented by rhizoliths, animal burrows and bioconstructions. The relatively high frequency of burrows and hives attributed to *Hodotermes*, the harvester termite, suggests that the

bioturbation occurred under a summer rainfall regime and that grass was an important food resource. Some of the rhizoliths are large enough to indicate the presence of trees. Traces left by the sand termite, *Psammotermes*, are rare in the Tsondab area, whereas they are extremely common at Rooilepel and other parts of the Sperrgebiet in Southern Namibia. This suggests that during the Early Miocene, the northern part of the proto-Namib Desert enjoyed a summer rainfall regime whereas the southern part lay within a winter rainfall zone.
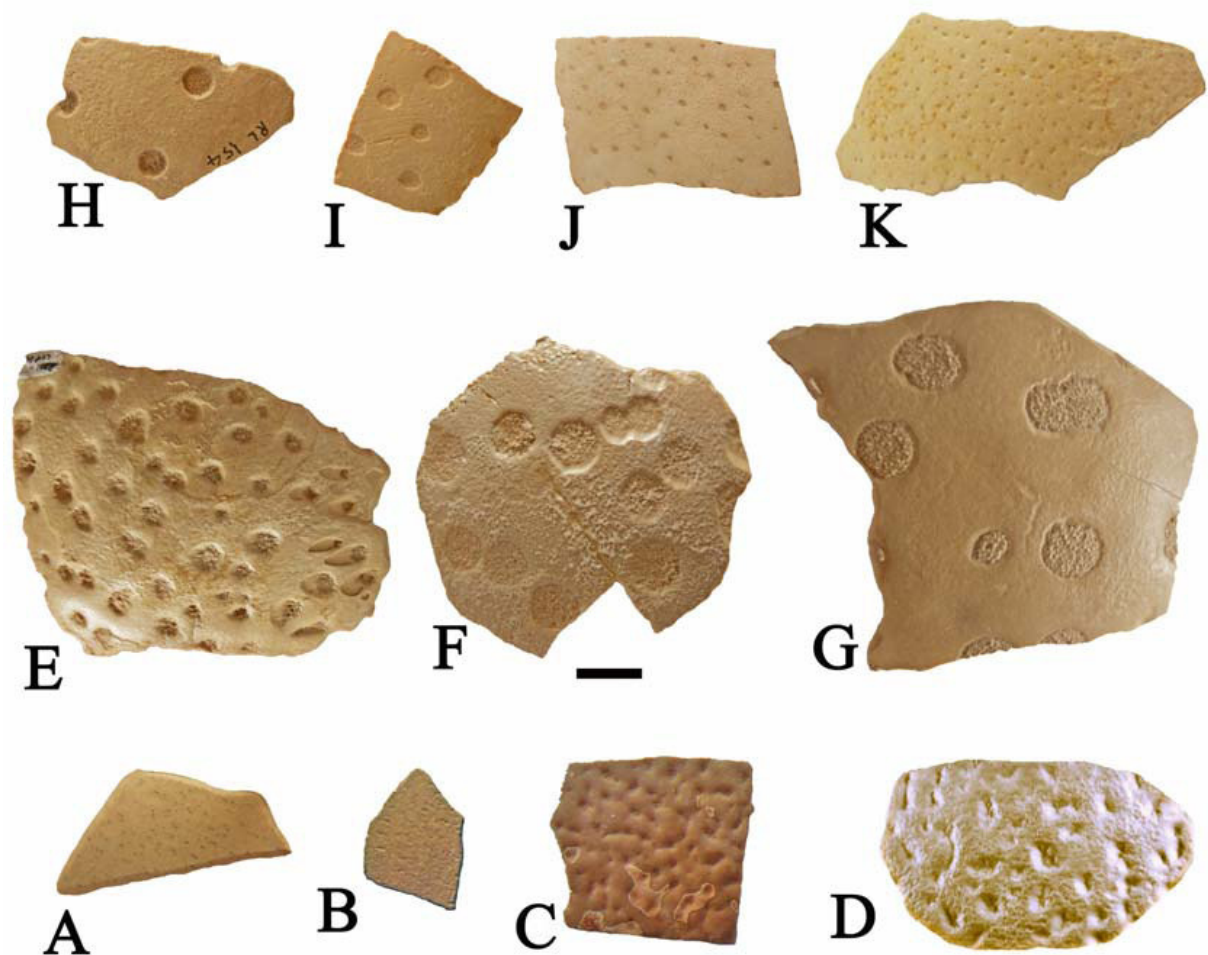
Figure 13: Succession of fossil eggshell types from the Namib Desert (A oldest to K youngest). A) *Tsondabornis minor*, B) *Tsondabornis psammoides*, C) *Namornis elimensis*, D) *Namornis oshanai*, E) *Diamantornis corbetti*, F) *Diamantornis spaggiarii*, G) *Diamantornis wardi*, H) *Diamantornis laini*, I) *Struthio karingarabensis*, J) *Struthio daberasensis*, K) *Struthio camelus* (scale – 10 mm).
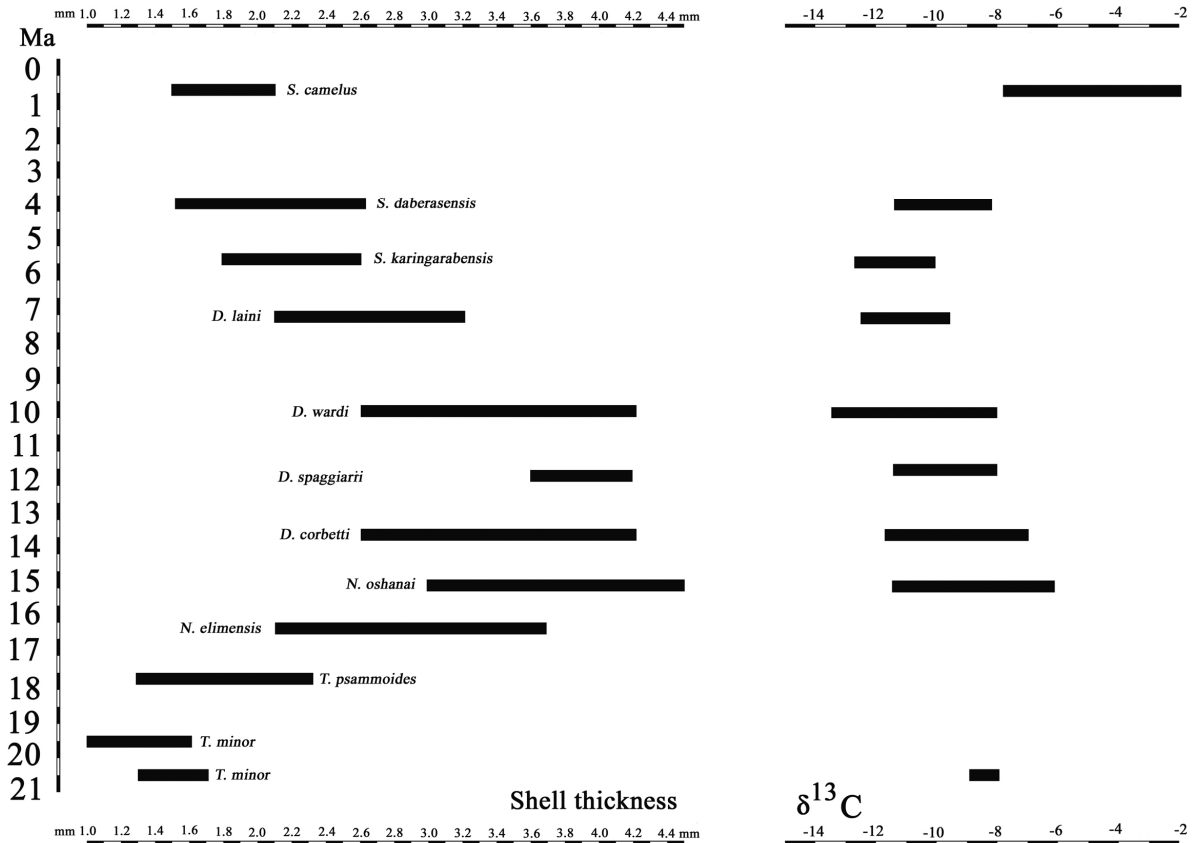
Figure 14: Variation in eggshell thickness and $\delta^{13}C$ values of fossil eggshells from the Miocene of Namibia. There appears to be an inverse correlation between the two trends, with thicker eggshells tending to have lower $\delta^{13}C$ values than thin eggs ($\delta^{13}C$ values from Ségalen *et al*., 2002).

Eggshell thickness in the Namib succession shows a trend of increase through the Early Miocene to the base of the Middle Miocene, followed by a slow decrease during the rest of the Miocene, speeding up during the Plio-Pleistocene (Fig. 14). Examination of the $d^{13}C$ values through the same succession of egg types reveals an inverse trend, with high values corresponding with thin eggshells, and lower values corresponding with thicker eggshells (Fig. 14). Ségalen *et al*., (2002) showed a correlation between the $d^{13}C$ values of the Namibian eggshells and the pCO_2 values in the atmosphere during the Miocene in the southern hemisphere (Pagani *et al*., 1999), with lower $d^{13}C$ values corresponding to higher values of pCO_2. The correlation between eggshell thickness and pCO_2 values noted herein, suggests that eggshell thickness in ratites is due not just to changes in the dimensions of the eggs (it has long been known that larger eggs have

thicker shells), but may also be related to the concentration of CO_2 in the atmosphere where the birds were living.

Palaeoecology

Birds have a range of reproductive strategies correlated to clutch size. K-strategy birds lay few eggs and parental investment in the hatched young tends to be energy expensive and often prolonged. In contrast, r-strategy birds lay large clutches of eggs and the young tend to become relatively independent soon after hatching. Present day ostriches are r-strategy birds, several females usually laying several dozen eggs in the same nest and the young are able to walk and forage soon after hatching.

It is clear from the mapped fossil occurrences that *Diamantornis wardi*, *Diamantornis laini* and *Struthio daberasensis* laid many eggs in the same nest, as eggshell frag-

ments of these species often occur in large concentrations indicating the former presence of many eggs in the same next. In contrast, the eggshell fragments of some species including *Namornis elimensis*, *Tsondabornis minor* and *Tsondabornis psammoides* tend to occur in small patches containing few fragments, suggesting that only one or two eggs were laid at each site. However, it cannot be ruled out that the occurrences of eggs of these species found so far represent "scatter" eggs (Sauer, 1968) in the same way that extant ostriches often lay an isolated egg away from the nest, immediately abandoning it. The possible exception is *Tsondabornis psammoides*, as one locality (Zebra Hill) yields many shell fragments in the surface deflation deposits. However, at all the other sites which yielded eggs of this taxon, shell fragments tended to be scarce, suggesting the former presence at each site of only one or two eggs.

Phylogeny

The transition from the basically aepyornithoid eggshell pattern of pores in slits and isolated dagger point pits in *Tsondabornis psammoides* to the more complex clustering of pores that occurs in *Namornis elimensis*, but with some arranged in sub-parallel slits, suggests that the struthious pattern was derived from the aepyornithoid pattern, as postulated by Sauer (1966) (see also Bibi *et al.*, 2006). During the same period, the basically smooth external surface of eggshells in *Tsondabornis minor* became weakly undulating in *Tsondabornis psammoides*, culminating in the strongly undulating surface in eggs of *Namornis elimensis* a trend continued in *Namornis oshanai* (Sauer, 1966). Eggs attributed to subsequent species of *Diamantornis* generally possess smooth shell between the pore complexes, morphology carried over into the eggs of *Struthio*.

Conclusions

Palaeontological field work in the Tsondab Vlei and Tsondab Flats to the west

has resulted in the recognition of two new kinds of extinct bird eggs. The older of the two, on the basis of superposition of strata is *Tsondabornis psammoides* nov. gen. nov. sp., the eggs of which are somewhat thicker than those of the extant ostrich *Struthio camelus*. This species was followed by a bird which laid much thicker eggs, *Namornis elimensis* nov. sp., the eggs of which were about twice as thick as those of the extant ostrich but thinner than those of the type species *Namornis oshanai*. In other parts of the Namib-Naukluft Park, eggs of younger species of bird have been found, including those of *Namornis oshanai*, *Diamantornis corbetti*, *Diamantornis wardi*, and *Diamantornis laini*, all of Miocene age, whereas in Pleistocene to Recent levels, eggs of *Struthio camelus* are common.

The main interest of this work concerns the downwards extension of the biostratigraphic scheme based on gigantic avian eggs from the Sperrgebiet and the southern sector of the Namib-Naukluft Park (Dauphin *et al.*, 1998; Pickford & Senut, 1999). As such the two new oo-species fill a gap that used to exist between the so-called "aepyornithoid" eggs from the Early Miocene fluvio-paludal deposits of the Sperrgebiet (Elisabethfeld, Grillental, Fiskus, Langental) (Senut *et al.*, 1995) and *Namornis oshanai* from the basal Middle Miocene levels at Rooilepel, Karingarab and Awasib (Pickford *et al.*, 1995) and by inference to Beisebvlakte, near Etosha (Sauer, 1966). The large morphometric gap that used to separate the aepyornithoid eggshells from those of *Namornis oshanai* is now reduced by the presence of two intermediate kinds. This indicates the likelihood of autochthonous evolution rather than extinction of the aepyornithoid type followed by immigration of *Namornis*. It also reduces the punctuated aspect of the evolution of Namibian fossil eggs, and suggests instead a gradual, albeit quite rapid, evolutionary process within the country (continent).

Fossil eggs hold tremendous potential for unravelling the history of sandstone deposition in the Central Namib Desert,

something that traditional mapping techniques have thus far failed to reveal. The distribution of fossil eggs in the Tsondab Formation indicates a complex history of interplay between aeolian deflation and deposition spanning the entire Miocene and Pliocene, resulting in sand bodies which are separated from each other by super-bounding and erosional surfaces (not necessarily horizontally disposed), a process that continues to the present day with the Sossus Sand Sea, much of the sand of which is derived by reworking from the Tsondab Formation.

The aeolianites that have yielded the eggs of *Tsondabornis psammoides* are younger than the Early Miocene fluvio-paludal sites in the Sperrgebiet (21-19 Ma) which yield eggs of *Tsondabornis minor* and bones of *Struthio coppensi*. However, it is stressed that there is a great deal of aeolianite beneath the levels that yielded the oldest eggs found in the Namib-Naukluft Park, so there remains the possibility that the onset of aeolianite deposition could have been earlier than previously thought, perhaps as early as 19 Ma (Fig. 14) (Ségalen *et al.*, 2004a). Further south in the Sperrgebiet the onset of aeolianite deposition coincided in time with eggshells of *Namornis oshanai*, which are younger than those of *Namornis elimensis*, indicating a later start of sand deposition in the south (ca 16 Ma) than in the north (Pickford & Senut, 1999) although arid conditions could have existed for some time prior to the first deposition of aeolianite.

The fact that struthious oo-species defined in Namibia have been recognised as far afield as Tanzania, Kenya and the Arabian Peninsula indicates that the birds producing them were able to diffuse widely and rapidly between Southwestern Africa, Eastern Africa and Arabia, which in turn suggests that an arid corridor existed between these regions for a considerable period of time.

Finally, in the succession of Namibian fossil eggs, there appears to be a correlation between eggshell thickness and the concentration of carbon dioxide (pCO_2) in the atmosphere.

References

Andrews, C.W., 1911 – Note on some fragments of fossil eggshell of a large struthious bird from Southern Algeria, with some remarks on some pieces of the eggshell of an ostrich from northern India. *In*: H. Schalow (Ed.) *Verhandlungen des Fünften Internationalen Ornithologen-Kongresses, Berlin, May 30 to 4 June, 1910*, pp. 169-174, Berlin, Deutsche Ornithologische Gesellschaft.

Besler, H., 1996 – The Tsondab Sandstone in Namibia and its significance for the Namib Erg. *South African Journal of Geology*, **99**: 77-87.

Besler, H., & Marker, M., 1979 – Namib Sandstone: a distinctive lithological unit. *Transactions of the Geological Society of South Africa*, **82**: 155-160.

Bibi, F., Shabel, A., Kraatz, B., & Stidham, T., 2006 – New fossil ratite (Aves: Palaeognathae) eggshell discoveries from the Late Miocene Baynunah Formation of the United Arab Emirates, Arabian Peninsula. *Palaeontologica electronica*, **9(1)2A**: 1-13.

Dauphin, Y., Pickford, M., & Senut, B., 1996 – Microstructures des coquilles

d'oeufs d'oiseaux fossiles de Namibie. *Revue de Paléobiologie*, **45:** 225-241.

Dauphin, Y., Pickford, M., & Senut, B., 1998 – Diagenetic changes in the mineral and organic phases of fossil avian eggshells from Namibia. *Applied Geochemistry*, **13**: 243-256.

Harris, J.M., & Leakey, M.G., 2003 – Lothagam birds. *In*: Leakey, M.G., & Harris, J.M., (Eds) *Lothagam: The Dawn of Humanity in Eastern Africa*. New York, Columbia University Press, pp. 161-166.

Harrison, T., & Msuya, C., 2005 – Fossil struthionid eggshells from Laetoli, Tanzania: Taxonomic and biostratigraphic significance. *Journal of Human Evolution*, **41**: 303-315.

Heine, K., 1985 – Late Quaternary development of the Kuiseb Valley and adjacent areas, Central Namib Desert, South West Africa/Namibia, and palaeoclimatic implications. *Zeitschriften für Gletscherkunde und Glazialgeologie*, **21**: 151-157.

Kingston, J., & Harrison, T., 2005 – Ostrich eggshells as palaeoenvironmental indicators in the Pliocene Laetoli succession, N. Tanzania. *PaleoAnthropology*, PAS **2005**: A37.

Lancaster, J., Lancaster, N., & Seely, M., 1984 – Climate of the Central Namib Desert. *Madoqua*, **14**: 5-61.

Lancaster, N., 1983 – Controls of dune morphology in the Namib Sand Sea. *In*: M.E. Brookfield & T.S. Ahlbrandt (Eds) *Eolian Sediments and Processes*. Elsevier, Amsterdam, pp. 261-289.

Lancaster, N., 1984a – Palaeoenvironments in the Tsondab Valley, Central Namib Desert. *Palaeoecology of Africa*, **16**: 411-419.

Lancaster, N., 1984b – Late Cenozoic fluvial deposits of the Tsondab Valley, Central Namib Desert. *Madoqua*, **13**: 257-269.

Lancaster, N., & Teller, J.T., 1988 – Interdune deposits of the Namib Sand Sea. *Sedimentary Geology*, **55**: 91-107.

Leeder, M.R., 1975 – Pedogenic carbonates and flood sediment accretion rates: a quantitative model for alluvial arid-zone lithofacies. *Geological Magazine*, **112**: 257-270.

Marker, M., 1977 – Aspects of the geomorphology of the Kuiseb River, South West Africa. *Madoqua*, **10**: 199-206.

Marker, M., 1979 – Relict fluvial terraces on the Tsondab Flats, Namibia. *Journal of Arid Environments*, **2**: 113-117.

Marker, M., 1980-1981 – The geological significance of some Central Namib materials. *Journal of the South West Africa Scientific Society*, **34-35**: 49-55.

Mein, P., & Dauphin, Y., 1995 – Des coquilles d'œufs de type *Aepyornis* dans le Bassin de Teruel (Pliocène basal, Espagne). *Neues Jahrbuch der Geologie und Paläontologie, Monatsheft*, **1995** : 182-191.

Mourer-Chauviré, C., Senut, B., Pickford, M., & Mein, P., 1996a – Le plus ancien représentant du genre *Struthio* (Aves, Struthionidae), *Struthio coppensi* n. sp. du Miocène inférieur de Namibie. *Comptes Rendus de l'Académie des Sciences, Paris*, **322:** 325-332.

Mourer-Chauviré, C., Senut, B., Pickford, M., Mein, P., & Dauphin, Y., 1996b – Ostrich eggs, legs and phylogenies. *South African Journal of Science*, **92**: 491-495.

Pagani, M., Arthur, M., & Freeman, K., 1999 – Miocene evolution of atmospheric carbon dioxide. *Paleoceanography*, **14**: 273-292.

Pickford, M., 2000 - Fossil spider's webs from the Namib Desert and the antiquity of *Seothyra* (Araneae, Eresidae). *Annales de Paléontologie*, **86**: 147-155.

Pickford, M., 2008a - Arthropod bioconstructions from the Miocene of Namibia and their palaeoclimatic implications. *Memoir of the Geological Survey of Namibia*, **20**: 53-64.

Pickford, M., 2008b - Freshwater and Terrestrial Mollusca from the Early Miocene deposits of the northern Sperrgebiet, Namibia. *Memoir of the Geological Survey of Namibia*, **20**: 65-74.

Pickford, M., & Dauphin, Y., 1993 – *Dia-*

mantornis wardi nov. gen. nov. sp., giant extinct bird from Rooilepel, Lower Miocene, Namibia. *Comptes Rendus de l'Académie des Sciences, Paris*, **316**: 1643-1650.

Pickford, M., & Senut, B., 1999 – Geology and Palaeontology of the Namib Desert, Southwestern Africa. *Memoir of the Geological Survey of Namibia*, **18**: 1-155.

Pickford, M., Abdel Ghany, M.S., Sileem, A.S.H., & Gamil, M.M., in press. A Descriptive Catalogue of Fossils from Wadi Natrun, Housed in the Cairo Geological Museum, Egypt.

Pickford, M., Senut, B., & Dauphin, Y., 1993 – Chronologie du Néogène continental de Namibie: apport des oeufs fossiles. *Palaeovox*, **2**: 66-67.

Pickford, M., Senut, B., & Dauphin, Y., 1995 – Biostratigraphy of the Tsondab Sandstone (Namibia) based on gigantic avian eggshells. *Geobios*, **28**: 85-98.

Rust, U., & Wienecke, F., 1980 – A reinvestigation of some aspects of the Kuiseb River Valley upstream of Gobabeb, South West Africa. *Madoqua*, **12**: 163-173.

Sauer, E.G.F., 1966 – Fossil eggshell fragments of a giant struthious bird (*Struthio oshanai*, sp. nov.) from Etosha Pan, South West Africa. *Cimbebasia*, **14**: 1-51.

Sauer, E.G.F., 1968 – Calculations of struthious egg sizes from measurements of shell fragments and their correlation with phylogenetic aspects. *Cimbebasia*, **Series A, 1**: 28-55.

Sauer, E.G.F., 1976 – Aepyornithoide eierschalen aus dem Miozän und Pliozän von Anatolien, Turkei. *Palaeontographica*, **A153**: 62-115.

Sauer, E.G.F., & Roth, P., 1972 – Ratite eggshells from Lanzarote, Canary Islands. *Science*, **176**: 43-45.

Seely, M., & Mitchell, D., 1986 – Termite casts in Tsondab Sandstone? *Palaeoecology of Africa*, **17**: 109-112.

Ségalen L., Renard M., A. Lee-Thorp J., Emmanuel L., Le Callonnec L., De Ra-

félis M., Senut B., Pickford M., Melice J.-L., 2006a - Neogene climate change and emergence of C_4 grasses in the Namib, southwestern Africa, as reflected in ratite ^{13}C and ^{18}O. *Earth and Planetary Science Letters*, **244 (3-4)**: 725-734.

Ségalen, L., Renard, M., Lee-Thorp, J., de Rafélis, M., Senut, B., & Pickford, M., 2006b – Neogene climatic change and emergence of C_4 grasses in southwestern and eastern Africa as reflected in continental carbonate ^{13}C and ^{18}O. *Lucy, 30 Years Later: Hominids and Environments in Africa from 7 to 1.5 Million Years Ago: New Discoveries and Lines of Research*. International Conference, CEREGE, Aix-en-Provence, 12-14 June, 2006, pp. 65-66.

Ségalen, L., Renard, M., Pickford, M., Senut, B., Cojan, I., Le Callonec, L., & Rognon, P., 2002 - Environmental and climatic evolution of the Namib Desert since the Middle Miocene: the contribution of carbon isotope ratios in ratite eggshells. *Comptes Rendus Geoscience*, **334**: 917-924.

Ségalen, L., Rognon, P., Pickford, M., Senut, B., Emmanuel, L., Renard, M., & Ward, J., 2004a - Reconstitution des morphologies dunaires et du régime des paléovents dans le Proto-Namib au cours du Miocène. *Bulletin de la Société géologique de France*, **175**: 537-546.

Ségalen, L., Renard, M., Senut, B., Pickford, M., & Lee-Thorp, J., 2004b - Palaeoclimate and palaeoenvironment reconstruction of the west coast of Southern Africa during the Neogene. *20th Colloquium of African Geology, 2-7 June, 2004, BRGM, Orléans, Abstracts Volume*, p. 371.

Selby, M., Hendey, C.H., & Seely, M., 1979 – A late Quaternary lake in the Central Namib Desert, southern Africa, and some implications. *Palaeogeography, Palaeoclimatology, Palaeoecology*, **26**: 37-41.

Senut, B., Dauphin, Y., & Pickford, M., 1998 – Nouveaux restes aviens du

Néogène de la Sperrgebiet (Namibie): Complément à la biostratigraphie avienne des éolianites du désert de Namib. *Comptes Rendus de l'Académie des Sciences, Paris*, **327**: 639-644.

Senut, B., & Pickford, M., 1995 – Fossil eggs and Cenozoic continental biostratigraphy of Namibia. *Palaeontologica africana*, **32**: 33-37.

Senut, B., Pickford, M., & Dauphin, Y., 1995 – Découverte d'oeufs de type « aepyornithoïde » dans le Miocène inférieur de Namibie. *Comptes Rendus de l'Académie des Sciences, Paris*, **320**: 71-76.

Senut, B., Pickford, M., & Ségalen, L., 2009 – Neogene desertification of Africa. *Comptes Rendus Geoscience*, **341**: 591-602.

Stidham, T., 2004 – Extinct ostrich eggshell (Aves; Struthionidae) from the Pliocene Chiwondo Beds, Malawi: implications for the potential biostratigraphic correlation of African Neogene deposits. *Journal of Human Evolution*, **46**: 489-496.

Teller, J., & Lancaster, N., 1986 – Lacustrine sediments at Narabeb in the Central Namib Desert, Namibia. *Palaeogeography, Palaeoclimatology, Palaeoecology*, **56**: 177-195.

Teller, J., & Lancaster, N., 1987 – Description of Late Cenozoic sediments at Narabeb, Central Namib Desert. *Madoqua*, **15**: 163-167.

Teller, J., Rutter, N., & Lancaster, N., 1990 – Sedimentology and Paleohydrology of Late Quaternary lake deposits in the Northern Namib Sand Sea, Namibia. *Quaternary Science Reviews*, **9**: 343-364.

Vigors, N.A., 1825 – Sketches in ornithology; or, observations on the leading affinities of some of the more extensive groups of birds. Arrangement of genera of birds. *Zoological Journal,* **2**: 368-405.

Walter, H., 1986 – The Namib Desert. *In*: M. Evenari, I. Noy-Meir & D.W. Goodall (Eds) *Ecosystems of the World 12B.*

Hot Deserts and Shrublands. Amsterdam, Elsevier, pp. 245-282.

Ward, J.D., 1987a – The Cenozoic succession in the Kuiseb Valley, Central Namib Desert. *Memoir of the Geological Survey of South-West Africa/Namibia*, **9**: 1-45.

Ward, J.D., 1987b – Tsondab Sandstone – extensive Tertiary desert deposits in the Central Namib. *South African Journal of Science*, **83**: 507.

Ward, J.D., 1988 – Eolian, fluvial and pan (playa) facies of the Tertiary Tsondab Sandstone Formation in the Central Namib Desert, Namibia. *Sedimentary Geology*, **55**: 143-162.

Yaalon, D., & Ward, J.D., 1982 – Observations on calcrete and recent calcic horizons in relation to landforms in the Central Namib Desert. *In*: Proceedings of the VIth SASQUA Conference. *Palaeoecology of Africa*, **15**: 183-186.

Namaia Pickford *et al.*, 2008, preoccupied by *Namaia* Green, 1963: proposal of a replacement name

Martin Pickford[1] and Mark D. Uhen[2]

1. Département Histoire de la Terre, UMR 7207 (CR2P) du CNRS, case postale 38, 57 rue Cuvier, 75005 Paris, France. e-mail: <pickford@mnhn.fr>
2. George Mason University, AOES Geology, MSN 6E2, Fairfax, Virginia, VA 22030, USA, e-mail : <muhen@gmu.edu>

The primate genus *Namaia* was erected by Pickford *et al.*, 2008, on the basis of a maxilla containing two molars found at the middle Eocene locality of Black Crow, Namibia. The name *Namaia* is however preoccupied by an ostracod genus, *Namaia* Green, 1963, found in the Mississippian Banff Formation at Bow River Valley, Alberta, Canada, hence the name of the genus (*Nama* means *bow* in the Indian Language). The type species is *Namaia reticulata* Green 1963.

We rebaptise the primate from Black Crow *Notnamaia*, not only to underscore that it is not the same as *Namaia*, but also because it was found in the southern part of Africa (Greek *notos* – south). The type species is *Notnamaia*

bogenfelsi (Pickford *et al.*, 2008). Coincidentally, one of the meanings of the German word *bogen* is *Bow*).

References

Green, R., 1963 – Lower Mississippian ostracodes from the Banff Formation, Alberta. *Research Council of Alberta*, **11** : 1-237.

Pickford, M., Senut, B., Morales, J., Mein, P., & Sanchez, I.M., 2008 - Mammalia from the Lutetian of Namibia. *Memoir of the Geological Survey of Namibia*, **20** : 465-514.

Contamination of Agricultural Products in the Surrounding of the Tsumeb Smelter Complex

Benjamin Mapani[1], Rainer Ellmies[2], Lothar Hahn[4], Gabi Schneider[3], Kaarina Ndalulilwa[3], Rosina Leonard[3], Mukuve Zeeuw[2], Norwel Mwananawa[2], Shopala Uugulu[2], Eline Namene[2], William Amaambo[2], Florence Sibanda[5], Maria Mufenda[3]

[1]*University of Namibia, Geology Department, Windhoek, Namibia*
[2]*Bundesanstalt für Geowissenschaften und Rohstoffe, Hannover, Germany*
[3]*Geological Survey of Namibia, Ministry of Mines and Energy, Windhoek, Namibia*
[4]*Deutsche Forschungsgemeinschaft (DFG), Bonn, Germany*
[5]*Department of Water Affairs, Ministry of Agriculture, Water and Forestry, Windhoek, Namibia*

Since the turn of the last century, the Tsumeb area was a major mining hub until 1999, and still continues to be a smelting centre for ores originating from the Democratic Republic of Congo, Zambia, Mauritania, Bulgaria and Chile. This has brought about a situation where the top soils surrounding the smelter, especially in the down wind direction, are highly contaminated with lead, zinc, copper, arsenic and cadmium. The contamination of the top soils and crops is a result of historical smelter emissions as well as due to windborne dust derived from the tailings and slag dumps of the smelter complex. A total of 43 samples of vegetative material were collected in areas with potential soil contamination in the surroundings of the Tsumeb smelter complex. The samples comprise fruit crops (marula, papaya), vegetable (tomato, parsley, carrot, bean, pumpkin, chillies) and a field crop (maize). Twelve topsoil samples were collected at specific sampling sites for correlation with vegetation samples. The concentrations of arsenic, lead and cadmium of most of the fruits and vegetables (marula fruits, pumpkins, chilli, and tomato) correlate with the heavy metal values of the underlying contaminated top soils. The guideline values of the WHO (Codex Alimentarius) and EU were applied for the interpretation of eventual health risks. All plant samples are characterised by high lead concentrations exceeding the guideline values. Crops from Tsumeb-Nomtsoub and the agricultural land to the west of the smelter show critical contaminations.

Introduction

The contamination of the agricultural land in the surroundings of the Tsumeb smelter complex has been well known for many years, though no quantitative data had been available. It can be traced back to emissions from the historical smelter activities as well as to windborne dust derived from the mine tailings and slag dumps in the smelter area.

The Geological Survey of Namibia monitored the environmental situation in Tsumeb in cooperation with the Czech Geological Survey (Kríbek and Kamona, 2005) and the University of Namibia in the past few years. This research has now revealed the exact extent and severity of soil contamination in the Tsumeb area (Geological Survey of Namibia, 2006a; 2006b; 2007a; 2007b; Iipinge, 2008). The previous research included groundwater quality, soil contamination, quality of fresh water fish and to a limited extent the contamination of grasses on surrounding farms.

For this study, a plant sampling campaign assisted by students from the Department of Geology at the University of Namibia (UNAM) was carried out in the Tsumeb area. The following metals were analysed: arsenic, cadmium, copper, lead, molybdenum and zinc.

Soil is a crucial component of rural and urban environments in a setting such as Tsumeb, as it forms the basis for crop cultivation and grazing of domestic animals. Heavy metals occur naturally in soils but rarely at toxic levels. In the case of Tsumeb, critical soil contamination with a number of metals has been caused by mining and processing of poly-metallic ores over a period of more than 100 years. Heavy metals have a deleterious effect on bacteria which are key players in nutrient turnovers in soil (Gremion, 2003). Due to the prevailing carbonate lithologies, the soils in the Tsumeb area have high a pH which is generally reducing the metal uptake of the plants (USDA-NRCS, 2000).

The study had two objectives: (i) The investigation of bioaccumulation of heavy metals in fruits and crops, and (ii) the determination of the specific contaminant uptake by various crops. In the absence of Namibia's own Minimum Risk Levels (MRLs), the UN Food and Agricultural Organisation (FAO)/World Health Organisation (WHO)
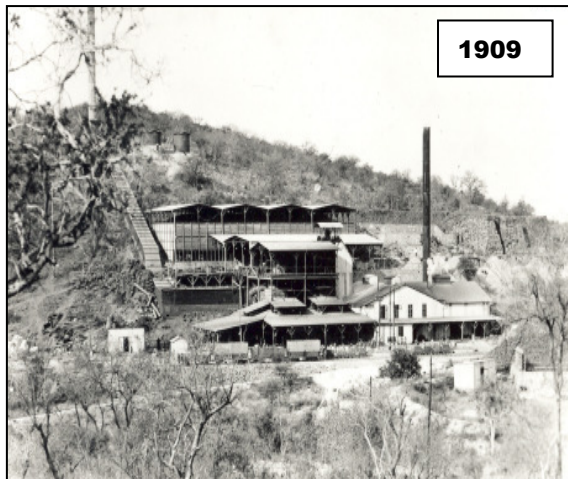
guidelines were used to evaluate crop contamination, together with German and Canadian guidelines for soil contamination.

History

Construction of a first smelter at Tsumeb started in 1906. This first smelter comprised two lead-copper blast furnaces with a cast iron water jacket, and the initial ignition of the first furnace took place in September 1907.

In the beginning, the smelter was not operating continuously, and also at a deficit. The reasons for this deficit were the enormous costs for first-class coke imported


from Germany, and for the additives, e.g. galena, which had to be mixed into the oxide ores, and which were imported from Norway. However, during World War I, when coke was imported from South Africa, and iron ore for flux was found near Kalkfeld close to the railway linking Tsumeb with the coast, the smelter became profitable. In 1923, a third blast furnace was added, and in 1924 one of the old furnaces was enlarged. In 1925, an electric Cottrell precipitator and a Dwight-Lloyd sinter plant for the recovery of cadmium and lead in flue dust in the off-gases were installed. This increased the lead production by 1 000 t annually. 1928 saw the enlargement of the third blast furnace, and the addition of a small rotary furnace as well as an oil-fired furnace for the smelting of lead bearing waste. Finally, in 1931, following the acquisition of a small reverberatory furnace to roast the cadmium-bearing flue dust, the first cadmium was produced (Schneider, 1992a). Due to the worldwide
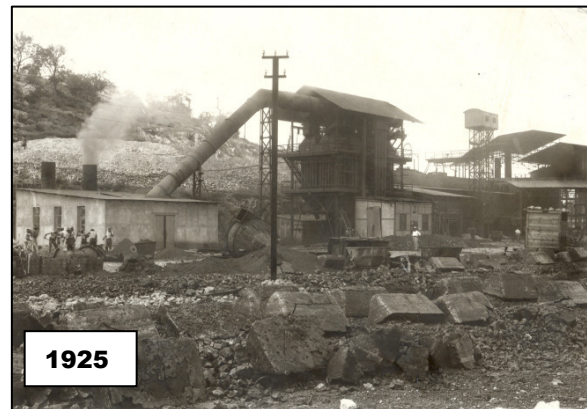
recession of the 1930ies with its associated low metal prices, the smelter came to a standstill, and remained inactive throughout World War II.

The smelting process at the first smelter at Tsumeb comprised the following steps: The dolomitic run-off-mine ore was stored in heaps of 8 000 t each, from where it was transferred by hand into charging trolleys with a capacity of 3 500 kg. After being mixed with aplite from the mine as silica flux, and hematite from Kalkfeld as iron flux, and after 12-13% of coke were added, the blast furnaces were charged with the material. Air was supplied to the furnaces with

their open throats by 5 rotary piston compressors. After tapping the molten charge flew out onto a settler furnace made from clay. During this process, lead and copper settled according to their specific gravity at the bottom, and the slag, which still contained 0.3% copper and 1.5% lead, remained on top. Once the settler furnace was full, it was also tapped, the copper was allowed to flow onto an iron tray for cooling and was subsequently crushed. The lead was collected in a container, from where it was transferred into forms to solidify. Lead and copper were then exported to Europe without any further value addition. The slag was removed for deposition as waste, but sometimes it was also crushed and used locally as aggregate for concrete (Bürg, 1942). The
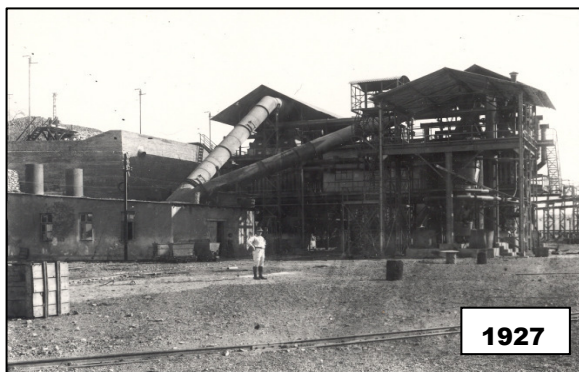

Tsumeb ores have always been very complex ores, containing a variety of accessory metals such as silver, arsenic, antimony, cadmium, cobalt, germanium, gallium, mercury, molybdenum, nickel, tin, tungsten and vanadium, some of which are highly toxic. Apart from cadmium, there was no effort made during the period of operation of the first smelter to recover other metals. During the smelting process, some of these metals went into the smelter products, and some into the slag, but others reached the environment via the smelter stack. All silver and nickel, stayed with the copper, while 100% of the germanium, gallium, tungsten and vanadium, 95% of the cobalt, and 30% of the tin were retained by the slag. However, only 50% of the molybdenum, 20% of the arsenic and the antimony, and 10% of the tin went with the copper, leaving 5% of the cobalt, 60% of the tin, 50% of the molybdenum, 80% of the ar-

senic and antimony, and an alarming 100% of the mercury to enter the atmosphere (pers. comm. H Nolte, September 2013).
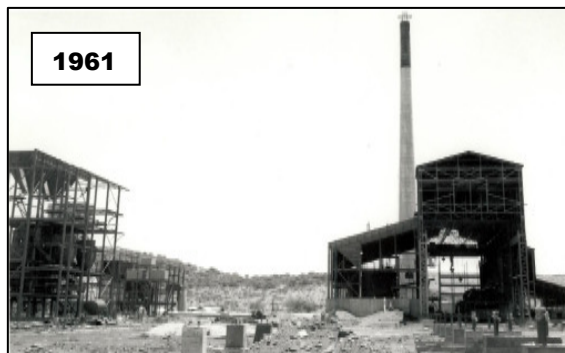
During the 1950ies, the Tsumeb concentrates were smelted and refined at a smelter in the USA. However, the ever-increasing transportation costs made it necessary to erect a new and larger smelter in Tsumeb between 1960 and 1962 (Schneider & Seeger, 1992). This smelter was built as an identical copy of the smelter used in the USA. It was commissioned in 1963, and featured integrated copper and lead sections, the latter with an associated lead refinery with an annual capacity of 90 000 tons. The copper section consisted of a reverberatory furnace with waste heat boiler, two converters, a holding furnace, a casting machine and a bag house. Modern filters were placed in the stacks and all areas where pollutants could reach the environment. Production started officially in March 1964, and at that stage the smelter produced more than 3 500 tons of blister copper and 6 000 tons of lead per month (Namibia Custom Smelters, 2013).
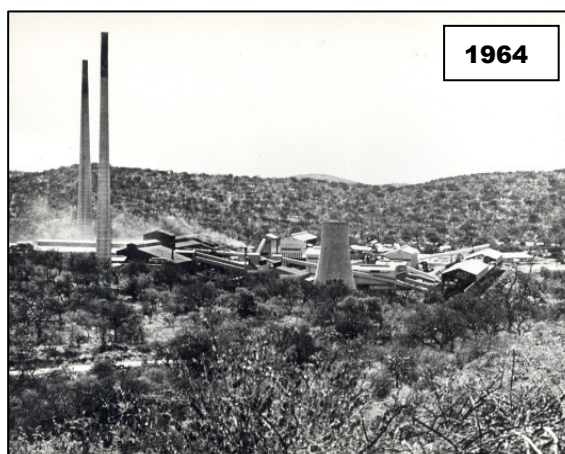

The smelter also featured an integrated arsenic plant consisting of four Godfrey roasters

with condensing kitchens and a common bag house, which produced 99% pure arsenic trioxide (Schneider & Genis, 1992).

Also in 1960, a separate germanium reduction plant was introduced. The tailings of the bulk-sulphide flotation circuit were treated with a magnetic separator to recover germanium concentrate. Germanium dioxide was produced from this germanium concentrate in the germanium reduction plant by complex leaching, evaporation, distillation and hydrolysis (Schneider, 1992b).

In 1965, an on-line cadmium plant was commissioned. It consisted of leaching, purification, precipitation, filtering, cementation, melting, refining and casting facilities and produced refined cadmium metal of 99.7% purity (Schneider, 1992a).

In 1986, the production of sodium antimonate was introduced. Antimony concentrates together with arsenic within the copper circuit in the Pierce-Smith converter in the dust which is subsequently fed, via the bag house and the arsenic plant into the lead circuit of the smelter. From the lead refinery, the antimony compounds, together with the arsenic go into the Wet Harris Plant, where they are reduced. The resulting native antimony is then treated with soda to remove impurities (Schneider, 1992c). Nevertheless, by the late 1970s, the modern filters that were installed when the smelter was built in the early 1960s, had become old and not

1992
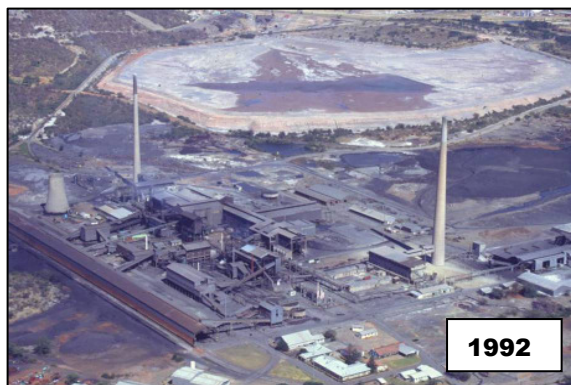
enough investment took place to replace them and to keep the smelter in an environmentally friendly condition. This state of affairs persisted up until the 1990s (pers. comm. H Nolte, September 2013).

Over the years, production had declined considerably, and by 1988 the annual output was some 13 000 tons of blister copper and 9 000 tons of lead only. In 1992, the lead section was closed. But in 1996, a new lead smelting furnace was built and commissioned. Based on Top Submerged Lance (TSL) technology, the Ausmelt TSL Process is an efficient, environmentally friendly and highly flexible pyro-metallurgical process for treating a wide range of feed materials. The process is based on injecting air, oxygen

1995

and fuel directly into the molten slag bath via a vertically suspended lance. Critical process phenomena, such as feed material dissolution, energy transfer, reaction and primary combustion, take place in the intensely agitated slag layer (www.outotech.com).

But then, and due to industrial action, the smelter was out of operation between 1996 and 2000. From 2000 to 2008, only the copper section of the smelter was operational, while the arsenic plant was run on a small scale. When the Namibian copper mining operations came to a standstill due to the world economic crisis in 2008, a decision was taken to divert to custom smelting, which was realised at the beginning of 2009.

However, the original lead smelting Ausmelt furnace had been refurbished to smelt copper concentrates and was re-

commissioned in 2008. The furnace is now charged with copper concentrates and various fluxes and fuelled with locally produced charcoal and heavy furnace oil. The iron and sulphur in the feed is utilised as the main energy source for smelting the concentrates. Oxygen enriched air is used for combustion. The molten material from the Ausmelt is tapped from tap holes and introduced to the reverberatory furnace –for holding and slag cleaning or alternatively slag is granulated while matte from the TSL can go directly to the converters. Molten matte tapped from the reverberatory furnace is transferred to the Pierce Smith converters for the production of blister copper. Air is blown into the matte and the oxygen reacts with sulphur, iron, lead and zinc. The sulphur from the metal sulphides provides the energy to complete the conversion of matte to blister copper. The blister copper (98.5 % Cu) is cast into 1.62 t bars for shipment to refiner-


2008

ies.

The granulated slag goes to the Slag Milling Plant for processing. Off-gases from the Ausmelt pass through a spray cooling system to cool it down to 120ºC before entering the bag house where dust is separated from gas before the cleaned gas is released to the atmosphere via a second stack. Dust recovered at the bag house is taken to the arsenic plant for processing.

Until recently, the smelter complex consisted of two primary smelting furnaces, namely the old reverberatory furnace and the refurbished Ausmelt furnace; three Pierce–Smith converter furnaces, bag houses and cooling towers, the arsenic treatment plant, and a slag milling plant. The Tsumeb smelter is one of only five commercial-scale smelters in Africa, and one of only few in the world that are able to treat arsenic- and lead-bearing copper concentrates and other poly-metallic ores. An oxygen plant was commissioned in 2012, and programmes to improve emissions control, such as the reduction of dust emissions from the converter furnaces, increase of baghouse capacity, upgrading of

2009
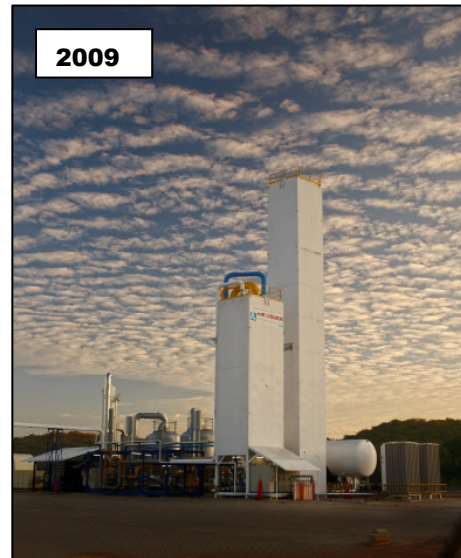
fume extraction systems, and a new extraction system at the arsenic plant are ongoing (www.dundee-precious.com).

In August 2013, the old reverberatory furnace was shut down completely because of its poor compliance to the improved environmental conditions. It will not be started up again, and thus the Ausmelt has become the only smelting furnace. An acid plant to

2012

capture the SO_2 emissions is currently under construction and will be commissioned towards the end of 2014 (pers. comm. H Nolte, September 2013).

Sampling and Analytical Methods

There are several sampling methods available to analyze heavy metals in soil samples. In this study, *x-ray fluorescence spectroscopy* (XRF) was used to quantify the contamination of the soil samples. The vegetative samples were analysed by *inductively coupled plasma-mass spectroscopy* (ICP-AES).
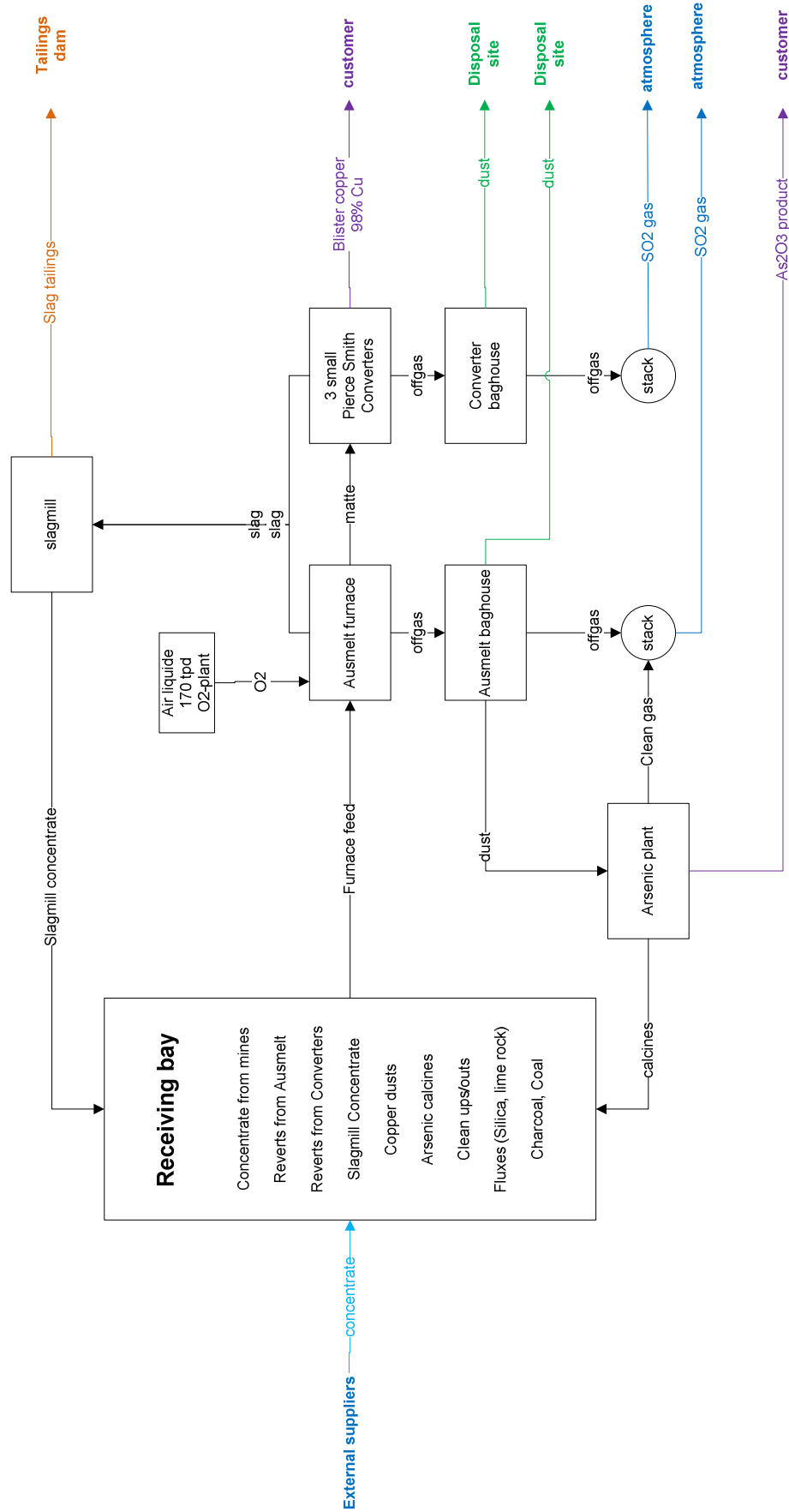
Plant sampling and analysis

A total of 43 plant samples were collected (Fig. 1) comprising of field crops (pumpkin – *Cucurbita sp.*, (Fig. 2a); maize – *Zea mays* (Fig. 2b)); fruit crops (marula – *Sclerocarya birrea* (Fig. 3); papaya – *Carica papaya* (Fig. 4a); chilli pepper – *Capsicum sp (*Fig. 4b)); vegetables (tomato – *Solanum lycopersicum*, parsley – *Pretroselinum crispum(*Fig. 5a); bean – genus *Fabaceae*; and carrot – *Daucus carota* (Fig. 5b)). Most of the vegetable and fruit samples were taken from commercial farms 1 to 1.5 km to the west of the smelter complex as well as private plantations in gardens between 0.3 and 1.5 km to the southwest of the historical smelter, in the Nomtsoub township of Tsumeb (Fig. 1). Marula fruits (Fig. 3), indigenous to the area, were also collected at distances between 200 m and 600 m from the fence of the smelter complex.

Figure 1: Plant sample locations marked by green points, Tsumeb, north-central Namibia (image Google Earth)

Two types of samples were collected from each sampling point, one plant sample was cleaned with distilled water while the other sample was not cleaned in order to investigate the eventual effect of superficial adsorption of dust. All samples were air dried.

The analyses of the vegetative material were performed by the Institute for Soil, Climate and Water in Pretoria, South Africa. Acid digestion of the material was applied. All samples were analysed for each element in duplicate, and mean values were calculated.

Soil Sampling and Analysis

The collection of the 12 soil samples was confined to the topsoil. Vegetation (leaves, branches) from sampling plots was removed and the upper three centimetres of the soil profile were taken. The <2 mm and <0.18 mm fractions of each homogenised soil sample were collected by sieving at each site. Previous studies showed a trend of only slight enrichment of arsenic, copper, lead, cadmium and zinc in the fine fraction compared to the coarser fraction (Geological Survey of Namibia, 2006b). Therefore, the <0.18 mm fraction was chosen as representative soil sample and used for analysis. The <2 mm fraction was taken to the Geological Survey of Namibia for analysis.

The semi-quantitative analysis of the soil samples took place onsite with a portable x-ray fluorescence (XRF) spectrometer XLt 700 Series Environmental Analyzer Version 4.2 of NITON Corporation, USA. The instrument is pre-calibrated by the manufacturer and the measurements taken were compared with readings from international standard samples (NIST 2709, NIST 2710, and RCRA). The detection limits vary between 10 and 30 mg/kg for the different elements. The confidence intervals (2 sigma; 95 %) depend on the measuring time, and typically range from ±5 to ±50%, using a measuring time of 60 seconds. Extended periods of measuring for 120 seconds to 180 seconds lower the range drastically to acceptable levels of 5-25%.
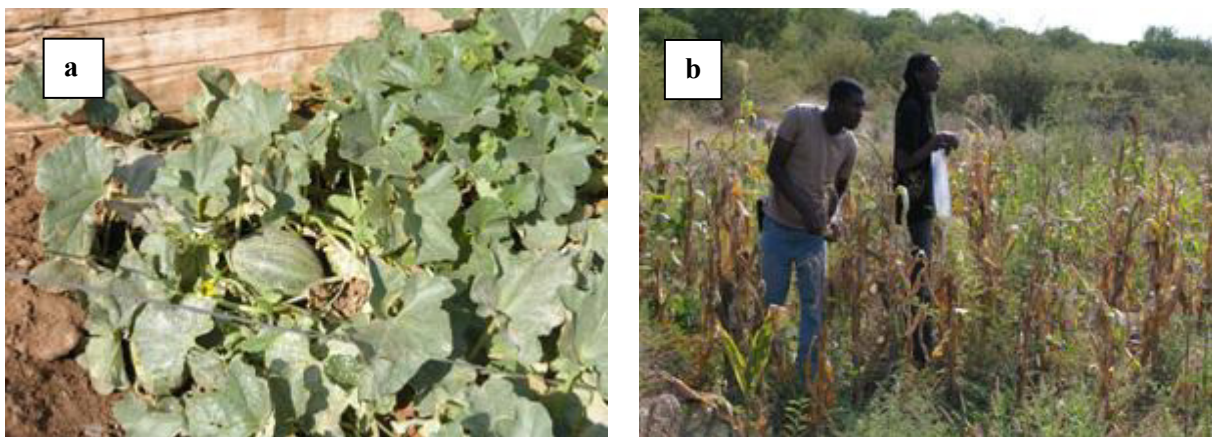
Figure 2: (a) Pumpkin (sample TV-131PM); and (b) maize (sample TV-130MZ) in gardens of Tsumeb - Nomtsoub, north of Rand Street

For standard analysis, about 100 g of the <0.18 mm fraction of each sample were used. The samples were placed into plastic bags and analysed in direct contact with the shutter window of the XRF. The samples were analysed for 60 seconds.

For the purpose of quality control, the soil samples were analysed in parallel at Analytical Laboratory Services in Windhoek applying inductively coupled plasma mass spectrometry (ICP). The reference method was EPA3050B (Environmental Protection Agency).
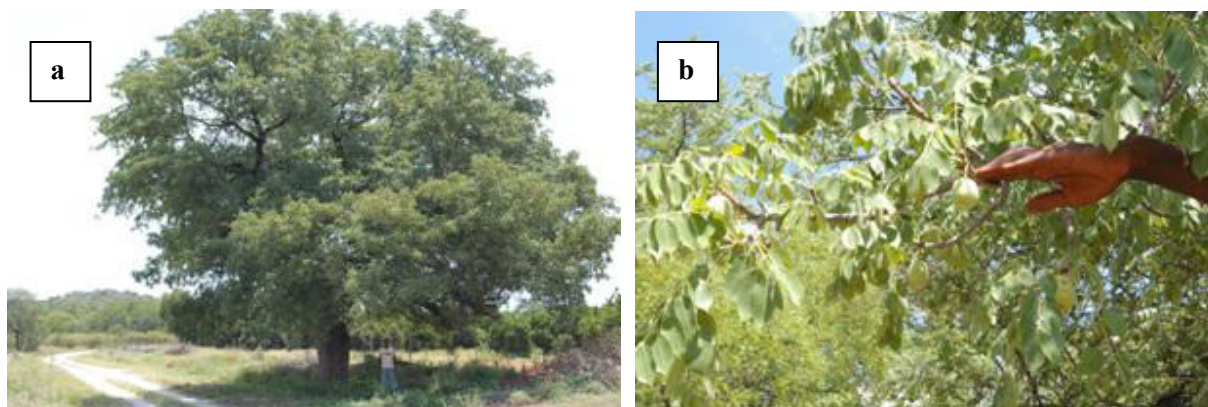
Figure 3: (a) Marula tree (person for scale under the tree); and (b) fruit, from the northern part of the Tsumeb town (hand for scale)
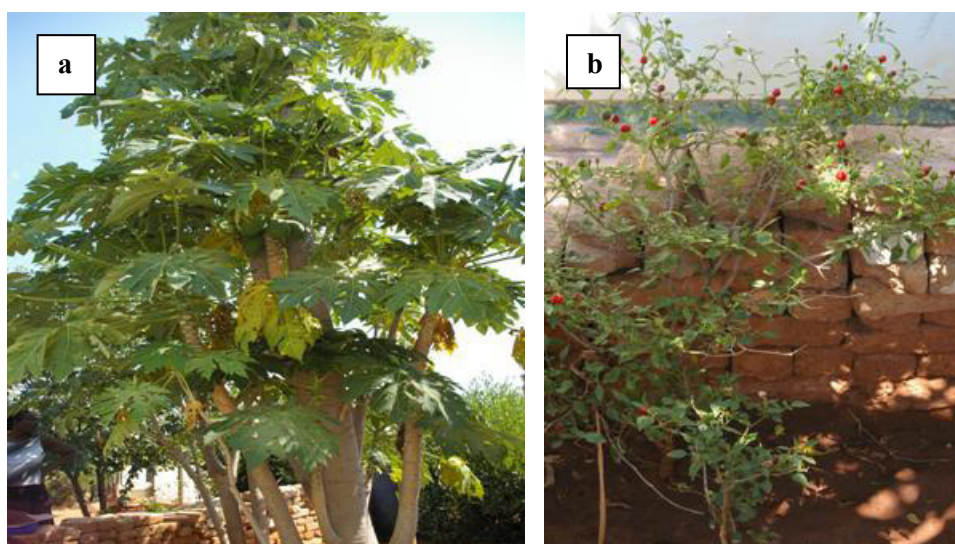
Figure 4: (a) Papaya fruit tree (TV-132PAW); and (b) chilli plants (TV-133CH), grown in the Nomtsoub township to the west of the smelter complex
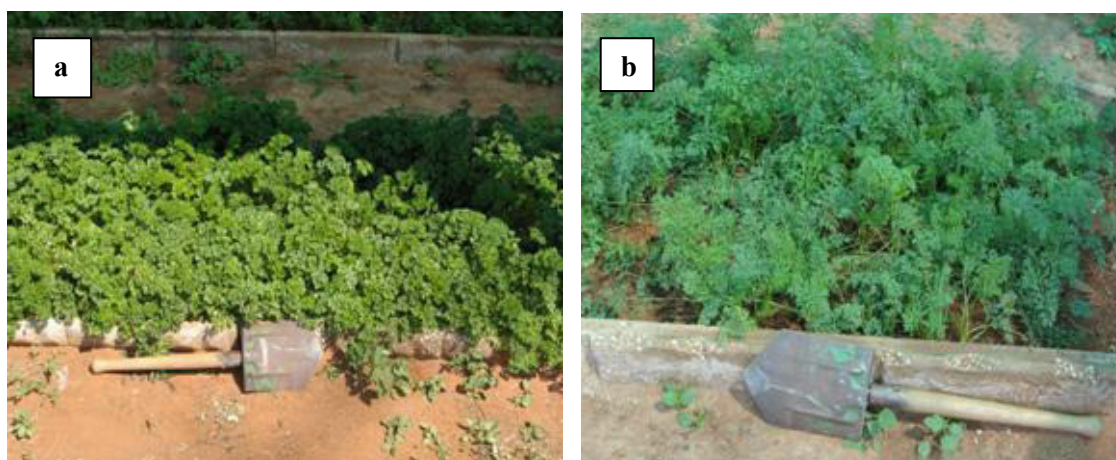
Figure 5: (a) Parsley plants (TV-119P); and (b) carrots (TV-120C) in a vegetable green house bed of the farm to the west of the smelter

Results of the Soil Survey

When comparing the ICP analysis of the top soils with the XRF spectrometer measurements, it becomes obvious that low to moderate concentrations of the heavy metals show an acceptable correlation. However, discrepancies between the two analytical methods exist with respect to the higher concentrations (Table 1). The data in Table 1 suggests that the portable XRF Niton XLt 700 version 4.2 series is sufficiently reliable. The matrix effect appears to be the main factor for major discrepancies.

Sample No	As mg/kg ICP	As* mg/kg	Cd mg/kg ICP	Cd* mg/kg	Cu mg/kg ICP	Cu* mg/kg	Pb mg/kg ICP	Pb* mg/kg	Zn mg/kg ICP	Zn* mg/kg	Mo mg/kg ICP
TSV-119	34	30	3		111	111	260	240	221	238	2
TSV-120	26	21	2		77	75	173	153	151	139	1
TSV-122	68	88	7		232	246	458	431	437	419	2
TSV-123	63	49	5		159	143	320	340	368	239	3
TSV-124	204	169	39		615	544	1090	1226	1580	858	4
TSV-125	849	929	224	214	2500	3308	3020	7315	6420	3231	23
TSV-126	307	192	49		531	457	831	1356	1520	606	6
TSV-127	393	366	63	28	915	1042	1190	2327	2300	1130	9
TSV-128	57	61	11		170	188	269	363	394	248	1
TSV-130	47	46	7		168	162	249	333	425	235	1
TSV-131	47	51	10		125	158	131	495	413	164	1
TSV-132	19	25	2		56	55	100	102	101	109	<1

- Portable XRF spectrometer

Table 1: Heavy metal concentrations of topsoil samples (180 µm fraction) of the Tsumeb area: Comparison between ICP values (Shaded) and semi-quantitative XRF spectrometer values

The evaluation of the hazardous potential of the top soils with respect to heavy metal contamination is based on German (Eikmann and Kloke, 1993) and Canadian (Canadian Environmental Council of Ministers of the Environment, 1999) guideline values for agricultural land use and gardening. These guidelines give the maximum allowable levels for toxic metals in soils and have been applied in this study (Table 2).

The majority of the topsoil samples revealed critical heavy metal contamination (Table 2). Concerning the strict Canadian guideline values, none of the investigated soils is suitable for agricultural land use. The top soils at the old railway station and to the west of it showed very high values for arsenic, cadmium, lead, copper and zinc, exceeding both, Canadian and German guideline values by far. The severe contamination in that area most probably traces back to metal-rich emissions derived from the historical smelter.

Arsenic ranges from 19-849mg/kg, thus some samples are below the German (50mg/kg) but still above the Canadian

guideline values (12mg/kg). Cadmium ranges from 2-224mg/kg, 67% of the soil samples are below the German guideline of 20mg/kg, while all are still above the Canadian guideline of 1.2mg/kg. Copper ranges from 56-2500mg/kg, 92% of the samples are below the German (1000mg/kg) guidelines, while 92% are above the Canadian guideline values of 63mg/kg. Lead values range from 100-3020mg/kg, whereby 25% are above German guideline values of 1000mg/kg, and 100% of samples are above the Canadian guideline of 70mg/kg. Zinc ranges from 101 to the extreme of 6420mg/kg and 33% of the samples are below the German guideline values of 600mg/kg, and 17% are below the Canadian value of 200mg/kg. In highly contaminated soils, the elements showed a trend with arsenic being widely distributed.

Garden soils from houses of the suburb of Tsumeb-Nomtsoub Extension 1 indicated elevated concentrations of the elements of concern but most values are slightly below the German guideline value. The agricultural land to the west and downwind of the Tsumeb smelter complex is in parts critically contaminated by arsenic and copper (Table 2).

Results of Plant Analysis

For interpretation purposes the guideline values of the WHO (Codex Alimentarius) and EU were applied (Table 3A).

All plant samples showed *lead* contaminations exceeding the EU and WHO guideline values of 0.3 and 0.4 mg/kg, respectively. The highest concentrations were found in parsley and carrots exceeding the WHO guideline value by up to almost 20 times for the un-cleaned vegetable. Proper washing of vegetables before preparation leads to a significant decrease of the contamination by approximately 50%. It showed that lead adhered more than the other elements to the surface of those crops and also that its chemical adsorption was high. However, both types of vegetable still exceed the WHO guideline value by roughly 7 times after cleaning with distilled water (Table

3B). Absorption of lead from soil is less than from lead dissolved in aqueous solutions. If ingested together with meals, absorption decreases (26% fasted; 2.5% when ingested with a meal) (ATSDR, 2005). In the Tsumeb area another major source of lead ingestion is through wind that has a high volume of suspended particles (Laidlaw and Filippelli, 2008).

The flesh of the marula samples ("cleaned samples") exceeds the WHO guideline value in all cases by 50% to 200% (Table 3B). Maize, beans and paw-paws are the least contaminated crops concerning lead in comparison to chilli, pumpkin and carrot. However, the lead concentrations in the cleaned samples still exceed the WHO guideline value in most cases.

The highest concentrations of cadmium were found in chilli, pumpkin and carrots, and are exceeding the EU guideline (0.2 mg/kg) value by four to six times. In contrast, maize and paw-paw samples contain cadmium in very low quantities far below the EU guideline value. Marula fruits are not critically contaminated with cadmium, except for one sample taken a few metres directly opposite of the historical smelter.

Parsley, carrots and pumpkin samples are significantly high in arsenic values (Table 3A). The washed vegetable samples exceeded the WHO guideline value of 0.5 mg/kg by two to four times (Table 3B). In contrast arsenic concentrations of maize, beans, chilli, and tomatoes are below the WHO guideline values. All analyses for maize are below the detection limit of the ICP-MS (<0.1 mg/kg). The arsenic concentrations in paw-paw and marula vary between 0.3 and 1.1 mg/kg, and, thus, exceed the guideline value only moderately.

None of the analysed plant samples show critical contamination in copper as they contained below 20mg/kg and zinc values were found to be below 50mg/kg though the soil was heavily contaminated.

The relative uptake of arsenic, lead and cadmium from the soil into the plant is shown by soil-plant transfer coefficients

Sample No.	Description	Latitude	Longi-tude	As mg/kg	Cd mg/kg	Cu mg/kg	Pb mg/kg	Zn mg/kg
TS V119t	Farm west of smelter	-19.20389	17.70638	34	3	111	260	221
TS V120t	Farm west of smelter	-19.20389	17.70638	26	2	77	173	151
TS V122t	Farm west of smelter	-19.20389	17.70638	68	7	232	458	437
TS V123t	Farm west of smelter	-19.20673	17.70670	63	5	159	320	368
TS V124t	Old railway station, garden	-19.23484	17.70846	204	39	615	1090	1580
TS V125t	West of old railway stat.	-19.23485	17.70639	849	224	2500	3020	6420
TS V126t	West of old railway stat.	-19.23368	17.70337	307	49	531	831	1520
TS V127t	West of old railway stat.	-19.23173	17.70379	393	63	915	1190	2300
TS V128t	Nomtsoub	-19.24031	17.70393	57	11	170	269	394
TS V130t	Nomtsoub	-19.24031	17.70213	47	7	168	249	425
TS V131t	Nomtsoub	-19.24016	17.69930	47	10	125	131	413
TS V132t	Nomtsoub	-19.24169	17.69968	19	2	56	100	101

Eikmann-Kloke Values for Soil Contamination, 1993 ("German guideline values")

BW III = "Soil Values III" point to human-, phyto-, zoo-, ecotoxicological risks: remediation required

		As mg/kg	Cd mg/kg	Cu mg/kg	Pb mg/kg	Zn mg/kg
BW III	Agriculture, gardening, crops, fruits	50	20	200	1000	600
BW III	Multifunction soils (parks, recreation)	80	50	600	2000	3000
BW III	Multifunction soils (industry)	200	60	2000	2000	3000

Germany – Soil Protection Law, 1999

Test values for the soil – human pathway (direct contact)

	As	Cd	Cu	Pb	Zn
Playground for children	25	10		200	
Residential areas (including house gardens)	50	20		400	

Canada – Soil Quality Guidelines for the Protection of Environmental and Human Health, 1999

		As	Cd	Cu	Pb	Zn
Agriculture		12	1.2	63	70	200
Residential		12	1.2	63	140	200
Commercial		12		91	260	360
Industrial		12		91	600	360

Table 2: Analytical results of the top soils and evaluation concerning the German (red) and Canadian (yellow) guideline value for agriculture, gardening, crops and fruits

Sample No.	Crop/ Topsoil	Zn mg/kg	Cu mg/kg	As mg/kg	Cd mg/kg	Pb mg/kg	Mo mg/kg
WHO Guidelines		**50**	**20**	**0.5**	**-**	**0.4**	**-**
EU Guidelines		**50**	**20**	**-**	**0.20**	**0.3**	**-**
TV-MA4 uncleaned	**Marula fruit**	17	10	0.9	0.37	2.7	0.5
TV-MA4 cleaned	**Marula fruit**	16	9	0.8	0.33	2.3	0.5
TSOS-114t	**Topsoil**	3279	2899	658.0	67.00	6471.0	---
TV-MA6 uncleaned	**Marula fruit**	19	6	1.1	0.13	2.2	0.6
TV-MA6 cleaned	**Marula fruit**	12	6	0.6	0.13	2.1	0.6
TSV-125t	**Topsoil**	6420	2500	849.0	224.00	3020.0	23.0
TV-MA7 uncleaned	**Marula fruit**	15	7	0.9	0.08	1.2	0.5
TV-MA7 cleaned	**Marula fruit**	14	6	0.8	0.10	0.9	0.5
TSV-126t	**Topsoil**	1520	531	307.0	49.00	831.0	6.0
TV-MA8 uncleaned	**Marula fruit**	13	8	1.2	0.08	2.7	0.4
TV-MA8 cleaned	**Marula fruit**	18	8	1.1	0.08	1.9	0.5
TSV-127t	**Topsoil**	2300	915	393.0	63.00	1190.0	9.0
TV-128PM uncleaned	**Pumpkin**	28	10	0.6	0.38	0.7	1.6
TV-128PM cleaned	**Pumpkin**	33	11	0.6	0.42	1.0	1.5
TV-129CH uncleaned	**Chilli**	21	9	0.2	1.21	0.8	1.0
TV-129CH cleaned	**Chilli**	16	8	0.1	1.31	0.7	0.8
TS-128t	**Topsoil**	394	170	57.0	11.00	269.0	1.0
TV-130TOM unclean.	**Tomato**	47	13	0.3	0.66	1.1	2.5
TV-130TOM cleaned	**Tomato**	45	14	0.2	0.58	0.6	2.3
TS-130t	**Topsoil**	425	168	47.0	7.00	249.0	1.0
TV-131PM unclean.	**Pumpkin**	46	12	1.1	0.75	2.0	0.5
TV-131PM cleaned	**Pumpkin**	44	11	1.2	0.80	1.5	0.5
TS-131t	**Topsoil**	413	125	47.0	10.00	131.0	1.0

Table 3A: Selected analysis for crops with heavy metal concentrations exceeding WHO and EU guidelines for agricultural plants (shaded) and associated top soils exceeding the German guideline values

(Tables 4 and 5). The metal distribution, in general, decreases from root to stem and leaf to edible parts (Adriano, 2001). Our study also shows that toxic elements are virtually excluded from the seed parts of the plant, as is shown by the maize sample.

The relative plant uptake for *lead* is very low. The lead concentration in the crops is between 0.15% and 2% of the lead concentration of the soil in which the crop grows. The higher value for *carrots* confirms

that lead primarily accumulates in the roots and is less trans-located to other parts of the plant as was found by Adriano (2001). Stem vegetables like *maize, beans* and *tomatoes* are less prone to lead contamination through the soil-plant pathway.

The coefficients for *cadmium* are significantly higher than those for lead which is supported by several other studies on the mobility of cadmium (Ramos et al., 2002; Smolders, 2001). The highest relative cad-

Sample No.	Crop	Zn mg/kg	Cu mg/kg	As mg/kg	Cd mg/kg	Pb mg/kg	Mo mg/kg
WHO Guidelines		**50**	**20**	**0.5**	**-.**	**0.4**	**-**
EU Guidelines		**50**	**20**	**-**	**0.2**	**0.3**	**-**
TV-MA1 uncleaned	Marula fruit	12.2	7.40	0.47	0.03	1.45	0.20
TV-MA1 cleaned	Marula fruit	16.5	7.30	0.34	0.03	0.67	0.12
TV-MA2 uncleaned	Marula fruit	11.2	4.32	0.50	0.04	1.33	0.22
TV-MA2 cleaned	Marula fruit	13.0	4.37	0.61	0.06	0.84	0.23
TV-MA3 uncleaned	Marula fruit	12.4	7.42	0.80	0.06	1.28	0.71
TV-MA3 cleaned	Marula fruit	10.3	5.96	0.76	0.06	1.10	0.65
TV-MA4 uncleaned	Marula fruit	16.8	9.52	0.92	0.37	2.42	0.52
TV-MA4 cleaned	Marula fruit	15.8	8.50	0.77	0.33	2.25	0.51
TV-MA5 uncleaned	Marula fruit	10.1	3.55	0.54	0.05	0.67	0.17
TV-MA5 cleaned	Marula fruit	13.0	4.58	0.53	0.15	0.73	0.26
TV-MA6 uncleaned	Marula fruit	18.6	6.35	1.09	0.13	2.20	0.57
TV-MA6 cleaned	Marula fruit	11.5	5.62	0.58	0.13	2.05	0.56
TV-MA7 uncleaned	Marula fruit	14.6	6.80	0.91	0.08	1.20	0.47
TV-MA7 cleaned	Marula fruit	13.8	6.45	0.75	0.10	0.94	0.50
TV-MA8 uncleaned	Marula fruit	13.0	8.15	1.19	0.08	2.66	0.36
TV-MA8 cleaned	Marula fruit	17.5	8.25	1.13	0.08	1.94	0.47
TV-119P uncleaned	Parsley	34.0	14.61	3.9	0.66	5.50	10.41
TV-119P cleaned	Parsley	31.1	10.14	2.1	0.44	2.67	9.48
TV-120C uncleaned	Carrot	29.4	7.81	1.70	0.71	7.51	1.25
TV-120C cleaned	Carrot	28.1	6.85	1.21	0.96	2.96	4.33
TV-120BS uncleaned	Bean seeds	24.1	9.08	0.12	0.18	0.33	2.51
TV-120B uncleaned	Bean skin	11.0	6.83	0.20	0.16	0.52	1.54
TV-120B cleaned	Bean skin	13.8	6.60	0.25	0.16	0.52	1.56
TV-122PAW unclean.	Pawpaw	18.0	4.77	0.94	0.06	2.35	2.21
TV-122PAW cleaned	Pawpaw	16.4	3.45	0.59	0.04	0.86	1.98
TV-123MZ uncleaned	Maize	31.2	2.78	<0.1	0.03	0.38	0.94
TV-123MZ cleaned	Maize	30.9	3.20	<0.1	0.03	0.40	0.93
TV-128PM uncleaned	Pumpkin	27.9	10.47	0.62	0.38	0.73	1.55
TV-128PM cleaned	Pumpkin	32.8	10.91	0.62	0.42	0.97	1.52
TV-129CH uncleaned	Chilli	20.5	8.84	0.19	1.21	0.84	1.01
TV-129CH cleaned	Chilli	16.4	7.54	0.13	1.31	0.69	0.79
TV-130MZ uncleaned	Maize	40.1	3.44	<0.1	0.04	0.49	1.01
TV-130MZ cleaned	Maize	37.7	3.68	<0.1	0.04	0.50	1.02
TV-130TOM uncleaned	Tomato	46.6	13.36	0.34	0.66	1.10	2.45
TV-130TOM cleaned	Tomato	44.9	13.78	0.16	0.58	0.62	2.26
TV-131PM uncleaned	Pumpkin	46.3	12.30	1.10	0.75	2.00	0.53
TV-131PM cleaned	Pumpkin	44.0	11.04	1.17	0.80	1.46	0.54
TV-132PAW uncleaned	Pawpaw	15.8	2.75	0.63	0.08	0.66	2.39
TV-132PAW cleaned	Pawpaw	18.0	2.80	0.55	0.07	0.73	1.95
TV-133CH uncleaned	Chilli	29.6	15.80	0.27	0.85	1.15	1.10
TV-133CH cleaned	Chilli	26.9	14.50	0.21	0.89	0.71	1.12
TV-134 cleaned	Ximenia Am.	10.3	5.80	0.64	0.28	0.98	1.40
TV-135MZ uncleaned	Maize	33.5	2.48	<0.1	0.03	0.61	0.80

Table 3B: Analytical results of uncleaned and cleaned vegetative material (Shaded: results exceeding guidelines)

mium uptake was found in *carrots, chilli* and *parsley* (Table 4). Following its uptake by the roots, cadmium translocation is rather limited throughout the plant. Cadmium uptake is influenced by the presence of zinc in soils and chloride salinity (Smolders, 2001). Cadmium distribution is very limited in cereal grains like *maize* and fruits of trees like *paw-paw* and *marula*. In areas where manganese is present in soils, as is the case in most tropical soils, the presence of Cd inhibits its uptake (Ramos *et al.*, 2002).

1The coefficients for arsenic reveal a generally low degree of contaminant uptake by the plants (Table 4). Stem crops (maize, chilli, tomato, beans) and fruit trees (marula, pawpaw) show the lowest values (Table 4). In contrast, arsenic uptake by root vegetables like carrots and leafy vegetables like parsley is high (Table 4).

Crop	Lead	Cadmium	Arsenic
Beans	0.25	8.50	0.80
Carrot	2.00	48.00	6.00
Chilli	0.50	28.50	0.50
Maize	0.15	0.60	<0.2
Marula fruit	0.46	0.21	0.96
Parsley	1.00	15.00	7.00
Pawpaw	0.50	2.30	1.30
Pumpkin	0.70	6.00	1.50
Tomato	0.20	8.00	0.30

Table 4: Plant uptake of contaminants from soil (concentration in plant material/concentration in soil in %)

Sample No.	Crop	Arsenic	Lead	Cadmium
TV-MA1	Marula fruit	0.02	0.01	-
TV-MA2	Marula fruit	0.02	0.01	-
TV-MA3	Marula fruit	0.01	0.01	-
TV-MA4	Marula fruit	0.001	0.0003	0.005
TV-MA5	Marula fruit	0.02	0.003	-
TV-MA6	Marula fruit	0.0007	0.0006	0.0005
TV-MA7	Marula fruit	0.002	0.001	0.002
TV-MA8	Marula fruit	0.003	0.002	0.001
TV-119P	Parsley	0.07	0.01	0.15
TV-120C	Carrot	0.06	0.02	0.48
TV-120B	Bean Skin	0.01	0.003	0.08
TV-120BS	Bean Seeds	0.006	0.002	0.09
TV-122PAW	Pawpaw	0.006	0.003	0.006
TV-123MZ	Maize	<0.002	0.001	0.006
TV-128PM	Pumpkin	0.01	0.004	0.04
TV-129CH	Chilli	0.002	0.003	0.12
TV-130TOM	Tomato	0.003	0.002	0.08
TV-130MZ	Maize	<0.002	0.002	0.006
TV-131PM	Pumpkin	0.02	0.01	0.08
TV-132PAW	Pawpaw	0.02	0.007	0.04
TV-133CH	Chilli	0.008	0.007	0.45

Table 5: Coefficients for contaminants in the crop samples compared to the adjacent soil

Element	WHO (2002)	EU (2001)
As (mg/kg)	0.5	-
Cu (mg/kg)	20	20
Pb (mg/kg)	0.4	0.3
Zn (mg/kg)	50	50
Cd (mg/kg)	Not available	0.2
Mo (mg/kg)	Not available	Not available

Table 6: Guideline values of the WHO (Codex Alimentarius) and the EU for agricultural plants

Conclusions

The selection of sample materials was based on some fruits and vegetables which are abundant on farms and in gardens in the area. The analysed fruit crops (marula, paw-paw), vegetables (tomato, parsley, carrot, bean, pumpkin, chilli) and field crops (maize) were collected from moderately to severely contaminated soils in the surroundings of the Tsumeb smelter complex.

Bioaccumulation of the toxic elements lead, cadmium and arsenic is evident in all plant samples. These elements can severely impact human health if contaminated fruits and vegetables are consumed regularly or in significant quantities.

All cleaned fruit and vegetable samples exceed the WHO and EU guideline values for lead by up to seven (7) times, and, thus, are not suitable for human consumption.

Parsley and carrot as well as chilli and pumpkin accumulated high concentrations of lead, arsenic and cadmium despite the fact that the underlying soils are only moderately contaminated. In addition, the crops were grown in green house structures where wind-borne contamination is reduced (Table 5). Thus, leaf vegetables like parsley and root vegetables like carrots seem to be extremely prone to the accumulation of the investigated toxic elements.

In contrast, maize and to a lesser extend stem vegetables like tomatoes and beans as well as fruits of paw-paw contain relatively low concentrations of the hazardous elements.

Thus, it is recommended to strictly cease any agricultural land use and vegetable gardening for human consumption in the blue zone of figure 6. Especially critical is the area towards the west and north of the smelter, where a buffer zone of 3 to 6 km should be established where no crops and vegetables should be grown at all.

Growing of leaf vegetables (parsley, spinach, lettuce) and root vegetables (carrots, potatoes) should be generally restricted in the wider surroundings of the smelter including the whole town and the farmland up to 10 km to the west of the smelter (red zone in figure 6). For those areas, especially maize but also stem vegetables (beans, tomatoes, green pepper) and fruit trees could serve as alternatives.

Heavy metal concentrations of uncleaned and cleaned vegetative material showed generally moderate differences. Some pesticides such monosodium methyl arsenate (MSMA) and disodium methyl arsenate (DSMA) contain arsenic, and may have been used in the past. At present, widely used in the area is the herbicide Methyl-chlorophenoxyacetic acid (MCPA) and the pesticide Cypermethrin, both of which are organic compounds without any heavy metals (pers. comm. AGRA, September 2013) However, the effect of dust adsorption on the surface of parsley and carrots is significant. Thus, leaf and root vegetables grown in the Tsumeb area have to be intensively washed before consumption. Farmer and supermarkets are advised to clean all root vegetables properly before distribution.
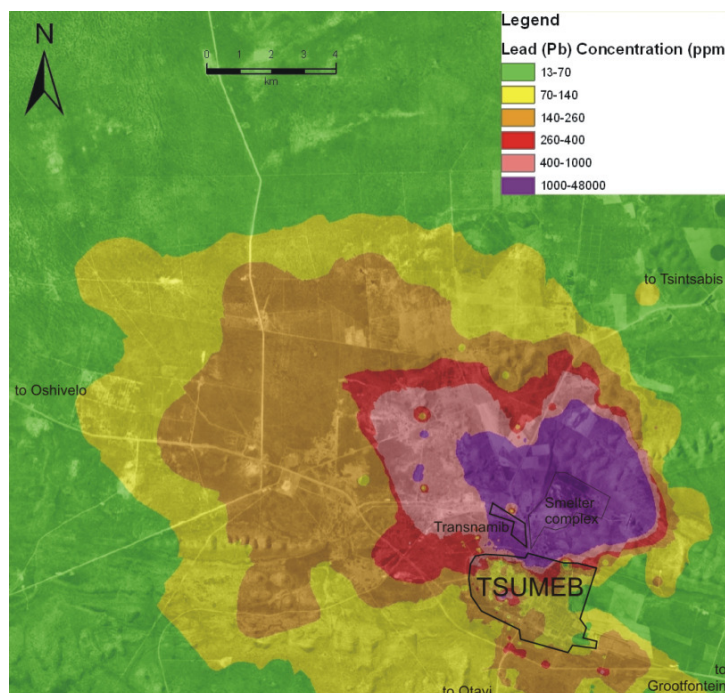
Figure 6: Lead contamination of surface soils in the Tsumeb area

Another issue of concern is the collection of marula fruit containing the contaminants directly in the flesh and in the adsorbed dust on the fruit's surface. Awareness has to be created on the severe hazardous risks posed by marula fruits collected in highly contaminated areas. Marula collection should be prevented in a radius of approximately 1 km around the smelter.

Element	Route of exposure	Duration	MRLs	Endpoint	Detected
Arsenic	Inhalation Ingestion Dermal	Acute Chronic	0.005mg/kg/day 0.0003mg/kg/day	Cancer, liver cardiovascular, gastrointestinal, kidney, neurological, Pulmonary, reproductive	Blood Urine Nails Hair
Cadmium	Ingestion Inhalation	Chronic	0.0002mg/kg/day TTD_{NEURO} = 0.0002mg/kg/day TTD_{CARDIO} = 0.005mg/kg/day TTD_{HEMATO} = 0.0008mg/kg/day TTD_{TESTIC} = 0.003mg/kg/day	Lung damage, stomach irritation, kidneys (main target), fragile bones, delayed development in children, testicular effects (necrosis & atrophy), BP	Blood, hair, urine or nails
Copper	Ingestion Inhalation	Acute	0.01mg/kg/day	gastrointestinal	Hair, nails, blood, urine and other tissues.
Lead	Inhalation Ingestion. Dermal (organic Pd)	Chronic	MRLs threshold not yet determined	Reduced fertility ≥40µg/dL Gastrointestinal Colic in children 60-100µg/dL Cardiovascular ≤10µg/dL	Blood, urine

Table 7: Minimal Risk Levels (ATSDR) - TTD – Target Organ Toxicity Dose, NEURO – Neurological effect, CARDIO – Cardiovascular effect, HEMA – Haematological effect, TESTIC – Testicular effect

Soil treatment can be done *in situ* (on-site) or *ex situ* (removed and treated elsewhere) e.g. by phyto-extraction. None of the metals investigated are biodegradable (USDA, 2000), which means that they will be resident in soils for some time to come. The best mitigation is zoning off areas that show the highest and unsafe levels of contamination of toxic metals such as arsenic, lead and cadmium. The path of exposure, effects and minimal risk levels for selected metals are given in Table 7.

Acknowledgements

References

ADRIANO, D.C. (2001): Trace elements in terrestrial environments. Biogeochemistry, bioavailability, and risks of metals. – 867 pp.; Springer.

ATSDR, 2005, ToxGuide for Arsenic, U.S. Department of Health and Human Service.

BÜRG, G. (1942): Die Nutzbaren Minerallagerstätten von Deutsch-Südwestafrika. Mitteilungen der Forschungsstelle für Kolonialen Bergbau, Bergakademie Freiberg, **2**, Walter De Gruyter, Berlin.

CANADIAN ENVIRONMENTAL COUNCIL OF MINISTERS OF THE ENVIRONMENT (1999): Soil Quality Guidelines for the Protection of Environmental and Human Health, updated 2006.

EIKMANN, T. UND KLOKE, A. (1993): Nutzungs- und schutzgutbezogene Orientierungswerte für (Schad-) Stoffe in Böden. – In: Rosenkranz, Einsele, Harreß (Hrsg.): Bodenschutz, Ergänzbares Handbuch; Erich Schmidt Verlag.

GREMION F. (2003): Analysis of Microbial Community Structures and Functions in Heavy Metal- Contaminated Soils Using Molecular Methods. 107 pp, PhD thesis, EPFL, Univ. Lausanne, Switzerland.

GEOLOGICAL SURVEY OF NAMIBIA (2006a): Geochemical Investigation of Soils in the Area of the Proposed Town Extensions Nomtsoub 6 and 7. Environmental Monitoring Series N° 1. – Geological Survey of Namibia, Windhoek, 15p.

GEOLOGICAL SURVEY OF NAMIBIA (2006b): Tsumeb - Hazardous Potential of the Current Waste Disposal Site of Tsumeb Regarding Groundwater Contamination Environmental Monitoring Series N°3. – Geological Survey of Namibia, Windhoek, 21p.

GEOLOGICAL SURVEY OF NAMIBIA (2007a): Mapping of soil contamination in Tsumeb. Environmental Monitoring Series N°7. Geological Survey of Namibia, Windhoek, 30p.

GEOLOGICAL SURVEY OF NAMIBIA (2007b): Tsumeb - Investigation on the eventual impact of the Tsumeb Smelter on fish farming at farm Mannheim 100/13. Environmental Monitoring Series N°14. Geological Survey of Namibia, Windhoek, 16p.

IIPINGE, S. (2008): Geochemical and mineralogical study of the heavy metal contamionants in the soils of the Tsumeb area, northern Namibia. Honours thesis, Rhodes University, Grahamstown, South Africa.

KRIBEK, B. AND KAMONA, F. (Eds., 2005): Assessment of the mining and processing of ores on the environment in mining districts of Namibia. – Final Report. Czech Geol. Surv., 102 p.; Prague.

LAIDLAW, M.A.S. AND FILIPPELLI, G.M. (2008). Resuspension of urban

soils as a persistent source of lead poisoning in children: A review and new directions. *Applied Geochemistry, 23, 2021-2039.*

NAMIBIA CUSTOM SMELTERS (2013): Overview and History of Namibia Custom Smelters. 4 pp., unpubl.

RAMOS, I., ESTEBAN, E., LUCENA, J.J. AND GARATE, A. (2002). Cadmium uptake and subcellular distribution in plants of Luctaca sp. Cd-Mn interaction. *Plant Science, 162, 761-767.*

SCHNEIDER, G.I.C. (1992a): Cadmium. *In*: The Mineral Resources of Namibia, Geol. Surv. Namibia, 2 pp.; Windhoek.

SCHNEIDER, G.I.C. (1992b): Germanium. *In*: The Mineral Resources of Namibia, Geol. Surv. Namibia, 2 pp.; Windhoek.

SCHNEIDER, G.I.C. (1992c): Antimony. *In*:   The Mineral Resources of Namibia, Geol. Surv. Namibia, 2 pp.; Windhoek.

SCHNEIDER, G.I.C. & GENIS, G. (1992): Arsenic. *In:* The Mineral Resources of Namibia, Geol. Surv. Namibia, 4 pp.; Windhoek.

SCHNEIDER, G.I.C. & SEEGER, K.G. (1992): Copper. In: The Mineral Resources of Namibia, Geol. Surv. Namibia, 118 pp.; Windhoek.

SMOLDERS, E. (2001). Cadmium uptake by plants. *International Journal of Occupational Medicine and Environmental Health, Vol. 14, No. 2, 177—183.*

USDA-NRCS, 2000, Heavy Metal Soil Contamination, Soil Quality-Urban Technical Note No.3

IMPACT OF ORE PROCESSING ON THE ENVIRONMENT IN THE TSUMEB AREA, NAMIBIA

Kříbek, B.[1], Majer, V.[1], Pašava, J.[1], Knésl, I.[1], Kamona, F.[2], Mapani, B.[2], Mwiya, S.[3], Kawali L.[3], Kandjii, I.[3], Keder, J.[4]

[1]*Czech Geological Survey, Geologická 6, 152 00 Prague 5, Czech Republic;bohdan.kribek@geology.cz*
[2]*University of Namibia, Faculty of Earth Sciences, Private Bag 13301 Windhoek, Namibia*
[3]*Geological Survey of Namibia, Ministry of Mines and Energy (MME), P.O. Box 2168, 1 Aviation Road, Windhoek, Namibia*
[4]*Czech Hydrometeorological Institute, Air Quality Protection Department, Na Šabatce 17, 14306 Prague 4, Czech Republic*

The environmental degradation in the Tsumeb Area, Namibia, is poorly qualified in spatial terms, since the availability of accurate and up-to-date regional geochemical data for both, unpolluted and polluted areas are limited. To determine an extent of the past industrial pollution, geochemical mapping of soils and grasses was carried out in the Tsumeb Area and the results were compared with those of numerical modeling of solid and gaseous emissions from the Tsumeb smelter, which is still in operation. The area was covered by a semi-regular network of topsoil sampling with a density of at least one composite sample for a 1 x 1 km basic cell using the methodology recommended by Salminen et al. (1998). The mapping in a scale of 1: 25 000 covered a total area of 429 km^2. As the anthropogenic contamination is usually restricted to the surface layer of soil, reference samples were taken from a depth of 80–90 cm of the soil profile. The Tsumeb region agriculture is mostly oriented on the livestock production. Therefore, different grass species collected from pasturelands were analysed for heavy metals contents. Soil, anthropogenic sediments and grass were analysed for As, Cd, Co, Cu, Ga, Ge, Hg, Mo, Pb, Zn, Tl, S_{sulf} and C_{org}. Statistical characteristics of analytical data were obtained using non-parametric statistical programme S-plus (MathSoft, USA). Geochemical data were expressed in the form of spot or isoline maps using SURFER (Golden Software Inc.) program. Numerical modeling was carried out using Symos´97 program (EIONET, 2003), which is based on the Gauss-type distribution of the emissions halo.

Sources of contamination

The following sources of contamination were identified in the studied area:
(1) Solid emissions from the copper and lead smelter contain high amounts of SO_2, high amounts of potentially toxic metals (up to 5.6 wt.% Cu, 0.5 wt. % Pb, 0.3 wt. % Zn) and increased amounts of Cd, As, Hg, Ga, Ge and Tl. Lead is mostly bound to relatively soluble sulfates, anglesite and lanarkite. Dust fall contains more than 85 wt. % of fine-grained particles (PM_{10}) that are hazardous with respect to the human respiratory system.
(2) Dust from the beaches of tailing impoundments contains up to 0.7 wt. % Pb, 0.57 wt.% Zn, 0.59 wt. % Cu and increased amounts of As, Cd and Tl. Approximately 14.7 wt. % of the PM_{10} particles was recorded in the dust fall.
(3) Slag deposits are composed mostly of medium-grained silicate glass particles with up to 11 wt. % Cu, 6 wt. % Zn, 4.4 wt. % Pb and high amounts of As, Cd, Co, Ga, Ge and Mo. Metals are bound partly to silicates, partly to easily soluble sulfide minerals or occur in native form.

## Distribution of heavy metals and sulfur in soils

To differentiate geological source, i.e. primary geochemical regional background of metals in soils and anthropogenic contamination, the concept of correlation between metals concentrations in topsoil and in the subsurface soil horizon (70 to 90 cm depth) was accepted. Using this concept, higher concentrations of metals in the surface layer of soil than in deeper

Using this concept, higher concentrations of metals in the surface layer of soil than in deeper soil horizon were considered to represent anthropogenic contamination caused mainly by airborne dust particles. In contrast, higher concentrations of metals in the lower soil horizon compared with topsoil were considered to reflect the natural geochemical contribution from bedrock (primary mineralization). For example, high concentrations of lead in topsoils were found west and north-west of the smelter and tailings impoundment (Fig. 1). The highest lead contents (> 1500 ppm) are interpreted to represent downwind dust contamination. Anomalous values of lead detected in subsurface soil in the area of the Tsumeb mine (Fig. 2) can be, however, related to primary sulfide mineralization.
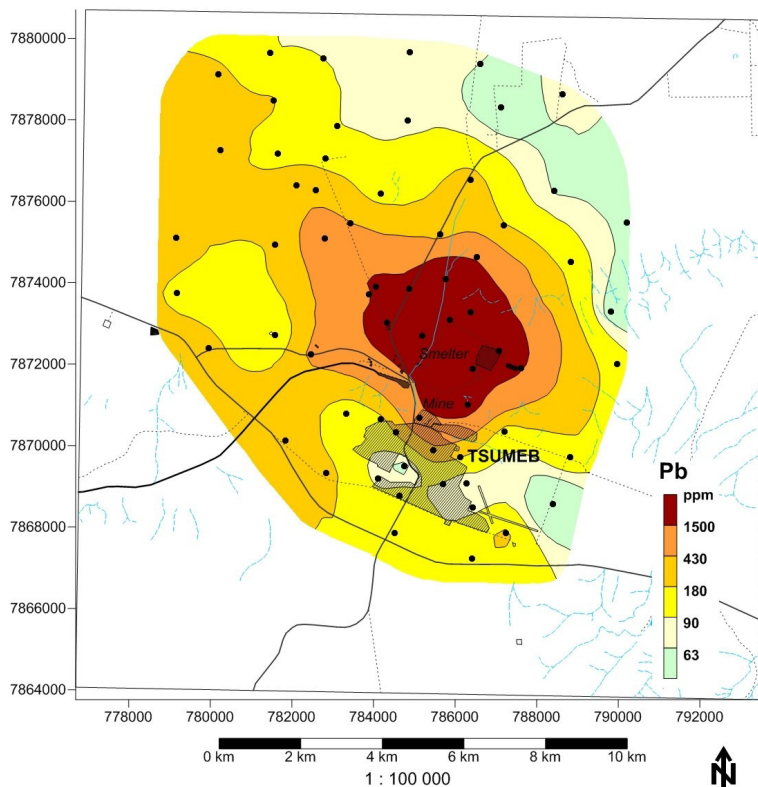
Figure 1: Distribution of lead in topsoils in the Tsumeb area. Black dots represent sampling points.
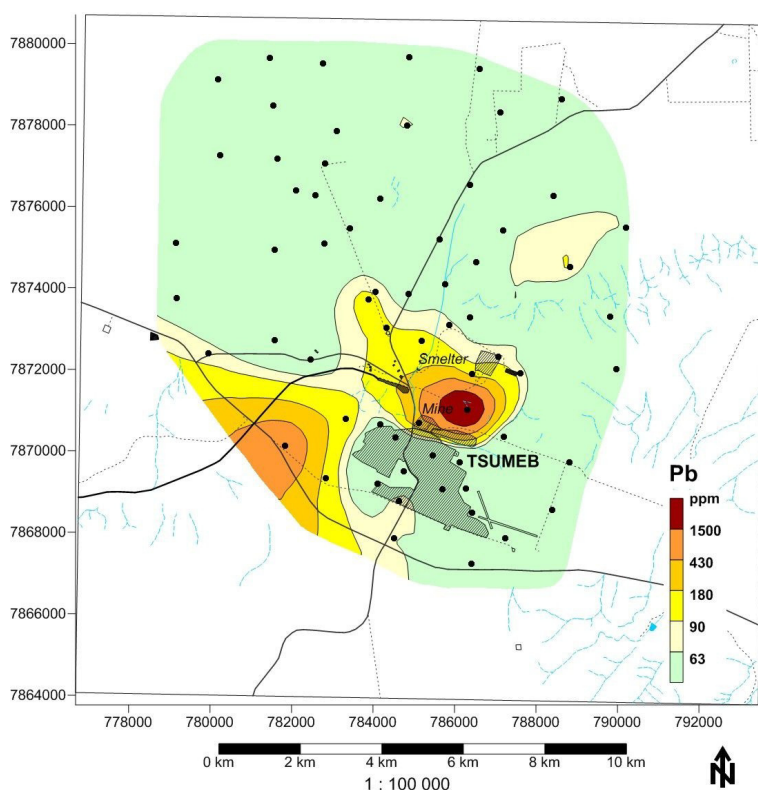
Figure 2: Distribution of lead in the subsurface soil horizon of the Tsumeb Area. Black dots represent sampling points.

The distribution of total sulfur in topsoils (**Fig. 3**) reflects the combined effect of sulfur emissions from the smelter, high content of sulfate around the closed Tsumeb mine (primary mineralization) and contamination of the Jordan River Valley with flotation wastes released during the failure of the of old tailing impoundment. It was established that the degree of industrial contamination may be the best expressed using the Coefficient of Industrial Pollution (CIP), which is a sum of the concentrations of selected metals in topsoil at the individual sampling point, divided by the median values of the same metals in topsoil of the whole region (**Fig. 4**):

$$CIP = \left(\frac{As}{m} + \frac{Cd}{m} + \frac{Cu}{m} + \frac{Hg}{m} + \frac{Pb}{m} + \frac{Zn}{m}\right)/6,$$

where *m* is a median value of the metal concentration.
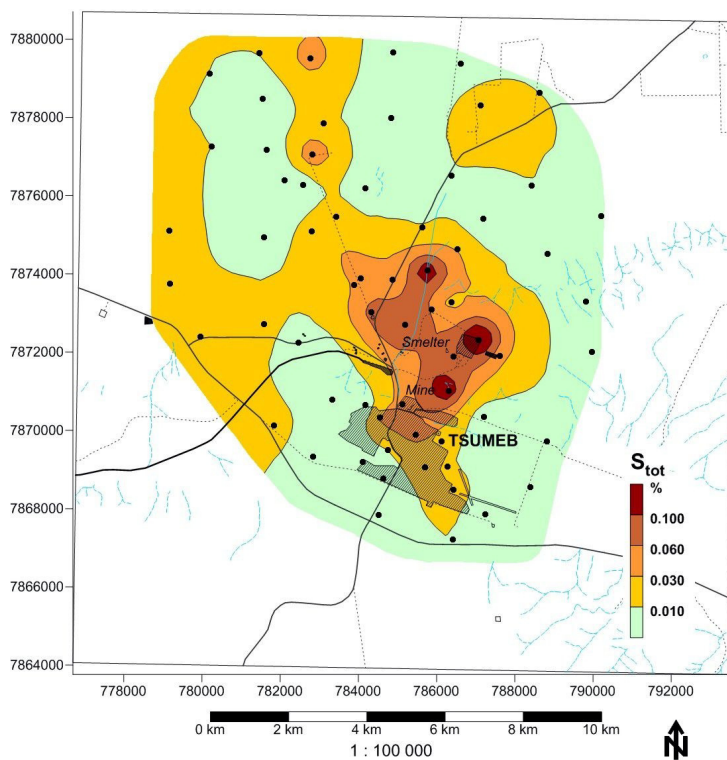
Figure 3: Distribution of total sulfur in topsoils of the Tsumeb Area. Black dots represent sampling points.
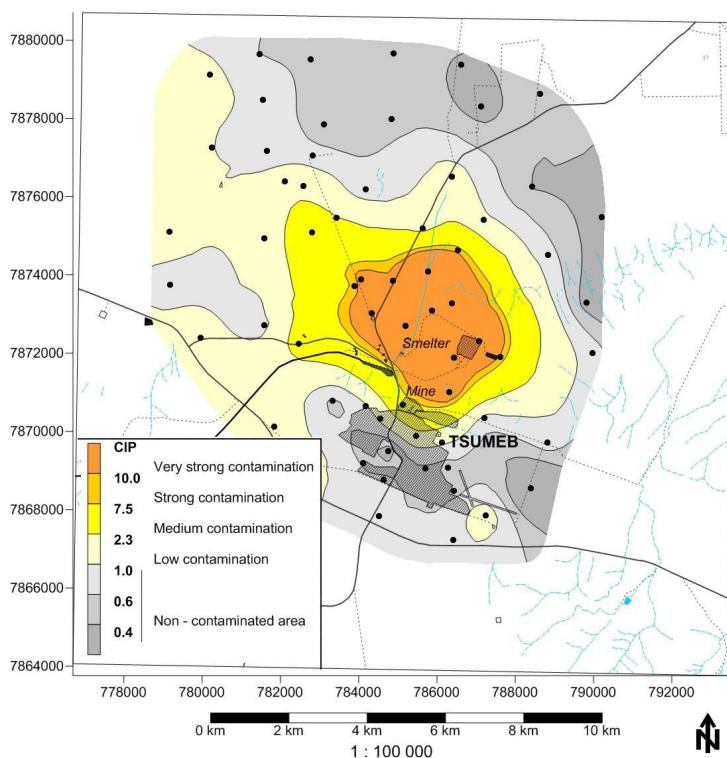
Figure 4: Coefficient of the industrial pollution (CIP) values in the Tsumeb Area. Black dots represent sampling points.

Distribution of heavy metals in plants

The Tsumeb region agriculture is mostly oriented on the livestock production. Therefore, different grass species from pasturelands were analysed for heavy metals/metalloids contents. It was found that 25.8 % of grass samples exceed the threshold of the As concentration in dry feedstock according to the Czech limits (CMR 987), 54.8 % exceed the threshold for Mo and 12.9 % the threshold for Pb (Fig. 5). The highest contents of metals (26.6 ppm As, 52.6 ppm Mo and 104 ppm Zn (on dry weight) were recorded in the grass species *Eargrotis cf. porosa* sampled in the grassland near the Tsumeb Smelter. A large number of grass samples from the Tsumore 761 Farm, 1335 Cadastre and peripheral parts of the Dannenberg 478 Farm is affected by contamination. Very high Pb concentrations in grass are found in the vicinity of the smelter. The contamination with Mo and especially with As is, however, traceable over a distance of 12 km NW from the Tsumeb Smelter.
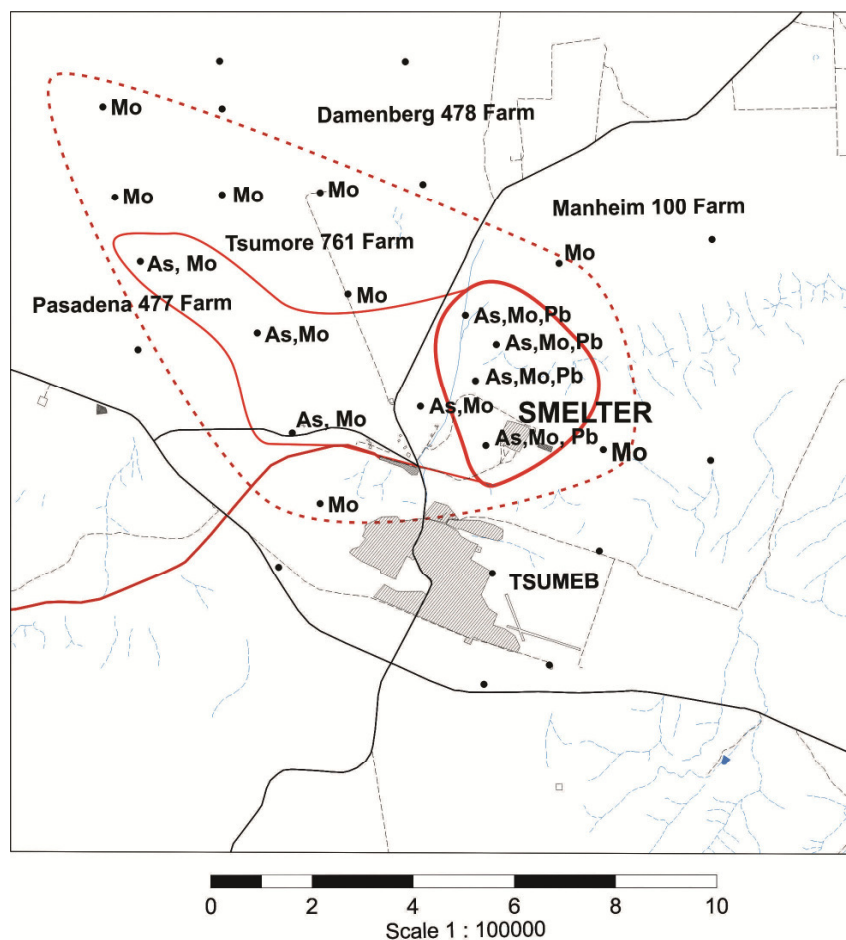
Figure 5: Metals in pasture grass in the Tsumeb Area. The assemblage of metals exceeding Czech limit for dry feedstock at individual sampling points is plotted by their symbols. Heavy red line restricts area contaminated by As, Mo and Pb, light red line restricts area contaminated by As and Mo and broken red line restricts area contaminated by Mo.

Numerical modeling of emissions from the Tsumeb Smelter

The results of the numerical modeling of the SO_2 emissions from the Tsumeb Smelter revealed a contamination of the Tsumeb Town area. However, according to the modeling results, the expected concentration of SO_2 is relatively low (< 0.1 $\mu g.m^{-3}$) and the health risk can be classified as acceptable according to Czech regulations. High SO_2 concentration haloes are expected to be located at the hilltops to the east and south of the smelter (Fig. 6).

The highest dust fall concentrations (> 100 $g.m^{-2}$) are expected to be found around the Tsumeb Smelter (Fig. 7). The Tsumeb residential area is less affected (< 0.X $g.m^{-2}$) due to a favorable landscape morphology between the

smelter and town (the Tsumeb Hills). A large area of dust fall contamination is expected to be located downwind, west of the Tsumeb Smelter. The results of numerical modeling of the SO_2 concentration and dust fall generally correspond with the results of environmental-geochemical mapping. Differences can be explained by additional sources of contamination (dust fall from tailing impoundments and slag deposits, mineralized dust from abandoned mines) that were not considered in the numerical model.
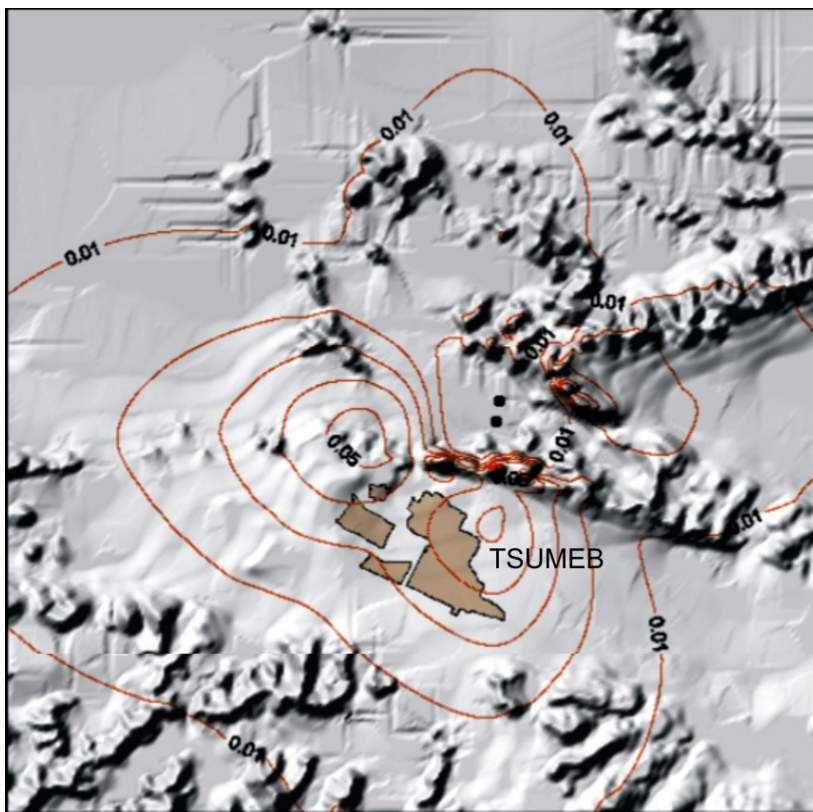
Figure 6: Numerical model of the SO_2 dispersion halo around the Tsumeb Smelter. Isolines represent annual average concentrations of SO_2 (in $\mu g.m^{-3}$). The position of smelter stacks is marked by black dots.
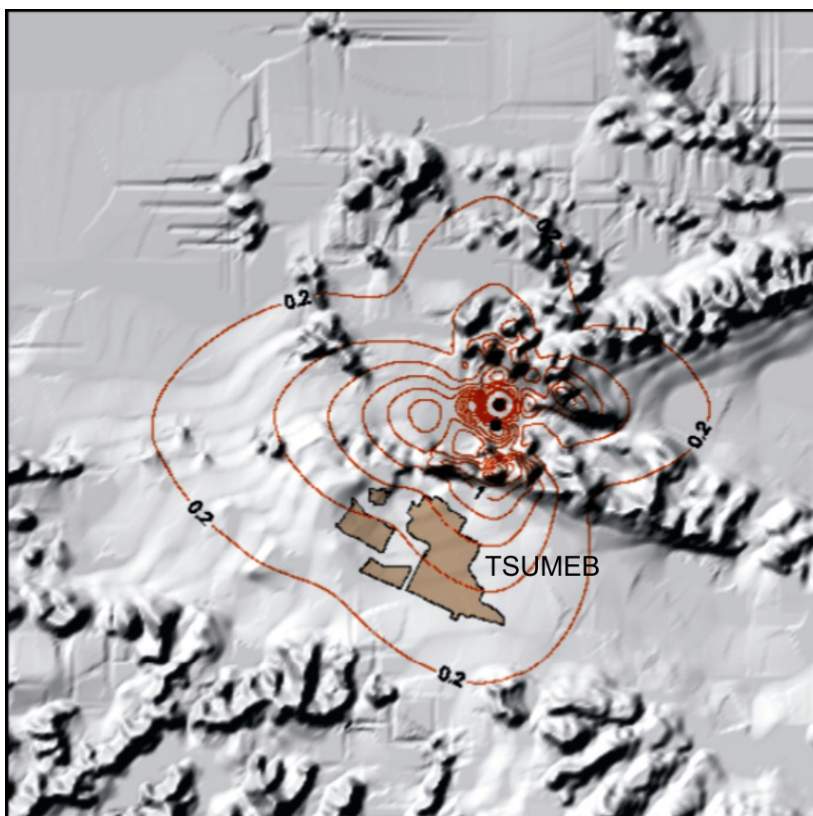
Figure 7: Numerical model of the dust dispersion halo around the Tsumeb Smelter. Isolines represent annual average concentrations of dust fall (in $g.m^{-2}$). The position of smelter stacks is marked by black dots.

Acknowledgments

References

CMR, 1987. Czech ministerial regulation No. 117/1987 Coll. on highest permissible content of heterogeneous substances in fodder. Ministry of Agriculture of the Czech Republic. Prague. 38 p.

EIONET (2003) European Topic Centre on Air and climate Change Long destcription of model "*Sysmos*97". http:// pandora.meng. auth.gr/mds/showlong.php?id=119, visited 01-08-2013.

Salminen R, Tarvainen T, Demetriadis ., Duriš M, Fordyce FM, Odor L, Plant JA, Siewers U, Williams L (1998) *FOREGS geo chemical mapping field manual.* Geological Survey of Finland, Guide 47. Geological Survey of Finland, Espoo, pp. 89.

Evidence of microbial activity involved with Neoproterozoic postglacial sediments from the Otavi Group, Namibia: a study of Sturtian oolitic carbonate sandstone with spectroscopic methods

Ildikó Gyollai [,2], Márta Polgári[2], Miklós Veres[3], Szabolcs Nagy[4], Friedrich Popp[5], Dieter Mader[1], Christian Koeberl[1,6]

[1]*Department of Lithospheric Research, University of Vienna, Althanstrasse 14, A-1090, Vienna, Austria;*
[2]*Research Centre for Astronomy and Geosciences, Geobiomineralization and Astrobiological Research Group Institute for Geology and Geochemistry, Hungarian Academy of Sciences, 1112 Budapest, Budaörsi út. 45, Hungary;*
[3]*Research Institute for Solid State Physics and Optics of Hungarian Academy of Sciences, Budapest, Hungary;* [4]*Department of Mineralogy, Geochemistry and Petrology, Szeged University, 6702 Szeged, Egyetem utca 2-6, Hungary;*
[5]*Department of Geodynamics and Sedimentology, University of Vienna, Althanstrasse 14, A-1090, Vienna, Austria;*
[6]*Natural History Museum, Vienna, A-1010, Burgring 7, Vienna, Austria*

Corresponding author: Márta Polgári, e-mail: rodokrozit@gmail.com

Abstract: Basal layers from Sturtian postglacial cap carbonate deposits of the Otavi Group, Namibia were studied using various spectroscopic methods in order to define their paleoenvironmental sedimentary conditions, as well as their presumptive micro-fossil record. Deposition of our sample set occurred in shallow water environments during the aftermath of the Sturtian „Snowball Earth" glaciation. Onion-like growth structures related to ironoxidizing bacteria and cyanobacteria were observed randomly in the interior of ooids and also within micritic matrix material. The Raman spectroscopic detection of various hydrocarbon phases contained in our samples strongly point to bacterial activity involved with sediments allocated to the immediate aftermath of Sturtian „Snowball Earth" glaciations. Backscattered electron imaging and cathodoluminescence microscopy of fine-grained detrital matrix material illustrate a variety of minerals, such as zircon, mica, feldspar, and apatite, all of which indicate detrital input derived from crystalline basement areas. Smectite around the ooids was most probably generated by diagenesis of iron-oxidizing bacterial films.

KEYWORDS: Sturtian glaciation, Neoproterozoic, ooid, oncolite, micro-Raman, cathodoluminescence, microbial record, cyanobacteria, iron-oxidizing bacteria, paleoenvironmental reconstruction

Introduction

Overview

Observational evidence suggests that Planet Earth went through several episodes of global or near-global glaciations during the Late Precambrian Period (Hoffman and Schrag, 2002). The so-called "Snowball Earth" hypothesis states that the Sturtian (~ 750 Ma) and Marinoan (~635 Ma) glaciations were of global extent and may have lasted for several million years (Hoffman et al., 1998). A variation of this hypothesis, called the "Slushball Earth", assumes intermediate conditions without substantial equatorial sea ice (Harland and Rudwick, 1964). While the "Snowball Earth glaciations"

would have ended abruptly in a greenhouse environment, the "Slushball Earth glaciations" ought to be characterized by a slower, gradual deglaciation process (Fairchild and Kennedy, 2007). Concerning the initiation of a global glaciation process a variety of causes have been discussed, including decreased solar luminosity, continental breakup tectonics and the passage of the Solar System through an interstellar cloud (Hoffmann and Schrag, 2002). At this stage, not only the probable cause of the glaciations is unclear, but also the cause and mechanism of deglaciation processes is debated. According to the so-called "Zipper-rift model" (Eyles and Januszczak, 2004) diachronous rifting of the former supercontinent

nent "Rodinia" might have led to a global glaciation, suggesting that some part of the specific diamictites have been formed from turbidity currents. However, our study confirms the existence of distinct ancient areas characterized by specific environmental conditions attended by the Sturtian deglaciation process. Our discovery of fossilized microbial textures is the focus of this study, which attempts to provide evidence of organic material incorporated within these putative microbial remains.

Geological background

Our research area is located in the Neoproterozoic Otavi Group of NW-Namibia. The Otavi Platform formed along the southern fringe of the Congo Craton and abuts on the continental slope facies further South and West (Fig. 1). Thus, the predominantly calcareous sedimentary successions of the unified Otavi Group were generated in a foreland position relative to the areas of the later Kaoko Belt in the West and to the Damara Belt in the South (Hoffman, 2005). The Otavi Group is subdivided into three subgroups, which are separated from each other by two glaciogenic diamictite units, the lower Chuos Formation and the upper Ghaub Formation (Hoffman, 2005; Hoffmann and Schrag, 2002). The cap carbonates succeeding these subunits might have been generated due to CO_2 oversaturation of the seawater (Le Hir et al., 2008; Kennedy et al., 2008) added by the input of methane outgassing from clathrates (Kennedy et al., 2008).
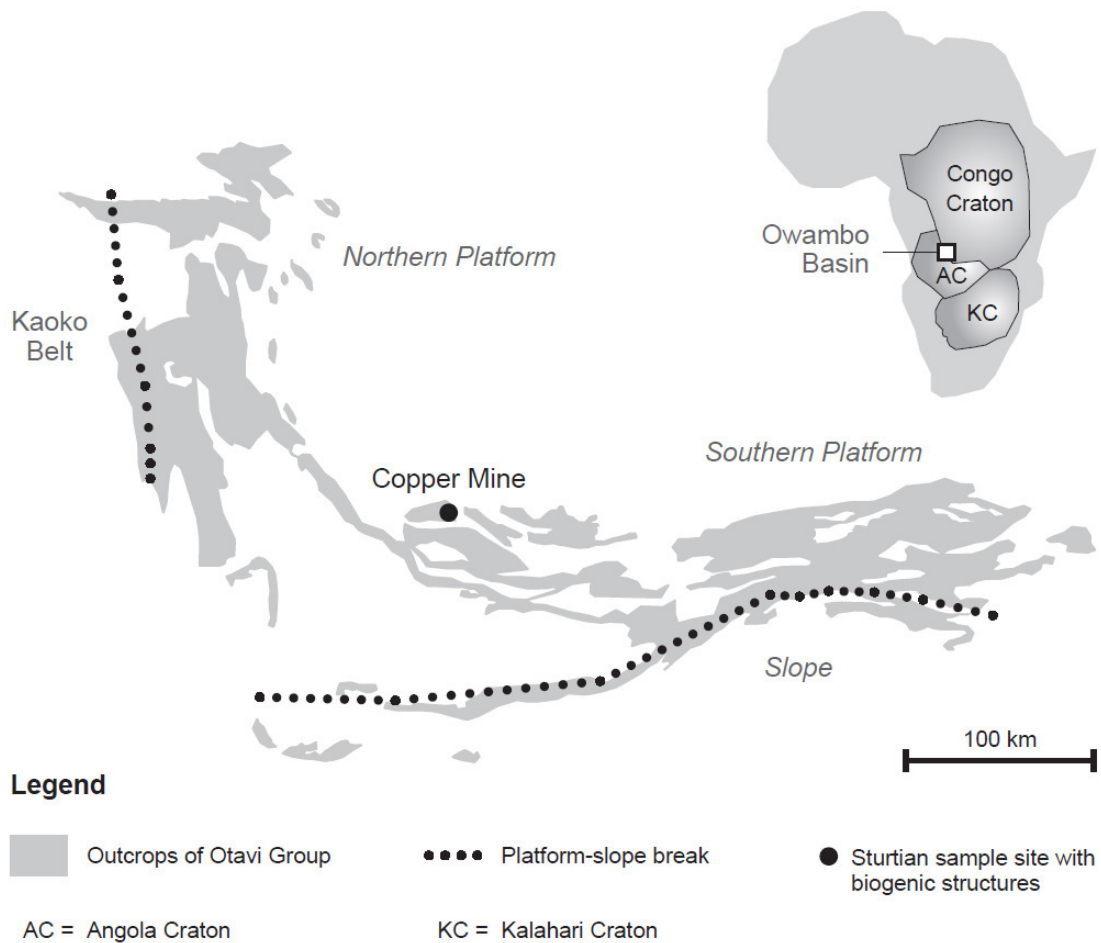

Figure 1: Geological map of the research area showing sampling site (Copper Mine; 9°25'18.43"S; 15° 9'50.90"E)(Modified after Hoffman, 2005).

Samples and methods

One representative oolitic carbonate sandstone sample (C8=basal layer of the Rasthof Fm.), collected from a distinct Otavi platform facies area was studied at the Copper Mine locality (19°25'18.43"S; 15° 9'50.90"E) in NW-Namibia. Macroscopic features show reddish brown- pale red color, grainstone texture with spherical carbonate components, and small quartz pebbles (Fig. 2A). Four ooid components were measured by micro-Raman spectroscopy in order to identify organic material incorporated within observed microbial structures. Pictured in Fig. 2B is a thin section of our Sturtian oolitic grainstone sample that shows the measured points. The first two investigated components were single cored ooids (ooid No. 1 and 2), while the rest have multiple cores (ooid No. 3 and 4).
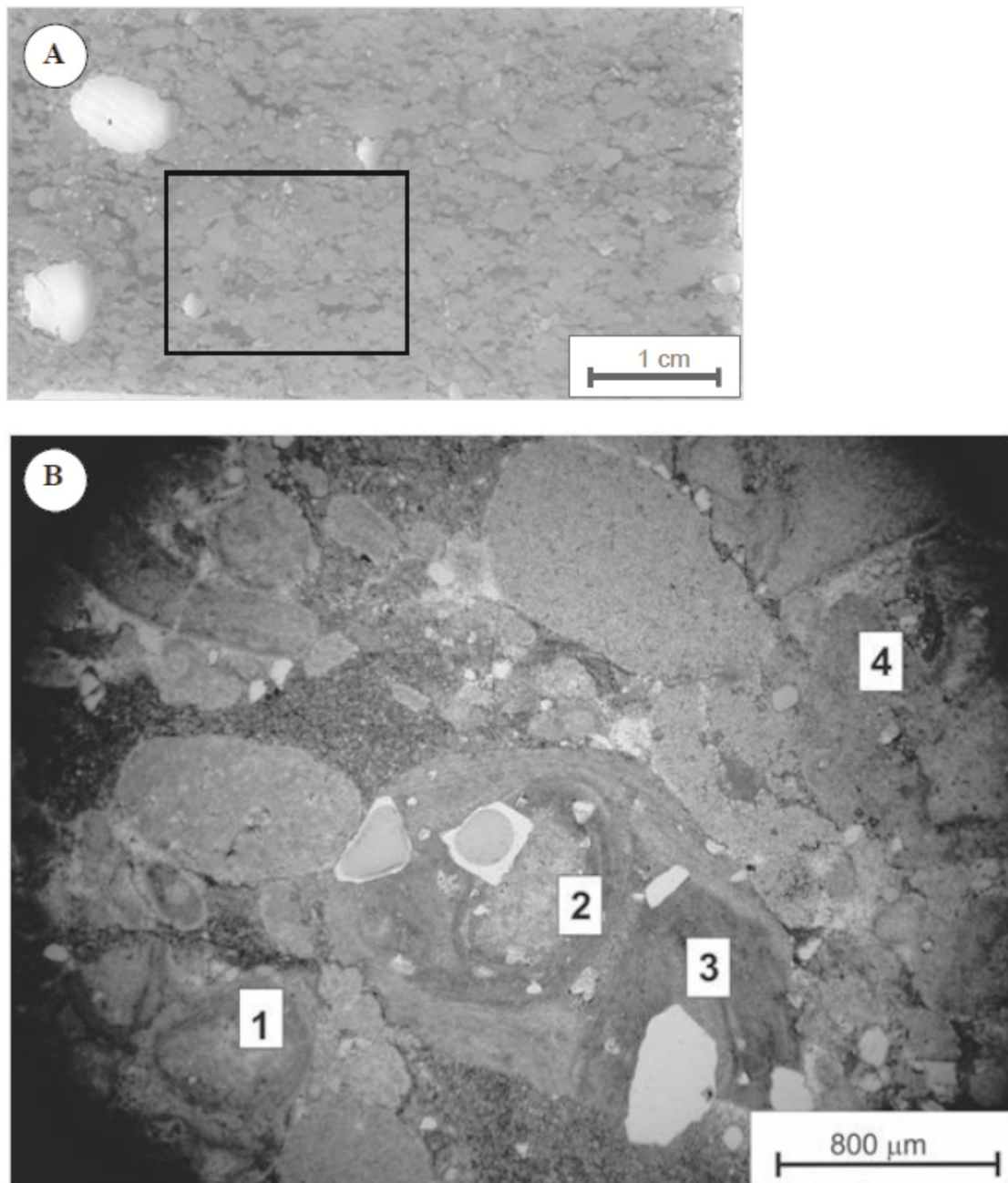
Figure 2: Sturtian oolitic grainstone sample. (A) photo of polished section (area of Raman measuring area – picture B is marked by black rectangle), (B) Raman measuring points signed on thin section ("ooids No. 1, 2, 3, 4"; optical microscopic photo, plain polarized light).

Scanning electron microscopy (SEM) studies were done on a polished thick section of the oolitic sandstone at the Department for Petrology and Geochemistry, Eötvös University, Budapest, Hungary. Chemical and mineral composition and distribution were determined by an Amray 1830 SEM with an EDAX PV9800 energy dispersive spectrometer detector, using 20 kW accelerating voltage, a beam current of 1nA with a defocused spot size of 10–50 nm and a collection time of 100 s.

The mineral assemblages and textures were also characterized by a NIKON ECLIPSE LV100POL optical microscope at University of Vienna and by a NIKON ECLIPSE 600 at the Institute for Geology and Geochemistry, RCAG, Hungarian Academy of Sciences, Budapest.
Raman spectra were recorded with a Renishaw Rm-2000 Raman spectrometer attached to a Leica DM/LM microscope (785 nm, 8mW laser line) at the Research Institute for Solid State Physics and Optics, Budapest.

Optical cathododoluminescence microscopy on a carbon coated polished thin section was performed with a Lumic HC5-LM system at the Department of Lithospheric Research, University of Vienna, using a beam energy of 14 keV and a beam current of ~0.20 mA. Image acquisitions were done with a KAPPA DX 40 C camera system.

Results

Petrography

The studied basal cap carbonate sample (C8) is an oolitic "wackestone" to "packstone" with respect to Dunham`s classification on dominant texture (Dunham, 1962) which formed at winnowed inner platform facies (Fig. 2). Some ooid grains are wrapped with micritic rims generating oncolite sedimentary structures. These oncoids can include one or more cores of different mineralogical composition. In cases of single cored oncoids the composition is micritic,

similarly to the matrix of the oncoid. If the oncoids are multicored their composition consists of detrital minerals, like quartz and mica. Recrystallized quartz lenses also occur among the oncoid´s cores. The micritic matrix contains mica, quartz, and carbonate. A few clasts are bordered/framed with fibrous mica. Quartz grains coated by sericite indicate very low grade metamorphic reactions. Based on microtexture, the dark micritic rims surrounding cores of dolomitic oncoids are assumed to be of bacterial origin (Fig. 2).

Microbial structures

Signs of Fe-oxidizing bacterial activity (FeOB) were observed in sample C8 located at the filamentous rims of the ooids and their onion-shape like internal structures (Fig. 3). Some supposable coccoidal iron oxidizing bacteria (FeOB) colonies are located perpendicularly to the growth rims of the ooids, being indicative of septum structures. These phenomena indicate that the putative FeOB colonies expanded upon ooid surfaces, and were repeatedly buried by following generations of carbonate films created by metabolism of calcimicrobae and cyanobacteria (Fig 4). Growth sequences of the observed FeOB colonies start randomly onto micritic carbonate nuclei then advancing towards their inner part. Compared to these carbonate nuclei quartz grains often offer a better preservation of this aspect (Fig. 4). Our samples exhibit mainly coccoidal colonies of FeOB. In general, the observed FeO colonies apparently developed in symbiosis of cyanobacteria and calcimicrobae with diatom-like microorganisms characterized by similar shape and SiO_2-bearing frustules incorporated in quartz.

Chemical composition and mineralogy - backscattered electron imaging

The bulk mineral composition of C8 oolitic packstone is 84 wt.% carbonate, 15 wt.% mica, 5 wt.% quartz and K-feldspar, and 1 wt.% hematite, as determined by optical microscopy.
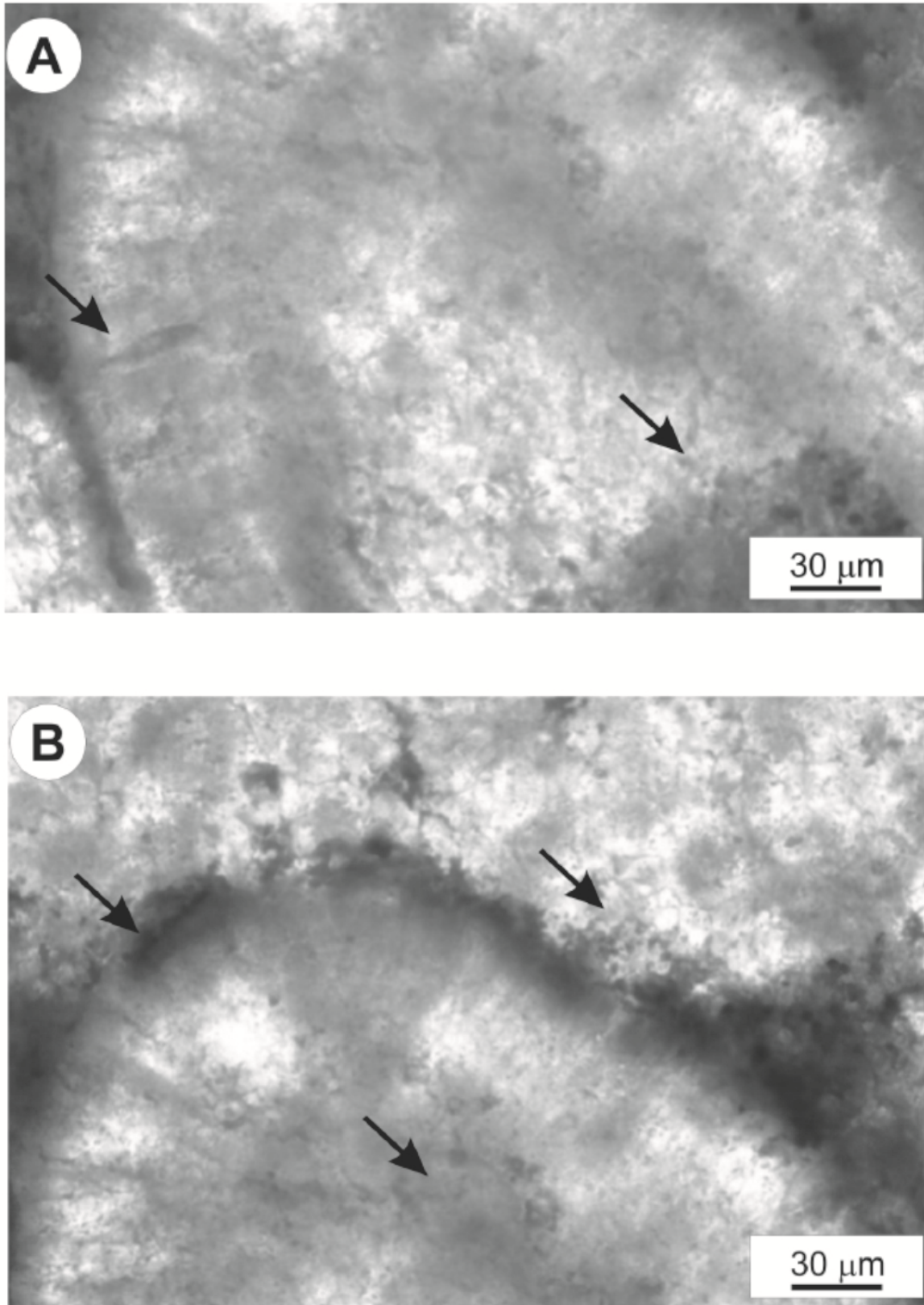
Figure 3: FeOB colonies on the surface of ooids and inside along of growth of ooids (in symbiosis with cyano-bacteria and calcimicrobae (shown by arrows). (A) FeOB colonies perpendicularly growth inside ooids, (B) FeOB colonies on surface of ooid.
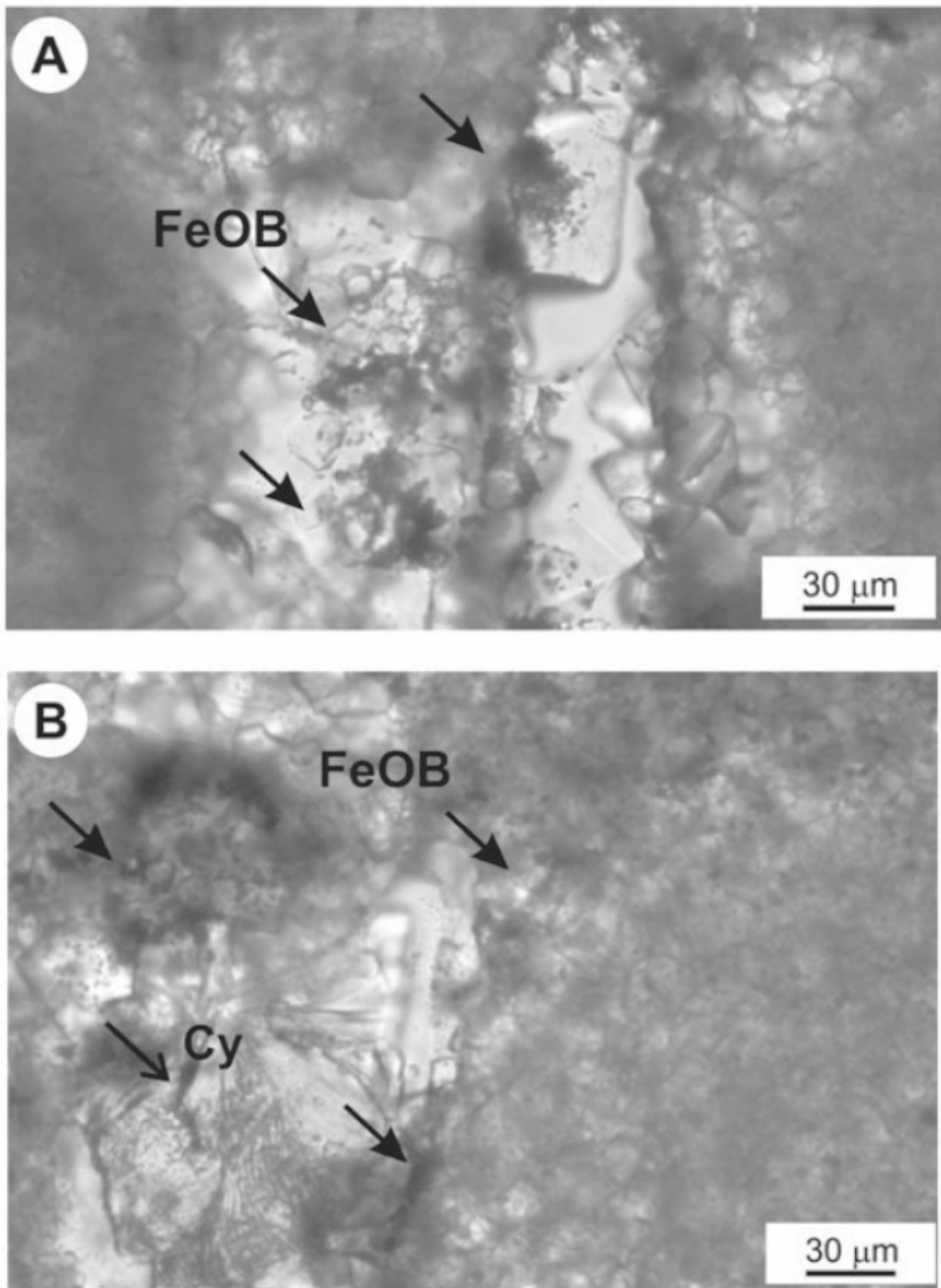
Figure 4: FeOB colonies on the surface of quartz pebbles (A) and in symbiosis with oscillatorian cyanobacteria (Cy) (B) (shown by arrows).

The analyzed ooids No. 1 and 2 have a single dolomite-core, the multi-cored ooid No. 3 consists of dolomite and microcline, and ooid No. 4 has a core of dolomite and quartz. According to SEM-EDS data and back-scattered electron (BSE) images, an analyzed 3 mm sized quartz of the oolitic packstone is surrounded by a rim of fine-grained kaolinite-barite-apatite mineral assemblage. This quartz grain is crossed by a diagenetic barite vein. The micritic ooids are usually surrounded by a smectite rim, which may contain galenite grains (Fig. 5).
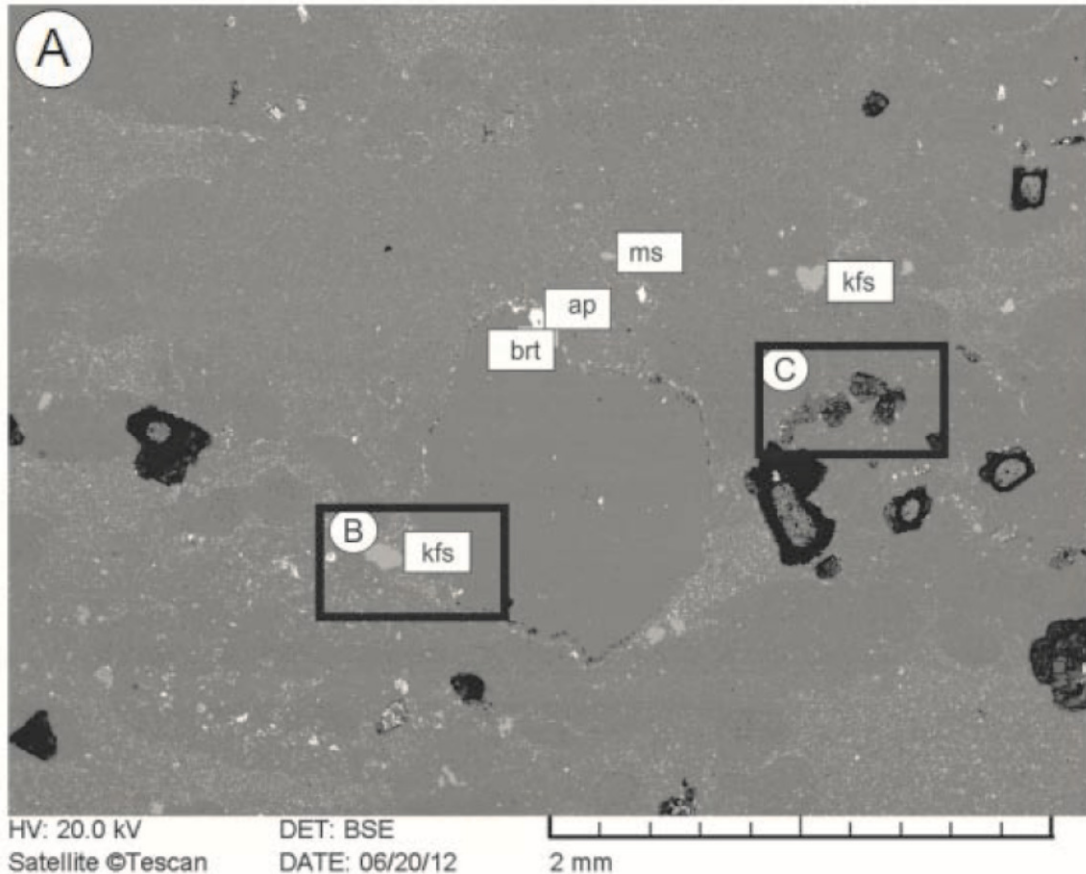
Figure 5: Backscattered electron image of an ooid in C8 Sturtian oolitic packstone-wackestone (A); (B) rim of quartz pebble; (C) smectite rim around ooid (Legend: brt=barite, smect= smectite, gal=galenite, kfs=K-feldspar, dol=dolomite, q=quartz, ap=apatite, ms=muscovite (B, C pictures are focused area of picture A, which are marked by black rectangle).

Textural characteristics by cathodoluminescence studies

The investigated ooid components show zoned luminescence (bright red zones in dull red material; Fig. 6). Several detrital mineral components can be observed inside the oncoid structure (blue luminescent quartz and feldspar). In general, the carbonate material between oolites has a brighter red luminescent color than the oolites themselves. Bright red luminescent clasts and small grained oolite components with bright red rim occur between larger oolite components (Fig. 7).

Raman spectroscopy

The points in our Sturtian oolitic grainstone ("ooid No. 1, 2, 3, 4") thin section that have been measured by Raman spectroscopy are shown in Fig. 2B, and the corresponding Raman vibration data are listed in Table 1.
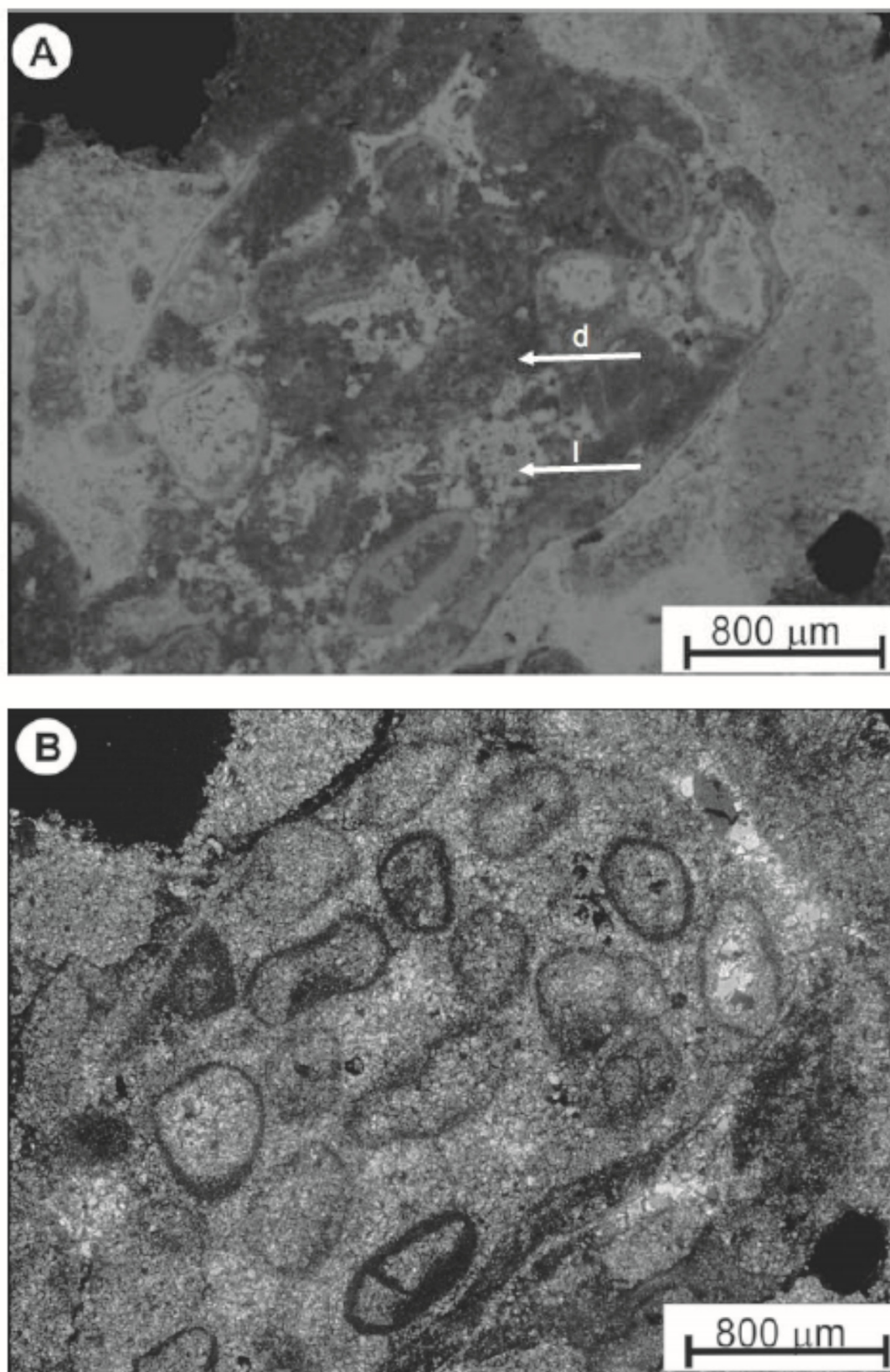
Figure 6: Multicore-oncoid where the core is surrounded by fine-grained material (bacterial film). Inside and between the cores, light-luminescent cements are observed (l-arrow), which are filled with small grained oolite components. The dull luminescent part (d-arrow) is built up from/by clayey and carbonaceous material. (A) cathodoluminescent light, (B) plain polarized light.
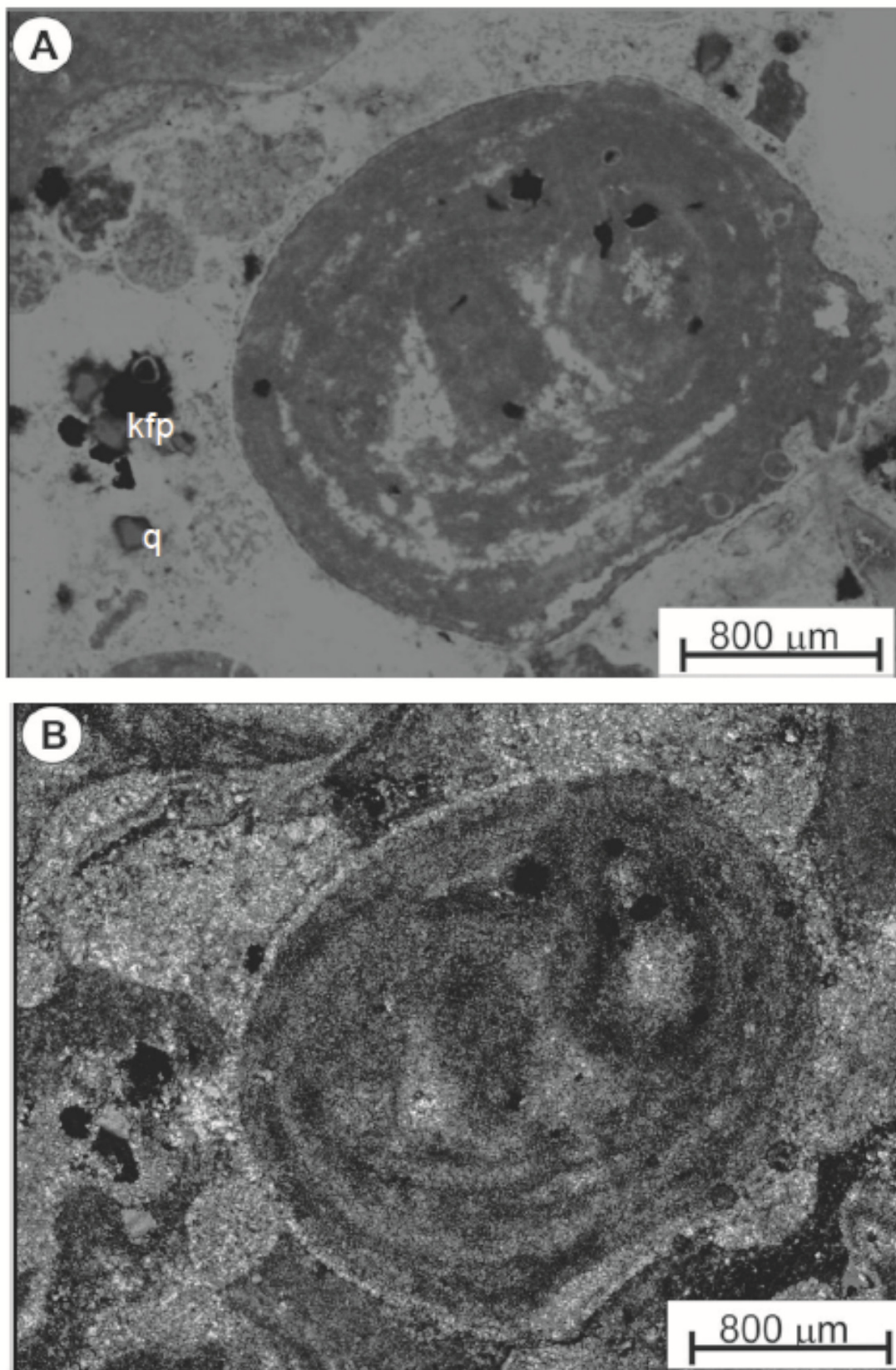
Figure 7: Ooids with growth rims, with brighter luminescent color. The middle luminescent grains are quartz (q) and feldspars (kfp) detrital grains (A) cathodoluminescent light, (B) plain polarized light.
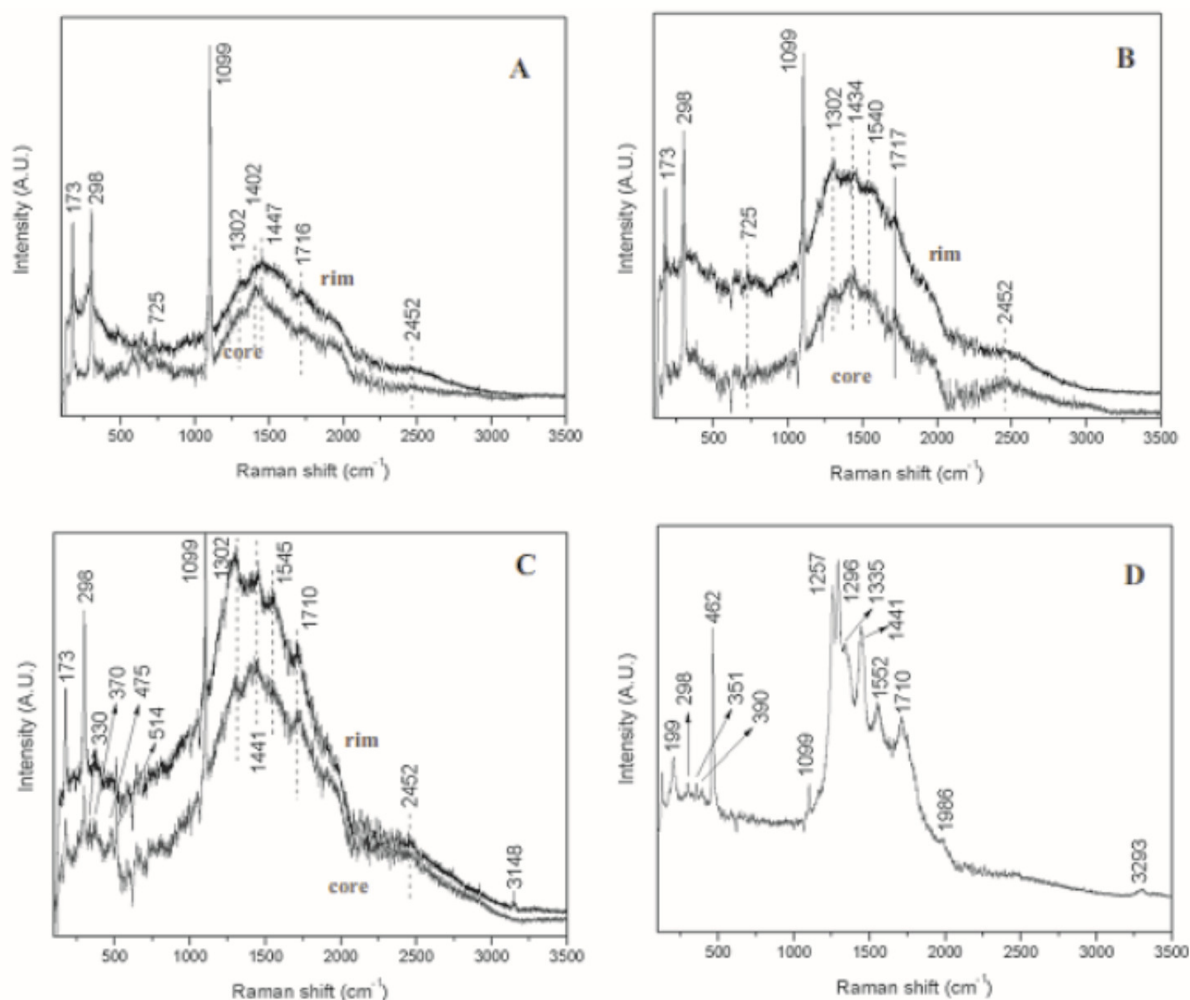
Ooid No. 1:

The spectra are dominated by the narrow bands of dolomite at 178, 300, 723, and 1097 cm^{-1} (Lewis and Edwards, 2001). Another remarkable feature of the spectra is the broad band in the 1000-2000 cm^{-1} region, which can be attributed to sp2 C=C bonds (up to 1650 cm^{-1}) and different carbonyl and cumulated double bonds of the amorphous carbon phase with some oxygen content. Other observable peaks at 1300 and 1450 cm^{-1} correspond to deformation vibrations of CH$_2$ and CH$_3$ groups, while the peak at 1402 belongs to asymmetric vibration of CH$_2$ and CH$_3$ groups. The peak of the carbonyl group can be detected at 1716 cm^{-1} (Fig. 8A; Table 1A).

Ooid No. 2:

The dolomite peaks appear at 173 cm^{-1} 298 cm^{-1}, 725 cm^{-1} and 1099 cm^{-1}, respectively. A broad band related to an amorphous carbon phase can be seen in the 1000-2000 cm^{-1} region. Narrow peaks at 1302 and 1402 cm^{-1} correspond to vibrations of CH$_2$ and CH$_3$ groups. The stretching vibration of the carbonyl group appears at 1717 cm^{-1} (Fig. 8B, Table 1B).

Figure 8: Raman spectra of ooid No. 1-4 (for measuring site see Fig. 2B, vibrations are listed in Table 1). (A) ooid No. 1, (B) ooid No. 2., (C) ooid No. 3, (D) ooid No. 4. Spectra in ooid No.1-3 were measured in core and rim region).

<u>*Ooid No. 3*</u>:

The peaks of dolomite appear at 173 cm^{-1}, 298 cm^{-1} and 1099 cm^{-1}, respectively. The peak at 724 cm^{-1} is of low intensity because of the polarization effect. The K-feldspar (microcline) shows minor peaks at 330 cm^{-1}, 364 cm^{-1}, and strong vibration of Si-O-Si/Si-O-Al bridges at 475 cm^{-1}, whereas the most characteristic Raman vibration is centered at 513 cm^{-1} concerning O symmetric motion in Si-O-Si bridges. The broad amorphous carbon band again appears in the 1000-2000 cm^{-1} region. Some narrow CH_2 and CH_3 vibrations can be detected at 1302 and 1441 cm^{-1}, together with the peak of C=O stretching vibration at 1710 cm^{-1} (Fig. 8C, Table 1C).

<u>*Ooid No. 4*</u>:

The peaks of dolomite appear at 299 cm^{-1} and 1099 cm^{-1}. The peak at 178 cm^{-1} overlaps with the band at 199 cm^{-1}, while the one at 724 cm^{-1} is affected by the polarization effect. The peaks of quartz appear at 199 cm^{-1}, 351 cm^{-1}, 390 cm^{-1} and 462 cm^{-1}. The vibrations of CH_3 and CH_2 groups are centered at 1296 cm^{-1}, 1335 cm^{-1} and 1441cm^{-1}. The C=O stretching vibration is at 1710 cm^{-1}, and a new peak can also be detected that can be attributed to some structural units with cumulated double or triple bonds. Amorphous carbon in the sample causes the broad band in the 1000-2000 cm^{-1} region (Fig. 8D, Table 1D).

Standard of dolomite	Hydrocarbon	Ooid 1core	Ooid 1rim
178 Eg** T(Ca, Mg, CO3)		73 (Dol)	173 (Dol)
300 Eg (T(Ca, Mg, CO3)		298 (Dol)	298 (Dol)
723 Eg v4 symmetric CO3 723 EG v4 symmetric CO3 Deformation		725 (Dol)	725 (Dol)
1097 Ag*** v1 symmetric C 1099 1099 Stretching	v v1 symmetric CO3	(Dol)	(Dol)
	1300 CH3-CH2 transverse vibrations of H atoms	1302	1302
	1400 assym. vibrations of CH3 and CH2 groups	1402	
1450 Eg v3 asymmetric CO3	1450 CH2 bend	1447	1447
	1710 C=O stretch	1716 1	716
	2450 graphite (minor peak)	2452	2452

Table 1A: Mineral and hydrocarbon phases with Raman vibrations in four ooids (1A: spectra of ooid No. 1)

Standard of dolomite RUFF Database	Hydrocorbon	Ooid 2 core	Ooid 2 rim
178 Eg T(Ca, Mg, CO3)		173 (Dol)	173 (Dol)
300 Eg (T(Ca, Mg, CO3)		298 (Dol)	298 (Dol)
723 Eg v4 symmetric CO3 deformation		725 (Dol)	725 (Dol)
723 Eg v4 symmetric CO3 deformation		1099 (Dol)	71099 (Dol)
1097 Ag v1 symmetric CO3 stretching	1300 CH3 and CH2 asym. vibr.	1302	1302
	1430-1450 sp2 C=C CH2 and CH3 group	1434	1434
1440 Eg v3 asymmetric	1532 COOH, 1500-1550 sp2 C	1540	1540
CO3 stretching	sp2 C		
	1710 C=O stretch	1717	1717
	2450 graphite (minor peak)	2452	2452

Table 1B: Mineral and hydrocarbon phases with Raman vibrations in four ooids (1B: spectra of ooid No. 2)

Discussion

The Raman spectroscopy is a powerful method to identify organic material as bio-marker of microbial structures. Precambrian microfossils were studied using this method by a number of research groups (Kudryavtsev et al., 2001; Kempe et al., 2005; Marshall et al., 2005). The aromatic ring deformation and symmetric breathing is attributed in the 1200-1400 cm^{-1} range (Mapelli et al., 1999). The peaks of organic material in Precambrian microfossils (e.g., acritarchs) occur around 1600 cm^{-1}, and there is a group of bands at 1300-1350 cm^{-1}, with broad peaks belonging to kerogen - aromatic (sp2) bonded C atoms joined together with peripheral sp2 and sp3-bonded hydro-carbons (Kempe et al., 2005). A variety of peaks of apparent C=C aromatic stretching bands at 1600 cm^{-1}, CH$_3$ terminal groups

(1345 cm^{-1}), C-H aliphatic stretching (3000-2700 cm^{-1}), and C=O vibration (1710 cm^{-1}) occur in the hydrocarbon phase (Marshall et al., 2005). In our samples the peak around 1710 cm^{-1}, related to the carbonyl group, is observed in all the measured ooids, which is similar to the published data of Marshall et al. (2005), while the other reported Raman shifts join the region occupied by the broad band of hydrogenated amorphous carbon phases, the large width of which is caused by the highly disordered character of the sample. This is a remarkable difference compared to the published data mentioned above. In spite of this, some characteristic CH vibrations were observed in form of narrow peaks in the 1300-1450 cm^{-1} region of our spectra (Fig. 8).

In general, the Raman spectrum of amorphous carbons consists of a broad band in the 1000-1800 cm^{-1} region (Dresselhaus and Dresselhaus, 1982; Ferrari and Robertson, 2000; Veres et al., 2006). For visible and near-infrared excitations it is dominated by the characteristic peaks of sp2 carbon atoms, since due to resonant processes the Raman scattering on these structural units is a few orders of magnitude higher than that on building blocks consisting of sp3 C atoms. The broad band is resulting from superposition of scattering contributions from different structural units and can be divided into several regions. For near infrared excitation used in this study, peaks between 1100-1200 cm^{-1} and 1400-1500 cm^{-1} correspond to vibrations of sp2 carbon chains (observed mainly in hydrogenated samples), between 1200-1350 cm^{-1} – to breathing vibrations of sp2 carbon rings (this is the so called D band) and above 1570 cm^{-1} – to stretching vibrations of sp2 carbon atoms in rings (the so called G band) (Veres et al., 2006). Features of the broad band observed in our spectra suggest that the amorphous carbon phase in the sample is dominated by sp2 (hydro) carbon chains, with relatively minor (graphitic) sp2 C ring content (Table 1). This is supported by the narrow peaks assigned to different vibrations of CH$_2$ and CH$_3$ groups. Components of the broad band in the >1650

cm^{-1} region, together with the carbonyl peak indicate the presence of oxygen in the amorphous carbon structure.

Comparing the broad amorphous carbon bands, ooid No. 2 and 3 have quite a similar structure, with somewhat higher graphitic content compared to ooid No. 1 (indicated by the higher intensities in the D and G band regions) (Fig 8A-C, Table 1 A-C). In ooid No. 1 and 2 the narrow hydrocarbon peaks are less intense (Fig 8A-B). These peaks have the highest intensity in the spectrum of ooid No. 4, where the C=O shows also the most pronounced vibration (Fig. 8D, Table 1D).

The observed features of amorphous carbon phases are similar to those found in cryptocrystalline silica varieties with traces of Miocene hydrothermal biomineralization (Müller et al., 2009) and indicate the organic, probably microbial origin of the amorphous carbon phases identified in the sample. Apart from organic matter, mineral components (dolomite, hematite, quartz, feldspar) were also identified by Raman spectroscopy.

The first peak of dolomite (178 cm^{-1}) shifted to 5 cm^{-1} wave number, and this was overlapped by the quartz band in the spectrum of ooid No. 4 (Table 1D). In ooids No. 3 and No. 4 the 723 cm^{-1} peak did not appear in the spectra, which is due to a polarization effect (Fig 8C-D, Table 1C-D.). Due to diagenesis and weathering the material was dolomitized and hematitized. A dolomitization process means infiltration of Mg-rich pore water, which changes original microbial carbonate (aragonite, calcite) to dolomite during the diagenesis. Hematite was probably formed by transformation of primary ferrihydrite originated via Fe-oxidizing bacterial activity (Konhauser, 1998). Alternatively, the hematite could be derived by continental weathering (iron-rich matrix) (Hoffman et al., 1998). The smectites around the ooids are derived most probably by diagenesis and/or weathering of microbial structures, whereas galenite formed in a biomineralization process (Erlich, 2010).

Dolomite	Microcline	Hydrocarbon	Ooid 3 core	Ooid 3 rim
178 Eg T(Ca, Mg, CO3)			173 (Dol)	173 (Dol)
300 Eg (T(Ca, Mg, CO3)			298 (Dol)	298 (Dol)
	330		330 (mcl)	330 (mcl)
	364		370 (mcl)	370 (mcl)
	475 s Si-O-Si/Si-O-Al		475 (mcl)	475 (mcl)
	513 vs (A.g.)		514 (mcl)	514 (mcl)
723 Eg ν4 symmetric CO3 deformation				
1097 Ag ν1 symmetric CO3 stretching			1099 (Dol)	1099 (Dol)
		1300 asymmetric vibrations of CH3 and CH2 group	1302	1302
1440 Eg ν3 asymmetric CO3 stretching		1450 CH2 bend	1441	1441
		1532-1550 COOH	1545	1545
		1710 C-O stretch	1710	1710
		2450 graphite (minor peak)	2452	2452
		2900-3300 CH stretching vibration		3148

Table 1C: Mineral and hydrocarbon phases with Raman vibrations in four ooids (1C: spectra of ooid No. 3)

Conclusions

A representative sample (C8) was analyzed for its organic geochemistry and mineral composition as well as for its textural characteristics. The presence of amorphous carbon was demonstrated in all of the measured points of the sample. Traces of hydrocarbons and C=O groups were detected, featuring highest concentrations in the dolomite-quartz matrix. Ooid 1 and 2 hold light hydrocarbon (with low C number) of the methyl group, whereas ooid 4 contains a more complex hydrocarbon, similar to butane.

We consider the hydrocarbons detected in our samples (C8) to originate from bacterial (probably cyanobacteria) communities which existed in shallow water environments

of the ancient Otavi platform. Smectite surrounding the ooid grains is most probably derived from diagenesis and/or weathering of microbial films. Numerous peaks attributed to the methyl group might indicate a contribution from methane outgassing and thus indicate the role of rapid global warming after Neoproterozoic "Snowball Earth" glaciations.

Standard quartz (Raman) shift) in cm-1)	Standard of dolomite RUFF Datebase	Hydrocarbon	Ooid 4
	178 Eg T(Ca, Mg, CO3)		
203			199 (Q)
	300 Eg (T(Ca, Mg, CO3)		298 (Dol)
353			351 (Q)
393.5			390 (Q)
461 vs			462 (Q)
	723 Eg v4 symmetric CO3 deformation		
	1097 Ag v1 symmetric CO3 stretching		1099 (Dol)
		1000-1275 C-O stretching	1257
		1300 asymmetric vibration of CH_2-CH_3 group	1296
		1335 amorphous carbon	1335
		1450 CH_2 bend	1441
		1532-1550 COOH	1552
		C=O stretch	1710
		2000 sp2 C	1986
		3300 C-H stretching of butane	3293

[*] Except No. 4, all of ooid specimens were measured at rim and in core. Mineral standards were taken from RUFF database. Hydrocarbon vibrations were interpreted following Kudryavtsev et al. (2001); Kempe et al. (2005); Marshall et al. (2005); Veres et al. (2006). Raman shifts are added in cm^{-1}. For measuring site see Fig. 2B, for spectra see Fig. 8A-D.

[**] Eg: marks minor vibrations in Raman spectrum.

[***] Ag: defines major vibration, which is most characteristic vibration for adjacent phase in Raman spectrum.

Table 1D: Mineral and hydrocarbon phases with Raman vibrations in four ooids (1D: spectra of ooid No. 4)

Acknowledgements

References

Dunham, R.J., 1962: Classification of carbonate rocks according to depositional texture.- In Ham, W.E. (ed.): Classification of carbonate rocks.- Amer. Assoc. Petrol. Geol. Memoir, **1**: 108 – 121.

Dresselhaus, M.S. and Dresselhaus, G. 1982. Light scattering in graphite intercalation compounds. *Light Scattering in Solids III, Top. App. Phys.*, **51**, 3-57.

Erlich, H. 2010. Biominerals. In: Erlich, H. *Biological Materials of Marine Origin - Biologically-Inspired Systems*, **1**, 25-50.

Eyles, N. and Januszczak, N. 2004. 'Zipper-rift': a tectonic model for Neoproterozoic glaciations during the breakup of Rodinia after 750 Ma. Earth-Sci. Rev., 65, 1-73.

Fairchild, I.J. and Kennedy, M.J. 2007. Neoproterozoic glaciation in the Earth system. *J. Geol. Soc. London*, **164**, 895-921.

Ferrari, A.C. and Robertson, J. 2000. Interpretation of Raman spectra of disordered and amorphous carbon. *Phys. Rev. B*, **61**, 14095–14107.

Harland, W.B. and Rudwick, M.J.S. 1964. The great Infra-Cambrian glaciation. *Scientific American* **211**, 28-36.

Hoffman, P.F. 2005. 28th DeBeers Alex Du Toit Memorial Lecture (2004): On Cryogenian (Neoproterozoic) ice-sheet dynamics and the limitations of the glacial sedimentary record. *S. Afr. J. Geol.*, **108**, 557-576.

Hoffman P.F. and Schrag D.P. 2002. The Snowball Earth hypothesis: testing the limits of global change. *Terra Nova,* **14**, 129-155.

Hoffman, P.F.; Kaufman, A.J.; Halverson, G.P. and Schrag, D.P. 1998. A Neoproterozoic snowball Earth. *Science*, **281**, 1342-1346.

Kempe, A.; Wirth, R.; Altermann, W.; Stark, R.W.; Schopf, J.W. and Heck, W.M. 2005. Focussed ion beam preparation and in situ nanoscopic study of Precambrian acritarchs.- *Precambrian Res.*, **140**, 36–54.

Kennedy, M.; Mrofka, D. and von der Borch, C. 2008. Snowball Earth termination by destabilization of equatorial permafrost methane clathrate. *Nature*, **453**, 642-645.

Konhauser, K.O. 1998. Diversity of bacterial iron mineralization. *Earth-Sci. Rev.,* **43/ 3–4**, 91-121.

Kudryavtsev, A.B.; Schopf, J.W.; Agresty, D.G. and Wdowiak T.J. 2001. In situ laser-Raman imagery of Precambrian microscopic fossils. *PNAS*, **98/ 3**, 823–826.

Le Hir, G.; Donnadieu, Y.; Godderis ,Y.; Pierrehumbert, R. T.; Halverson, G. P.; Macouin , M.; Nedelec, A.; and Ramstein, G. 2008. The snowball Earth aftermath: Exploring the limits of continental weathering processes. *Earth Planet. Sci. Lett.*, **277**, 453-463.

Lewis, I.R. and Edwards, H. 2001. *Handbook of Raman Spectroscopy: From the Research Laboratory to the Process Line.* Taylor and Francis, 1072 pp.

Mapelli, C.; Castiglioni, C.; Zerbi, G. and Mullen, K. 1999. Common force field for graphite and polycyclic aromatic hydrocarbons. *Phys. Rev.* **B60**, 12710–12725.

Marshall, C.P.; Javaux, E.J.; Knoll, A.H. and Walter, A.M. 2005. Combined micro-Fourier transform infrared (FTIR) spectroscopy and micro-Raman spectroscopy of Proterozoic acritarchs: A new approach to palaeobiology. *Precambrian Res.*, **138**, 208–224.

Müller, A.; Polgári, M.; Gucsik, A.; Nagy, Sz.; Veres, M.; Pál-Molnár, E.; Götze, J.; Cserháti, C.; Németh, T. and Hámor-Vidó, M. 2009. Cathodoluminescent features and Raman spectroscopy of Miocene hydrothermal biomineralization embedded in cryptocrystalline silica varieties, Central Europe, Hungary. Abstract

volume, Conference on Micro Raman Spectroscopy and Luminescence Studies in the Earth and Planetary Sciences, *AIP Proceedings CP1163, Micro-Raman Spectroscopy and Luminescence Studies in the Earth and Planetary Sciences* (Gucsik A. (ed)., p. 207-218.

Veres, M.; Tóth, S. and Koós, M. 2006. New aspects of Raman scattering in carbon-based amorphous materials. Diamond and Related Materials, **17**, 1692-1696.

Note on the fossil fauna and flora in tufa at Ongongo Springs, Damaraland, Namibia

H. Mocke

Geological Survey of Namibia, National Earth Science Museum, 1 Aviation Road, Private Bag 13297, Windhoek
e-mail: hmocke@mme.gov.na

Knowledge of Quaternary fossils in Namibia is poor, although several sites were identified by Hermann Korn and Henno Martin (Korn and Martin, 1937). The Ongongo Springs in Western Namibia are associated with thick layers of tufa (freshwater carbonate) containing a rich collection of impressions of macroscopic fossil plant leaves, roots, branches and trunks. The leaf impressions show mostly primary venation, making their identification difficult. The absence of organic material within the preserved leaves, roots, stems and trunks renders C14 dating impossible. Dating of tufas has been attempted in the past, but the results are not reliable as contaminations easily occur, due to their porous nature.

At Ongongo a possible sedge leaf was noted as were impressions of the leaves of sycamore fig, *Ficus sycomorus* (Family Moraceae) and mopane, *Colophospermum mopane* (Family Fabaceae). However, no fruits or seeds were found. To date only a single vertebrate fossil has been reported by a visitor to the springs. It was suggested to be the impression of a frog skeleton. Land snails were observed in the tufas and surrounding calcretes and are comparable to the modern genus *Sculptaria*.

Introduction

Ongongo Springs is located at S 19° 08′25.3′′ E 13° 49′09.5′′ ca. 30 km south of the village of Sesfontein in Damaraland and close to another spring and small community settlement called Warmquelle (*German: Hot Spring*), which is located about 45 km south of the Ongongo Springs camp.

It is currently run as a communal camp site by the local inhabitants, and has become an attractive tourist destination.

Travertine is the most common spring deposit, with tufa being a porous variety of travertine. Both consist of $CaCO_3$ and tend to have a creamy to off-white colour. Such spring deposits form by the precipitation of mineral matter dissolved in waters of hot or cold springs which emerge from permeable rocks or from weak zones in the earth's crust, such as faults, fissures and fractures. At the Ongongo site the predominant component of the spring deposit is tufa (Fig. 1).

Upon closer inspection of the tufas at Ongongo, impressions of leaves, casts of twigs and branches, and moulds of molluscs and possibly the bone impressions of a frog could be seen. The organic matter is not preserved however. Due to the porous nature of tufa there are constant additions from the surrounding environment and hence much contamination, making dating unreliable. Dating has been attempted on tufa deposits in the Namib Naukluft without success (pers. comm. Dr A Stone). The tufa may be Quaternary in age, since the leaf impressions identified in the tufa are those of still resident plant species in the area, like the sycamore fig, *Ficus sycomorus* (Family Moraceae) and mopane, *Colophospermum mopane* (Family Fabaceae).

In Namibia there are several sites preserving tufa (Fig. 2), but our knowledge about them and the fossils they preserve is poor. Hermann Korn and Henno Martin (1937, 1955) recorded several sites in Namibia, including a 5m-high hill of fossil tufa on Farm Doornkom 173, 65km SSE of Otjiwarongo, with casts of reeds. They reported a similar deposit on Farm Sukses 133 West of Maltahöhe. Tufa from Farm Blässkranz, hosted calcified casts of the reed, *Phragmites australis*, as well as other plant varieties. Near Outjo, spring waters calcified a honeycomb, estimated to be 1 million years old and at Bushman Hill spring waters petrified filamentous algae, estimated to be 10 000 years old. Miller (2008) reported both ac-

tively forming and fossil tufas at the Naukluft Mountains, where calcified plant remains and fresh-water crabs, *Potamonautes perlatus*, have been found. Ward (1987) recorded 17 tufa deposits along the edge of the lower Kuiseb River canyon section, on tributary valley walls and areas where water seeps occur. Ward named these deposits the Hudaob Tufa Formation. Another tufa deposit has been noted at Ruacana (pers. comm. Dr M Pickford).
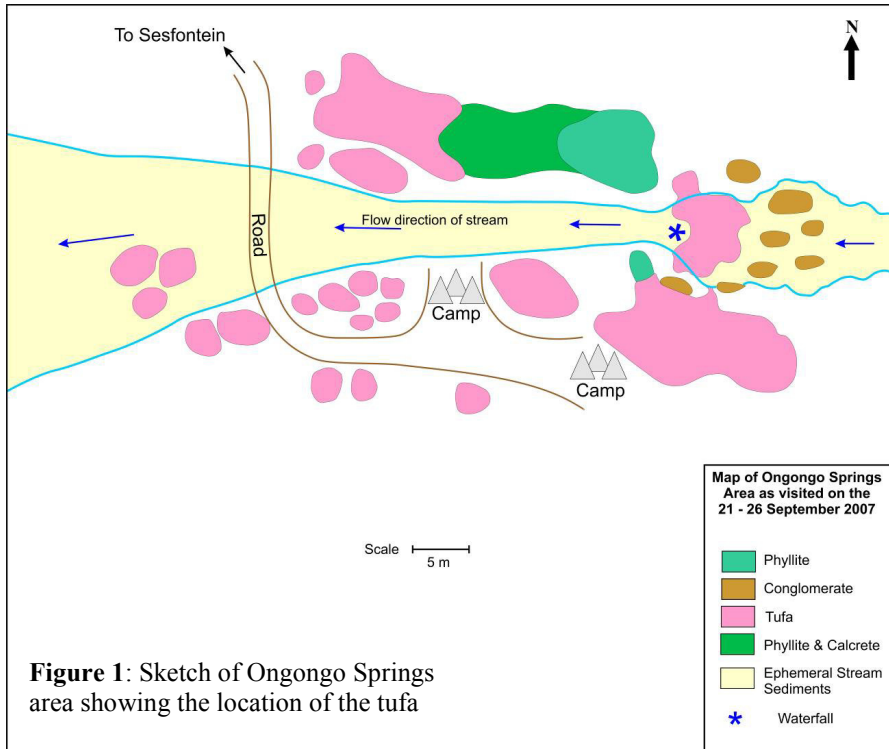
Figure 1: Sketch of Ongongo Springs area showing the location of the tufa
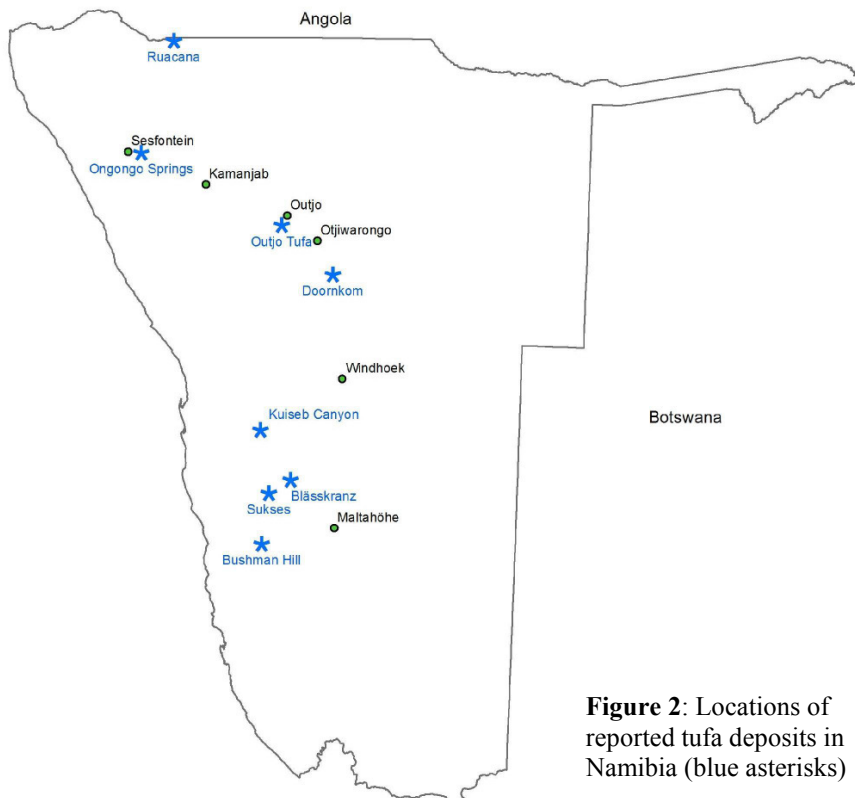
Figure 2: Locations of reported tufa deposits in Namibia (blue asterisks)

Geological setting

The geology of the Ongongo area consists of phyllites and conglomerates of the late Neo-proterozoic Sesfontein Formation (Mulden Group, Damara Supergroup) overlain by surficial sediments. At the site of the springs huge boulders of tufa are present within a narrow river cut through the conglomerates of the Warmquelle Member and the grey, pearly phyllites of the Sesfontein Formation (Fig. 3).
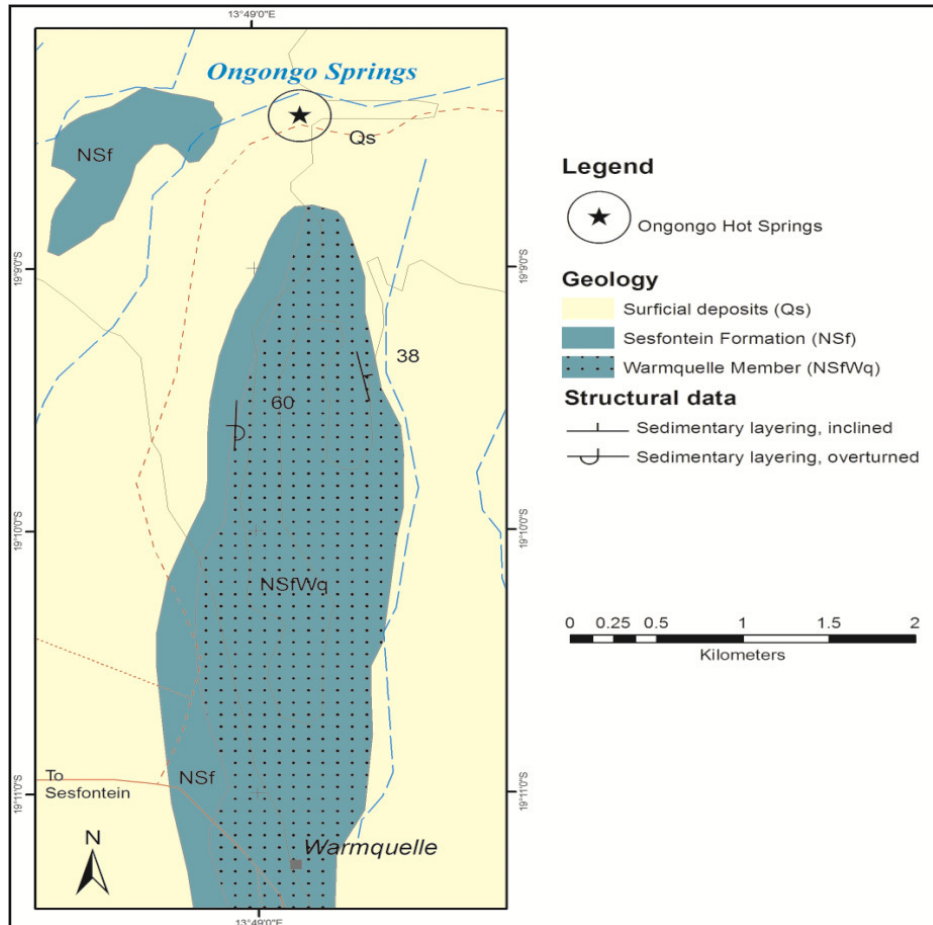

Figure 3: Regional Geology of the Ongongo Springs area

Preservation and description of material

Flora

Leaf impressions were noted within the Ongongo tufas. Roots, trunks and stems were infilled with tufa and form the predominant component of the preserved material.

Comparison of well-preserved leaf specimens with extant plant leaves growing in the area, indicate that the venation characters are particularly similar to sycamore fig and mopane trees. However, carbonaceous material was not preserved and all material was layered randomly with no indication of flow direction.

Ficus sycomorus (Family Moraceae)

Figure 4: Description of material

The apex of the leaf was not preserved. The mid rib and lateral veins are conspicuous with a deep depression where the petiole would have inserted into the base of the leaf blade. The preserved leaf margin is slightly lobate. The base of the leaf blade is slightly heart-shaped. The preserved specimen is comparable in dimensions to that of the extant sycamore fig leaf (Fig. 5), and is com-

Figure 4: Impression of leaf resembling wild fig (scale in cm)

Figure 5: Extant wild fig growing in the Ongongo area (scale in cm)

Colophospermum mopane
(Family Fabaceae)

Figure 6: Description of material
Only the central part of a single leaflet, part of a bi-foliate leaf is preserved. The radiating veins are well preserved and are comparable to those seen in extant species of mopane (Fig. 7) still growing in the vicinity. Other, better preserved specimen were noted during low light situations but were inaccessible for sampling.

Figure 6: Impression of part of a leaflet with radiating veins (scale in cm)

Figure 7: Extant mopane leaf (scale in cm)

?Sedge (Family Cyperaceae)

Figure 8: Description of material

Part of a sedge leaf was preserved with clearly visible parallel veins. Unfortunately no seeds were found, which would have helped with the definite identification of the species. Sedges, such as the one illustrated in figure 9, are growing profusely along the run-off of the spring's area.

Figure 8: Impression of sedge leaf with parallel veins (scale in cm)

Figure 9: Extant sedge living in river course (scale in cm)

Fauna

Sculptaria, terrestrial snail
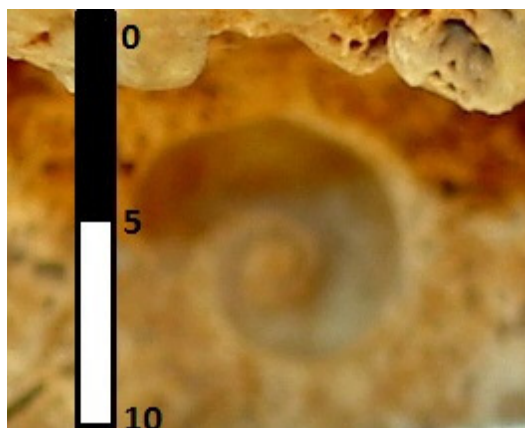
Figures 10, 11, 12: Description of material

Small impression of snail with flattened whorls, about 8 mm in diameter, preserved in tufa and calcrete, but aperture not preserved, see figure 12. This impression can be ascribed to a terrestrial snail, similar in general morphology to the modern species *Sculptaria* (Pickford, pers. comm.). More recent specimens were observed in finely laminated sediments and calcretes in the immediate area surrounding the spring pool as seen in figures 10 and 11.

Figure 11: View of aperture opening of *Sculptaria* (scale in cm)

Figure 10: Dorsal view of modern Snail, *Sculptaria* in the area (scale in cm)

Figure 12: Impression of snail in tufa (scale in cm)

?Vertebrate

Figure 13: Description of material

Impressions of possibly ribs and vertebrae preserved within tufa at the edge of the spring run-off. The impressions were reported and photographed by a visitor to the springs. It has been suggested that the sample is the impression of a frog skeleton based on the interpretation of the shapes of the impressions, which are similar to ribs and vertebrae, as well as the scale of the material (pers. Comm. Dr M. Pickford). However, given the complexity of the specimen and the lack of bone material, this could not be confirmed.

Figure 13: Impression of a possible frog. Photo taken by Martin Prinsloo

Layered *Procavia capensis* dung

Figure 14: Description of material

Well layered *Procavia capensis* dung was observed within one of the hollows of the tufa boulders about 4.5 m above the spring pool. This is well compacted and not too granular in nature, though it would be younger in age than the tufa.

Figure 14: Layered *Procavia capensis* dung

Palaeoecology

According to the vegetation map of Giess (1998), the Ongongo area is located within the Mopane Savanna vegetation type. As the name suggests the dominant plant species of this vegetation type is *Colophospermum mopane*, or mopane tree. The Mopane Savanna vegetation type is closely related to the Mountain Savanna vegetation type, which includes the entire Karstveld and includes *Ficus sycomorus*, or wild fig trees. Both tree species occur in the Ongongo area today.

The mopane can occur either as a shrub or tree. Towards the western Namib, where the annual rainfall ranges from 50-100 mm, the mopane is often confined to depressions or dry riverbeds (Giess, 1998). In areas of higher annual rainfall ranging from 500-600 mm, towards Ovamboland and the Grootfontein District, the mopane usually grows as a tree.

The nearest rainfall monitoring station to the Ongongo area is located at Kamanjab which has an average annual rainfall of 303.5 mm (data from the Meteorological Division, Windhoek). The tufa outcrop area under observation is located in a river bed which receives more moisture compared to surrounding areas, due to the Ongongo spring and often contains standing water pools. According to the National Drought Task Force (1997) climate classification based on annual rainfall averages, the Ongongo area has an arid to semi-arid climate.

The average annual temperatures for the Ongongo area range from 20 ˚C to more than 22 ˚C (Mendelsohn *et al.*, 2002). According to the same authors the average maximum temperatures during the hottest month of the year for the same area ranges from 30 ˚C to 34 ˚C. According to (Sweet, 1999) the annual potential evapo-transpiration rate for Namibia exceeds annual precipitation by ratios of up to 30:1, excluding deserts, resulting in the aggravation of drought conditions throughout most of the country.

Conclusions

The fossiliferous tufa described here is located at S 19˚ 08´25.3´´ E 13˚ 49´09.5´´. In order to establish an age for the impressions, it is necessary to develop reliable dating techniques for spring deposits.

Fossils identified include
- *Ficus sycomorus* (Family Moraceae)
- *Colophospermum mopane* (Family Fabaceae)
- ?Sedge (Family Cyperaceae)
- *Sculptaria,* terrestrial snail (Invertebrata)
- ?Frog (Vertebrata)
- *Procavia capensis* dung (Vertebrata)

This biota indicates the presence of the Mopane Savanna vegetation type, an arid to semi-arid climate, an average annual rainfall of 50 mm to above 300 mm, and high rates of evapo-transpiration at the time of deposition, similar to today's climatic conditions in that area.

References

Giess, W. 1998. Contributions to the Flora of Namibia. *Dinteria* No. 4, Third Revised Edition, Namibia Scientific Society, Windhoek, 112pp.

Korn, H. and Martin, H. 1937. Die jüngere geologische und klimatische Geschichte Südwestafrikas. Zentralblatt für Mineralogie, *Geologie und Paläontologie*, B11, 456-473.

Korn, H. and Martin, H. 1955. The Pleistocene in South West Africa. *Proceedings of the 3rd Pan-African Congress on Prehistory*, Livingstone, 14-22.

Mendelsohn, J., Jarvis, A., Roberts, C. and Robertson, T. 2002. *Atlas of Namibia: A Portrait of the Land and its People.* David Philip Publishers, Cape Town, South Africa, 200pp.

Miller, R. McG. 2008. *The Geology of Namibia. Volume 3- Palaeozoic to Cenozoic*, Ministry of Mines & Energy, Geological Survey, Chapters 24-25, 690 pp.

NDTF, 1997. Towards a drought policy for Namibia. *A discussion document prepared by the National Drought Task Force for a workshop at Neudamm Agricultural College 11-13 March 1997*. National Drought Task Force, Windhoek.

Sweet, R.J. 1999. *Livestock—Coping with drought: Namibia—case study*. Paper pre-

pared for FAO electronic conference on drought, FAO, Rome.

Ward, J. D. 1987. The Cenozoic succession in the Kuiseb Valley, central Namib Desert. *Memoir Geological Survey Namibia*, 9, 124pp.

COMMUNICATIONS OF THE GEOLOGICAL SURVEY OF NAMIBIA

Communications first appeared in 1985 with the aim to disseminate information about research and mapping projects carried out by Geological Survey staff, as well as by visiting scientists, on an annual basis. Although for a number of years this goal has not been met, it is planned with this issue to return to its original objective. If warranted by the number of contributions, bi-annual publication will be considered. Communications is published in digital format and distributed to universities and research institutions worldwide; copies can also be purchased at the Geological Survey's sales office at 1 Aviation Road, Windhoek.

INSTRUCTIONS FOR CONTRIBUTORS

General

1. Manuscripts must be written in English.
2. A short abstract of less than 200 words must accompany research papers and reports.
3. Short geological notes (commonly less than 1000 words) may also be submitted. Notes do not require an abstract.
4. Contributions have to be submitted in digital format. The preferred format for text is Microsoft Word, for figures jpg or tiff.
5. Papers will be reviewed by external and internal referees; reports will be reviewed by internal referees. In addition, manuscripts submitted by students should be critically reviewed by their supervisors before submission. It is the responsibility of the supervisor to ensure that a high standard is maintained.
6. Proof copies will be sent to the corresponding author for final checking before publication and should be returned within two weeks.

Text

1. A recent issue of *Communications* should be consulted for the general style and format to be adopted.
2. The format and sequence of headings are as follows:
   a. Bold Upper and Lower Case (centred)
   b. Free-standing italics (centred)
   c. Italics, above the line and at the margin
   d. Italics, indented at the line
   If further subdivision is needed, numerals or letters (lower case) should be used.
3. An alphabetical list of all references must follow the text, with a format as follows:
   Gevers, T.W. and Frommurze, H.F. 1929. The tin-bearing pegmatites of the Erongo Area, SWA. *Trans. Geol. Soc. S. Afr.*, **32**, 111-149.
   Blignault, H.J. 1977. *Structural-metamorphic imprint on part of the Namaqua Mobile Belt in South-West Africa.* Ph.D. thesis (unpubl.), Univ. Cape Town, 197 pp.
   (N.B. standard abbreviations for journals preferred!)

Illustrations

1. Figures and photographs must be of good quality; ensure that lettering is readable after reduction.
2. Figures and tables may be included in the text document to indicate their positioning, but must also be provided separately in one of the above-mentioned formats.
3. Figure captions must be provided as a separate list.
4. Headings of tables and appendices should appear above the table.
5. All illustrations or photographs are termed figures, and are referred to as Fig. or Figs in the text.